Dynamics and transport in the vicinity of a quantum phase transition in dimension two

Félix Rose

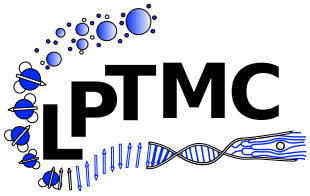

Thèse de doctorat
de l'Université Pierre et Marie Curie

Spécialité : Physique

École doctorale : « Physique en Île-de-France »

réalisée au

Laboratoire de physique théorique de la matière condensée

présentée par

Félix Rose

pour obtenir le grade de :

Docteur de l'Université Pierre et Marie Curie

Sujet de la thèse :

Dynamique et transport au voisinage d'une transition de phase quantique en dimension deux

soutenue le 19 septembre 2017

devant le jury composé de :

M.	**Sylvain Capponi**	**Rapporteur**
M.	**Nicolas Wschebor**	**Rapporteur**
Mme	**Silke Biermann**	**Président du jury**
M.	**Serge Florens**	**Examinateur**
M.	**Christophe Mora**	**Examinateur**
M.	**Jean-Paul Blaizot**	**Invité**
M.	**Nicolas Dupuis**	**Directeur de thèse**

Contents

Remerciements

> Welcome to the premiere of *Cleaver*, the story of a young man who goes to pieces, then manages to find himself again. In all seriousness, however, I'd like to say a few words. Much like a child, a film has many parents, that is to say many individuals who act like parents, or that by aversion, the film is their baby.
>
> I, as an executive producer, am one of those individuals.
>
> — "Stage 5", *The Sopranos*

Il est communément admis que le plus important dans un manuscrit de thèse est l'introduction, permettant de comprendre la portée du travail réalisé et de situer ce dernier dans son contexte. Ce n'est pas complètement faux mais généralement, ce qui est le plus lu, ce qui passe à la postérité, est ce que vous lisez maintenant : les remerciements. Autant dire qu'un lourd poids sur mes épaules alors que j'écris ces lignes et que je dois de manière concise, complète, et si possible amusante, chanter les louanges de ceux qui m'ont accompagné et aidé pendant ces trois années.

En premier lieu, je veux remercier Nicolas, mon directeur de thèse. Si cette thèse a été pour moi un formidable moment intellectuel, c'est en partie grâce à toi ; disponible et attentionné, tu auras su me motiver, me guider, et toujours m'aider quand j'en avais besoin, toujours avec bonté et humour, imperturbable face aux difficultés. Ensuite, je remercie Bertrand, pas seulement pour fayoter auprès du nouveau directeur, mais pour ton talent de conteur, avec lequel tu m'as non seulement initié aux arcanes de la renormalisation mais également partagé tes histoires et ta sagesse, avec la concision qui te caractérise.

Mon passage au sein du LPTMC aura été plaisant, en bonne partie, grâce aux permanents avec qui j'ai eu du plaisir à interagir. Je salue d'abord le groupe du midi. Claude, Jean-Noël, Hélène et Rémi m'auront offert de passionnantes conversations, de nombreux traits d'humour et beaucoup de soutien moral dans les moments difficiles. Julien aura su paradoxalement me rassurer avec son pessimisme et je retiendrai de lui sa bienveillance rarement égalée. Je garderai également de bons souvenirs d'Annie et de ses gâteaux et sa vodka, Dominique et son humeur joviale, Diane et son efficacité, Gilles qui aura motivé l'approximation « full Pol Pot », Marco et ses plats Picard, ainsi que Pascal et son aide informatique précieuse.

Bien sûr, il ne m'est pas possible d'oublier mes compagnons de cordée, les autres impermanents qui ont partagé mon quotidien ces trois années durant. Thibault, mon grand frère de thèse qui m'a pavé la voie, sera noté pour ses discussions toujours profondes, que ce soit à propos de physique ou de Feldenkrais. Son alter ego Andréas n'est pas en reste ; souvent opposé à Thibault, que ce soit dans les opinions ou le caractère, il n'en reste pas moins incontournable. Pierre m'aura apporté de nombreux fous rires et Elena autant de sourires. Auront supporté ma compagnie en tant que voisins

de bureau le bavard Thiago, le siffleur Fred, et bien sûr Ariane, dont le passage bien que bref n'en fut pas moins remarqué. Le père Simon a été une carte maitresse du groupe lors de son passage, et Boris restera dans nos mémoires comme le pape de la PPG. Olivier aura marqué le laboratoire par son sérieux, sa dévotion et son tableau bien rempli. Nicolas et Charlotte, l'état lié du laboratoire, m'auront beaucoup appris en matière de montage de meubles Ikéa. C'aura été un plaisir d'échanger avec Elsa, bien moins glaciale que ce que son allure de reine des neiges préfigure. Il en va de même avec Chloé, qui aura su face aux adversités de la thèse toujours retomber sur ses pattes. Charlie, l'adepte des betteraves et pois chiches m'aura initié quand à lui, entre autres, au gloups et au zbrah (ne parlons pas du reste — ce qui se passe à Lyon reste à Lyon). Charlie, Fred et Thibault, constituaient la cellule syndicale des doctorants du laboratoire. Je ne peux m'empêcher de remarquer un fort recouvrement avec le groupe des thésards du NPRG, peut-être signe d'une affection partagée pour les causes perdues sous-jacente ?

Ce fut également un plaisir d'échanger et travailler avec Adam et Federico, dont je me souviendrai des conseils et de l'animation qu'ils auront insufflé à Leucade et Trieste.

Enfin, je remercie Sylvain Capponi et Nicolas Wshebor d'avoir rapporté ma thèse et attentivement lu le manuscrit, ainsi que Jean-Paul Blaizot, Silke Biermann, Serge Florens et Christophe Mora pour avoir participé au jury de thèse, et l'ensemble du jury pour les commentaires et corrections apportés au manuscrit.

Pour terminer sur une note plus personnelle, je voudrais sortir du LPTMC pour remercier également mes autres amis. Les trois années que durent une thèse ne peuvent se résumer qu'à ce qui se passe dans le laboratoire, et votre présence à été essentielle pour moi. Par manque de place et pour ne pas faire de jaloux je me contente de vous citer par ordre alphabétique, sans distinction de classe ni de race. Merci Adrien, Alexandre, Arnaud, Betty, Camille, Cécile, Claire, Émilie, Fabrice, Guillaume, Hédy, Julie, Kiril, Léa, Louis-Marie, Luca, Manon, Marc, Marie, Marion, Michael, Paul, Quentin, Razvan, Sarah, Solenn, Sophie, Svyatoslav, Tal, Thibault, Tony, et tous ceux que j'oublie (ils se reconnaitront).

Et, bien sûr, merci Alex et Olga, sans qui rien de tout ça n'aurait été possible.

1

Introduction

> Like most North Americans of his generation, Hal tends to know way less about why he feels certain ways about the objects and pursuits he's devoted to than he does about the objects and pursuits themselves. It's hard to say for sure whether this is even exceptionally bad, this tendency.
>
> — David Foster Wallace, *Infinite Jest*.

The study of phases of matter occupies a major spot in condensed matter physics. In many-body systems, that is, physical systems with a macroscopic number of degrees of freedom, the interplay of interactions and quantum statistics (and, in some cases, topology) explains well-known as well as more exotic behaviors, from Bose–Einstein condensation and metallic conduction to superconductivity and fractional quantum Hall effect.

The simplest case is that of a system whose elementary excitations can be described in terms of weakly interacting quasiparticles, such as Fermi liquids. Although a quasiparticle model is simple to study, it may be nontrivial to identify the elementary excitations starting from a microscopic model.

Of particular interest are materials whose low-energy excitations cannot be understood in terms of quasiparticles. These are said to be strongly correlated systems. In many cases, these strong correlations are linked to the existence of a zero-temperature *quantum phase transition* (QPT). By contrast to classical phase transitions, caused by thermal fluctuations, a QPT is a qualitative change in the ground state of a system driven by quantum fluctuations as an external parameter, e.g. a magnetic field or doping, is tuned. In the vicinity of a continuous (second-order) QPT, the correlation length associated to quantum fluctuations becomes very large with respect to the microscopic scales of the system, which is therefore strongly correlated [1].

Examples

A very simple example of QPT is given by cobalt niobate ($CoNb_2O_6$) [2], in which the degrees of freedom are the spins of cobalt ions. Under a magnetic field, this system is described by the transverse-field Ising model. In the absence of external magnetic field, spins tend to align in a ferromagnetic order along an easy axis z. The system is invariant under the reflection with respect to the orthogonal plane to z, the ground state has a two-fold degeneracy, with the spins aligned along z, pointing either all up or down. If one switches on a magnetic field in the plane orthogonal to z, Zeeman effect tends to align the spins with the magnetic field. In the limit of an infinitely strong transverse field, the ground state is nondegenerate, with all spins aligned with the magnetic field. Now, tuning the field from infinite to zero strength, one cannot smoothly connect the two

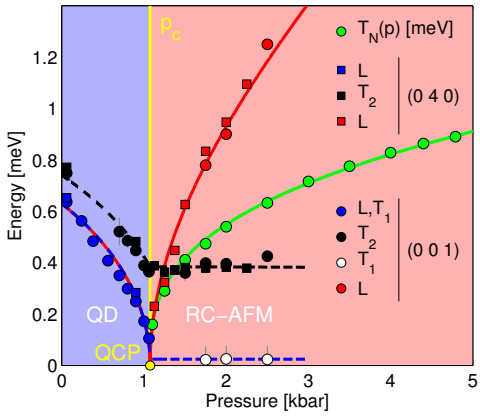

FIGURE 1.1: Phase diagram of $TlCuCl_3$ under pressure and excitation gaps measured through inelastic neutron scattering. At low pressure, the ground state is made of spin singlets and there are three degenerate triplet excitation branches (L, $T_{1,2}$). At higher pressures the system shows magnetic ordering, and there are two gapless modes ($T_{1,2}$), corresponding to transverse fluctuations of the magnetic moment, and one longitudinal gapped mode (L). Because of a weak anisotropy in the magnet, one of the transverse modes (T_2) is actually gapped. Above the Néel temperature T_N the magnet loses antiferromagnetic ordering. All excitations energies as well as T_N vanish at the quantum critical point. Original reference: [3].

scenarios (nondegenerate paramagnetic ground state respecting the Hamiltonian symmetry and two degenerate ferromagnetic ground states breaking down the Hamiltonian symmetry): there is necessarily a critical value of the field for which a phase transition occurs.

Quantum antiferromagnets also provide examples of QPTs [3–5]. We present for instance in Fig. 1.1 the experimental phase diagram and excitations of the quantum magnet $TlCuCl_3$, in which spins in the magnet form dimers. As pressure is applied to the system, the paramagnetic ground state made by spin singlets gives way to an antiferromagnetic phase.

QPTs can also be observed in ultracold atom systems. In a system of interacting bosons trapped in an optical lattice, tuning e.g. the lattice potential triggers a transition between an insulating phase where the bosons are localized at each site and a superfluid phase where a macroscopic fraction of the bosons condense in the one-particle zero-momentum state. This Mott insulator-superfluid transition has been observed experimentally in realizations of the Bose–Hubbard model [6–10].

The disorder driven superconductor-insulator transition is also a bosonic QPT [11]. While weak disorder does not modify qualitatively the superconducting ground state, strong disorder decomposes the homogeneous ground state into individual superconducting islands. In that case, the QPT takes place at a critical value of disorder for which phase fluctuations between the superconducting islands destroy the global phase coherence, while the pairing gap itself does not vanish as each island individually remains superconducting.

There are several examples of QPTs in fermion systems, such as heavy fermion compounds [12, 13]. These are typically materials with f-electron orbitals, which bear their name from the fact that conduction electrons display a very large effective mass (about 1000 that of a free electron). Due to the presence of local magnetic moments interacting with conduction electrons (Kondo lattice), there is a QPT as the Kondo coupling is varied, through external pressure or doping, between a Fermi liquid paramagnetic state where Kondo screening suppresses magnetic order and an antiferromagnetic ground state stabilized by RKKY interactions.

Another fermionic example is given by unconventional high-temperature superconductivity in cuprates. Although it is not fully understood yet, several proposals link this unconventional superconductivity to the collective behavior of electrons associated with the presence of a zero-temperature QPT under the superconducting dome [14, 15]. These strong collective fluctuations could provide us with an explanation of the strange properties of the metallic phase, such as the pseudo-gap or the resistivity linear in temperature.

Phenomenology

Let us now discuss briefly generic properties of QPTs. A question one may ask oneself is how the quantum phase transitions discussed above, which occur at zero temperature and are driven by quantum fluctuations, are related to classical phase transitions. One may indeed be more familiar with transitions of the latter type, such as the liquid-gas transition in fluids or the ferromagnetic-paramagnetic transition in magnets. In these classical transitions, it is the competition between energetic and entropic terms in the free energy which determines the phase of the system, the entropy favoring disordered phases of matter and the energy ordered ones (i.e., broken symmetry phases). The tuning parameter determining which term is dominant is the temperature.

Before further discussing the link with QPTs, let us recall two essential properties of second-order (continuous) classical phase transitions: universality and scaling. As these transitions are characterized by a diverging correlation length, long-distance physics (in the critical regime) can be parameterized by scaling functions depending on dimensionless ratios of a small set of macroscopic variables, such as the correlation length, the length scale at which is probed the system, and so on. This property is called scaling. Universality means that quantities characterizing the long-distance physics in the vicinity of the transition, including these scaling functions, do not depend on the microscopic details of the model but merely on very broad determinants, such as dimensionality or the symmetry of the Hamiltonian. For instance, the long-distance physics of water near its critical point and that of an uniaxial anisotropic magnet near its Curie temperature are the same: these two transitions are said to belong to the same universality class. The theoretical framework that allows to understand these remarkable properties is the renormalization group (RG).

The connection between QPTs and classical phase transitions is made through path integral formulation, which allows to rephrase a quantum statistical physics problem in terms of a classical theory. The price to pay is the introduction of an extra imaginary time direction, with a finite width equal to the inverse temperature. In the case of a continuous QPT, there are at the transition two diverging correlation lengths, ξ and ξ_τ, corresponding to the space and time directions. The model is a priori anisotropic and there is no reason for them to scale identically; one defines the dynamical critical exponent z by comparing the scaling of the two lengths near the transition, $\xi_\tau \sim \xi^z \sim |\delta - \delta_c|^{-z\nu}$, with δ the nonthermal control parameter triggering the QPT at a value δ_c. The time correlation length defines an energy scale $\Delta \sim \xi_\tau^{-1}$ which vanishes at the transition.

Note that second order finite-temperature transitions are always driven by classical (thermal) fluctuations. Indeed at finite temperature the thermal de Broglie wavelength of the critical excitations λ_{dB} is finite while the correlation length ξ diverges at the transition. Because of this, close enough to the transition, $\xi \gg \lambda_{dB}$ and the system can be effectively described in classical terms. As we shall see in the following, the presence of a zero-temperature QPT nonetheless strongly affects the finite-temperature physics.

Because of the quantum-classical mapping, the above discussion about second order classical phase transitions apply to second order QPTs. In particular, scaling and universality hold. Examples

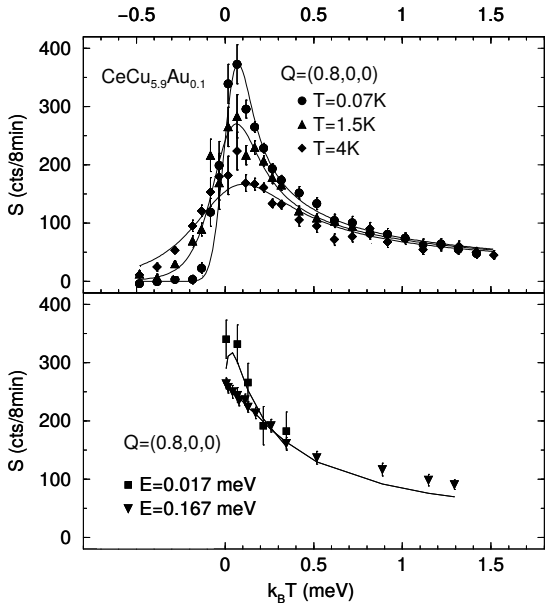

(a) Susceptibility measured at fixed temperatures (top) and energy (bottom).

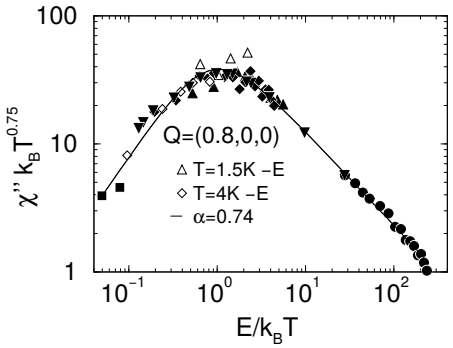

(b) Scaling analysis.

FIGURE 1.2: Imaginary part χ'' of the spin susceptibility of the heavy fermion alloy $CeCu_{6-x}Au_x$ near its QPT. The transition occurs as Au is substitued for the Cu atoms; for values of x larger than $x_c \simeq 0.1$ the heavy fermion paramagnet gives way to an ordered antiferromagnet. The system is driven near the QCP and $\xi = \infty$, $\Delta = 0$. The susceptibility (taken for a given wavevector) is measured as a function of energy at fixed temperature (top left) and as a function of temperature at fixed energy (bottom left). A scaling analysis (right) shows that the data collapses on a single curve, proving that near the QCP the suceptibility is a function of the ratio $E/k_B T$ of incident energy $E = \hbar\omega$ to temperature T. The collapse involves one free parameter α, related to the dynamical exponent z through $\alpha = 2/z$; the value of the fit $\alpha \simeq 0.74$ deviates from the mean-field result $\alpha = 1$. The full line correspond to a phenomenological prediction for $\alpha = 0.74$. Original reference: [16].

of scaling are given by the pressure P or the order parameter susceptibility χ, which scale in d space dimensions (below the upper critical dimension) like

$$P(T,\Delta) = P(T=0,\Delta) + aT^{(d+z)/z}\mathcal{F}\left(\frac{\Delta}{k_B T}\right), \quad \chi(\mathbf{p},\omega,T,\Delta) = b\xi^{\gamma/\nu}\mathcal{G}\left(\mathbf{p}\xi, \frac{\hbar\omega}{k_B T}, \frac{\Delta}{k_B T}\right), \quad (1.1)$$

with a and b nonuniversal prefactors, and γ, ν critical exponents. Here $\mathbf{p}$ and ω denote the momenta and frequency at which the system is probed. The scaling functions $\mathcal{F}(x)$, $\mathcal{G}(u,v,w)$ do only depend on the universality class of the theory. An example of scaling in the vicinity of a QPT, observed in the susceptibility of a heavy fermion compound, is given in Fig. 1.2.

From these considerations, one may draw a qualitative typical phase diagram of the model. At zero temperature, there is a quantum phase transition at δ_c. This transition separates a disordered symmetric phase, with a vanishing order parameter, from a broken symmetry ordered phase where the order parameter is finite. Spontaneous symmetry breaking causes long-range order (LRO).

Let us now look at what happens at small but finite temperature. In the functional integral formulation, the time direction becomes finite with length $L_\tau = \hbar/k_B T$. In the disordered phase, the

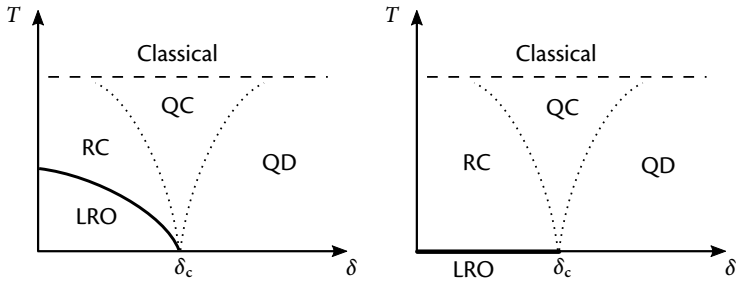

(a) LRO at finite temperature. (b) No LRO at finite temperature.

Figure 1.3: Qualitative phase diagram of a quantum phase transition. At zero temperature, the symmetric phase is separated from the broken symmetry phase displaying long range order (LRO) by a quantum phase transition at a critical value δ_c of the coupling δ. At finite temperature, there are crossover lines separating the quantum disordered (QD), quantum critical (QC) and renormalized classical (RC) regimes. Depending on the model and dimension, LRO may persist at finite temperature, in which case it is separated from the disordered phase by a line of classical critical points terminating at the QCP.

system does not realize that the temperature is nonzero as long as $\xi_\tau \ll L_\tau$, i.e. $k_B T \ll \Delta$. Recall that Δ is a zero-temperature energy scale; in the disordered phase Δ is the gap, while in the ordered phase it is convenient to use the gap of the point on the disordered phase sharing the same value of $|\delta - \delta_c|$. The zero-temperature physics describe qualitatively the system, whose behavior is dominated by quantum fluctuations, hence this regime is called quantum disordered (QD). For temperatures larger than the gap, $k_B T \gtrsim \Delta$, thermal fluctuations become important and this picture breaks down.

In the ordered phase, two scenarios are possible, depending on the model and dimension. Indeed, by turning on the temperature, the time dimension becomes compact, and the dimensionality of the theory is reduced. This may suppress long-range order (e.g. because of Mermin–Wagner theorem), in which case the system is disordered at any finite temperature. Disorder is mainly due to thermal fluctuations, although quantum fluctuations affect the properties of the model, hence the denomination of renormalized classical (RC) regime. Otherwise, a LRO phase persists in the RC regime and is separated from the finite temperature disordered phase by a line of classical (thermal) phase transitions terminating at the QCP. As in the disordered case, this picture holds as long as $k_B T \ll \Delta$.

Finally, let us discuss what happens in the regime where $k_B T \gtrsim \Delta$. Although the transition happens at zero-temperature, finite-temperature physics is strongly affected by the QCP, hence the name of quantum critical regime. As Δ is much smaller than the temperature, the physics is controlled by the thermal excitations above the QCP ground state, with only one energy scale, $k_B T$. This leads to exotic behavior: for instance, specific heat scales like $T^{d/z}$. We graphically summarize the phase diagram in Fig. 1.3.

The quantum $O(N)$ model

As we saw above, QPTs occur in a broad variety of physical systems, including spins, bosons and fermions. We shall in this thesis restrict ourselves to the study of universal properties of one specific family of universality classes, those of the relativistic quantum $O(N)$ model. The microscopic action

describing these models is

$$S[\boldsymbol{\varphi}] = \int \mathrm{d}^d\mathbf{r} \int_0^{1/T} \mathrm{d}\tau \, \frac{1}{2}(\partial_\mu \boldsymbol{\varphi})^2 + U(\boldsymbol{\varphi}^2/2), \tag{1.2}$$

with $\boldsymbol{\varphi}(\mathbf{r}, \tau)$ a N-component real field defined over a $(d+1)$-dimensional space-time. We denote time and space directions by $\mu = 0, 1, \ldots, d$ and perform an implicit sum on μ, $(\partial_\mu \boldsymbol{\varphi})^2 = \sum_\mu (\partial_\mu \boldsymbol{\varphi})^2$. Here and in the following we work in natural units $\hbar = k_\mathrm{B} = 1$. The theory is invariant under rotations of the field and bears a relativistic space-time symmetry at zero temperature. It exhibits a QPT between a symmetric (disordered) phase where the expectation value of the field vanishes and an ordered phase where the $\mathrm{O}(N)$ symmetry is broken as the field acquires a finite expectation value. In three space dimensions and above, the theory is noninteracting at low energies and is qualitatively described by mean-field theory (with logarithmic corrections in three dimensions). Because of this, we are mostly interested in the case of two dimensions, in which the transition belongs to the three-dimensional classical $\mathrm{O}(N)$ universality class, which is controlled by a strongly-interacting (Wilson–Fisher) fixed point.

Although in condensed matter and quantum optics Galilean invariance is more common than relativistic invariance, several of the QPTs we enumerated above are described in the low-energy sector by the quantum $\mathrm{O}(N)$ model. When the Mott insulator-superfluid transition occurs at fixed (integer) density, because of an emergent particle-hole symmetry, it is described by the relativistic $\mathrm{O}(2)$ model, the real and imaginary part of the bosonic field being mapped on a two-component real field [1]. The disorder driven superconductor-insulator transition is another example. In that case the relevant degree of freedom of the model is the local phase, the fluctuations of which can be described by the XY model, which also belongs to the $\mathrm{O}(2)$ universality class.

Finally, the low-energy action of the fluctuations around the Néel order in an insulating antiferromagnet is given by the action of the $\mathrm{O}(3)$ nonlinear σ model and additional topological terms [17]. Dropping the latter (something not always justified in small dimensions and in the disordered phase), one recovers the universality class of the relativistic $\mathrm{O}(3)$ model.

Outline of the manuscript

The tool we use to study the universal properties of the relativistic quantum $\mathrm{O}(N)$ model is the Nonperturbative Renormalization Group (NPRG). Based on a functional implementation of Wilsonian RG, it is a framework tailored to devise nonperturbative approximation schemes. In Chapter 2, we present in detail the NPRG and give its implementation on the $\mathrm{O}(N)$ model, as well as examples of approximation schemes and results obtained using them. We then study the universal properties of the quantum $\mathrm{O}(N)$ model in Chapters 3 to 5, examining first the thermodynamics of the model, then its zero-temperature dynamical properties: excitation spectrum, transport.

- In Chapter 3, we examine the thermodynamics of the model, and determine the universal scaling functions describing the gap and the pressure of the model in the whole critical regime. We show a mapping between the two-dimensional quantum theory at finite temperature and a classical model in three dimensions confined along a direction, establishing a correspondence between the thermodynamics of the quantum model and Casimir forces in the classical model and allowing us to compare our results with numerical simulations of three-dimensional spin systems.

- In Chapter 4, we study the excitation spectrum in the ordered phase of the model. For $N \geq 2$, the $\mathrm{O}(N)$ symmetry is continuous and mean-field theory predicts the existence of $N-1$ gapless Goldstone modes and one massive amplitude "Higgs" mode. Whether this picture remains true beyond mean field in two space dimensions has been debated; we show that there indeed is a well-defined resonance in the scalar susceptibility for $N = 2$ and (to some extent) 3 and compare our results to Monte Carlo simulations. For $N = 1$, the symmetry is discrete, there are no Goldstone modes and the ordered phase is gapped. We determine in that case the bound state spectrum of the model and the universal ratio of its energy to the one-particle excitation gap.

- Finally, in Chapter 5, we study the transport properties of the model, namely, its conductivity, which we determine at zero temperature for all frequencies in the universal regime. In particular, in the disordered phase, the system behaves like a capacitor with a capacitance C_{dis} while in the ordered phase, one of the two components of the conductivity tensor is an inductance L_{ord}. The ratio $C_{\mathrm{dis}}/L_{\mathrm{ord}}$ is a universal number which we determine. We also compute the universal conductivity at the QCP and compare with QMC and conformal bootstrap results. Furthermore we show that, in the ordered phase, the other component of the conductivity tensor at zero frequency is "superuniversal", depending neither on the distance to the QPT nor on N.

2

Introduction to the nonperturbative renormalization group

> To the last we have learned nothing. In all of us, deep down, there seems to be something granite and unteachable. No one truly believes, despite the hysteria in the streets, that the world of tranquil certainties we were born into is about to be extinguished.
>
> — J. M. Coetzee, *Waiting for the Barbarians*.

In this chapter, we present the Non-Perturbative Renormalization group (NPRG), sometimes also called the "functional" or "exact" RG. We aim for a concise yet self-contained introduction that focuses more on practical than conceptual aspects. For more information we refer to reviews [18, 19] and especially [20].

Let us explain the principles of Wilson-like renormalization group (RG) as well as the ideas behind it. In high-energy and statistical physics, ultraviolet divergences arise within the context of field theories. Even in the presence of a finite ultraviolet cutoff, these are problematic: the divergences mean that the theory strongly depends on the cutoff, while we know that in the vicinity of a second-order phase transition universal physics should not depend on the microscopic details of the model. These divergences are not necessarily a fundamental property of such theories, but rather arise from the continuum formulation adopted. In a system close to a second-order phase transition, all scales up to the correlation length contribute to the physics. Fluctuations at arbitrary small scales cause these divergences. By contrast, a continuum description of, say, hydrodynamics in the laminar regime, does not cause any problem; for instance, in the description of a macroscopic wave, the only relevant length scale is its wavelength and nothing much happens at smaller scales.

Wilson's idea to cure the divergences caused by the presence of fluctuations at all scales is to integrate the latter in a smart way. Rather than taking all fluctuations into account simultaneously, they are integrated over successively, starting with microscopic scales and iteratively adding modes at larger and larger scales. By doing so, some contributions from the modes become less and less important: part of the microscopic physics is washed out. On the other hand, other contributions are amplified through these steps, and define the long-distance physics of the system. By integrating small-scale fluctuations, we construct an effective theory for the long-distance physics; the trajectory taken by the effective microscopic action through theory space as this transformation is iterated is the RG flow. At the phase transition, the system is scale-invariant (at distances large with respect to the microscopic scales), and the RG flow leads to a fixed point. In the vicinity of the critical point, the physics is still governed by the fixed point: for length scales smaller than the correlation length,

it looks critical, and the flow stalls close to the critical point. At larger length scales, the system "realizes" it is not critical, and the flow is driven away from the fixed point towards a phase. The behavior of the flow near the fixed point determines the universal physics in the vicinity of criticality.

The conceptually simplest example of such an RG procedure is Kadanoff's celebrated block-spin RG [21]. Consider a system of lattice spins $\{\sigma_i\}$ described by an Hamiltonian $H[\{\sigma_i\}, \{g_i\}]$, where $\{g_i\}$ is the set of coupling constants describing the interaction between the spins. We adopt a very general notation even if the Hamiltonian is described by only a few couplings, e.g. a nearest-neighbor ferromagnetic interaction. The partition function reads

$$\mathcal{Z} = \sum_{\{\sigma_i\}} \exp(-H[\{\sigma_i\}, \{g_i\}]). \tag{2.1}$$

The block-spin RG transformation consists in three steps. In the first one, we form blocks B_i regrouping neighboring spins, to which we attribute a spin value (e.g. by majority rule). Then, we integrate out the local spins by summing over them in the partition function, to obtain an effective Hamiltonian H^{eff} for the blocks B_i,

$$\mathcal{Z} = \sum_{\{Bi\}} \sum_{\sigma_i \in B_i} \exp(-H[\{\sigma_i\}, \{g_i\}]) = \sum_{\{Bi\}} \exp(-H^{\text{eff}}[\{B_i\}, \dots]), \tag{2.2}$$

where we do not precise the coupling constants. Finally, we rescale the space to map the lattice formed by the block into the initial lattice. The effective Hamiltonian for the blocks is recast into an Hamiltonian for the coarse-grained spins (which we still note σ_i) but with different coupling constants. The total transformation reads

$$H[\{\sigma_i\}, \{g_i\}] \to H[\{\sigma_i\}, \{g_i'\}]. \tag{2.3}$$

The integration of local degrees of freedom is incorporated into the new coupling constants $\{g_i'\}$. The RG flow is the map that describes the evolution of the coupling constants through iterations of this transformation. If the initial condition were the ferromagnetic Ising model, for instance, the system would admit a fixed point with a finite nearest-neighbor ferromagnetic coupling. Away from the transition, this coupling would either flow to zero (in the paramagentic phase) or to infinity (in the ferromagnetic phase). Note that even if there are initially only a small number of coupling constants, an infinite number of couplings between the blocks is generated by even a single step of the RG flow, and in principle one has to keep track of all possible couplings allowed by symmetry. Although this approach is instructive, it is often unpractical and hard to generalize. We shall now discuss Wilson's RG and the closely related NPRG, which are implemented on continuum field theories and in Fourier space.

The NPRG is very close in concept to the Wilsonian renormalization group [22–24], which is the basis for many perturbative RG approaches in condensed matter physics. Let us recall its principle, using the classical O(N) theory in D space dimensions (or, equivalently, the quantum O(N) model in $d+1 = D$ space-time dimensions at zero temperature) as an example. The partition function reads

$$\mathcal{Z} = \int \mathcal{D}[\boldsymbol{\varphi}] \exp(-S[\boldsymbol{\varphi}]), \tag{2.4}$$

with $\boldsymbol{\varphi}(\mathbf{x})$ a N-component real field and S the action invariant under global rotations of the field. We assume the theory is regulated in the ultraviolet by a cutoff Λ, which in a condensed matter setting would correspond to the inverse lattice spacing.

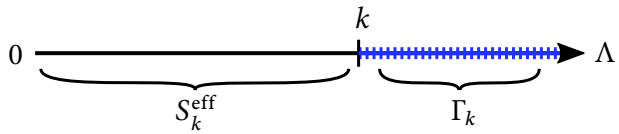

Figure 2.1: Comparison of Wilsonian RG and NPRG. In the former method, fluctuations at high energy are encoded into an (effective) microscopic action for the low-energy modes. In the latter, these fluctuations are directly incorporated into an effective action.

For the Wilsonian RG, the separation of fast and slow scales is done by decomposing the field modes $\boldsymbol{\varphi}$ into a slow and a fast component, $\boldsymbol{\varphi} = \boldsymbol{\varphi}_{\text{s}} + \boldsymbol{\varphi}_{\text{f}}$. The fast part $\boldsymbol{\varphi}_{\text{f}}$ only comprises Fourier components of momenta larger than some scale k; it corresponds to small-distance, high-energy fluctuations of the field, in opposition to the slow part $\boldsymbol{\varphi}_{\text{s}}$. Having isolated the fast part, we integrate it out, resulting in an effective action S_k^{eff} for the slow modes:

$$\mathcal{Z} = \int \mathcal{D}[\boldsymbol{\varphi}_{\text{s}}]\mathcal{D}[\boldsymbol{\varphi}_{\text{f}}]\, \exp(-S[\boldsymbol{\varphi}_{\text{s}}, \boldsymbol{\varphi}_{\text{f}}]) = \int \mathcal{D}[\boldsymbol{\varphi}_{\text{s}}]\, \exp(-S_k^{\text{eff}}[\boldsymbol{\varphi}_{\text{s}}]), \tag{2.5}$$

$$\exp(-S_k^{\text{eff}}[\boldsymbol{\varphi}_{\text{s}}]) = \int \mathcal{D}[\boldsymbol{\varphi}_{\text{f}}]\, \exp(-S[\boldsymbol{\varphi}_{\text{s}}, \boldsymbol{\varphi}_{\text{f}}]). \tag{2.6}$$

In a last step, a rescaling of the space is performed which brings back the ultraviolet cutoff to Λ, and, in parallel, the field is renormalized. The procedure can be iterated and an exact flow equation that describes the evolution of S_k^{eff} as k is lowered from Λ to 0 can be derived. The fluctuations are incorporated into the coupling constants defining S_k^{eff}.

The most successful implementation of this RG procedure on S_k^{eff} has been rederived by Polchinski with an arbitrary cutoff function [25] (rather than the sharp cutoff shown above) and is often called "Wilson–Polchinski RG". However, despite its conceptual elegance, the method is ill-suited for approximation schemes beyond perturbation theory or the local potential approximation (the latter is discussed in Section 2.3.1). Because of this, even though Wilsonian RG was developed in the 1970s, it has mostly been used as the basis for perturbative RG approaches, until its reformulation using the effective action formalism (which we call NPRG). Although the ideas behind NPRG had been in the air for some time [26, 27], a breakthrough came in the 1990s with the modern formulation of NPRG [28–31]. The reason why Wilsonian RG had remained relatively unexploited is that computing correlation functions using S_k^{eff} is technically strenuous (one has to determine the partition function in presence of an external source with a nontrivial action S_k^{eff}) and, in practice, results are highly sensitive to approximation schemes and the cutoff function. What allowed the rise of NPRG is the idea to consider the effective action $\Gamma[\boldsymbol{\phi}]$, the Legendre transform of the free energy, rather than the microscopic action. In a very similar fashion to what is done in Wilsonian RG, we build a k-dependent effective action Γ_k incorporating only fluctuations at momenta scales larger than k, see Fig. 2.1. Γ_k is more convenient to manipulate than S_k^{eff}, and is much more suited to the implementation of approximation schemes.

Through the remainder of the chapter, we retain the above defined $\mathrm{O}(N)$ theory to illustrate the principle of NPRG, even though its scope is not limited to such theories. In Section 2.1, we define the effective action of the theory and show how to deduce physical properties from it. In Section 2.2, we explain how the k-dependent effective action is constructed and how its flow is determined. Finally, in Section 2.3, we detail approximation procedures which allow in practice to study critical physics.

2.1 The effective action formalism

In this section, we define the effective action of a theory, the central object in the NPRG formalism, using the O(N) model as an example. To describe a theory, one needs, in general, the knowledge of the partition function, which yields the free energy, and the correlation functions, $\langle \varphi_{i_1}(\mathbf{x}_1)\cdots\varphi_{i_n}(\mathbf{x}_n)\rangle$. The standard way to access this information is to (formally) linearly couple $\boldsymbol{\varphi}$ to an external source $\mathbf{J}$. The partition function reads

$$\mathcal{Z}[\mathbf{J}] = \int \mathcal{D}[\boldsymbol{\varphi}] \exp\left(-S[\boldsymbol{\varphi}] + \int_{\mathbf{x}} \mathbf{J}\cdot\boldsymbol{\varphi}\right). \tag{2.7}$$

Then, the free energy $\ln\mathcal{Z}$ is the generating functional of the connected correlation functions. It contains all the physical information of the theory. The order parameter, the expectation value of $\boldsymbol{\varphi}$, is given by

$$\boldsymbol{\phi}[\mathbf{x};\mathbf{J}] = \langle\boldsymbol{\varphi}(\mathbf{x})\rangle = \frac{\delta \ln\mathcal{Z}[\mathbf{J}]}{\delta\mathbf{J}(\mathbf{x})}. \tag{2.8}$$

The effective action Γ is the Legendre transform of $\ln\mathcal{Z}$ with respect to $\mathbf{J}$,

$$\Gamma[\boldsymbol{\phi}] = -\ln\mathcal{Z}[\mathbf{J}[\boldsymbol{\phi}]] + \int_{\mathbf{x}} \mathbf{J}[\boldsymbol{\phi}]\cdot\boldsymbol{\phi}. \tag{2.9}$$

In Eq. (2.9), $\mathbf{J}$ is a functional of $\boldsymbol{\phi}$ obtained by inverting (2.8). Γ is the Gibbs free energy. By definition of the Legendre transform, it is a convex function of the field. Since the free energy is also convex (its Hessian is the two-point connected correlation function) it can be reconstructed from the effective action. Thus, Γ contains all the physical information on the system. It satisfies the equation of state

$$\frac{\delta\Gamma[\boldsymbol{\phi}]}{\delta\boldsymbol{\phi}(\mathbf{x})} = \mathbf{J}[\mathbf{x};\boldsymbol{\phi}], \tag{2.10}$$

and in absence of external sources the order parameter $\boldsymbol{\phi}(\mathbf{x})$ is the field configuration that extremizes Γ. The thermodynamic properties of the system can be deduced from the effective potential

$$U(\rho) = V^{-1}\,\Gamma[\boldsymbol{\phi}]\big|_{\boldsymbol{\phi}=\text{const.}} \tag{2.11}$$

defined by the effective action evaluated in a uniform field $\boldsymbol{\phi}(\mathbf{x}) = \boldsymbol{\phi}$ (V is the volume, set to 1 in the following). From now on, we set $\mathbf{J}$ to zero. Due to symmetry, $U(\rho)$ only depends on the O(N) invariant $\rho = \boldsymbol{\phi}^2/2$. We denote ρ_0 the position of the minimum.[1] The norm of the order parameter is given by $|\boldsymbol{\phi}| = \sqrt{2\rho_0}$. Thus, if $\rho_0 > 0$, there is an infinity of possible degenerate values for the order parameter (two possible values for $N = 1$ as $\mathrm{O}(1) \simeq Z_2$): the O(N) symmetry is spontaneously broken as the system selects one of these minima. Conversely, in the fully symmetric phase, $\rho_0 = 0$ and the order parameter is zero. Note that as the effective action is convex, in the ordered phase $U(\rho)$ has a "flat bottom"; it is constant and equal to its minimum in the whole range $[0,\rho_0]$.

Γ is the generating functional of one particle irreducible (1PI) vertices. Correlation functions can be reconstructed from the 1PI vertices, defined by

$$\Gamma^{(n)}_{\{i_j\}}[\{\mathbf{x}_i\};\boldsymbol{\phi}] = \frac{\delta^n\Gamma[\boldsymbol{\phi}]}{\delta\phi_{i_1}(\mathbf{x}_1)\cdots\delta\phi_{i_n}(\mathbf{x}_n)}. \tag{2.12}$$

[1] The position of the minimum of the potential is often referred to as the minimum of the potential.

The correlation functions evaluated in a uniform field configuration are determined by the vertices

$$\Gamma^{(n)}_{\{ij\}}(\{\mathbf{x}_i\},\boldsymbol{\phi}) = \Gamma^{(n)}_{\{ij\}}[\{\mathbf{x}_i\};\boldsymbol{\phi}]\Big|_{\boldsymbol{\phi}=\text{const.}}, \tag{2.13}$$

e.g., the n-point connected correlation function $\langle\varphi_{i_1}(\mathbf{x}_1)\cdots\varphi_{i_n}(\mathbf{x}_n)\rangle_c$ can be expressed in terms of vertices $\Gamma^{(i\leq n)}$. In particular, the connected propagator $G_{ij}(\mathbf{p},\phi) = \langle\varphi_i(\mathbf{p})\varphi_j(-\mathbf{p})\rangle - \langle\varphi_i(\mathbf{p})\rangle\langle\varphi_j(-\mathbf{p})\rangle$ is given by the matrix equation

$$G(\mathbf{p},\boldsymbol{\phi}) = [\Gamma^{(2)}(\mathbf{p},\boldsymbol{\phi})]^{-1}. \tag{2.14}$$

Because of translational invariance G and $\Gamma^{(2)}$ only depend on one momenta and we define e.g. $\Gamma^{(2)}(\mathbf{p},\boldsymbol{\phi})$ by $\Gamma^{(2)}_{ij}(\mathbf{p},\mathbf{p}',\boldsymbol{\phi}) = \delta_{\mathbf{p}+\mathbf{p}',0}\Gamma^{(2)}_{ij}(\mathbf{p},\boldsymbol{\phi})$.[2]

Within Landau theory, at the mean-field level, the partition function is approximated by its saddle point value, and it is easy to see that the effective action is equal to the microscopic action,

$$\Gamma^{\text{MF}}[\boldsymbol{\phi}] = S[\boldsymbol{\phi}]. \tag{2.15}$$

The convexity of Γ is broken down by the mean field approximation. In the Gaussian approximation, the action is expanded up to quadratic order around the saddle point value of the field and the effective action is equal to

$$\Gamma^{1\text{ loop}}[\boldsymbol{\phi}] = S[\boldsymbol{\phi}] + \frac{1}{2}\operatorname{Tr}\ln S^{(2)}[\boldsymbol{\phi}], \tag{2.16}$$

where $S^{(2)}$ is the second order functional derivative of S and the trace runs over both space and internal $\mathrm{O}(N)$ variables.

For $N \geq 2$, The $\mathrm{O}(N)$ symmetry allows to decompose $\Gamma^{(2)}$ on two independent tensors,

$$\Gamma^{(2)}_{ij}(\mathbf{p},\boldsymbol{\phi}) = \delta_{ij}\Gamma_A(\mathbf{p},\rho) + \phi_i\phi_j\Gamma_B(\mathbf{p},\rho), \tag{2.17}$$

where Γ_A and Γ_B depend on ρ and not on the direction of $\boldsymbol{\phi}$. This yields in turn the longitudinal (L) and transverse (T) components of the propagator,

$$G_{ij}(\mathbf{p},\boldsymbol{\phi}) = \delta_{ij}G_{\mathrm{T}}(\mathbf{p},\rho) + \frac{\phi_i\phi_j}{2\rho}(G_{\mathrm{L}}(\mathbf{p},\rho) - G_{\mathrm{T}}(\mathbf{p},\rho)), \tag{2.18}$$

$$G_{\mathrm{T}}(\mathbf{p},\rho) = [\Gamma_A(\mathbf{p},\rho)]^{-1}, \quad G_{\mathrm{L}}(\mathbf{p},\rho) = [\Gamma_A(\mathbf{p},\rho) + 2\rho\Gamma_B(\mathbf{p},\rho)]^{-1}. \tag{2.19}$$

In the symmetric phase at $\mathbf{J} = 0$ both components are equal (we denote them G or $G_{\mathrm{L,T}}$) whereas in the broken symmetry phase the longitudinal and transverse components respectively correspond to fluctuations along the direction of the order parameter and in orthogonal directions. We recall that for $N = 1$ $\Gamma^{(2)}$ has no matrix structure and there is only one component to the propagator.

2.2 Scale-dependent effective action

Having introduced the effective action of the theory, we can now detail the NPRG procedure. We seek for a way to implement a Wilson-like RG on the effective action in momentum space.

[2] We adopt the standard condensed matter notations for Fourier transforms. Defining $\int_{\mathbf{x}} \equiv \int \mathrm{d}^D\mathbf{x}$ in real space and $\int_{\mathbf{p}} \equiv (2\pi)^{-D}\int \mathrm{d}^D\mathbf{p}$ in reciprocal space, the Fourier transform of a function $f(\mathbf{x})$ is $f(\mathbf{p}) = \int_{\mathbf{x}} \exp(-\mathrm{i}\mathbf{p}\cdot\mathbf{x})f(\mathbf{x})$ and conversely $f(\mathbf{x}) = \int_{\mathbf{p}} \exp(\mathrm{i}\mathbf{p}\cdot\mathbf{x})f(\mathbf{p})$. If the volume V is finite the integrals over momenta reduce to sums and $\int_{\mathbf{p}} \equiv V^{-1}\sum_{\mathbf{p}}$.

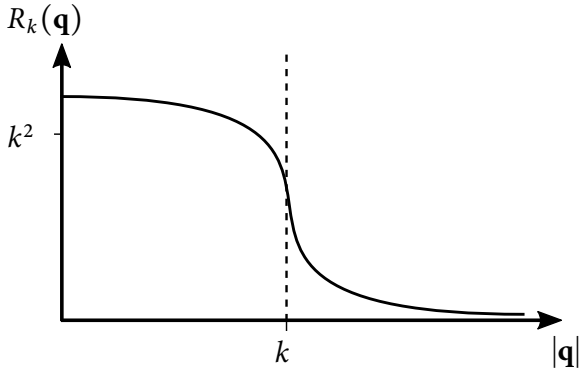

FIGURE 2.2: Sketch of the shape of the regulator in momentum space. At small momenta with respect to k it is large (of order of k^2) whereas it decays fast at larger momenta.

Consider an arbitrary momentum scale k between 0 and Λ. We want to construct an effective action Γ_k that incorporates fluctuations only at momentum scales larger that k. This is done by adding to the action a regulator term,

$$S[\boldsymbol{\phi}] \to S_k[\boldsymbol{\phi}] = S[\boldsymbol{\phi}] + \Delta S_k[\boldsymbol{\phi}], \qquad \Delta S_k[\boldsymbol{\phi}] = \frac{1}{2}\int_{\mathbf{q}} \boldsymbol{\phi}(-\mathbf{q}) \cdot R_k(\mathbf{q})\boldsymbol{\phi}(\mathbf{q}). \tag{2.20}$$

Here, the regulator R_k is an arbitrary function verifying

$$R_k(\mathbf{q}) = \begin{cases} k^2 & \text{for } |\mathbf{q}| \ll k, \\ o(1) & \text{for } |\mathbf{q}| \gg k. \end{cases} \tag{2.21}$$

R_k vanishes for $k = 0$. Physically, the regulator is akin to a momentum dependent term in front of the operator $\boldsymbol{\phi}^2$. At small momenta, the regulator is very large, and imposes an important energetic cost: fluctuations for momenta smaller than k are in effect frozen. Conversely, the regulator vanishes for fast modes and they contribute fully to the functional integral. By gradually lowering the scale k, modes are progressively taken into account. A sketch of such a regulator is given in Fig. 2.2. Examples of suitable regulators are the Θ-regulator

$$R_k(\mathbf{q}) \propto \alpha k^2(1 - \mathbf{q}^2/k^2)\Theta(1 - \mathbf{q}^2/k^2) \tag{2.22}$$

and the exponential regulator

$$R_k(\mathbf{q}) \propto \alpha k^2 \frac{\mathbf{q}^2/k^2}{\exp(\mathbf{q}^2/k^2) - 1}, \tag{2.23}$$

with α a constant numerical prefactor of order one. We use the proportionality symbol as we allow for an additional k-dependent constant in front of the propagator, see Section 2.3.2.

Quantitatively, one defines k-dependent partition function and effective action as

$$\mathcal{Z}_k[\mathbf{J}] = \int \mathcal{D}[\boldsymbol{\varphi}] \exp\left(-S[\boldsymbol{\varphi}] + \int_{\mathbf{x}} \mathbf{J} \cdot \boldsymbol{\varphi} - \Delta S_k[\boldsymbol{\varphi}]\right), \tag{2.24}$$

$$\Gamma_k[\boldsymbol{\phi}] = -\ln \mathcal{Z}_k[\mathbf{J}] + \int_{\mathbf{x}} \mathbf{J}[\boldsymbol{\phi}] \cdot \boldsymbol{\phi} - \Delta S_k[\boldsymbol{\phi}]. \tag{2.25}$$

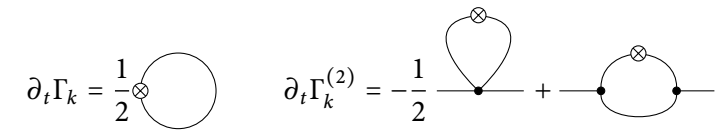

(a) Wetterich equation. (b) Flow of $\Gamma_k^{(2)}$.

Figure 2.3: Diagrammatic representation of the flow equations. The full lines stand for the full propagator $G_k = (\Gamma_k^{(2)} + R_k)^{-1}$ at scale k, dots with n legs for the vertex $\Gamma^{(n)}$, and crossed circles for $\partial_t R_k$. The signs and symmetry factors are determined the following way: for each functional derivative one has to enumerate all possible ways to add an external leg to the diagrams, either by acting on a propagator (which yields a minus sign) or on a vertex.

The k-dependent effective action $\Gamma_k[\phi]$ is the *modified* Legendre transform of the free energy: note the additional $\Delta S_k[\phi]$ term, present to ensure a good limit when $\Delta S_k \to \infty$ (see below).

Obviously for $k = 0$ the regulator vanishes and the original effective action is recovered. For $k = \Lambda$, in the limit of an infinite regulator $\Delta S_\Lambda = \infty$, all fluctuations are frozen by the regulator and only configurations of the field that minimize the action contribute: Landau theory is exact. Thus

$$\Gamma_{k=0}[\phi] = \Gamma[\phi], \qquad \Gamma_{k=\Lambda}[\phi] = S[\phi]. \tag{2.26}$$

Note that in practice ΔS_Λ is always large but finite. It remains correct to approximate the initial condition $\Gamma_{k=\Lambda}$ by S as long as one is only interested in the universal quantities, which depend solely on the universality class of the problem and not on the underlying microscopic theory. For nonuniversal quantities (e.g. the critical temperature), greater care should be taken in determining the initial condition.

To interpolate between the $k = \Lambda$ and $k = 0$ limits, one derives the flow equation, often dubbed the "Wetterich equation" [28],

$$\partial_t \Gamma_k[\phi] = \frac{1}{2} \operatorname{Tr}[\partial_t R_k (\Gamma_k^{(2)}[\phi] + R_k)^{-1}], \tag{2.27}$$

represented diagrammatically in Fig. 2.3 (left). In the above equation, $t = \ln(k/\Lambda)$ is the (negative) RG "time", and $\partial_t = k\partial_k$. Defining the operator $\tilde{\partial}_t = (\partial_t R_k)\partial_{R_k}$, which corresponds to a time derivative that only acts on the time dependence of R_k, the equation is recast as

$$\partial_t \Gamma_k[\phi] = \frac{1}{2} \tilde{\partial}_t \operatorname{Tr} \ln(\Gamma_k^{(2)}[\phi] + R_k), \tag{2.28}$$

a form which is more convenient for many calculations.

This functional nonlinear integro-differential partial derivative equation connects the mean-field solution to the complete effective action. It is exact; the only underlying assumption is that the functional integral and the $k \to 0$ limit commute. It is also impossible to solve in general, but it is a good starting point either to reproduce perturbation theory (see below) or to devise fundamentally nonperturbative approximations.

Let us remark that the flow is regularized by R_k both in the infrared and in the ultraviolet. Because of ΔS_k, at finite k infrared modes always have a "mass" and the propagators do not develop poles,

even at criticality or in the presence of Goldstone modes, while the $\partial_t R_k$ in the trace decays fast enough at large momentum to ensure convergence in the ultraviolet.

Note that the flow has a one-loop structure: if one sets the right hand side of (2.27) to its mean-field value $\mathrm{Tr}[\partial_k R_k (S^{(2)}[\phi] + R_k)^{-1}] = \partial_k \mathrm{Tr} \ln(S^{(2)}[\phi] + R_k)$ one recovers

$$\Gamma^{1\text{ loop}}[\phi] = S[\phi] + \frac{1}{2}\mathrm{Tr} \ln S^{(2)}[\phi]. \tag{2.29}$$

This means that sensible approximation schemes will always reproduce one-loop results in the weak coupling limit.

2.3 Approximation schemes

Before detailing approximation schemes, let us make some very general remarks. The main difficulty in solving the flow equation is that Γ is a functional. However, often, the knowledge of the effective potential and low order vertices is sufficient to describe the system. By taking the functional derivative of the flow of Γ_k, it is possible to derive the flow of the k-dependent effective potential U_k and the vertices $\Gamma_k^{(n)}$ in an uniform field configuration $\phi(\mathbf{x}) = \phi$, which are easier to deal with as they are mere functions of ϕ. For instance,

$$\partial_t U(\rho) = \frac{1}{2}\int_{\mathbf{q}} \partial_t R_k(\mathbf{q}) G_{k,ii}(\mathbf{q},\phi), \tag{2.30}$$

$$\begin{aligned}\partial_t \Gamma^{(2)}_{k,ij}(\mathbf{p},\phi) = {} & \frac{1}{2}\int_{\mathbf{q}} [\tilde\partial_t G_{k,i_1i_2}(\mathbf{q},\phi)]\Gamma^{(4)}_{k,iji_2i_1}(\mathbf{p},-\mathbf{p},\mathbf{q},-\mathbf{q},\phi) \\ & - \int_{\mathbf{q}} [\tilde\partial_t G_{k,i_1i_2}(\mathbf{q},\phi)]\Gamma^{(3)}_{k,i_2i_3i}(\mathbf{q},-\mathbf{p}-\mathbf{q},\mathbf{p},\phi) \\ & \times G_{k,i_3i_4}(\mathbf{p}+\mathbf{q},\phi)\Gamma^{(3)}_{k,i_4i_1j}(\mathbf{p}+\mathbf{q},-\mathbf{q},-\mathbf{p},\phi).\end{aligned} \tag{2.31}$$

Here $G_k = (\Gamma^{(2)} + R_k)^{-1}$ is the full propagator and $\tilde\partial_t G_{k,ij}(\mathbf{q},\phi) = -\partial_t R_k(\mathbf{q}) G_{k,il}(\mathbf{q},\phi) G_{k,lj}(\mathbf{q},\phi)$. These equations are represented in Fig. 2.3. It is easy to see that the flow of the n-th vertex involve $\Gamma^{(n+1)}$ and $\Gamma^{(n+2)}$: we have replaced the functional PDE (2.27) by an infinite hierarchy of regular PDEs. A class of NPRG approximation schemes rely on truncating in some way this hierarchy by approximating the higher-order vertices to obtain a finite number of coupled PDEs for the lower-order vertices. The Blaizot–Méndez-Galain–Wschebor (BMW) approximation and variants are based on this idea, see Section 2.3.4.

In a second class of approximations, an *Ansatz* is given for the k-dependent effective action. We thus project the exact flow equation on a smaller subspace of functionals which we can handle. Examples of this kind of approximations include the derivative expansion (DE) and its simplifications, and the local potential approximation″ (LPA″), detailed respectively in Sections 2.3.1 and 2.3.3.

An important point when considering approximations is that the regulator term preserves the $\mathrm{O}(N)$ symmetry. It is crucial to devise approximations respecting this symmetry; in that case, expressions (2.17) and (2.18) are still valid (note that the propagator includes R_k),

$$\Gamma^{(2)}_{k,ij}(\mathbf{p},\phi) = \delta_{ij}\Gamma_{k,A}(\mathbf{p},\rho) + \phi_i\phi_j\Gamma_{k,B}(\mathbf{p},\rho), \tag{2.32}$$

$$G_{k,ij}(\mathbf{p},\phi) = \delta_{ij}G_{k,\mathrm{T}}(\mathbf{p},\rho) + \frac{\phi_i\phi_j}{2\rho}(G_{k,\mathrm{L}}(\mathbf{p},\rho) - G_{k,\mathrm{T}}(\mathbf{p},\rho)), \tag{2.33}$$

$$G_{k,\mathrm{T}}(\mathbf{p},\rho) = [\Gamma_{k,A}(\mathbf{p},\rho) + R_k(\mathbf{p})]^{-1}, \quad G_{k,\mathrm{L}}(\mathbf{p},\rho) = [\Gamma_{k,A}(\mathbf{p},\rho) + 2\rho\Gamma_{k,B}(\mathbf{p},\rho) + R_k(\mathbf{p})]^{-1}. \tag{2.34}$$

For more complicated models it may be harder to find a regulator that preserves the symmetry group.

Lastly, note that although the final result $\Gamma_{k=0}$ does not depend on the chosen regulator, as soon as an approximation is made, it induces a (usually small) dependence of the results on the shape of the regulator. To give quantitative results we minimize this dependency by applying the principle of minimal sensitivity, that is, we seek for a local extremum of a given physical quantity taken as a function of the regulator. In practice, when computing a physical quantity Q with, for instance, the exponential regulator (2.23), we seek for an optimal value of α such that $\partial_\alpha Q(\alpha) = 0$.

We shall now explain these approximations by order of conceptual difficulty. We start with the DE in Section 2.3.1, and explain how to study critical physics in Section 2.3.2. We then describe in Section 2.3.3 the conceptually similar LPA″, before finishing with the BMW approximation, in Section 2.3.4.

2.3.1 Derivative expansion

In the DE, we propose an *Ansatz* for the k-dependent effective action. We impose the conditions that it is local (as allowed by the presence of a regulator at finite k) and respects the $\mathrm{O}(N)$ symmetry. On top of this, we perform a gradient expansion of Γ_k, that is, we only include terms with up to a certain number of derivatives. One may wonder whether this is well justified. Indeed at criticality (the regime we wish to explore) we expect the effective action to be singular. However the presence of the cutoff R_k regulates the theory in the infrared, hence validating the expansion. This also means that, at finite k, the expansion is only valid for momenta $p \lesssim k$. Setting k to 0, the DE is, through this argument, strictly speaking only valid at zero momenta. In many cases it is possible to extract finite-momentum information; for instance, should there be an energy scale in the problem that plays the role of an infrared cutoff (e.g. an energy gap), the DE would be valid at smaller finite momenta scales. In the absence of a gap, the external momentum $\mathbf{p}$ often acts as an infrared cutoff and the physical result can in practice be obtained by stopping the DE flow at a scale $k \sim |\mathbf{p}|$.

For instance the most general form of the action at order $O(\partial^2)$ is

$$\Gamma_k[\boldsymbol{\phi}] = \int_{\mathbf{x}} \frac{1}{2} Z_k(\rho)(\partial_\mu \boldsymbol{\phi})^2 + \frac{1}{4} Y_k(\rho)(\boldsymbol{\phi}\cdot\partial_\mu\boldsymbol{\phi})^2 + U_k(\rho). \tag{2.35}$$

All vertices can be expressed in term of the three functions $U_k(\rho)$, $Z_k(\rho)$ and $Y_k(\rho)$. $U_k(\rho)$ is the effective potential. We note the derivation with respect to ρ with primes and define $W_k(\rho) = U_k'(\rho)$. $Z_k(\rho)$ and $Y_k(\rho)$ renormalize the kinetic part of the action; at order two of the DE, the components of the propagator at scale k read

$$G_{k,\mathrm{T}}(\mathbf{p},\rho) = [Z_k(\rho)\mathbf{p}^2 + W_k(\rho) + R_k(\mathbf{p})]^{-1}, \tag{2.36}$$

$$G_{k,\mathrm{L}}(\mathbf{p},\rho) = [(Z_k(\rho) + \rho Y_k(\rho))\mathbf{p}^2 + W_k(\rho) + 2\rho W_k'(\rho) + R_k(\mathbf{p})]^{-1}. \tag{2.37}$$

The fact that there are two functions $Z_k(\rho)$ and $Y_k(\rho)$ reflect that, for $N \geq 2$, transverse and longitudinal fluctuations have different stiffness. For $N = 1$, $(\phi\partial_\mu\phi)^2 = 2\rho(\partial_\mu\phi)^2$ and the $Y_k(\rho)$ part of the *Ansatz* can be included in the $Z_k(\rho)$ term.

The flow of $U_k(\rho)$ (or $W_k(\rho)$) is deduced from Eq. (2.30) and reads

$$\partial_t U_k(\rho) = \frac{1}{2}\int_{\mathbf{q}} \partial_t R_k(\mathbf{q})[G_{k,\mathrm{L}}(\mathbf{q},\rho) + (N-1)G_{k,\mathrm{T}}(\mathbf{q},\rho)]. \tag{2.38}$$

For $Z_k(\rho)$ and $Y_k(\rho)$, we use Eq. (2.31). The flow generates contributions at all powers in $\mathbf{p}$ to $\Gamma_k^{(2)}$ one has to project the flow onto the *Ansatz*, using

$$Z_k(\rho) = \partial_{\mathbf{p}^2}\Gamma_{k,A}(\mathbf{p},\rho)|_{\mathbf{p}=0}, \qquad Y_k(\rho) = \partial_{\mathbf{p}^2} 2\Gamma_{k,B}(\mathbf{p},\rho)|_{\mathbf{p}=0}. \tag{2.39}$$

The flow equations for $Z_k(\rho)$ and $Y_k(\rho)$ are given for instance in [18, 32].

Upon integration of the flows, one obtains the effective potential $U(\rho) = U_{k=0}(\rho)$. The position of its minimum, $\rho_0 = \lim_{k\to 0}\rho_{0,k}$, indicates the phase. If $\rho_0 = 0$ the system is disordered with an inverse correlation length $\xi^{-1} = \sqrt{W_{k=0}(0)/Z_{k=0}(0)}$. Conversely, for $\rho_0 > 0$, the system is ordered with a spontaneous magnetization $\sqrt{2\rho_0}$.

What we presented above is the "full potential" DE, so called because no assumption is made on $U_k(\rho)$ $Z_k(\rho)$ and $Y_k(\rho)$. If we further approximate $Y_k(\rho) = 0$ and $Z_k(\rho) = 1$, we obtain the local potential approximation (LPA). Allowing $Z_k(\rho)$ to be a number nets the LPA′. Also, it is possible to truncate the DE by expanding the functions around the minimum $\rho_{0,k}$, to keep track only of a small set of coupling constants.

2.3.2 Critical physics and dimensionless equations

In this Section we explain how to study the critical physics of the model within DE. Most of the remarks here will be relevant to other approximation schemes.

Second order phase transitions are characterized by scale invariance which translates into a fixed point of the corresponding RG equations. However, even at criticality, the above flow equations do not admit fixed point solutions for the functions $U_k(\rho)$, $Z_k(\rho)$ and $Y_k(\rho)$. The reason for this is that the regulator introduces itself a new momentum scale k and explicitly breaks down scale invariance. We thus rewrite the flow equations by introducing dimensionless variables and functions,

$$\tilde{q} = |\mathbf{q}|/k, \quad \tilde{\rho} = Z_k k^{2-D}\rho, \tag{2.40}$$

$$\tilde{U}_k(\tilde{\rho}) = k^{-D}U_k(\rho), \quad \tilde{Z}_k(\tilde{\rho}) = Z_k^{-1}Z_k(\rho), \quad \tilde{Y}_k(\tilde{\rho}) = Z_k^{-2}k^{D-2}Y_k(\rho). \tag{2.41}$$

In the above expressions Z_k is a number, not to be confused with the function $Z_k(\rho)$. Aside from Z_k the dimensional factors come from trivial dimensional analysis. To understand the origin of Z_k, recall that at the critical point and small $\mathbf{p}$, $G(\mathbf{p}) \sim |\mathbf{p}|^{-2+\eta}$, with η the anomalous dimension. However, in the presence of the regulator, the theory is always infrared-regular and in the critical regime one expects the propagator to scale like

$$G_k(\mathbf{p})^{-1} \sim \begin{cases} k^{-\eta}\mathbf{p}^2 + Ck^2 & \text{for } |\mathbf{p}| \ll k, \\ |\mathbf{p}|^{2-\eta} & \text{for } |\mathbf{p}| \gg k, \end{cases} \tag{2.42}$$

with C some constant (recall that at finite k due to the presence of the regulator the theory is massive). Because of this, the field renormalization term $Z_k(\rho)$ (determined by the $|\mathbf{p}| \ll k$ behavior of $\Gamma_k^{(2)}$)

scales like $k^{-\eta}$ and has no fixed point.[3] We thus extract this dependency into $Z_k \sim k^{-\eta}$, which we define by imposing

$$\tilde{Z}_k(\tilde{\rho}_{\mathrm{RG}}) = 1 \tag{2.43}$$

for a certain arbitrary renormalization point $\tilde{\rho}_{\mathrm{RG}}$, which may depend on k (in practice, one uses either $\tilde{\rho}_{0,k}$ or $\tilde{\rho} = 0$). We define the running anomalous dimension by

$$\partial_t \ln Z_k = -\eta_k. \tag{2.44}$$

Since the inverse propagators scale like $Z_k k^2$, it is convenient to define the regulator by

$$R_k(\mathbf{q}) = Z_k k^2 r(\mathbf{q}^2/k^2), \tag{2.45}$$

with $r(y)$ some dimensionless function (e.g. $r(y) = \alpha y/(\exp(y) - 1)$ for an exponential regulator).

The dimensionless flow equation for the potential read

$$\partial_t \tilde{U}_k(\tilde{\rho}) = -D\tilde{U}_k(\tilde{\rho}) + (D - 2 + \eta_k)\tilde{\rho}\tilde{U}'_k(\tilde{\rho}) + k^{-D}\partial_t U_k(\rho)|_{\tilde{\rho}}. \tag{2.46}$$

The first two terms come from the dimension of $U_k(\rho)$ and ρ respectively, while the last one is the flow of $U_k(\rho)$ in dimensionful variables. Similar equations can be obtained for the other functions. At criticality, the flow equations admit fixed points when expressed in dimensionless variables. Note that, from a numerical point of view, it is also most of the time more convenient to handle dimensionless equations, as their solutions remain nonsingular functions of order one as k goes to 0.

It is possible to extract the critical exponents from these dimensionless flow equations. At the critical point in the critical regime (small k), η_k reaches a plateau equal to η (within LPA, there is no renormalization of the field and $\eta = 0$ by construction). To determine ν, we remark that it is the exponent that controls the speed at which the flow exits the critical regime. Because of this, it is possible to show that, for a flow close to criticality, for $\xi^{-1} \ll k \ll p_{\mathrm{G}}$ (ξ^{-1} being the actual inverse correlation length and p_{G} the Ginzburg scale signaling the onset of the critical regime, see also Chapter 3, Eq. (3.4)), $\tilde{\rho}_{0,k}$ behaves like

$$\tilde{\rho}_{0,k} = \tilde{\rho}_{0,\mathrm{c}} + Ck^{-1/\nu} + \cdots, \tag{2.47}$$

with $\tilde{\rho}_{0,\mathrm{c}}$ the fixed point value and C some constant [21]. The same form is true for other quantities, e.g. $\tilde{W}(0)$. We extract ν from this relation.

Values obtained for the critical exponents for the DE and other approximation methods are listed in Tables 2.1 and 2.2.

2.3.3 LPA″

As explained in Section 2.3.1, the DE in general fails to describe finite momentum physics. For example, even at criticality, only the small momenta behavior of the propagator in presence of the regulator $G_k^{-1}(\mathbf{p}) \sim \mathbf{p}^2 + Ck^2$ is obtained and the anomalous dimension has to be extracted from

[3] Note that within DE only the regime $|\mathbf{p}| \ll k$ is captured and the propagator scales like $G_k^{-1}(\mathbf{p}) = Z_k\mathbf{p}^2 + Ck^2 \sim k^{-\eta}\mathbf{p}^2 + C'k^2$. As we wrote in the previous Section an heuristic way to determine a quantity at a finite momentum $\mathbf{p}$ is to stop the flow at a scale $k \sim |\mathbf{p}|$; in this case as the mass term is negligible as k goes to zero doing so one recovers the critical scaling $G^{-1}_{k\sim|\mathbf{p}|}(\mathbf{p}) \sim |\mathbf{p}|^{2-\eta}$.

N	DE	LPA″	BMW	MC		FT		CB [33]
1	0.638	0.631	0.632	0.63002(10)	[34]	0.6306(5)	[35]	0.629971(4)
2	0.668	0.679	0.673	0.6717(1)	[36]	0.6700(6)	[35]	0.67191(12)
3	0.706	0.725	0.714	0.7112(5)	[37]	0.7060(7)	[35]	0.7121(28)
4	0.741	0.765	0.754	0.749(2)	[38]	0.741(6)	[39]	
5	0.774	0.799	0.787			0.766	[40]	
6	0.803	0.836	0.816			0.790	[40]	
8	0.848	0.866	0.860			0.830	[40]	
10	0.879	0.892	0.893			0.859	[40]	
100	0.989	0.990	0.990			0.989	[41]	
1000	0.999	0.999	0.999			0.999	[41]	

TABLE 2.1: Critical exponent ν for the three dimensional classical $\mathrm{O}(N)$ universality class obtained in the NPRG approach, from the full potential DE at order $O(\partial^2)$, LPA″ and BMW approximation (results from the author, obtained with the exponential regulator with $\alpha = 2.25$), compared to Monte Carlo (MC) simulations, (perturbative) field theories (FT) and conformal bootstrap (CB). The exponent has been determined before within NPRG for most values of N, see e.g. [42] for the DE, [43] for the LPA″ and [44, 45] for the BMW approximation. For coherence we provide our own results, which are in agreement with the above references.

N	DE	LPA″	BMW	MC		FT		CB [33]
1	0.0443	0.0506	0.0411	0.03627(10)	[34]	0.0318(3)	[35]	0.036298(2)
2	0.0467	0.0491	0.0423	0.0381(2)	[36]	0.0334(2)	[35]	0.03852(64)
3	0.0463	0.0459	0.0411	0.0375(5)	[37]	0.0333(3)	[35]	0.0385(11)
4	0.0443	0.0420	0.0386	0.0365(10)	[38]	0.0350(45)	[39]	
5	0.0413	0.0382	0.0354			0.034	[40]	
6	0.0381	0.0346	0.0321			0.031	[40]	
8	0.0319	0.0287	0.0264			0.027	[40]	
10	0.0270	0.0243	0.0220			0.024	[40]	
100	0.00296	0.00289	0.00233			0.0027	[41]	
1000	0.000296	0.000293	0.000233			0.00027	[41]	

TABLE 2.2: Same as Table 2.1 but for the anomalous dimension η.

the scaling behavior of Z_k. A solution is given by the LPA″ approximation, proposed earlier by Hasselmann and collaborators [46, 47], who used it to determine the critical exponents of the O(N) model [43], see Tables 2.1 and 2.2. The LPA″ grants access to finite-momentum physics by offering a momentum-dependent *Ansatz* for the effective action, close to that of LPA′, which reads

$$\Gamma_k^{\mathrm{LPA}'}[\boldsymbol{\phi}] = \int_{\mathbf{x}} \frac{1}{2} Z_k (\partial_\mu \boldsymbol{\phi})^2 + \frac{1}{4} Y_k (\boldsymbol{\phi} \cdot \partial_\mu \boldsymbol{\phi})^2 + U_k(\rho) \tag{2.48}$$

with $U_k(\rho)$ a function and Z_k, Y_k mere numbers (note that in standard LPA′ Y_k is dropped; we retain it here). Consider the first term, which we rewrite

$$\int_{\mathbf{x}} \frac{1}{2} \boldsymbol{\phi} \cdot [-Z_k \partial_\mu^2] \boldsymbol{\phi}. \tag{2.49}$$

We can promote the number Z_k to some function of $-\boldsymbol{\partial}^2 \equiv -\partial_\mu^2$, using a formal series expansion:

$$\int_{\mathbf{x}} \frac{1}{2} \boldsymbol{\phi} \cdot [-Z_k(-\boldsymbol{\partial}^2)\boldsymbol{\partial}^2] \boldsymbol{\phi}, \qquad Z_k(x) = \sum_{n \geq 0} z_{k,n} x^n. \tag{2.50}$$

Applying the same procedure for Y_k, one obtains the LPA″ *Ansatz*

$$\Gamma_k^{\mathrm{LPA}''}[\boldsymbol{\phi}] = \int_{\mathbf{x}} \frac{1}{2} \partial_\mu \boldsymbol{\phi} \cdot Z_k(-\boldsymbol{\partial}^2) \partial_\mu \boldsymbol{\phi} + \frac{1}{4} \partial_\mu \rho \cdot Y_k(-\boldsymbol{\partial}^2) \partial_\mu \rho + U_k(\rho). \tag{2.51}$$

The *Ansatz* is defined by $U_k(\rho)$, a function of the field, and $Z_k(\mathbf{p}^2)$ and $Y_k(\mathbf{p}^2)$, functions of the modulus square of the momentum (in the following we note for simplicity $Z_k(\mathbf{p})$, $Y_k(\mathbf{p})$). Similarly to what is done within DE, their flow is obtained by evaluating $\Gamma_k^{(2)}$ at $\rho_{0,k}$,

$$Z_k(\mathbf{p}) = \frac{\Gamma_{k,A}(\mathbf{p}, \rho_{0,k}) - \Gamma_{k,A}(\mathbf{p} = 0, \rho_{0,k})}{\mathbf{p}^2}, \tag{2.52}$$

$$Y_k(\mathbf{p}) = 2 \frac{\Gamma_{k,B}(\mathbf{p}, \rho_{0,k}) - \Gamma_{k,B}(\mathbf{p} = 0, \rho_{0,k})}{\mathbf{p}^2}. \tag{2.53}$$

This *Ansatz* includes arbitrary high-order derivatives of the field and thus allows for finite momentum description of the physics. For instance, the propagator components read

$$G_{k,\mathrm{T}}(\mathbf{p}, \rho) = [Z_k(\mathbf{p})\mathbf{p}^2 + W_k(\rho) + R_k(\mathbf{p})]^{-1}, \tag{2.54}$$

$$G_{k,\mathrm{L}}(\mathbf{p}, \rho) = [(Z_k(\mathbf{p}) + \rho Y_k(\mathbf{p}))\mathbf{p}^2 + W_k(\rho) + 2\rho W_k'(\rho) + R_k(\mathbf{p})]^{-1}, \tag{2.55}$$

and at the critical point, for small momenta $\mathbf{p}$,

$$Z_{k=0}(\mathbf{p}) \propto |\mathbf{p}|^{-\eta}, \qquad G_{k=0,\mathrm{T}}(\mathbf{p}, \rho_0) \propto |\mathbf{p}|^{-2+\eta}. \tag{2.56}$$

The LPA″ is a hybrid between field truncation methods [28, 30] and DE. Indeed, the full field dependence of the potential is kept, while the other functions do not depend on the field, but are arbitrary functions of the momentum. The LPA″ is qualitatively different from the DE, as no ρ dependence of $Z_k(\mathbf{p})$ and $Y_k(\mathbf{p})$ is allowed. The main advantage of LPA″ over DE is that it grants access to finite momentum physics.

Just like one can add higher order gradient terms to the DE, a systematic expansion of LPA″ is possible by adding independent terms with higher powers of the field, for instance adding

$$\int_{\mathbf{x}} \frac{1}{2}\left(\frac{\boldsymbol{\phi}^2}{2}\right)^n \partial_\mu \boldsymbol{\phi} \cdot Z_{k,n}(-\boldsymbol{\partial}^2)\partial_\mu \boldsymbol{\phi} \tag{2.57}$$

yields a contribution

$$\rho^n \mathbf{p}^2 Z_{k,n}(\mathbf{p}) \tag{2.58}$$

to both inverse propagators.

2.3.4 The Blaizot–Méndez-Galain–Wschebor approximation

Here, we consider another approximation scheme, the Blaizot–Méndez-Galain–Wschebor (BMW) approximation [44, 45, 48] which does not rely on an *Ansatz* for the effective action. Rather, we obtain closed flow equations for the effective potential and $\Gamma^{(2)}$. Let us start from the exact equations (2.30) and (2.31). To close them, we need to find an approximate form for $\Gamma_k^{(3)}(\mathbf{p}+\mathbf{q}, -\mathbf{p}, -\mathbf{q}, \boldsymbol{\phi})$ and $\Gamma_k^{(4)}(\mathbf{p}, -\mathbf{p}, \mathbf{q}, -\mathbf{q}, \boldsymbol{\phi})$ (up to a permutation of momenta; we also drop temporarily the $\mathrm{O}(N)$ indices which are not relevant to the argument).

There are two ingredients in the BMW approximation. The first one is to notice that in the flow equations the regulator $\partial_t R_k(\mathbf{q})$ plays the role of a ultraviolet regulator. Because of this, the main contribution to the flow comes from momenta $|\mathbf{q}| \lesssim k$; it is thus a reasonable approximation to set $\mathbf{q}$ to 0 in the two above vertices (the propagators remain unchanged):

$$\Gamma_k^{(3)}(\mathbf{p}+\mathbf{q}, -\mathbf{p}, -\mathbf{q}, \boldsymbol{\phi}) \to \Gamma_k^{(3)}(\mathbf{p}, 0, -\mathbf{p}, \boldsymbol{\phi}), \quad \Gamma_k^{(4)}(\mathbf{p}, -\mathbf{p}, \mathbf{q}, -\mathbf{q}, \boldsymbol{\phi}) \to \Gamma_k^{(4)}(\mathbf{p}, -\mathbf{p}, 0, 0, \boldsymbol{\phi}). \tag{2.59}$$

The second ingredient is the *exact* identity [48, 49]

$$\Gamma^{(n+1)}_{k,i_1\dots i_n i_{n+1}}(\mathbf{p}_1, \dots, \mathbf{p}_n, 0, \boldsymbol{\phi}) = \frac{\partial \Gamma^{(n)}_{k,i_1\dots i_n}(\mathbf{p}_1, \dots, \mathbf{p}_n, \boldsymbol{\phi})}{\partial \phi_{i_{n+1}}}, \tag{2.60}$$

which can be intuited by remarking that the derivative of $\Gamma_k^{(n)}(\boldsymbol{\phi})$ with respect to the field $\boldsymbol{\phi}$ is akin to the functional derivative of $\Gamma_k^{(n)}[\boldsymbol{\phi}]$ with respect to a constant field $\boldsymbol{\phi}(\mathbf{p}=0)$, which defines $\Gamma_k^{(n+1)}$ (see Eq. (2.12)).[4]

Thus, within BMW, the closed flow equations read (we restore the $\mathrm{O}(N)$ indices)

$$\begin{aligned} \partial_t U(\rho) &= \frac{1}{2}\int_{\mathbf{q}} \partial_t R_k(\mathbf{q}) G_{k,ii}(\mathbf{q}, \boldsymbol{\phi}), \\ \partial_t \Gamma^{(2)}_{k,ij}(\mathbf{p}, \boldsymbol{\phi}) &= \frac{1}{2}\int_{\mathbf{q}} [\tilde{\partial}_t G_{k,i_1 i_2}(\mathbf{q}, \boldsymbol{\phi})] \partial_{\phi_{i_1}\phi_{i_2}} \Gamma^{(2)}_{k,ij}(\mathbf{p}, \boldsymbol{\phi}) \end{aligned} \tag{2.62}$$

[4] A rigorous proof is given by expanding the effective action around any constant field configuration $\bar{\boldsymbol{\phi}}$,

$$\Gamma_k[\boldsymbol{\phi}] = \sum_n \sum_{i_1\dots i_n} \frac{1}{n!}\int_{\mathbf{x}_i} \mathrm{d}\mathbf{x}_1 \cdots \mathrm{d}\mathbf{x}_n [\phi_{i_1}(\mathbf{x}_1) - \bar{\phi}_{i_1}] \cdots [\phi_{i_n}(\mathbf{x}_n) - \bar{\phi}_{i_n}] \Gamma^{(n)}_{k,i_1\dots i_n}(\mathbf{x}_1, \dots, \mathbf{x}_n; \bar{\boldsymbol{\phi}}). \tag{2.61}$$

The left hand side does not depend on $\bar{\boldsymbol{\phi}}$; taking the derivative of the above expression with respect to $\bar{\phi}_j$ yields the identity.

$$-\int_{\mathbf{q}}[\tilde{\partial}_t G_{k,i_1 i_2}(\mathbf{q},\boldsymbol{\phi})]\partial_{\phi_{i_2}}\Gamma^{(2)}_{k,ii_3}(\mathbf{p},\boldsymbol{\phi})G_{k,i_3 i_4}(\mathbf{p}+\mathbf{q},\boldsymbol{\phi})\partial_{\phi_{i_1}}\Gamma^{(2)}_{k,i_4 j}(\mathbf{p},\boldsymbol{\phi}). \tag{2.63}$$

This is not the end of the story. From (2.60) we notice that

$$\Gamma^{(2)}_{k,ij}(\mathbf{p}=0,\boldsymbol{\phi}) = \partial_{\phi_i\phi_j}U_k(\rho) = \delta_{ij}W_k(\rho) + \phi_i\phi_j W_k'(\rho). \tag{2.64}$$

Because of this, the flow of W_k can be obtained from either (2.62) or (2.63). Since approximations have been made, these two equations do not agree. We chose to obtain the flow of W_k from the formally exact equation (2.62) rather than from (2.63), which is approximated, and isolate the zero-momentum components of $\Gamma^{(2)}_k$:

$$\Gamma_{k,A}(\mathbf{p},\rho) = \mathbf{p}^2(1+Y_{k,A}(\mathbf{p},\rho)) + W_k(\rho), \qquad \Gamma_{k,B}(\mathbf{p},\rho) = \mathbf{p}^2 Y_{k,B}(\mathbf{p},\rho) + W_k'(\rho). \tag{2.65}$$

The flow of $Y_{k,A}$ and $Y_{k,B}$ is then obtained by subtracting to (2.63) its $\mathbf{p}=0$ part.

Note that although BMW nets the effective potential and propagators with a good precision (see Tables 2.1 and 2.2 for the critical exponents) it only provides little information on high-order vertices since only $\Gamma^{(n>2)}_k(\mathbf{p},-\mathbf{p},0,\dots,0)$ is determined.

There are several ways the BMW approximation can be systematically improved. One is to further expand the vertices around $\mathbf{q}=0$, e.g.

$$\Gamma^{(3)}_k(\mathbf{p}+\mathbf{q},-\mathbf{p},-\mathbf{q},\boldsymbol{\phi}) \to \Gamma^{(3)}_k(\mathbf{p},0,-\mathbf{p},\boldsymbol{\phi}) + \mathbf{q}\cdot\partial_{\mathbf{q}}[\Gamma^{(3)}_k(\mathbf{p}+\mathbf{q},-\mathbf{p},-\mathbf{q},\boldsymbol{\phi})]|_{\mathbf{q}=0}. \tag{2.66}$$

Another idea is to approximate $\Gamma^{(n+1)}$ and $\Gamma^{(n+2)}$ for some $n>2$, to obtain closed flow equations for U_k and $\Gamma^{(i\leq n)}$ in a similar manner to (2.59). However, solving the resulting equations is a daunting numerical task as high-order vertices do depend on several independent momenta.

3

Thermodynamics

Never underestimate the pleasure we feel from hearing something we already know.

— E. Fermi, cited by S. Weinberg.

In this Chapter, we study the thermodynamics of the relativistic quantum O(N) model for all values of $N \geq 1$. We restrict ourselves to the case of two space dimensions, where the theory is strongly coupled. We discuss the phase diagram of the model, as well as its thermodynamical properties and universal scaling functions which characterize the transition. The phase diagram of the model is well known [1] and its thermodynamics have been studied before our work [50]; we provide here the best nonpertubative estimates of the universal scaling functions to date [51]. Relying on the connection between quantum and classical statistical physics, we make a connection between the thermodynamics of the quantum model and the critical Casimir forces arising in classical physics. The outline of the chapter is the following. In Section 3.1, we recall the expression of the action of the O(N) model, give the qualitative phase diagram and define the physical quantities of interest as well as the universal ratios and scaling functions defining the thermodynamics, before explaining in Section 3.2 what critical Casimir forces are and how they relate to thermodynamics. In Section 3.3 we provide the exact large-N results for the quantum thermodynamics. In Section 3.4, we determine using a nonperturbative approach the thermodynamical properties of the two-dimensional O(N) model for $N = 1, 2, 3$ and compare our results to Monte Carlo simulations for classical spin models in three dimensions. Finally, in Section 3.5 we discuss the possible observation of the computed scaling functions.

Part of the work presented in this Chapter has been published [51].

3.1 Generalities

The model is defined by the action

$$S[\boldsymbol{\varphi}] = \int_{\mathbf{x}} \frac{1}{2}(\nabla\boldsymbol{\varphi})^2 + \frac{1}{2c_0^2}(\partial_\tau\boldsymbol{\varphi})^2 + \frac{r_0}{2}\boldsymbol{\varphi}^2 + \frac{u_0}{4!N}(\boldsymbol{\varphi}^2)^2, \tag{3.1}$$

where $\mathbf{x} = (\mathbf{r}, \tau)$, $\boldsymbol{\varphi}(\mathbf{x})$ is a N-component real field, $\tau \in [0, \beta]$ an imaginary time with $T = \beta^{-1}$ the temperature. In this Chapter we only consider the model in $d = 2$ space dimensions. r_0 and u_0 are temperature-independent coupling constants and c_0 the bare velocity of the field. The renormalized

velocity of the field, defined precisely below, is denoted by c. In the following, we set $c = 1$ by rescaling τ by a c factor; restoring c if needed for clarity. The model is regularized in the ultraviolet by a cutoff Λ.[1]

At zero temperature, for a critical value r_{0c} of the quadratic coupling r_0 (at fixed u_0 and c_0), the model undergoes a second order quantum phase transition between a disordered phase ($r_0 \geq r_{0c}$) and an ordered phase ($r_0 \leq r_{0c}$) where the O(N) symmetry is spontaneously broken. The quantum critical point at $r_0 = r_{0c}$ belongs to the universality class of the classical $D = 3$ O(N) model, with a dynamical exponent $z = 1$ (this value follows from the space-time isotropy of the system at $T = 0$) and the phase transition is governed by the three-dimensional Wilson–Fisher fixed point. The zero-temperature disordered phase is gapped, with a gap m_0 and a finite correlation length $\xi = 1/m_0$. The excitation spectrum of the ordered phase depends on the value of N. For $N = 1$, the broken symmetry is the discrete symmetry O(1) $\simeq Z_2$, and the ordered phase is also gapped. For $N \geq 2$, the O(N) symmetry is continuous and there are $N - 1$ gapless Goldstone modes.

The Goldstone modes correspond to fluctuations of the field in the direction orthogonal to the order parameter (transverse fluctuations). If one parameterizes the field as $\boldsymbol{\varphi} = \phi_0(\sigma, \boldsymbol{\pi})$, with σ and $\boldsymbol{\pi}$ the fluctuations in the longitudinal and transverse directions and ϕ_0 the modulus of the order parameter, the fluctuations of the field in the longitudinal direction are gapped at the mean-field level and the transverse fluctuations are described by a non-linear σ model (NLσM) with the constraint $\sigma^2 + \boldsymbol{\pi}^2 = 1$. Within the NL$\sigma$M, the Goldstone modes are effectively noninteracting at low energy, and the effective low-energy microscopic action for the transverse modes reads

$$S[\boldsymbol{\pi}] = \frac{\rho_s}{2} \int_{\mathbf{x}} (\partial_\mu \boldsymbol{\pi})^2. \tag{3.2}$$

This defines the stiffness (or rigidity, or helicity modulus) ρ_s. It is a quantity associated with the energy cost of twisting the direction of the field. In other terms, the propagator for the transverse modes, given by ϕ_0^2 times the propagator of the $\boldsymbol{\pi}$ modes, is gapless and reads for $\mathbf{p}, \omega_n \to 0$

$$G_T(\mathbf{p}, i\omega_n) = \frac{\phi_0^2}{\rho_s(\mathbf{p}^2 + \omega_n^2)}. \tag{3.3}$$

For $d = 2$, ρ_s has the dimension of an energy and defines an energy scale in the ordered phase. The corresponding length, $\xi_J = c/\rho_s$, is the Josephson length which separates the critical regime and the Goldstone regime: at scales larger than ξ_J, the physics is dominated by the (effectively noninteracting) transverse modes and governed by the action (3.2).

Another characteristic scale one can construct is the Ginzburg momentum scale [52],

$$p_G \sim c u_0, \tag{3.4}$$

which signals the onset of the critical regime. Indeed, for instance at the critical point r_{0c}, at high energy ($\mathbf{p}^2 + \omega_n^2 \gg p_G^2$) the Gaussian approximation remains qualitatively correct and the propagator scales like $G_{L,T} \sim 1/(\mathbf{p}^2 + \omega_n^2)$ while in the critical regime $\mathbf{p}^2 + \omega_n^2 \ll p_G^2$ the propagator develops an anomalous dimension, $G_{L,T} \sim (\mathbf{p}^2 + \omega_n^2)^{(-2+\eta)/2}$.

Phase diagram

At finite temperature, it is possible to distinguish several regimes in the vicinity of the QCP, by comparing the temperature T to either ρ_s or m_0 (depending on whether at $T = 0$ the system is

[1] To maintain the Lorentz invariance of the action at zero temperature, the cutoff is implemented on both frequencies and momenta in a covariant way.

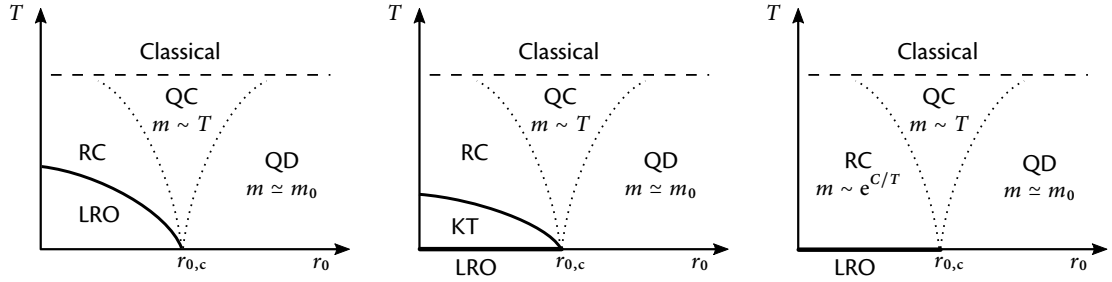

(a) Quantum Ising model. (b) Quantum XY model. (c) $N \geq 3$.

Figure 3.1: Qualitative phase diagram of the quantum $\mathrm{O}(N)$ model in two space dimensions. At zero temperature, the symmetric phase is separated from the broken symmetry phase with long range order (LRO) by a quantum phase transition at a critical value r_{0c}. Crossover lines separate the quantum disordered (QD), quantum critical (QC) and renormalized classical (RC) phases. For $N = 1$ (left), the symmetry is discrete and LRO persists at finite temperature, separated from the finite-temperature disordered phase by a transition line belonging to the two-dimensional classical Ising universality class. Similarly, for $N = 2$ (center), there is a topological Kosterlitz–Thouless (KT) phase at finite temperature, separated from the finite-temperature disordered phase by a transition line belonging to the two-dimensional classical XY universality class. For $N \geq 3$ (right) there is no finite-temperature transition.

ordered or disordered). The phase diagram, which we represent in Fig. 3.1, strongly depends on the dimension and we recall that here $d = 2$.

As long as $T \ll m_0$, temperature has little effect on the zero-temperature disordered phase: the system, disordered at $T = 0$ due to quantum fluctuations, remains so at finite temperature, with a gap $m(T) \simeq m_0$ unaffected by temperature; this is the quantum disordered (QD) regime.

Above the zero-temperature ordered phase, the situation depends on N. The system is always disordered for $N \geq 2$, in agreement with the Mermin-Wagner theorem. For $N = 1$ (respectively $N = 2$), an ordered phase (respectively a quasi-ordered BKT phase) exists at small finite temperature for $r_0 \leq r_{0c}$, separated from a higher-temperature disordered symmetric phase by a transition line terminating at $r_0 = r_{0c}$ for $T = 0$. Near this finite temperature transition, the gap vanishes for $N = 1$ as $m(T) \sim |T - T_c|^{\nu_{3D}}$, with ν_{3D} the three-dimensional Ising exponent; for $N = 2$, the BKT phase is gapless and above T_c near the transition the gap vanishes with an essential singularity $m(T) \sim \exp(-A/\sqrt{T - T_c})$, with A nonuniversal [53]. For $N \geq 3$ the system is gapped at any finite temperature and the gap vanishes when T goes to zero like $m(T) \sim \exp[-4\pi\rho_s(T = 0)/(N-2)T]$, as the physics is controlled by the Goldstone modes (in that case the system is described by a non-linear σ model [21]). In any case, in the high-temperature disordered phase above the zero-temperature ordered phase, the low-energy physics of the model is that of the classical $\mathrm{O}(N)$ model in dimension two, albeit with a renormalization of its coupling constants due to quantum fluctuations, hence the denomination of renormalized classical (RC) regime. As in the QD regime, this picture only holds for $T \ll \rho_s$ ($T \ll m_0$ for the Ising model).

Let us now investigate what happens in the regime $T \gg m_0, \rho_s$, i.e. at finite temperature above the quantum critical point. The only relevant energy scale is the temperature. This implies that in this regime, dubbed the quantum critical (QC) regime, scaling functions are defined by power laws of the temperature. In particular the excitation gap has to scale like temperature, $m(T) \sim T$.

It is possible to define crossover lines $m_0 \sim T$ and $\rho_s \sim T$ which separate the QC regime from the QD ($m_0 \gg T$) and RC regimes ($\rho_s \gg T$). As m_0 and ρ_s vanishes like $|r_0 - r_{0c}|^\nu$ at the QCP, the QC regime widens as the temperature increases, hence the name of "quantum critical fan" for the QC regime.

Energy scales and universal physics

The thermodynamics is defined by the long-wavelength physics which is entirely contained in the free energy (and thus the partition function) in the presence of an homogeneous external source. The free energy defines the equation of state; we now discuss its scaling properties in the vicinity of the quantum critical point. This regime is defined by the fact that the characteristic length scales of the system, the correlation length $\xi \sim |r_0 - r_{0c}|^{-\nu}$ and the correlation length in the time direction $\xi_\tau \sim \xi^z$ (here in our units $\xi_\tau = \xi$ as $z = 1$) are large with respect to the microscopic length scales of the model, such as Λ^{-1} or the Ginzburg length p_G^{-1}. In that regime, the scaling hypothesis [21, 54] holds. It predicts that, for any physical quantity X, since the singular behavior of X at the transition is due to the divergence of ξ and ξ_τ as well as finite-size effects at finite temperature (due to the presence of a finite time dimension $L_\tau \sim 1/T$), the singular part of X is given by a homogeneous function of ξ, ξ_τ, L_τ, and any other parameter on which X depends, such as a magnetic field or an external momenta. In turn, this homogeneous function can be recast as a function of the dimensionless ratios of its arguments with, as a prefactor, $\xi^{-[X]}$, $[X]$ being the scaling dimension of X. The scaling function is universal up to two multiplicative constants, one a prefactor of its argument and the other a prefactor of the function itself.

Take for instance the susceptibility (two-point correlation function) of the classical Ising model. Its singular part can be expressed, from the above scaling analysis, as

$$\chi(\mathbf{p}, T) = \mathcal{A}^\pm \xi^{2-\eta} \chi^\pm(\mathbf{p}\xi), \tag{3.5}$$

with ξ the correlation length and $\chi^+(x)$ and $\chi^-(x)$ two universal functions, the indices + and − respectively denoting the disordered and ordered phase. The two amplitudes $\mathcal{A}^\pm$ are not universal, and depend on the microscopic details of the system. Remark that however, their ratio $\mathcal{A}^+/\mathcal{A}^-$ is universal. An heuristic explanation is that the non-universal prefactors, being of the same nature, are both "built" the same way, incorporating the same dependence on nonuniversal quantities. These dependencies cancel when taking the ratio and the result is a universal number. To show it more rigorously one remarks that all theories belonging to the same universality class are related to each other by either a rescaling of the field or of the distance to the critical point [18, 55]. The ratio of the two correlation functions being invariant under such transformations, the ratio of the amplitudes is universal.

Let us go back to the quantum O(N) model. To L_τ and ξ correspond two energies, T and a characteristic zero-temperature scale, Δ, which vanishes at the transition. In the symmetric phase, we chose Δ to be equal to the excitation gap (inverse correlation length) $m_0(r_0 - r_{0c}) \sim (r_0 - r_{0c})^\nu$, while in the broken symmetry phase, we define it as the gap in the disordered phase at the point located symmetrically with respect to the QCP with a negative sign[2], i.e.,

$$\Delta = \mathrm{sgn}(r_0 - r_{0c}) m_0(|r_0 - r_{0c}|). \tag{3.6}$$

[2] This is a choice we make for convenience reasons. Another possible (more natural) convention for Δ would be to define it as $\Delta = \rho_s$. As ρ_s/Δ is universal both choices are equivalent.

The scaling argument proves that the excitation gap $m(T,\Delta)$ at finite temperature in the critical regime near the QCP is determined by a universal scaling function, depending only on the scaling variable $x = \Delta/k_B T$ (we restore k_B and $\hbar$),

$$m(T,\Delta) = k_B T F_N\left(\frac{\Delta}{k_B T}\right), \tag{3.7}$$

using the fact that the regular part of m vanishes at the QCP. Technically, m is defined by two scaling functions, one for each zero-temperature phase; with our convention for Δ, $F_N(x)$ describes the RC regime for $x \ll -1$, the QD regime for $x \gg 1$, and the QC regime for $|x| \ll 1$. In the phase diagram (r_0, T), going from $x = -\infty$ to $x = +\infty$ corresponds to sweeping the parameter r_0 from $-\infty$ to $+\infty$ at fixed $T > 0$.[3]

We now turn our attention to the universal properties of the thermodynamics. They are encoded in the free energy density $\mathcal{W}$, whose singular part we denote $\mathcal{W}_s$. Unlike the regular part, $\mathcal{W}_s$ displays universal scaling [21]. By dimensional analysis, as $[\mathcal{W}] = d+1$,

$$\mathcal{W}_s(T,\Delta) = -N\frac{(k_B T)^{d+1}}{(\hbar c)^d}\mathcal{F}_N\left(\frac{\Delta}{k_B T}\right), \tag{3.8}$$

with $\mathcal{F}_N(x)$ a universal function, depending only on the dimension, value of N, and the phase of the system (note that we rescale it by N to have a finite limit for $N \to \infty$).

The internal energy density $\epsilon = \partial[\beta\mathcal{W}]/\partial\beta$ follows a related scaling form,

$$\epsilon(T,\Delta) = \epsilon(T=0,\Delta) - N\frac{(k_B T)^{d+1}}{(\hbar c)^d}\vartheta_N\left(\frac{\Delta}{k_B T}\right), \qquad \vartheta_N(x) = d\mathcal{F}_N(x) - x\mathcal{F}_N'(x). \tag{3.9}$$

Finally, the entropy (per unit volume) is the derivative of the free energy with respect to the temperature, $S = -\partial\mathcal{W}/\partial T$, and is defined by the the scaling function $(d+1)\mathcal{F}_N(x) - x\mathcal{F}_N'(x)$,

$$S(T,\Delta) = N\frac{(k_B T)^d}{(\hbar c)^d}\left[(d+1)\mathcal{F}_N\left(\frac{\Delta}{k_B T}\right) - \frac{\Delta}{k_B T}\mathcal{F}_N'\left(\frac{\Delta}{k_B T}\right)\right]. \tag{3.10}$$

We stress again that the scaling functions $F_N(x)$, $\mathcal{F}_N(x)$ and $\vartheta_N(x)$ are independent of the microscopic parameters c_0, r_0 and u_0. The latter only intervene indirectly through Δ and c.

Another universal quantity is the spin stiffness ρ_s in the zero-temperature ordered phase, expressed in units of Δ. Note that since for $N = 1$ there are no transverse fluctuations ρ_s is not defined. For $N \geq 3$ the system is always disordered at finite temperature and ρ_s is not defined for $T > 0$. For $N = 2$ the stiffness is defined in the KT phase and, noting T_{KT} the temperature of the transition, there is a jump from $\rho_s(T_{KT}^+) = 0$ to $\rho_s(T_{KT}^-) = (2/\pi)T_{KT}$ at the transition [56]. This jump is universal, and independent in particular of the value of T_{KT} (which can be tuned by r_0).

3.2 Link with classical critical Casimir forces

Before examining in detail the thermodynamics of the quantum O(N) model, we first discuss critical Casimir forces, in the context of classical statistical field theory. While these different physical phenomena may seem completely unrelated, they are nonetheless linked by the celebrated quantum-classical mapping, which is, in that case, more than a computational trick. The mapping will also allow us to compare results derived from the three-dimensional classical model to our computations for the quantum system in two dimensions.

[3] In presence of an ultraviolet cutoff Λ r_0 cannot be more negative than $O(-\Lambda^2)$.

3.2.1 From the quantum Casimir effect to critical Casimir forces

The name "Casimir effect" is attributed to a range of phenomena in which a system is subject to forces originating from its confinement. First, we briefly recall here what is the "original" Casimir effect in quantum field theory, proposed by Casimir in 1948 [57]. Consider, in d space dimensions, two perfectly conducting metallic plates of area L^{d-1} separated by a length $L_\perp$ ($L \gg L_\perp$). Due to the quantum fluctuations of the electromagnetic (EM) field, they experience an attractive force. Indeed, temporarily restoring physical units, the Hamiltonian of the EM field between the two plates reads

$$\hat{H} = \sum_{\mathbf{k}} \hbar\omega_{\mathbf{k}}(\hat{n}_{\mathbf{k}} + \frac{1}{2}). \tag{3.11}$$

The sum here carries over all allowed momenta $\mathbf{k}$. In the absence of the plates, all values are authorized for $\mathbf{k}$, whereas in their presence boundaries conditions impose a quantification on $\mathbf{k}$: the field vanishes on both plates. In the absence of EM field, the presence of the plates changes the energy by an amount

$$\Delta E(L_\perp) = \sum_{\mathbf{k}\ \text{quantized}} \frac{\hbar\omega_{\mathbf{k}}}{2} - \sum_{\mathbf{k}} \frac{\hbar\omega_{\mathbf{k}}}{2}. \tag{3.12}$$

Although each term is formally divergent, the difference can be regularized by noticing that in the ultraviolet the plates will be transparent to the field and cutting off the sums accordingly. It can be shown that when the cutoff is sent to infinity the difference converges to a number independent of the shape of the cutoff, which can be determined with complex analysis formulas.

To this difference in energy corresponds a force per surface area, dubbed the "Casimir force",

$$f_{\mathrm{C}} = -\frac{1}{L^{d-1}} \frac{\mathrm{d}[\Delta E(L_\perp)]}{\mathrm{d}L_\perp} \tag{3.13}$$

It can be computed for various geometries of the plates and dimensions. Its general form can be deduced by dimensional analysis. The relevant energy scale is $\hbar c L_\perp^{-1}$ while the relevant length scale is $L_\perp$, thus, by dimensional analysis

$$f_{\mathrm{C}} = C\frac{\hbar c}{L_\perp^{d+1}}, \tag{3.14}$$

where the constant C has been determined by Casimir ($C = -\pi^2/240$ for $d = 3$). Note that the above scaling argument alone indicates neither the magnitude of the force nor does it tell whether it is attractive or repulsive and the computation must be performed to answer these questions.

After Casimir's original paper, people investigated whether a similar effect could be found in other systems. The key ingredients intervening in the Casimir effect are the quantum fluctuations of the EM field (within classical electrodynamics the plates feel no force) and the fact that the EM forces are long-ranged (this assumption is implicit, as obviously the photon is massless, but the plates have to "know" about each other for any force to be felt). This led Fisher and de Gennes to predict in 1978 the existence of a Casimir force in a confined system near a bulk classical phase transition [58]. In this setting, thermal fluctuations play the role of quantum fluctuations, while the divergence of the bulk correlation length ensures that the interactions are long-range. The Casimir effect has been observed experimentally in binary mixtures [59] and liquid helium films [60, 61].

The mechanism is the same in essence as for the quantum electromagnetism phenomenon. Consider a D-dimensional classical system confined in a film geometry of area $A = L^{D-1}$ (L is sent

Quantum	$d+1$	β	$r_0 - r_{0c}$	Δ	Free energy	Internal energy
Classical	D	$L_\perp$	$T - T_c$	ξ^{-1}	Excess free energy	Casimir force

Table 3.1: Dictionary relating a confined classical field theory to the equivalent quantum field theory at finite temperature.

to infinity) and thickness $L_\perp$ near its bulk critical temperature T_c. Let us consider the free energy per unit volume $\mathcal{W}$. Switching back to natural units ($\hbar = k_B = 1$), we write

$$\mathcal{W}(t, L_\perp) = \mathcal{W}_b(t) + TL_\perp^{-1} g_{ex}(t, L_\perp). \tag{3.15}$$

Here, t denotes the reduced temperature $(T - T_c)/T_c$, $\mathcal{W}_b$ is the bulk free energy per unit volume and $\mathcal{W}_{ex} = TL_\perp^{-1} g_{ex}(t, L_\perp)$ the excess contribution from the presence of a boundary. The Casimir force per unit area expressed in temperature units is

$$f_C(T, L_\perp) = -\frac{1}{AT}\frac{\partial[AL_\perp \mathcal{W}_{ex}(t, L_\perp)]}{\partial L_\perp} = -\frac{\partial g_{ex}(t, L_\perp)}{\partial L_\perp} \tag{3.16}$$

As the regular part of the free energy is nearly independent of $L_\perp$ in the critical regime, a scaling analysis near T_c, coupled to a finite size scaling analysis [51], predicts that g_{ex} has the universal scaling form (for $D < 4$)

$$g_{ex}(T, L_\perp) = L_\perp^{1-D} \mathcal{F}(L_\perp/\xi), \tag{3.17}$$

with $\mathcal{F}$ a universal function, and $\xi \sim |t|^{-\nu}$ the bulk correlation length. Hence, the scaling law of the Casimir force is

$$f_C(T, L_\perp) = L_\perp^{-D} \vartheta(L_\perp/\xi), \qquad \vartheta(x) = (D-1)\mathcal{F}(x) - x\mathcal{F}'(x). \tag{3.18}$$

3.2.2 Quantum-classical mapping and link with quantum thermodynamics

Now, let us consider a quantum phase transition in $d + 1 = D$ dimensions belonging to the same universality class than the above classical phase transition; that is, the zero temperature quantum field theory (QFT) is described by the same low-energy action than the bulk classical field theory (CFT). Note that this implies that the theory is relativistic (i.e., Lorentz-invariant, with c playing the role of a fictitious speed of light) at zero temperature and that the dynamical exponent z is equal to one as the bulk CFT is presumed isotropic. At finite temperature, the time direction of the QFT is singled out and has a finite width β. Mathematically, the action is exactly the same as that of the classical model in the presence of a confined direction (the time) of width $L_\perp$ (β). Because of this correspondence, the partition function of the quantum and classical models are identical, and the universal quantities and scaling functions of both models are the same, although they describe different physics; see Table 3.1 for a correspondence dictionary.

In particular, the scaling functions $\mathcal{F}_N$ and ϑ_N of the free energy and the internal energy density of the d-dimensional quantum O(N) model [defined by Eqs. (3.7) and (3.9)] and the scaling functions $\mathcal{F}$ and ϑ of the excess free energy and the Casimir force of the D-dimensional classical O(N) model [defined by Eqs. (3.17) and (3.18)] are identical, up to a scale factor of N. This is a remarkable result: completely different physical phenomenons, the thermodynamics of a quantum system and the Casimir force in a classical system, are governed by the same mathematical functions.

Thanks to this, the scaling functions of the Casimir forces in three-dimensional critical classical systems can be compared to those of the free energy and internal energy in two-dimensional quantum systems. We exploit this in Section 3.4.1 to compare the NPRG approach to classical Monte-Carlo results.

Note that, contrary to the quantum model which has periodic boundaries conditions in the time direction, the boundary conditions of the confined classical model have not been specified. They are important as they define the universality class of the scaling functions. Thus to make the correspondence, the classical system must have periodic boundary conditions in the confined directions. Remark that our correspondence implies that the critical Casimir forces in a system with PBCs are always attractive, as $-\vartheta_N$, by definition (3.9), is proportional to the thermal energy, which is positive. Conversely, the mapping shows that the results for three-dimensional classical systems with periodic boundary conditions, unphysical at first sight, can be compared with experiments in quantum systems.

3.3 Large-N solution

A first step in the quantitative study of the quantum $\mathrm{O}(N)$ model is to investigate the large-N limit. In that case, the model is exactly solvable as the saddle-point approximation becomes exact. We present here a sketch of the derivation and the results, which yield $m(T,\Delta)$ and the universal functions F_∞ and $\mathcal{T}_\infty$; see [50] for a detailed resolution. To look into the large-N limit serves several goals. First, we can establish rigorously the qualitative phase diagram detailed in Section 3.1. Second, it brings some information about the finite-N physics, even though $1/N$ expansion remains a perturbative method. Lastly, it serves as a useful benchmark to test approximations and numerical solutions.

Let us present briefly how the results are derived. In this section, we use a cutoff Λ acting only on momenta, and do not distinguish between the bare velocity c_0 and the renormalized one c since they coincide in the large-N limit. We start from the action (3.1), and introduce two auxiliary fields: τ, which will be equal to $\boldsymbol{\varphi}^2$, and λ, a Lagrange multiplier which enforces this constraint. Indeed from the identity

$$\delta(\boldsymbol{\varphi}^2-\tau) \propto \int \mathrm{d}\lambda\, \exp\left(-\frac{\mathrm{i}\lambda}{2}(\boldsymbol{\varphi}^2-\tau)\right) \tag{3.19}$$

we rewrite the partition function $Z=\int \mathcal{D}[\boldsymbol{\varphi}]\,\exp(-S[\boldsymbol{\varphi}]) = \int \mathcal{D}[\boldsymbol{\varphi},\tau]\,\delta(\boldsymbol{\varphi}^2-\tau)\exp(-S[\boldsymbol{\varphi}])$ as

$$Z \propto \int \mathcal{D}[\boldsymbol{\varphi},\tau,\lambda]\exp\left(-\int_{\mathbf{x}}\frac{\mathrm{i}\lambda}{2}(\boldsymbol{\varphi}^2-\tau)+\frac{1}{2}(\partial_\mu\boldsymbol{\varphi})^2+\frac{r_0}{2}\tau+\frac{u_0}{4!N}\tau^2\right), \tag{3.20}$$

$$Z \propto \int \mathcal{D}[\boldsymbol{\varphi},\lambda]\exp\left(-\int_{\mathbf{x}}\left[\frac{1}{2}\left(\partial_\mu\boldsymbol{\varphi}\right)^2+\frac{\mathrm{i}\lambda}{2}\boldsymbol{\varphi}^2-\frac{3N}{2u_0}(r_0-\mathrm{i}\lambda)^2\right]\right), \tag{3.21}$$

where ∂_μ denotes $c^{-1}\partial_\tau$ for $\mu=0$ and ∇_i for $\mu=i>0$. In the last line we integrate out τ.

We single out the first component of the field and rewrite $\boldsymbol{\varphi}=(\sigma,\boldsymbol{\pi})$ where σ and $\boldsymbol{\pi}$ are respectively the first and the next $N-1$ components of the field. One may now integrate out the $\boldsymbol{\pi}$ fields and then rescale $\sigma\to\sqrt{N}\sigma$ to obtain the effective microscopic action for the remaining modes

$$S[\sigma,\lambda]=N\int_{\mathbf{x}}\left[\frac{1}{2}(\nabla\sigma)^2+\frac{\mathrm{i}\lambda}{2}\sigma^2-\frac{3}{2u_0}(\mathrm{i}\lambda-r_0)^2\right]+\frac{N-1}{2}\operatorname{Tr}\ln g^{-1}(\lambda). \tag{3.22}$$

Here g^{-1} is the propagator of the $\boldsymbol{\pi}$ modes in presence of λ,

$$g^{-1}(\mathbf{x},\mathbf{x}') = \delta(\mathbf{x}-\mathbf{x}')[-\partial_\mu^2 + \mathrm{i}\lambda(\mathbf{x})]. \tag{3.23}$$

In the large-N limit, $S[\sigma,\lambda]$ scales like N and the saddle-point approximation becomes exact: the partition function function is given by the action evaluated at the fields minimizing the action. Equivalently, the effective action is equal to the microscopic action. From this one can determine the thermodynamics. In a constant field, σ^2 and $m = c\sqrt{\mathrm{i}\lambda}$ respectively correspond to the modulus square of the order parameter and the excitation gap.[4] The ordered phase is characterized by $\sigma > 0$, $m = 0$; the disordered phase by $\sigma = 0$, $m > 0$, and at the QCP $\sigma = m = 0$. Let us now present the results.

3.3.1 Zero temperature

At zero temperature the critical coupling r_{0c} takes a nonzero value $r_{0c} = -u_0\Lambda c/24\pi$. In the disordered phase the gap m_0 verifies

$$\frac{6m_0^2}{u_0c^2} + \frac{m_0}{4\pi} = \frac{6}{u_0}(r_0 - r_{0c}). \tag{3.24}$$

By comparing both terms in the left-hand side of the above equation, one defines the Ginzburg momentum scale $p_G = cu_0/24\pi$. This scale determines the range of the critical regime. Near the critical point $m_0 \ll p_G$, the gap scales like $m_0 \propto (r_0 - r_{0c})$. As $z = 1$, we deduce a non-trivial value for the critical exponent $\nu = 1$. Far from the QCP, $m_0 \gg cp_G$, we retrieve the mean-field result $m_0 \propto (r_0 - r_{0c})^{1/2}$. Our definition of Δ yields

$$\Delta(r_0) = \frac{24\pi}{u_0}(r_0 - r_{0c}). \tag{3.25}$$

We now discuss the ordered phase. $m_0 = 0$ and the modulus square of the order parameter is $2\rho_0 = -(6N/u_0)(r_0 - r_{0c})$, hence $\beta = 1/2$ (thus by hyperscaling $\eta = 2 - D + 2\beta/\nu = 0$). In the large-$N$ limit, the transverse propagator is not renormalized: $G_T(\mathbf{p},\mathrm{i}\omega_n) = 1/(\mathbf{p}^2 + \omega_n^2)$ at low energy. Since the stiffness is defined by $G_T(\mathbf{p},\mathrm{i}\omega_n) = [2\rho_0/\rho_s]/(\mathbf{p}^2 + \omega_n^2)$ (see Eq. (3.3)), one has

$$\frac{\rho_s}{N\Delta} = \frac{2\rho_0}{N\Delta} = \frac{1}{4\pi}. \tag{3.26}$$

3.3.2 Finite temperature

At finite temperature, in the critical regime $\Delta, T \ll cp_G$, the gap m and the scaling function F_∞ defined in Eq. (3.7) by $m(T,\Delta) = TF_\infty(\Delta/T)$ is given by

$$m(T,\Delta) = 2T\,\mathrm{arsinh}\left[\frac{1}{2}\exp\left(\frac{\Delta}{2T}\right)\right], \qquad F_\infty(x) = 2\,\mathrm{arsinh}\left[\frac{1}{2}\exp\left(\frac{x}{2}\right)\right]. \tag{3.27}$$

From this, we highlight the three regimes discussed in Section 3.1 and illustrated in Fig. 3.1. They are defined by comparing the two energies Δ and T, i.e. the ratio $x = \Delta/T$ to ± 1. Indeed, $x \ll -1$,

[4] $\mathrm{i}\lambda$ is real and positive at the saddle point.

$|x| \ll 1$ and $x \gg 1$ respectively correspond to the RC, QC and QD regimes. In these limiting cases

$$m(T,\Delta) = \begin{cases} T\exp(\Delta/2T) & \text{for } \Delta < 0,\ |\Delta| \gg T, \\ 2\,\mathrm{arsinh}(1/2)\,T & \text{for } |\Delta| \ll T, \\ \Delta & \text{for } \Delta > 0,\ \Delta \gg T, \end{cases} \qquad F_\infty(x) = \begin{cases} \exp(x/2) & \text{for } x \ll -1, \\ 2\,\mathrm{arsinh}(1/2) & \text{for } |x| \ll 1, \\ x & \text{for } x \gg 1. \end{cases} \tag{3.28}$$

This illustrates the qualitative phase diagram of Fig. 3.1 (right). Indeed, we recover the expected behaviors in the three regimes: in the QD regime, the system is gapped at zero temperature, and as long as $T \ll \Delta$ the gap is unaffected by temperature, $m(T \ll \Delta, \Delta > 0) \simeq m(T = 0, \Delta)$. In the RC regime, the system is disordered at finite temperature, but the gap vanishes exponentially as T goes to zero. Finally, in the QC regime the gap is equal to the temperature with a universal prefactor, $m/T = 2\,\mathrm{arsinh}(1/2) \simeq 0.962424$.

The function $F_\infty(x)$ intervenes in the expression of the free energy, given by the action taken at the saddle point. Because of this, the scaling function $\mathcal{F}_\infty(x)$ [defined by Eq. (3.7)] of the free energy reads [50]

$$\mathcal{F}_\infty(x) = \frac{1}{2\pi}\left[\frac{x^3}{12}\Theta(x) - \frac{x}{4}F_\infty(x)^2 + \frac{1}{6}F_\infty(x)^3 + F_\infty(x)\,\mathrm{Li}_2(\mathrm{e}^{-F_\infty(x)}) + \mathrm{Li}_3(\mathrm{e}^{-F_\infty(x)})\right], \tag{3.29}$$

where $\Theta(x)$ is the step function and $\mathrm{Li}_s(z)$ a polylogarithm, given for $|z| < 1$ by

$$\mathrm{Li}_s(z) = \sum_{n=1}^{\infty} \frac{z^n}{n^s}. \tag{3.30}$$

Both $F_\infty(x)$ and $\mathcal{F}_\infty(x)$ are represented in Fig. 3.2, together with NPRG-based determinations of $F_N(x)$ and $\mathcal{F}_N(x)$ for small N.

The limiting behavior of $\mathcal{F}_\infty$ is given by

$$\mathcal{F}_\infty(x) = \begin{cases} \zeta(3)/2\pi & \text{for } x \ll -1, \\ 2\zeta(3)/5\pi & \text{for } |x| \ll 1, \\ x\mathrm{e}^{-x}/2\pi & \text{for } x \gg 1, \end{cases} \tag{3.31}$$

where ζ is the Riemann zeta function; $\zeta(3)/2\pi \simeq 0.191313$ and $2\zeta(3)/5\pi \simeq 0.153051$. For large x, deep in the disordered phase, the gap is large and the free energy does not depend on temperature, hence the exponential decay of $\mathcal{F}_\infty(x)$. For large negative x, the low-energy physics is governed by the transverse fluctuations, whose dynamics is given by the nonlinear σ model. Since the correlation length is exponentially large, the thermodynamics is dominated by the $N-1$ modes corresponding to transverse fluctuations of the local order parameter (see the discussion in [50]), and the free energy is given by that of $N-1$ free two-dimensional bosons with a linear dispersion relation. An elementary calculation then yields

$$\mathcal{F}_\infty(x \to -\infty) = \zeta(3)/2\pi. \tag{3.32}$$

3.4 Nonperturbative determination

We present an approximation scheme based on NPRG to determine the thermodynamics of the quantum $\mathrm{O}(N)$ model, namely the scaling functions and the universal ratio ρ_s/Δ. First, we recall

how to determine these quantities within the effective action formalism developed in 2.1. They are given by the potential $U(\rho) = \Gamma(\boldsymbol{\phi})/V$ (here $\rho = \boldsymbol{\phi}^2/2$ is the O(N) invariant, and V the volume) and the retarded propagator $G(\mathbf{p}, \mathrm{i}\omega_n, \boldsymbol{\phi}) = \Gamma^{(2)-1}(\mathbf{p}, \mathrm{i}\omega_n, \boldsymbol{\phi})$. In the disordered phase the excitation gap is given by the closest pole to zero in the propagator evaluated at the minimum of the potential $\rho_0 = 0$, whereas in the ordered phase ρ_s is determined by the low-momenta behavior of the transverse propagator, see Eq. (3.3). The free energy density is given by $-U(\rho_0)$.

Now, one needs to develop a NPRG scheme to determine $U(\rho)$ and $G(\mathbf{p}, \mathrm{i}\omega_n, \boldsymbol{\phi})$. At zero temperature, the two-dimensional quantum O(N) model reduces to the three-dimensional classical O(N) model and all procedures discussed in Section 2.3 can be used directly. At finite temperature, the situation is slightly more complicated. The space-time isotropy is broken and this has to be taken into account. In particular, propagators and vertices that, at zero temperature, depend on a three-dimensional momentum $\mathbf{p}$ now depend a two-dimensional momentum $\mathbf{p}$ and a Matsubara frequency $\omega_n = 2\pi n T$.[5]

The derivative expansion scheme we exposed in Section 2.3.1 is sufficient for the study of thermodynamics. Denoting by k the renormalization scale, following the standard NPRG procedure, we add a k-dependent regulator term,

$$\Delta S_k[\boldsymbol{\phi}] = \frac{1}{2}\int_{\mathbf{q},\omega_n} \boldsymbol{\phi}(-\mathbf{q}, -\mathrm{i}\omega_n)\cdot R_k(\mathbf{q},\omega_n)\boldsymbol{\phi}(\mathbf{q},\mathrm{i}\omega_n), \tag{3.33}$$

where the cutoff function $R_k(\mathbf{q},\omega_n)$ acts symmetrically on space and time, $R_k(\mathbf{q},\omega_n) \equiv R_k(\mathbf{q}^2 + \omega_n^2/c_k^2)$, so that at zero temperature Lorentz invariance is preserved. We use the exponential regulator (2.23). The renormalized velocity c_k is defined below by Eq. (3.41).

We write the most general action respecting the O(N) symmetry at order two in the derivatives,

$$\Gamma_k[\boldsymbol{\phi}] = \int_{\mathbf{x}} \frac{1}{2}Z_k^{\mathbf{r}}(\rho)(\nabla\boldsymbol{\phi})^2 + \frac{1}{2}Z_k^{\tau}(\rho)(\partial_\tau\boldsymbol{\phi})^2 + \frac{1}{4}Y_k^{\mathbf{r}}(\rho)(\boldsymbol{\phi}\cdot\nabla\boldsymbol{\phi})^2 + \frac{1}{4}Y_k^{\tau}(\rho)(\boldsymbol{\phi}\cdot\partial_\tau\boldsymbol{\phi})^2 + U_k(\rho). \tag{3.34}$$

Note that, unlike in the *Ansatz* (2.35), there are two pairs of functions $Z_k^{\mathbf{r}}(\rho)$ and $Z_k^{\tau}(\rho)$, and $Y_k^{\mathbf{r}}(\rho)$ and $Y_k^{\tau}(\rho)$, to take into account the space-time anisotropy. At zero temperature, Lorentz invariance is restored and $Z_k^{\mathbf{r}}(\rho) = Z_k^{\tau}(\rho)$, $Y_k^{\mathbf{r}}(\rho) = Y_k^{\tau}(\rho)$ (with $c_k = c_\Lambda = 1$). The propagators read

$$G_{\mathrm{T}}(\mathbf{p},\mathrm{i}\omega_n,\rho)^{-1} = \mathbf{p}^2 Z_k^{\mathbf{r}}(\rho) + \omega_n^2 Z_k^{\tau}(\rho) + W_k(\rho) + R_k(\mathbf{p}^2 + \omega_n^2/c_k^2), \tag{3.35}$$

$$G_{\mathrm{L}}(\mathbf{p},\mathrm{i}\omega_n,\rho)^{-1} = \mathbf{p}^2[Z_k^{\mathbf{r}}(\rho) + \rho Y_k^{\mathbf{r}}(\rho)] + \omega_n^2[Z_k^{\tau}(\rho) + \rho Y_k^{\tau}(\rho)] + W_k(\rho) + 2\rho W'(\rho) + R_k(\mathbf{p}^2 + \omega_n^2/c_k^2). \tag{3.36}$$

The flow of $U_k(\rho)$ is given by Eq. (2.30). That of the other four functions is determined by projecting the flow of $\Gamma_k^{(2)}$,

$$Z_k^{\tau}(\rho) = \frac{\Gamma_{k,\mathrm{A}}(\mathbf{p}=0,\mathrm{i}\omega_1,\rho) - \Gamma_{k,\mathrm{A}}(\mathbf{p}=0,0,\rho)}{\omega_1^2}, \qquad Z_k^{\mathbf{r}}(\rho) = \partial_{\mathbf{p}^2}\Gamma_{k,\mathrm{A}}(\mathbf{p},\mathrm{i}\omega_n=0,\rho)|_{\mathbf{p}=0}, \tag{3.37}$$

$$Y_k^{\tau}(\rho) = 2\frac{\Gamma_{k,\mathrm{B}}(\mathbf{p}=0,\mathrm{i}\omega_1,\rho) - \Gamma_{k,\mathrm{B}}(\mathbf{p}=0,0,\rho)}{\omega_1^2}, \qquad Y_k^{\mathbf{r}}(\rho) = \partial_{\mathbf{p}^2} 2\Gamma_{k,\mathrm{B}}(\mathbf{p},\mathrm{i}\omega_n=0,\rho)|_{\mathbf{p}=0}. \tag{3.38}$$

[5] A mundane consequence is that the computation time of the numerical resolution of flow equations is highly increased. For instance $G_{\mathrm{L,T}}$ depends on three variables, ρ, $|\mathbf{p}|$, ω_n, rather than the two variables ρ and $|\mathbf{p}|$ at zero temperature.

The flow of $Z_k^{\mathrm{r}}(\rho)$ and $Y_k^{\mathrm{r}}(\rho)$ is formally the same as that of $Z_k(\rho)$ and $Y_k(\rho)$ within DE at zero temperature, notwithstanding that the threshold functions themselves are different as they involve sums over Matsubara frequencies rather than integrals. The flows of $Z_k^{\tau}(\rho)$ and $Y_k^{\tau}(\rho)$ involve differences rather than a derivative, as ω_n can only take discrete values; at very small temperatures, it reduces to a derivative.[6] We recall that $\omega_0 = 0$ and $\omega_1 = 2\pi T$.

Now, one has to write the equations in a dimensionless form, as is done in Section 2.3.2. Frequencies are put in a dimensionless form using the velocity, $\tilde{\omega}_n = \omega_n/(kc_k)$. As in the classical model, $Z_k^{\mathrm{r}}(\rho)$ and $Z_k^{\tau}(\rho)$ incorporate the anomalous dimensions of the propagator. They are thus rewritten following Eq. (2.41),

$$\tilde{Z}_k^{\mathrm{r}}(\tilde{\rho}) = Z_k^{\mathrm{r}\,-1} Z_k^{\mathrm{r}}(\rho), \qquad \tilde{Z}_k^{\tau}(\tilde{\rho}) = Z_k^{\tau\,-1} Z_k^{\tau}(\rho), \tag{3.39}$$

with Z_k^{r}, Z_k^{τ} mere numbers. As in Eq. (2.43) Z_k^{r}, Z_k^{τ} are defined using an arbitrary renormalization point, which we chose to be $\tilde{\rho}_{0,k}$, such that $\tilde{Z}_k^{\mathrm{r}}(\tilde{\rho}_{0,k}) = \tilde{Z}_k^{\tau}(\tilde{\rho}_{0,k}) = 1$. From this, one defines two running anomalous dimensions η_k and $\tilde{\eta}_k$ like in Eq. (2.44) by

$$\partial_t \log Z_k^{\mathrm{r}} = -\eta_k, \qquad \partial_t \log Z_k^{\tau} = -\tilde{\eta}_k. \tag{3.40}$$

The presence of two running exponents is due to the anisotropy of the model at finite temperature. The velocity is defined by

$$c_k = \sqrt{Z_k^{\mathrm{r}}/Z_k^{\tau}}. \tag{3.41}$$

At the QCP, lengths and times respectively scale like k^{-1} and k^{-z}, and thus $c_k \sim k^{z-1}$, which leads us to define the running dynamical exponent z_k as $\partial_t \log c_k = z_k - 1$, and

$$z_k = 1 + \frac{\tilde{\eta}_k - \eta_k}{2}. \tag{3.42}$$

At the zero-temperature QCP, this yields the critical exponents $\eta = \eta_k$ and $\tilde{\eta} = \tilde{\eta}_k$. Due to Lorentz invariance, at zero temperature c is not renormalized and $\eta = \tilde{\eta}$ and $z = 1$.

3.4.1 Results

First, we determine at zero temperature the ratio $\rho_s/N\Delta$ for different approximations. The result is shown in Table 3.2; the different methods are consistent both with existing Monte-Carlo simulations [64–67] and with the large-N result.

We now turn our attention to DE at finite temperature. The flow equations are solved numerically using an explicit Euler method (see Appendix A) with $\delta t = -10^{-5}$ ($t = \ln(k/\Lambda)$), $u_0 = 150$ and $\Lambda = 1$. We use a $\tilde{\rho}$ grid of 80 points $0 \leq \tilde{\rho} \leq \tilde{\rho}_{\max}$, $\tilde{\rho}_{\max} = 8N$; the integrals are computed with Simpson's method, with a step $\delta\tilde{q} = 0.02$ and a cutoff $\tilde{q}_{\max} = 6$. The high precision of the integrals is necessary as the change in the free energy with the temperature is a subtle effect. The sum over Matsubara frequencies is cut for large frequencies by the regulator; when there are more than 30 frequencies contributing to the sum it is a good approximation to replace it by an integral over frequencies.

The result for the scaling functions of the gap F_N and the free energy density $\mathcal{F}_N$ [defined by Eq. (3.7)] for $N = 1$, 2 and 3 as well as the large-N exact result are shown in Fig. 3.2. For small values

[6] In other contexts, the flow of quantities similar to $Z_k^{\tau}(\rho)$ are defined with a derivative with respect to ω_n, even at finite temperature. In our case that choice leads to instabilities in the flow.

N	DE	LPA″	BMW	MC	ED
2	0.207	0.195	0.193	0.220 [62]	0.17(2) [63]
3	0.147	0.140	0.137	0.114 [62]	
4	0.118	0.115	0.111		
6	0.0935	0.0947	0.0903		
8	0.0846	0.0876	0.0829		
10	0.0810	0.0844	0.0803		
1000	0.0795	0.0798	0.0796		

Table 3.2: Universal ratio $\rho_s/N\Delta$ for the two dimensional quantum $O(N)$ universality class obtained in the NPRG approach, from the full potential DE, LPA″ and BMW (results from the author), compared to Monte Carlo (MC) simulations and exact diagonalization (ED). The exact result in the large-N limit is $1/4\pi \simeq 0.0796$.

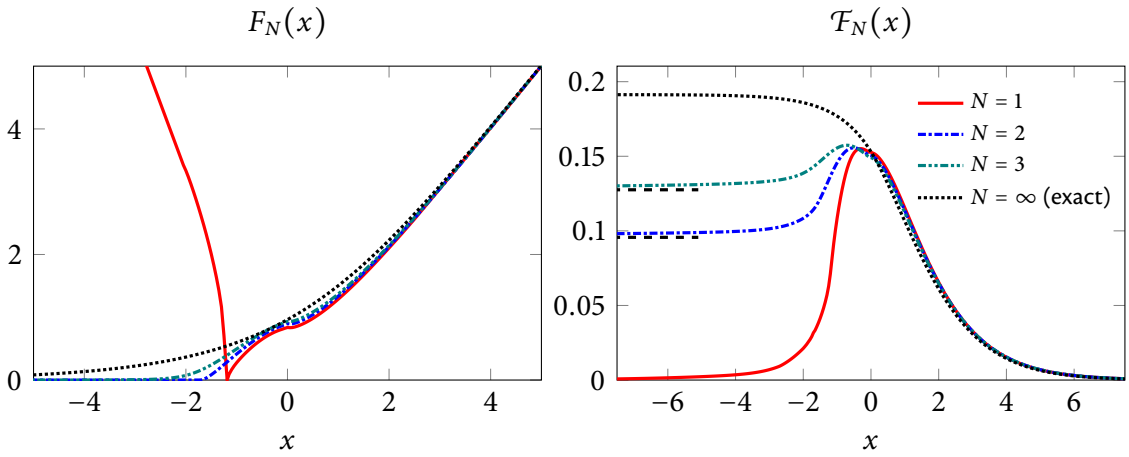

Figure 3.2: Scaling functions $F_N(x)$ and $\mathcal{F}_N(x)$ for the two-dimensional quantum $O(N)$ universality class obtained from the NPRG for $N = 1$, 2, and 3, shown together with the exact solutions $F_\infty(x)$ and $\mathcal{F}_\infty(x)$ in the large-N limit. The exact limit $\mathcal{F}(x \ll -1) \simeq [(N-1)/N]\zeta(3)/2\pi$ is given for $N = 2$ and 3 by black dashed lines.

of N, F_N and $\mathcal{F}_N$ differ significantly from the $N \to \infty$ limit. In the QD ($x \gg 1$) regime, the limit $N \to \infty$ is a good approximation; the gap at finite temperature is nearly equal to the zero-temperature gap and the temperature-dependence of the free energy decays exponentially.

In the QC and RC regimes, this is no longer the case. The function F_N shows an inflexion point for x close to zero and $\mathcal{F}_N$ has a local maximum for some value of $|x| \lesssim 1$.

In the RC regime, the behavior depends strongly on N. For $N \geq 3$, the gap is always finite, but suppressed exponentially. For $N = 2$, it vanishes smoothly at a critical value $x_2^c \simeq -1.7$ below which the system is in the BKT phase. Note that DE fails to completely capture the physics of the two-dimensional classical KT model: while the high-temperature phase is correctly reproduced, the correlation length is always finite and there is no proper transition. However below a certain temperature (with which we define the "transition") one finds a line of quasi-fixed points implying a very large correlation length; see [68] for a throughout discussion. For $N = 1$, the gap vanishes at a value $x_1^c \simeq -1.19$, then rises again in the Ising ordered phase, which is gapped due to the absence of

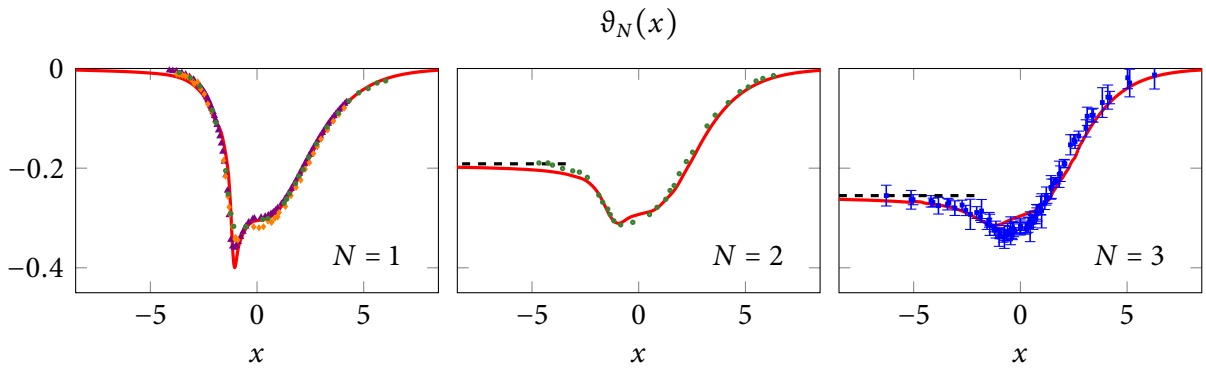

FIGURE 3.3: Casimir scaling function $\vartheta_N(x)$ for the two-dimensional quantum O(N) universality class obtained from the NPRG (full red lines), compared to classical Monte-Carlo simulations of the corresponding three-dimensional spin models (symbols). Violet triangles, yellow diamonds, green circles and blue squares are respectively taken from [66], [67], [65] and [64]. Note that in [64], the overall scale of the $N = 3$ scaling function was not determined. We have rescaled the MC data so that they satisfy the known asymptotic value when $x \ll -1$, $-2(N-1)\zeta(3)/2\pi$; the rescaled function compares very well with the NPRG result. The $x \to -\infty$ result is given by dashed black lines.

Goldstone modes. For $x \to -\infty$, deep in the ordered phase, the gap at small finite temperature is given by the zero-temperature gap the and $F_1(x)$ grows linearly while $\mathcal{T}_1(x)$ decays exponentially as one gets closer to $T = 0$.

The RC scaling of $\mathcal{T}_N(x)$ for $N \geq 2$ can be understood with the same argument than in the large-N limit [see the derivation of Eq. (3.32)]. This means that $\mathcal{T}_N(x)$ is given by the large-N result, up to a $(N-1)/N$ factor, as in the limit $N \to \infty$ we identify $N-1$ with N, and

$$\mathcal{W}_s(T \ll |\Delta|, \Delta < 0) \simeq -(N-1)\frac{\zeta(3)}{2\pi}\frac{T^3}{c^2}. \tag{3.43}$$

From $\mathcal{T}_N$ we deduce the scaling function ϑ_N of the internal energy density [Eq. (3.9)]. Thanks to the link between the thermodynamics of the two-dimensional quantum O(N) model and the critical Casimir forces of the three-dimensional model explained in Section 3.2, we compare in Fig. 3.3 our NPRG result for $N = 1$, 2 and 3 to Monte-Carlo simulations for the equivalent classical spin systems. For all three cases we find very good agreement between the NPRG and simulation results. In particular, the non-monotonous form for $\vartheta_N(x)$ is well reproduced and the amplitude and position of the minimum of the scaling function are accurately predicted, with some small differences between NPRG and simulations occurring in the region around $x \simeq -1$, with the former showing a more pronounced minimum for $N = 1$. Monte Carlo calculations predict the value of the minimum to be about $\vartheta_{N=1,\min} \simeq -0.32$–$36$ with no consensus among the studies, while NPRG predicts $\vartheta_{N=1,\min}$ to be closer to -0.4.[7]

[7] The determination of $\vartheta_N(x)$ is done through the numerical differentiation of $\mathcal{T}_N(x)$, which is a source of numerical noise, hence the uncertainty in the NPRG determination of $\vartheta_{N=1,\min}$.

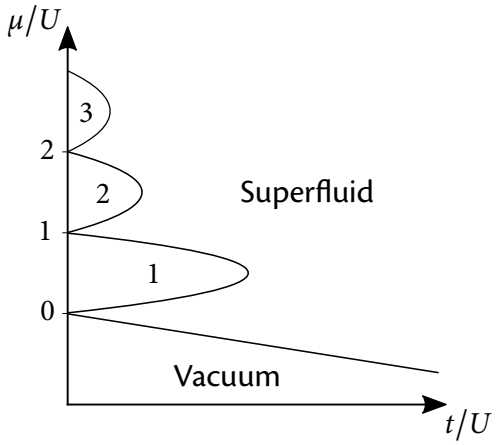

Figure 3.4: Qualitative phase diagram of the Bose–Hubbard model. The integers inside the lobes indicate the average number of particles $\langle \hat{n}_i \rangle$ per site in the Mott insulator phase.

3.5 Comparison with experiments

As a conclusion to this Chapter, let us discuss the possible experimental observation of the thermodynamics of the relativistic quantum O(N) model in bosonic gases trapped in two-dimensional optical lattices [6–9]. We first describe the superfluid-insulator transition that undergo interacting bosons in a lattice and show its relation to the O(2) model.

The physics of interacting bosons in an optical lattice is given by the Bose–Hubbard Hamiltonian,

$$\hat{H} = -t \sum_{\langle i,j \rangle} (\hat{b}_i^\dagger \hat{b}_j + \hat{b}_j^\dagger \hat{b}_i) + \frac{U}{2} \sum_i \hat{n}_i (\hat{n}_i - 1) - \mu \hat{n}_i . \tag{3.44}$$

Here the indices i, j, denote the lattice sites, $\hat{b}_i^\dagger$ (respectively $\hat{b}_i$) denotes the operator that creates (anihilates) a boson at the site i, and $\hat{n}_i = \hat{b}_i^\dagger \hat{b}_i$ is the particle number operator at the site i. The first term describes the hopping between neighboring sites $\langle i, j \rangle$ with an energy t and the second one the repulsive interaction between the bosons at each site with an energy $U > 0$. We work in the grand canonical ensemble and μ denotes the chemical potential.

In the Hamiltonian (3.44), there is a competition between the hopping term, which favors delocalization of bosons across the lattice, and the repulsive interaction which hinders transport. The phase diagram of the model can be established at the mean-field level [Fig. 3.4]. At large t/U, the hopping term dominates and the system is superfluid, with a finite portion of the bosons in a delocalized state. For small t/U the picture depends on the chemical potential μ, which controls the average number of bosons per site $\langle \hat{n}_i \rangle$. For integer $\langle \hat{n}_i \rangle$ the ground state is insulating with a finite energy cost to add, remove or move a boson from a site. If $\langle \hat{n}_i \rangle$ is not an integer, even at very large U a fraction of the bosons remain delocalized and the ground state is always superfluid. The order parameter of the transition is the expectation value of the creation operator, $\langle \hat{b}_i \rangle$, which vanishes in the insulating phase and is finite in the superfluid phase.

To study the quantum phase transition, one may write an effective low-energy action for the system near the transition. This can be done through the standard path integral formulation[8] or

[8] In that case, one proceeds in two steps. First, using the coherent state path integral representation, one rewrites the partition function as a functional integral over complex fields $b_i(\tau)$. Then, an additional Hubbard–Stratanovith transformation is needed to decouple neighboring sites.

phenomenologically, by performing a gradient expansion [1, 69].

The resulting action reads

$$S_{\text{eff}}[\psi,\psi^*] = \int \mathrm{d}^2\mathbf{r} \int_0^{1/T} \mathrm{d}\tau\, \psi^* \left(-Z_A\nabla^2 + Z_C\partial_\tau - V_A\partial_\tau^2 + r_0\right)\psi + u_0|\psi|^4 + \cdots \tag{3.45}$$

where the dots denote higher-order terms. $\psi(\mathbf{r},\tau)$ is a bosonic complex field, with $\tau \in [0, 1/T]$. The effective parameters Z_A, Z_C, V_A, r_0 and u_0 can be related to the underlying microscopic parameters t, μ and U. As the microscopic parameter is tuned, the system undergoes a phase transition from an insulating phase (with $\langle\psi\rangle = 0$) to a superfluid one (with $\langle\psi\rangle \neq 0$). Generically, the microscopic effective action is not Lorentz-invariant, as evidenced by the presence of a single time derivative term. However, the Z_C term may vanish.

Let us now characterize when does Z_C vanish. To do so, we exploit the U(1) invariance of the Hamiltonian. Consider the local microscopic action

$$S[\psi,\psi^*] = \int_0^{1/T} \mathrm{d}\tau\, \psi^*(\partial_\tau - \mu)\psi + V(\psi,\psi^*), \tag{3.46}$$

with V a U(1)-invariant potential. S is invariant under the time-dependent gauge transform

$$\psi \to \mathrm{e}^{\mathrm{i}\alpha(\tau)}\psi, \qquad \psi^* \to \mathrm{e}^{-\mathrm{i}\alpha(\tau)}\psi^*, \qquad \mu \to \mu + \mathrm{i}\partial_\tau\alpha(\tau). \tag{3.47}$$

That property remains true when adding hopping terms to S. Thus, due to the U(1) invariance of the Hamiltonian (3.44), S_{eff} is invariant under the time-dependent gauge transform (3.47). This also appears explicitly when deriving the action through the standard path integral formulation. That invariance in turn implies that Z_C and r_0 are related by the Ward identity $Z_C = -\partial_\mu r_0$.[9] This means that Z_C vanishes precisely at the top of the lobes in Fig. 3.4. At these points, the system displays an emergent Lorentz symmetry and the transition is in the universality class of the quantum O(2) model.

Let us explain how could the scaling function $\mathcal{F}_2$ be measured in a gas of bosons trapped in an optical lattice. In the grand canonical ensemble, $\mathcal{F}_2(x)$ is the scaling function of the pressure of the system. Indeed, the pressure P is the conjugate variable to the volume V of the system, and

$$P = -\frac{\partial[V\mathcal{W}]}{\partial V} = -\mathcal{W} \tag{3.48}$$

as $V\mathcal{W}$ is the total grand potential. The regular part of the pressure depends weakly on the temperature at the quantum phase transition, which allows us to write near the tip of the lobes[10]

$$P(T,\Delta) = P(T=0,\Delta) + 2\frac{(k_{\mathrm{B}}T)^3}{(\hbar c)^2}\mathcal{F}_2\left(\frac{\Delta}{k_{\mathrm{B}}T}\right), \tag{3.49}$$

The equation of state of a two-dimensional gas of bosons has already been measured in the dilute regime [70, 71]. It turns out that the Mott insulator-superfluid transition away from the tips of the Mott lobes (i.e. induced by a density change) is in the universality class of the dilute Bose gas. Experimentally, the condensate is trapped in an harmonic potential, $V(\mathbf{r})$. Within the local density

[9] Here and in the reminder of this section ∂_μ denotes the derivative with respect to the chemical potential.

[10] See [50, 51] for a more detailed justification of this scaling law which has been confirmed through RG.

approximation, the system is described by a position-dependent density $\rho(\mathbf{r})$ and chemical potential $\mu(\mathbf{r}) = \mu - V(\mathbf{r})$. By studying the tails of the condensate, where the interactions are assumed to be weak enough so that the equation of state is that of an ideal Bose gas, one determines the temperature T and the chemical potential μ. That way, the authors of [70, 71] are able to measure in a single experiment $\rho(\mathbf{r})$ and $\mu(\mathbf{r})$ for various $\mathbf{r}$ and thus $\rho(\mu)$ for a range of μ. From this, one may deduce the universal scaling function of ρ (or of the pressure P as $\rho = \partial_\mu P$) as a function of $\mu/k_\mathrm{B}T$ (in the vacuum phase μ is the single-particle gap as it is the energy needed to add a boson to the system).

4

Excitation spectrum

> La meilleure des idées progressistes est celle qui renferme une assez forte dose de provocation pour que son partisan puisse se sentir fier d'être original, mais qui attire en même temps un si grand nombre d'émules que le risque de n'être qu'une exception solitaire est immédiatement conjuré par de bruyantes approbations de la multitude victorieuse.
>
> — Milan Kundera, *Le livre du rire et de l'oubli*.

Having dealt with the thermodynamics of the $\mathrm{O}(N)$ model, we now study its dynamical properties. In this Chapter, we focus our attention on the spectral properties of the model at zero temperature.

We shall examine the physics of the model in the ordered phase for $N \geq 2$ and for $N = 1$, which are radically different. In the first case, the $\mathrm{O}(N)$ symmetry is continuous and the spontaneous symmetry breaking associated with the phase transition gives rise to $N - 1$ gapless Goldstone bosons. In addition to these, mean-field theory predicts the existence of a "Higgs" amplitude mode corresponding to fluctuations of the norm of the order parameter. The existence of the amplitude mode near the QCP when all fluctuations are taken into account beyond mean-field has been a subject of debate, the resolution of which we contributed through our computation of the scalar susceptibility, detailed in Section 4.1.

On the other hand, for $N = 1$ (which corresponds to the scalar ϕ^4 theory) the symmetry group $\mathrm{O}(1) \simeq Z_2$ is discrete and the symmetry broken phase is gapped. In $2 + 1$ dimensions, a classical argument predicts the existence of a bound state at an energy between the gap and the multiparticle continuum, which has been corroborated by resummed perturbation theory and observed numerically. In Section 4.2, we provide a nonperturbative calculation to study the existence and the energy of the bound state in the vicinity of criticality for all dimensions between $1 + 1$ and $3 + 1$.

Part of the work presented in this Chapter has been published [72, 73].

4.1 "Higgs" amplitude mode

In the following, we focus on the zero-temperature limit, in which the action takes the form of the classical $\mathrm{O}(N)$ model in $D = d + 1$ dimensions,

$$S[\boldsymbol{\phi}] = \int_x \frac{1}{2}(\partial_\mu \boldsymbol{\varphi})^2 + \frac{r_0}{2}\boldsymbol{\varphi}^2 + \frac{u_0}{4!N}(\boldsymbol{\varphi}^2)^2, \tag{4.1}$$

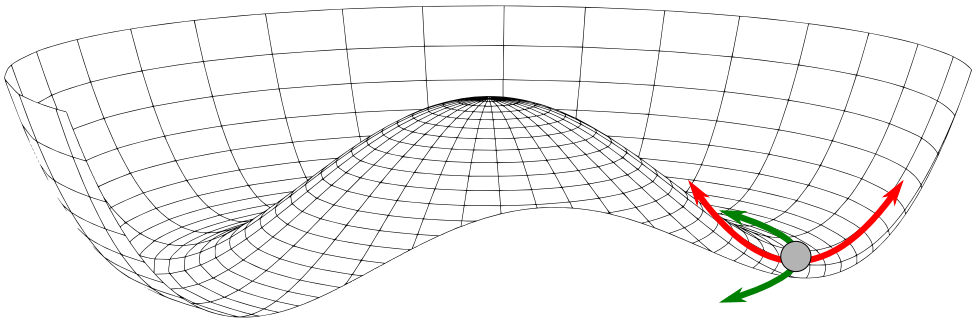

FIGURE 4.1: Sketch of the potential $U(\boldsymbol{\varphi}) = (r_0/2)\boldsymbol{\varphi}^2 + (u_0/4!N)(\boldsymbol{\varphi}^2)^2$ in the ordered phase for $N = 2$. Excitations around the minimum of the potential are represented by the arrows; the green arrow corresponds to gapless transverse fluctuations while the red one corresponds to massive amplitude fluctuations.

with a space variable $\mathbf{x} = (\mathbf{r}, \tau)$.

In Fourier space we identify the last component p_D of a momenta $\mathbf{p}$ in the classical model to the Matsubara frequency ω_n in the quantum model, $p_D = \omega_n$. A correlation function in the classical model $\chi(\mathbf{p})$ ($\mathbf{p}$ has D components) is identified to $\chi(\mathbf{p}, \mathrm{i}\omega_n)$ in the quantum model ($\mathbf{p}$ has $D-1 = d$ components), which yields the retarded dynamical correlation function $\chi(\mathbf{p}, \omega) = \chi(\mathbf{p}, \mathrm{i}\omega_n \to \omega + \mathrm{i}0^+)$. We shall use the notations $\chi(\omega)$ or $\chi(\mathrm{i}\omega_n)$ for the response function at $\mathbf{p} = 0$, and the spectral function $\chi''(\omega) = \mathrm{Im}[\chi(\omega)]$. In the following, we adopt the quantum language.

The concept of the amplitude mode in the ordered phase of the $\mathrm{O}(N)$ model can be easily grasped from a mean-field analysis we now provide. In the ordered phase ($r_0 < 0$), the order parameter $\boldsymbol{\phi} = \langle \boldsymbol{\varphi} \rangle$ is finite. Its modulus is $\phi_0 = \sqrt{-6Nr_0/u_0}$. For further convenience, we decide it lies along the first axis. We rewrite the field as

$$\boldsymbol{\varphi} = (\phi_0 + \sigma, \boldsymbol{\pi}). \tag{4.2}$$

The mean-field susceptibilities, defined by the two components of the bare propagator evaluated at the minimum of the potential, are

$$\chi^0_{\mathrm{L}}(\mathbf{p}, \mathrm{i}\omega_n) = \langle \sigma(\mathbf{p}, \mathrm{i}\omega_n)\sigma(-\mathbf{p}, -\mathrm{i}\omega_n) \rangle = (\mathbf{p}^2 + \omega_n^2 + 2|r_0|)^{-1}, \tag{4.3}$$

$$\chi^0_{\mathrm{T}}(\mathbf{p}, \mathrm{i}\omega_n) = \langle \pi_i(\mathbf{p}, \mathrm{i}\omega_n)\pi_i(-\mathbf{p}, -\mathrm{i}\omega_n) \rangle = (\mathbf{p}^2 + \omega_n^2)^{-1}, \tag{4.4}$$

which respectively correspond to fluctuations of the longitudinal component of the field σ and of the transverse component $\boldsymbol{\pi}$ (there is no summation over repeated indices in the definition of χ^0_{T}). The $N-1$ transverse modes are gapless (Goldstone bosons) while the longitudinal mode is gapped, with a gap $m_{\mathrm{H}} = \sqrt{2}\Delta$, $\Delta = \sqrt{|r_0|}$ being the single-particle gap in the disordered phase at the symmetric point with respect to the QCP. The ratio m_{H}/Δ is in fact a universal number, a result which holds beyond mean-field. These excitations are schematically represented in Fig. 4.1.

Importance of relativistic invariance

As the above picture relies heavily on the shape of the "Mexican hat" potential, it is tempting to believe that the existence of a massive amplitude mode does not depend on the kinetic term

in the action. This is wrong. Consider, for instance, the Galilean-invariant action describing a non-relativistic interacting Bose gas

$$S[\psi,\psi^*] = \int_{\mathbf{r},\tau} \psi^* \left(\partial_\tau - \mu - \frac{\nabla^2}{2}\right)\psi + g(\psi^*\psi)^2, \tag{4.5}$$

with ψ a bosonic complex field. μ is the chemical potential and g the interaction. The equation of motion of ψ is given by the Gross–Pitaevskii equation. The low energy excitations in the superfluid phase are gapless Bogoliubov modes, which couple density (amplitude) and phase (transverse) fluctuations. This can be seen in the operator formalism: one writes $\hat{\psi} = \sqrt{\hat{\rho}}e^{i\hat{\theta}}$, with $\hat{\rho}$ the density and $\hat{\theta}$ the phase of the condensate. The phase and the density are conjugate variables, $[\hat{\rho},\hat{\theta}] = i$, and thus correspond to only one degree of freedom, yielding the Bogoliubov mode. Hence, there is no amplitude mode, despite the shape of the potential.

Link with the Higgs boson

The massive amplitude mode is often dubbed the "Higgs" mode due to the partial similarity with the eponymous mechanism, which answers an apparent paradox in high-energy physics. A field theory that describes fundamental forces (electromagnetism, strong and weak interaction) has to be Lorentz- and gauge-invariant. These symmetries, however, forbid the presence of "massive" terms for the gauge bosons (i.e., quadratic in the gauge field) in the Lagrangian of the theory. This is incompatible with the experimental data which had shown W and Z bosons to be massive. The Higgs mechanism [74–76] consists in the existence of a scalar field which couples to gauge bosons. Upon spontaneous symmetry breaking, the scalar field takes a finite expectation value, thus giving an effective mass to the gauge bosons. The excitation mode of the scalar field around its expectation value is the celebrated Higgs boson observed at CERN [77]. In our problem, the field $\boldsymbol{\varphi}$ plays a role analogous to that of the Higgs scalar field, and its gapped longitudinal excitation that of the massive Higgs boson. There are, however, several differences. There is no gauge field that couples to $\boldsymbol{\varphi}$. Furthermore, the symmetry is continuous, hence the presence of transverse modes.

Before the prediction of the Higgs boson in high-energy physics, the existence of a similar mechanism in superconductors had also been predicted [78] and observed [79–81], see also [82] for a pedagogical discussion. In that setting, the amplitude mode corresponds to fluctuations of the modulus of the superconducting gap. The equation of motion for BCS superconductivity is second-order, enabling the existence an Higgs mode, as a consequence of an (approximate) particle-hole symmetry (assuming the density of states is constant near the Fermi energy). The amplitude mode in a superconductor may be hard to detect. First, since it does not carry spin or charge it does not couple easily to external probes. Second, it may not be a well-defined excitation as it couples to quasi-particle (pair breaking) excitations. It has been argued that the Higgs mode can nevertheless be observed in systems where superconductivity coexists with a charge density wave (CDW) order. On the one hand, the coupling between superconductivity and CDW lowers the Higgs mode energy below the threshold for quasiparticle excitation. On the other hand it makes the Higgs mode Raman active and therefore easily observable [80, 81].

Distinguishing longitudinal and amplitude mode

Above, we use indistinctly the terms "longitudinal" and "amplitude" mode to denote the fluctuations of the field in the direction of the order parameter. This is somewhat imprecise as strictly speaking

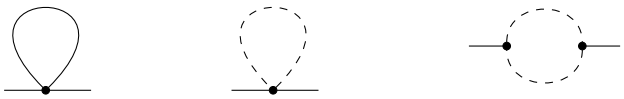

(a) Infrared-regular diagrams. (b) Polarization bubble.

FIGURE 4.2: Feynman diagrams contributing to the longitudinal self-energy at one loop order. Solid lines represent the σ propagators, dashed lines the $\boldsymbol{\pi}$ propagators and dots the interaction. In the infrared limit, the divergent polarization bubble contains the most pertinent contribution.

the amplitude mode corresponds to the fluctuations of the modulus (amplitude) of the order parameter, which is a different excitation. At the mean-field level, both modes display a well-defined gapped excitation, which is why the two modes are sometimes conflated. However, in cases where mean field is qualitatively wrong, the two modes may display different physics. In Section 4.1.1, we perturbatively determine the longitudinal susceptibility, which diverges in the infrared for $d < 3$, contrary to what happens at the mean-field level. In that case there is no well-defined longitudinal mode. In Section 4.1.2 we define and compute within perturbation theory the scalar susceptibility, the response function of the field squared, which by contrast does not diverge at small momenta and frequencies even in small dimensions and is thus the correct response function to examine in order to (possibly) observe the Higgs mode.

4.1.1 Longitudinal fluctuations beyond mean field

Let us first discuss the longitudinal mode. Whether it remains a well-defined excitation in the vicinity of criticality beyond mean-field is a nontrivial question. We discuss it in this Section using perturbation theory; a NPRG-based study is presented later. The answer depends heavily on dimensionality. In three space dimensions, the theory is controlled by a Gaussian fixed point and renormalizes to a noninteracting theory: mean-field is qualitatively correct.[1] This has been evidenced by experiments in quantum antiferromagnets [3, 83, 84], cold atoms [85] as well as quantitative theoretical studies [86, 87].

By contrast, in $2 < d + 1 < 4$ dimensions, the theory is controlled by the Wilson–Fisher (non Gaussian) fixed point and the existence of the longitudinal mode is not guaranteed. In fact, it has been believed for a very long time that no "amplitude" mode could exist [1, 88–91]. The argument is that, if one studies perturbatively the longitudinal mode by expanding the action around the minimum of the potential, cubic and quartic interaction terms appear, e.g. $\sigma\boldsymbol{\pi}^2$, $\boldsymbol{\pi}^2\boldsymbol{\pi}^2$, etc. While these terms are irrelevant for $d+1 \geq 4$, they are crucial for the $2 < d+1 < 4$ physics. This implies that the coupling of longitudinal fluctuations to transverse modes is important and, as these modes are not gapped, the massive longitudinal excitation decays into massless Goldstone bosons. Because of that, the longitudinal mode is damped and cannot be observed.

Remark that, in the ordered phase, the system is described by a non-linear σ model (NLσM), where $\sigma^2 + \boldsymbol{\pi}^2 = 1$, where we have rewritten $\boldsymbol{\varphi} = \phi_0(\sigma, \boldsymbol{\pi})$. Then for small fluctuations $\sigma \simeq 1 - \boldsymbol{\pi}^2/2$,

[1] Up to logarithmic corrections in three space dimensions, which lead to a weak infrared divergence of the longitudinal susceptibility.

and, using Wick's theorem,[2] the connected longitudinal correlation function is given by

$$\phi_0^2\langle\sigma\sigma\rangle_c|_{\mathbf{p},i\omega_n} \sim \frac{1}{4}\phi_0^2\langle\boldsymbol{\pi}^2\boldsymbol{\pi}^2\rangle|_{\mathbf{p},i\omega_n} = \frac{N-1}{2}\phi_0^2\int_{\mathbf{q},i\omega_m}\langle\pi_i\pi_i\rangle|_{-\mathbf{q},-i\omega_m}\langle\pi_i\pi_i\rangle|_{\mathbf{p}+\mathbf{q},i\omega_n+i\omega_m}. \tag{4.6}$$

In $D < 4$, the behavior of the last term at small $\mathbf{p}$ and ω_n indicates that $\langle\sigma(\mathbf{p},i\omega_n)\sigma(-\mathbf{p},-i\omega_n)\rangle_c$ diverges in the infrared like $(\omega_n^2+\mathbf{p}^2)^{(d-3)/2}$, in sharp contrast with the mean-field result (4.3).

Let us be more quantitative. To that effect we shall study the longitudinal susceptibility first at one-loop order, within a weak coupling approach, then in the large N limit. Although these approaches do not capture the small-N critical behavior they still do provide insight into the physics of the ordered phase.

We shall start with the weak coupling approach. We develop the action around the mean-field minimum. The full susceptibility of the σ modes is given by

$$\chi_L^{1\text{ loop}}(\mathbf{p},i\omega_n) = \frac{1}{[\chi_L^0(\mathbf{p},i\omega_n)]^{-1} - \Sigma_\sigma(\mathbf{p},i\omega_n)} \tag{4.7}$$

where $\chi_L^0(\mathbf{p},i\omega_n)$ is the mean-field susceptibility and Σ_σ the longitudinal self energy. Let us assume that the self-energy remains small in the infrared, and expand the longitudinal susceptibility in powers of the interaction. As is discuted below, this assumption proves to be wrong. One then has

$$\chi_L^{1\text{ loop}}(\mathbf{p},i\omega_n) = \chi_L^0(\mathbf{p},i\omega_n) + [\chi_L^0(\mathbf{p},i\omega_n)]^2\Sigma_\sigma(\mathbf{p},i\omega_n) + O(u_0^2). \tag{4.8}$$

At the lowest order in the interaction, in the infrared, the diagram that contributes the most to Σ_σ is the polarization bubble,

$$\Pi^0(\mathbf{p},i\omega_n) = \int_{\mathbf{q},i\omega_m}\chi_T^0(\mathbf{q},i\omega_m)\chi_T^0(\mathbf{p}+\mathbf{q},i\omega_n+i\omega_m), \tag{4.9}$$

given by the convolution of two massless $\boldsymbol{\pi}$ propagators. The bubble and other diagrams contributing to Σ_σ are represented in Fig. 4.2. Unlike the other diagrams, Π^0 diverges in the infrared like $(\omega_n^2+\mathbf{p}^2)^{(d-3)/2}$ at zero temperature. In $d = 2$

$$\Pi^0(\mathbf{p},i\omega_n) = \frac{1}{8\sqrt{\mathbf{p}^2+\omega_n^2}} \quad \text{for } \mathbf{p},\omega_n \to 0. \tag{4.10}$$

Replacing this into Eq. (4.8), one obtains that the longitudinal susceptibility $\chi_L^{1\text{ loop}}$ diverges in the infrared like $(\omega_n^2+\mathbf{p}^2)^{(d-3)/2}$, and in $d = 2$ its corresponding spectral function $\chi_L^{1\text{ loop}\prime\prime}$ behaves like $\chi_L^{1\text{ loop}\prime\prime}(\mathbf{p},\omega) \sim \Theta(\omega^2-\mathbf{p}^2)/\sqrt{\omega^2-\mathbf{p}^2}$.

Note that the above expansion is ill-justified, since to expand in powers of u_0 the susceptibility we have to assume that the self-energy remains small, which is not the case (Σ_σ diverges in the infrared). In fact, this evidences the breakdown of perturbation theory in $D < 4$. For a more rigorous

[2] In the NLσM, the interaction is asymptotically weaker as the energy decreases and the Goldstone (transverse) modes are controlled by a Gaussian (noninteracting) action at low energies. That the system is described by the NLσM can be justified by NPRG: upon renormalization of the model in the ordered phase, the (dimensionless) gap of the longitudinal mode diverges. Furthermore, the inverse of the position of the minimum of the potential ($1/\rho_{0,k}$) plays the role of the coupling constant of the NLσM and its β function is given by that of the NLσM [50].

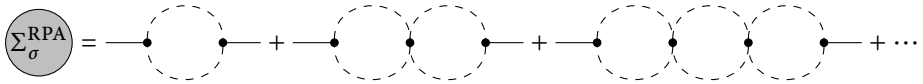

(a) RPA self-energy.

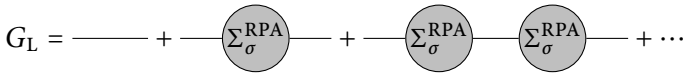

(b) Longitudinal susceptibility.

FIGURE 4.3: Diagrams in the large N limit. Dots and lines have the same meaning than in Fig. 4.2.

argument, let us consider the large-N limit. The self-energy is then exactly determined by the sum of RPA diagrams (see Fig. 4.3),

$$\Sigma_\sigma^{\mathrm{RPA}}(\mathbf{p}, \mathrm{i}\omega_n) = \frac{m_{\mathrm{H},0}^2 u_0 \Pi^0(\mathbf{p}, \mathrm{i}\omega_n)}{6 + u_0 \Pi^0(\mathbf{p}, \mathrm{i}\omega_n)}, \tag{4.11}$$

where $m_{\mathrm{H},0}$ is the mean-field value of the longitudinal mode gap given by the pole in χ_{L}^0. (Note that we incorporate nontrivial large-N effects in $\chi_{\mathrm{L}}^{0\,-1}(\mathbf{p}, \mathrm{i}\omega_n) = \mathbf{p}^2 + \omega_n^2 + m_{\mathrm{H},0}^2$, as $m_{\mathrm{H},0}$ vanishes at a critical value $r_{0\mathrm{c}} \neq 0$.) The susceptibility reads

$$\chi_{\mathrm{L}}(\mathbf{p}, \mathrm{i}\omega_n) = \frac{1}{[\chi_{\mathrm{L}}^0(\mathbf{p}, \mathrm{i}\omega_n)]^{-1} - \Sigma_\sigma(\mathbf{p}, \mathrm{i}\omega_n)} = \frac{1}{\mathbf{p}^2 + \omega_n^2 + \dfrac{6m_{\mathrm{H},0}^2}{6 + u_0 \Pi^0(\mathbf{p}, \mathrm{i}\omega_n)}}. \tag{4.12}$$

In the infrared Π^0 dominates all other terms and the longitudinal susceptibility behaves like

$$\chi_{\mathrm{L}}(\mathbf{p}, \mathrm{i}\omega_n) \simeq \frac{u_0}{6m_{\mathrm{H},0}^2} \Pi^0(\mathbf{p}, \mathrm{i}\omega_n) \sim (\omega_n^2 + \mathbf{p}^2)^{(d-3)/2}. \tag{4.13}$$

χ_{L} is therefore completely dominated by the transverse fluctuations in the infrared. The physical consequence of this divergence is that even if there were an excitation at some finite energy, its corresponding peak in the spectral function would be broadened into a hard to detect shoulder. In summary, the longitudinal response function does not display a well-defined resonance. In the next Section, we show how, by contrast, the scalar susceptibility may display such a resonance. If present and well defined, this resonance would correspond to an amplitude mode.

4.1.2 Finding the right response function

Although the longitudinal susceptibility does not allow to observe the amplitude mode, a recent paper has suggested that the scalar susceptibility could be a good candidate to observe the amplitude mode [92]. The scalar susceptibility describes fluctuations of the amplitude of the field, rather than of its longitudinal component.

Let us give the intuition which leads to consider this spectral function before defining it. In the ordered phase, fluctuations of the field around the order parameter $\boldsymbol{\phi}_0$ can be parameterized in two ways:

$$\boldsymbol{\varphi} = (\phi_0 + \sigma, \boldsymbol{\pi}) = (\phi_0 + n)\boldsymbol{\Omega}. \tag{4.14}$$

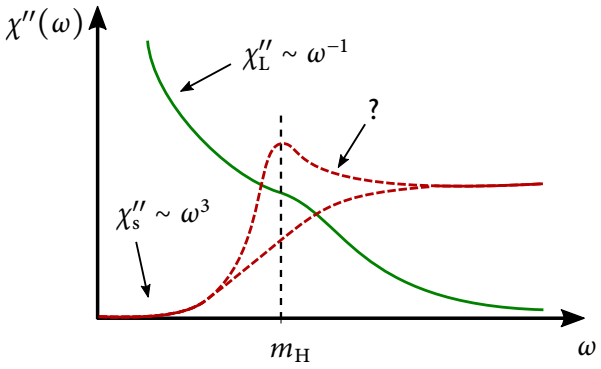

Figure 4.4: Sketch of the spectral function of the longitudinal and scalar susceptibility deep in the ordered phase. At small frequencies, the longitudinal susceptibility diverges like ω^{-1} while the scalar susceptibility vanishes as ω^3. Because of this, the amplitude mode resonance at $\omega = m_{\rm H}$ is broadened and not visible on the longitudinal spectral function, but may remain observable in the scalar spectral function. The dashed lines for $\chi_{\rm s}(\omega \sim m_{\rm H})$ represent the two possible scenarios, with the scalar susceptibility either displaying a well-defined resonance or not.

The first representation has been used in the previous Section. In the second one, $\mathbf{\Omega}$ is a unit vector defining the direction of the field and n describes fluctuations of the amplitude of $\boldsymbol{\varphi}$ around its average value ϕ_0. The difference between the two representations is akin to the difference between Cartesian and spherical coordinates. Naively, one may think that examining the fluctuations of the longitudinal component σ and the amplitude n would yield similar results. However, it is not the case. Rewriting the action in terms of n and $\mathbf{\Omega}$, one sees that the potential term depends solely on n and the kinetic term becomes

$$(\partial_\mu \boldsymbol{\varphi})^2 = (\partial_\mu n)^2 + (\phi_0 + n)^2 (\partial_\mu \mathbf{\Omega})^2. \tag{4.15}$$

The amplitude-direction coupling $n(\partial_\mu \mathbf{\Omega})^2$ contains two derivatives while there are none in the longitudinal-transverse coupling $\sigma \boldsymbol{\pi}^2$. This means that the amplitude field couples weakly to the Goldstone modes and one may expect the response function of the n field to be infrared regular.

Working with the unit constraint on the $\mathbf{\Omega}$ field is not convenient. Rather than the n field response function, we consider the scalar susceptibility,

$$\chi_{\rm s}(\mathbf{r} - \mathbf{r}', \tau - \tau') = \langle \boldsymbol{\varphi}^2(\mathbf{r}, \tau) \boldsymbol{\varphi}^2(\mathbf{r}', \tau') \rangle - \langle \boldsymbol{\varphi}^2(\mathbf{r}, \tau) \rangle \langle \boldsymbol{\varphi}^2(\mathbf{r}', \tau') \rangle, \tag{4.16}$$

which is the correlation function of the square of the field $\boldsymbol{\varphi}$. The expected behavior of $\chi_{\rm s}$, compared to that of the longitudinal susceptibility, is represented in Fig. 4.4. Whether or not there is a true resonance at $m_{\rm H}$ reflecting a well-defined excitation remains however to be seen.

As for the longitudinal mode, it is possible to compute $\chi_{\rm s}$ in the weak coupling limit. Due to the coupling to the Goldstone modes, at low frequencies in $d = 2$ $\chi_{\rm s}(\mathbf{p}, \mathrm{i}\omega_n) \sim (\mathbf{p}^2 + \omega_n^2)^{3/2}$ does not diverge. As the spectral function vanishes like $\chi_{\rm s}(\omega) \sim \omega^3$, it is possible that the spectral function presents a pronounced peak at a frequency close to $m_{\rm H,0}$.

Now, let us examine the large N limit. Expanding around the minimum of the field, it is possible to relate $\chi_{\rm s}$ to propagators $\langle \sigma\sigma^2 \rangle$, $\langle \sigma^2\sigma^2 \rangle$, $\langle \sigma\pi_i^2 \rangle$, and so on, which are computed by summing the RPA diagrams as was done for the longitudinal susceptibility [92]. One finds

$$\chi_{\rm s}(\mathbf{p}, \mathrm{i}\omega_n) = \frac{12N}{u_0} \frac{(\mathbf{p}^2 + \omega^2) u_0 \Pi^0(\mathbf{p}, \mathrm{i}\omega_n) + 6m_{\rm H,0}^2}{(\mathbf{p}^2 + \omega^2)(u_0 \Pi^0(\mathbf{p}, \mathrm{i}\omega_n) + 6) + 6m_{\rm H,0}^2}. \tag{4.17}$$

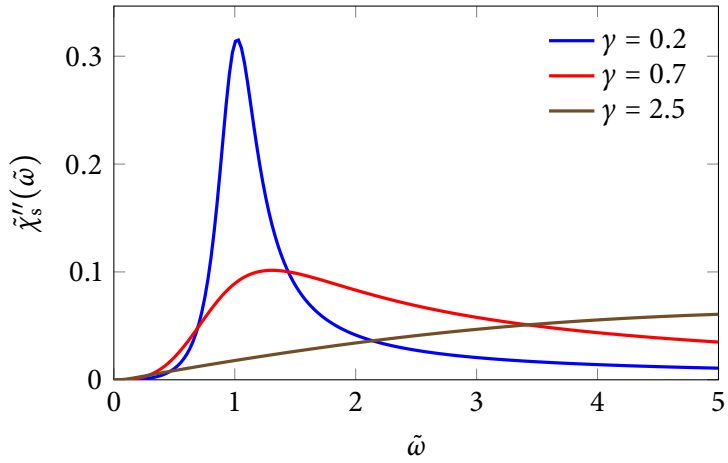

FIGURE 4.5: Large-N spectral function $\tilde{\chi}_s''(\tilde{\omega})$ in the ordered phase for various values of γ. For small values of γ there is a sharp resonance at $\omega \simeq m_{H,0}$. As γ increases the peak gets shifted to larger values of γ and is smoothed. For large values of γ the peak disappears.

Let us perform the analytic continuation. We set $\mathbf{p} = 0$ and $i\omega_n = \omega + i0^+$. Then

$$\chi_s''(\omega) = \frac{N}{4} \frac{\omega^3}{(\omega^2 - m_{H,0}^2)^2 + (u_0/48)^2 \omega^2}. \tag{4.18}$$

Let us write this in a dimensionless form,

$$\tilde{\chi}_s''(\tilde{\omega}) = \frac{1}{4} \frac{\gamma \tilde{\omega}^3}{(\tilde{\omega}^2 - 1)^2 + 4\gamma^2 \tilde{\omega}^2}, \tag{4.19}$$

with the dimensionless variables

$$\tilde{\omega} = \omega/m_{H,0}, \qquad \gamma = u_0/16 m_{H,0}, \qquad \tilde{\chi}_s''(\tilde{\omega}) = \chi_s''(\omega/m_{H,0})/N\gamma m_{H,0}. \tag{4.20}$$

The resulting spectral function is displayed in Fig. 4.5 for several values of γ, which controls the presence of a resonance. In the deep ordered phase, $\gamma \ll 1$, the spectral function displays a well-defined peak of width γ at an energy of the order of $m_{H,0}$. Indeed, this corresponds to the weak coupling limit, where the Gaussian approximation is qualitatively correct. For $\tilde{\omega} \ll 1$, $\tilde{\chi}_s''(\tilde{\omega}) \sim (\gamma/4)\tilde{\omega}^3$, while for $\tilde{\omega} \gg 1$, $\tilde{\chi}_s''(\tilde{\omega}) \sim (\gamma/4)\tilde{\omega}^{-1}$.

By contrast, for $\gamma \gtrsim 1$, which corresponds to the vicinity of the phase transition[3] (critical regime), the resonance is washed out. In that case three regimes can be distinguished: for $\tilde{\omega} \ll \gamma^{-1}$, $\tilde{\chi}_s''(\tilde{\omega}) \sim (\gamma/4)\tilde{\omega}^3$, for $\gamma^{-1} \ll \tilde{\omega} \ll \gamma$, $\tilde{\chi}_s''(\tilde{\omega}) \sim \tilde{\omega}/16\gamma$, and for $\tilde{\omega} \gg \gamma$, $\tilde{\chi}_s''(\tilde{\omega}) \sim (\gamma/4)\tilde{\omega}^{-1}$.

To summarize, these results indicate that the scalar spectral function may be a good candidate for the observation of the amplitude mode. In particular, they agree on the infrared behavior of the scalar spectral function, which vanishes as ω^3. However, these perturbative results are inconclusive as to its fate in the vicinity of criticality for small N. The large-N approach indicates that there is no Higgs mode in the critical regime, while the weak coupling limit claims the presence of a well-defined amplitude mode. The two approaches yield opposite results.

[3] Indeed, $\gamma \sim p_G/m_0$, with $p_G \sim u_0$ the Ginzburg scale and $m_0 \sim m_{0,H}$ the single-particle gap at the symmetric point in the disordered phase. The critical regime is precisely characterized by the condition $m_0 \ll p_G$ which means that there is a broad range of scales at which the system is critical, see the definition of p_G by Eq. (3.4).

Since neither approach is valid in the vicinity of criticality at small N, it is necessary to go beyond perturbation theory.

State of the art

Before detailing our own calculation of the scalar susceptibility and the results concerning the Higgs mode, let us briefly present the state of the art at the time of our work [72]. It has been studied though various techniques: next to leading order large-N [93], (Q)MC simulations [62, 94–96], NPRG using a simplified BMW approximation [50], and dimensional expansion about $D = 4$. For $N = 2$, these studies have shown the existence of an amplitude mode which persists arbitrarily close to the QCP. However, there were some uncertainty regarding the precise value of the mass (studies gave values between 2.2 and 3.1, in units of the single-particle gap in the disordered phase at the same distance to the transition). Furthermore, several questions remained: what happens for larger values of N, e.g. 3 or 4? Is there a signature of the amplitude mode in the disordered phase, as predicted by some QMC studies [94]? The following study answers these interrogations. We further detail our findings and compare our results to these references as well as to studies posterior to ours in Section 4.1.4.

4.1.3 Nonperturbative computation of the scalar susceptibility

We shall now present a NPRG-based scheme to compute the scalar susceptibility at all momenta and frequencies.

The first difficulty to overcome is that χ_s is a 4-point correlation function. As such, within the usual effective action formalism, it would be related to high-order vertices depending on several momenta $\Gamma^{(3)}(\mathbf{p}_1, \mathbf{p}_2, \boldsymbol{\phi})$, $\Gamma^{(4)}(\mathbf{p}_1, \mathbf{p}_2, \mathbf{p}_3, \boldsymbol{\phi})$. Here and in the following, as we restrain ourselves to zero temperature, we adopt the notations of the classical $(2+1)$-dimensional $\mathrm{O}(N)$ model. Devising an approximation to accurately compute these vertices is difficult and dealing with functions of several momentum variables very challenging computationally. Instead of this, we shall use the fact that χ_s only involves two space-time positions: it is the correlator of the composite $\boldsymbol{\varphi}^2$ field. We now will demonstrate how the BMW approximation can be used to determine χ_s.

Let us introduce a new source h which couples to $\boldsymbol{\varphi}^2$. In presence of an external field $\mathbf{J}$, the partition function reads (we go back to the notation $\mathbf{x} = (\mathbf{r}, \tau)$)

$$\mathcal{Z}[\mathbf{J}, h] = \int \mathcal{D}[\boldsymbol{\varphi}] \exp\left[-S[\boldsymbol{\varphi}] + \int_{\mathbf{x}} (\mathbf{J}\cdot\boldsymbol{\varphi} + h\boldsymbol{\varphi}^2)\right]. \tag{4.21}$$

Now, the average value of the field

$$\boldsymbol{\phi}[\mathbf{x}; \mathbf{J}, h] = \langle \boldsymbol{\varphi}(\mathbf{x})\rangle = \frac{\delta \ln \mathcal{Z}[\mathbf{J}, h]}{\delta \mathbf{J}(\mathbf{x})} \tag{4.22}$$

depends on both sources. The source h allows us to compute the scalar susceptibility [defined by Eq. (4.16)]

$$\chi_s(\mathbf{x} - \mathbf{x}') = \left.\frac{\delta^2 \ln \mathcal{Z}[\mathbf{J}, h]}{\delta h(\mathbf{x}) \delta h(\mathbf{x}')}\right|_{\mathbf{J}=0,\ h=0}. \tag{4.23}$$

Effective action formulation

The effective action formalism in presence of h is very similar to that developed in Section 2.1, as h is treated as an external field. Γ is the Legendre transform of the free energy with respect to $\mathbf{J}$ (but not h)

$$\Gamma[\boldsymbol{\phi}, h] = -\ln \mathcal{Z}[\mathbf{J}, h] + \int_{\mathbf{x}} \mathbf{J} \cdot \boldsymbol{\varphi}. \tag{4.24}$$

In (4.24), $\mathbf{J}$ is a functional of both $\boldsymbol{\phi}$ and h obtained by inverting (4.22). From Γ we define the 1PI vertices

$$\Gamma^{(n,m)}_{\{i_j\}}[\{\mathbf{x}_i\}, \{\mathbf{y}_i\}; \boldsymbol{\phi}, h] = \frac{\delta^{n+m}\Gamma}{\delta\phi_{i_1}(\mathbf{x}_1)\cdots\delta\phi_{i_n}(\mathbf{x}_n)\delta h(\mathbf{y}_1)\cdots\delta h(\mathbf{y}_m)}. \tag{4.25}$$

The correlation functions evaluated at $h = 0$ and in a uniform field configuration are determined by the vertices

$$\Gamma^{(n,m)}_{\{i_j\}}(\{\mathbf{x}_i\}, \{\mathbf{y}_i\}, \boldsymbol{\phi}) = \Gamma^{(n,m)}_{\{i_j\}}[\{\mathbf{x}_i\}, \{\mathbf{y}_i\}; \boldsymbol{\phi}, h]\Big|_{h=0,\ \boldsymbol{\phi}=\text{const.}}. \tag{4.26}$$

For $h = 0$ the vertices $\Gamma^{(n,0)}$ are the same as the vertices $\Gamma^{(n)}$ of the theory in the absence of the additional h source. For instance, $\Gamma^{(2,0)}$ is the inverse propagator.

We recall that the response functions are determined by propagators taken at the minimum of the potential, and longitudinal and transverse susceptibilities are given by

$$\chi_{\mathrm{L,T}}(\mathbf{p}) = G_{\mathrm{L,T}}(\mathbf{p}, \rho_0). \tag{4.27}$$

In the disordered phase ($\rho_0 = 0$) the single-particle excitation gap Δ manifests itself as a sharp peak in the spectral function $\chi''_{\mathrm{L,T}}(\omega)$ for $|\omega| = \Delta$. $\chi''_{\mathrm{L,T}}(\omega)$ vanishes for $|\omega| < \Delta$. In the ordered phase the stiffness ρ_s (introduced in the Chapter 3) is defined by

$$\chi_{\mathrm{T}}(\mathbf{p} \to 0) \simeq \frac{2\rho_0}{\rho_s \mathbf{p}^2}. \tag{4.28}$$

As explained in Section 3.1 for two systems located symmetrically with respect to the QCP (i.e., corresponding to the same value of $|r_0 - r_{0c}|$) the ratio ρ_s/Δ is a universal number depending only on N as $|r_0 - r_{0c}|$ goes to zero. Because of this, we use Δ as a characteristic energy scale in both phases. Introducing $\delta = r_0 - r_{0c}$ the detuning from the transition, the energy scale is given by $\Delta = \Delta(|\delta|)$. Unlike in Chapter 3 with this convention Δ is positive in the ordered phase.

In the universal regime, near the QCP the susceptibilities $\chi_{\mathrm{L,T}}(\mathbf{p})$ and the corresponding spectral functions $\chi''_{\mathrm{L,T}}(\omega) = \mathrm{Im}[\chi_{\mathrm{L,T}}(\mathbf{p} \to (0, \ldots, 0, -i\omega + 0^+))]$ take the dimensionless form

$$\chi_{\mathrm{L,T}}(\mathbf{p}) = C\Delta^{\eta-2}\tilde{\chi}_{\mathrm{L,T}}(\tilde{p}), \qquad \chi''_{\mathrm{L,T}}(\omega) = C\Delta^{\eta-2}\tilde{\chi}''_{\mathrm{L,T}}(\tilde{\omega}), \tag{4.29}$$

where the dimensionless variables are $\tilde{p} = |\mathbf{p}|/\Delta$ and $\tilde{\omega} = \omega/\Delta$. The exponent $\eta - 2$ stems from the scaling dimension of the operator $\boldsymbol{\varphi}(\mathbf{x})$, $(D - 2 + \eta)/2$. $\tilde{\chi}_{\mathrm{L,T}}(\tilde{p})$ and $\tilde{\chi}''_{\mathrm{L,T}}(\tilde{\omega})$ are universal scaling functions which depend on N and the phase considered. C is a nonuniversal constant (depending on r_0, u_0 and Λ as well as on the response function). $\tilde{\chi}''_{\mathrm{L,T}}(\tilde{\omega})$ is an odd function of $\tilde{\omega}$. At the QCP $\tilde{\chi}_{\mathrm{L,T}}(\tilde{p}) \sim \tilde{p}^{-2+\eta}$ and $\tilde{\chi}''_{\mathrm{L,T}}(\tilde{\omega}) \sim \tilde{\omega}^{-2+\eta}$.

Let us relate the scalar susceptibility to the 1PI vertices. From (4.23) we deduce that

$$\chi_s(\mathbf{x} - \mathbf{x}') = -\left.\frac{\bar{\delta}^2\Gamma[\bar{\boldsymbol{\phi}}[h], h]}{\bar{\delta}h(\mathbf{x})\bar{\delta}h(\mathbf{x}')}\right|_{h=0}, \tag{4.30}$$

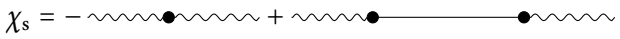

FIGURE 4.6: Diagrammatic representation of the scalar susceptibility. Dots with n straight lines and m wavy lines stand for the vertex $\Gamma^{(n,m)}$ and full lines represent the propagator $G = \Gamma^{(2,0)-1}$.

where $\bar{\boldsymbol{\phi}}[h]$ is the h-dependent order parameter for vanishing $\mathbf{J}$ and $\bar{\delta}/\bar{\delta}h(\mathbf{x})$ a total derivative acting both on the explicit h dependence of Γ and the implicit dependence on h in $\bar{\boldsymbol{\phi}}[h]$. As $\bar{\boldsymbol{\phi}}[h]$ extremizes Γ, i.e.

$$\left.\frac{\delta\Gamma[\boldsymbol{\phi},h]}{\delta\boldsymbol{\phi}}\right|_{h=0,\ \bar{\boldsymbol{\phi}}[h]} = \Gamma^{(1,0)}[\bar{\boldsymbol{\phi}}[h],h] = 0, \tag{4.31}$$

one has

$$\frac{\bar{\delta}^2\Gamma[\bar{\boldsymbol{\phi}}[h],h]}{\bar{\delta}h(\mathbf{x})\bar{\delta}h(\mathbf{x}')} = \Gamma^{(0,2)}[\mathbf{x},\mathbf{x}';\bar{\boldsymbol{\phi}}[h],h] + \int_{\mathbf{y}} \Gamma_i^{(1,1)}[\mathbf{x},\mathbf{y};\bar{\boldsymbol{\phi}}[h],h]\frac{\delta\bar{\phi}_i(\mathbf{y})}{\delta h(\mathbf{x}')}. \tag{4.32}$$

To compute the very last term in Eq. (4.32) we remark that $\Gamma_i^{(1,0)}[\mathbf{y};\bar{\boldsymbol{\phi}}[h],h] = 0$; taking a functional derivative with respect to $h(\mathbf{x}')$ and inverting the resulting relation one finds

$$\frac{\delta\bar{\phi}_i(\mathbf{y})}{\delta h(\mathbf{x}')} = -\int_{\mathbf{y}'} \Gamma_{ij}^{(2,0)-1}[\mathbf{y},\mathbf{y}';\bar{\boldsymbol{\phi}}[h],h]\Gamma_j^{(1,1)}[\mathbf{y}',\mathbf{x}';\bar{\boldsymbol{\phi}}[h],h]. \tag{4.33}$$

Finally we deduce

$$\chi_s(\mathbf{x}-\mathbf{x}') = -\Gamma^{(0,2)}(\mathbf{x},\mathbf{x}',\bar{\boldsymbol{\phi}}) + \int_{\mathbf{y},\mathbf{y}'} \Gamma_i^{(1,1)}(\mathbf{x},\mathbf{y},\bar{\boldsymbol{\phi}})\left[\Gamma^{(2,0)-1}\right]_{ij}(\mathbf{y},\mathbf{y}',\bar{\boldsymbol{\phi}})\Gamma_j^{(1,1)}(\mathbf{y}',\mathbf{x}',\bar{\boldsymbol{\phi}}), \tag{4.34}$$

or, in Fourier space,

$$\chi_s(\mathbf{p}) = -\Gamma^{(0,2)}(\mathbf{p},\bar{\boldsymbol{\phi}}) + \Gamma_i^{(1,1)}(\mathbf{p},\bar{\boldsymbol{\phi}})\left[\Gamma^{(2,0)-1}\right]_{ij}(\mathbf{p},\bar{\boldsymbol{\phi}})\Gamma_j^{(1,1)}(\mathbf{p},\bar{\boldsymbol{\phi}}). \tag{4.35}$$

This is represented in Fig. 4.6. The second term in the right-hand side of Eq. (4.35) is the one-particle reducible part of χ_s. As h transforms as a scalar under $\mathrm{O}(N)$ rotations, vertices $\Gamma^{(0,2)}$ and $\Gamma^{(1,1)}$ can be rewritten as

$$\Gamma_i^{(1,1)}(\mathbf{p},\boldsymbol{\phi}) = \phi_i f(\mathbf{p},\rho), \qquad \Gamma^{(0,2)}(\mathbf{p},\boldsymbol{\phi}) = \gamma(\mathbf{p},\rho), \tag{4.36}$$

with f and γ two functions of $|\mathbf{p}|$ and ρ. Thus

$$\chi_s(\mathbf{p}) = -\gamma(\mathbf{p},\rho_0) + \frac{2\rho_0 f^2(\mathbf{p},\rho_0)}{\Gamma_A(\mathbf{p},\rho_0) + 2\rho_0\Gamma_B(\mathbf{p},\rho_0)}. \tag{4.37}$$

In the universal regime in the vicinity of the QCP, χ_s adopts the scaling form

$$\chi_s(\mathbf{p}) = \mathcal{B} + \mathcal{A}\Delta^{3-2/\nu}\tilde{\chi}_s(\tilde{p}), \qquad \chi_s''(\omega) = \mathcal{A}\Delta^{3-2/\nu}\tilde{\chi}_s''(\tilde{\omega}), \tag{4.38}$$

with $\tilde{\chi}_s(\tilde{p})$ and $\tilde{\chi}_s''(\tilde{\omega})$ universal functions (depending on N and the phase of the system) and $\mathcal{A}$, $\mathcal{B}$ nonuniversal constants. $\tilde{\chi}_s''$ is an odd function of $\tilde{\omega}$. The exponent $3-2/\nu$ (in $d=2$) comes from the fact that the composite operator $\boldsymbol{\varphi}^2$ has scaling dimension $D-1/\nu$; this is deduced from the fact that the relevant coupling r_0 has scaling dimension $1/\nu$. At the QCP $\chi_s(\mathbf{p}) - \chi_s(0) \sim |\mathbf{p}|^{3-2/\nu}$ and $\chi_s''(\omega) \sim \omega^{3-2/\nu}$. An estimate of ν can be obtained from this scaling expression.

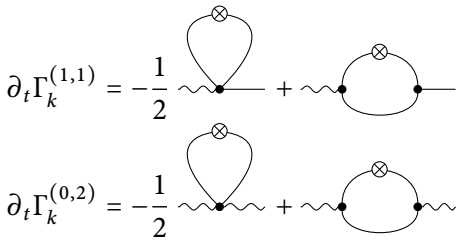

FIGURE 4.7: Diagrammatic representation of the flow equations $\Gamma_k^{(1,1)}$ and $\Gamma_k^{(0,2)}$. The flow of $\Gamma_k^{(2,0)}$ is shown in Fig. 2.3. The full lines stand for the full propagator $(\Gamma_k^{(2)} + R_k)^{-1}$ at scale k, dots with n solid lines and m wavy lines for the vertex $\Gamma_k^{(n,m)}$, and crossed circles for $\partial_t R_k$.

NPRG formalism and BMW approximation

To determine the scalar susceptibility, one has to compute f and γ or, equivalently, the vertices $\Gamma^{(0,2)}$ and $\Gamma^{(1,1)}$ at all momenta, in addition to the inverse propagator $\Gamma^{(2,0)}$. To that effect we introduce the NPRG formalism, following step by step Section 2.2, the sole difference being the presence of the additional field h. We define the k-dependent partition function and (modified) effective action,

$$\mathcal{Z}_k[\mathbf{J},h] = \int \mathcal{D}[\boldsymbol{\varphi}] \exp\left[-S[\boldsymbol{\varphi}] - \Delta S_k[\boldsymbol{\varphi}] + \int_{\mathbf{x}} (\mathbf{J}\cdot\boldsymbol{\varphi} + h\boldsymbol{\varphi}^2)\right], \tag{4.39}$$

$$\Gamma_k[\boldsymbol{\phi},h] = -\ln \mathcal{Z}_k[\mathbf{J},h] + \int_{\mathbf{x}} \mathbf{J}\cdot\boldsymbol{\phi} - \Delta S_k[\boldsymbol{\phi}], \tag{4.40}$$

where $\Delta S_k[\boldsymbol{\varphi}]$ is an infrared regulator term. Assuming that for $k = \Lambda$ the fluctuations are completely suppressed the initial condition reads

$$\Gamma_\Lambda[\boldsymbol{\phi},h] = S[\boldsymbol{\phi}] - \int_{\mathbf{x}} h\boldsymbol{\phi}^2. \tag{4.41}$$

On the other hand $\Gamma_{k=0}[\boldsymbol{\phi},h] = \Gamma[\boldsymbol{\phi},h]$ as $R_{k=0}$ vanishes.

The flow equation

$$\partial_t \Gamma_k[\boldsymbol{\phi},h] = \frac{1}{2}\,\mathrm{Tr}\big[\partial_t R_k (\Gamma_k^{(2,0)}[\boldsymbol{\phi},h] + R_k)^{-1}\big] \tag{4.42}$$

interpolates between $k = \Lambda$ and $k = 0$. We recall the flow equations (2.30) and (2.31) for the potential and the inverse propagator in a uniform field and vanishing h (where we drop, for the sake of clarity, the $\boldsymbol{\phi}$ dependences),

$$\partial_t U = \frac{1}{2}\int_{\mathbf{q}} \partial_t R_k(\mathbf{q}) G_{k,ii}(\mathbf{q}), \tag{4.43}$$

$$\begin{aligned}\partial_t \Gamma^{(2,0)}_{k,ij}(\mathbf{p}) = {}& \frac{1}{2}\int_{\mathbf{q}} [\tilde\partial_t G_{k,i_1i_2}(\mathbf{q})]\Gamma^{(4,0)}_{k,iji_2i_1}(\mathbf{p},-\mathbf{p},\mathbf{q},-\mathbf{q}) \\ & - \int_{\mathbf{q}} [\tilde\partial_t G_{k,i_1i_2}(\mathbf{q})]\Gamma^{(3,0)}_{k,i_2i_3i}(\mathbf{q},-\mathbf{p}-\mathbf{q},\mathbf{p}) G_{k,i_3i_4}(\mathbf{p}+\mathbf{q})\Gamma^{(3,0)}_{k,i_4i_1j}(\mathbf{p}+\mathbf{q},-\mathbf{q},-\mathbf{p}).\end{aligned} \tag{4.44}$$

The flows of the vertices $\Gamma_k^{(0,2)}$ and $\Gamma_k^{(1,1)}$ for a uniform $\boldsymbol{\phi}$ and vanishing h, which we represent in Fig. 4.7, are similarly derived

$$\partial_t \Gamma^{(1,1)}_{k,i}(\mathbf{p}) = \frac{1}{2}\int_{\mathbf{q}} [\tilde\partial_t G_{k,i_1i_2}(\mathbf{q})]\Gamma^{(3,1)}_{k,ii_2i_1}(\mathbf{p},\mathbf{q},-\mathbf{q},-\mathbf{p})$$

$$- \int_{\mathbf{q}} [\tilde{\partial}_t G_{k,i_1 i_2}(\mathbf{q})] \Gamma^{(3,0)}_{k,i_2 i_3 i}(\mathbf{q}, -\mathbf{p}-\mathbf{q}, \mathbf{p}) G_{k,i_3 i_4}(\mathbf{p}+\mathbf{q}) \Gamma^{(2,1)}_{k,i_4 i_1}(\mathbf{p}+\mathbf{q}, -\mathbf{q}, -\mathbf{p}), \quad (4.45)$$

$$\partial_t \Gamma^{(0,2)}_k(\mathbf{p}) = \frac{1}{2} \int_{\mathbf{q}} [\tilde{\partial}_t G_{k,i_1 i_2}(\mathbf{q})] \Gamma^{(2,2)}_{k,i_2 i_1}(\mathbf{q}, -\mathbf{q}, \mathbf{p}, -\mathbf{p})$$
$$- \int_{\mathbf{q}} [\tilde{\partial}_t G_{k,i_1 i_2}(\mathbf{q})] \Gamma^{(2,1)}_{k,i_2 i_3}(\mathbf{q}, -\mathbf{p}-\mathbf{q}, \mathbf{p}) G_{k,i_3 i_4}(\mathbf{p}+\mathbf{q}) \Gamma^{(2,1)}_{k,i_4 i_1}(\mathbf{p}+\mathbf{q}, -\mathbf{q}, -\mathbf{p}). \quad (4.46)$$

We close these equations by applying the BMW procedure described in Section 2.3.4. The BMW approximation amounts to setting $\mathbf{q} = 0$ in the vertices (but not the propagators) in Eqs. (4.45) and (4.46), which allows us to close the flow equations. For the vertices $\Gamma^{(2,1)}_k$, $\Gamma^{(3,1)}_k$ and $\Gamma^{(2,2)}_k$ the approximation reads

$$\Gamma^{(2,1)}_{k,ij}(\mathbf{q}, -\mathbf{p}-\mathbf{q}, \mathbf{p}) \to \Gamma^{(2,1)}_{k,ij}(0, -\mathbf{p}, \mathbf{p}) = \partial_{\phi_i} \Gamma^{(1,1)}_{k,j}(-\mathbf{p}), \quad (4.47)$$
$$\Gamma^{(3,1)}_{k,ijl}(\mathbf{q}, -\mathbf{q}, \mathbf{p}, -\mathbf{p}) \to \Gamma^{(3,1)}_{k,ijl}(0, 0, \mathbf{p}, -\mathbf{p}) = \partial_{\phi_i \phi_j} \Gamma^{(1,1)}_{k,l}(\mathbf{p}), \quad (4.48)$$
$$\Gamma^{(2,2)}_{k,ij}(\mathbf{q}, -\mathbf{q}, \mathbf{p}, -\mathbf{p}) \to \Gamma^{(2,2)}_{k,ij}(0, 0, \mathbf{p}, -\mathbf{p}) = \partial_{\phi_i \phi_j} \Gamma^{(0,2)}_k(\mathbf{p}). \quad (4.49)$$

The new flow equations for $\Gamma^{(0,2)}_k$ and $\Gamma^{(1,1)}_k$ are

$$\partial_t \Gamma^{(1,1)}_{k,i}(\mathbf{p}) = \frac{1}{2} \int_{\mathbf{q}} [\tilde{\partial}_t G_{k,i_1 i_2}(\mathbf{q})] \partial_{\phi_{i_1} \phi_{i_2}} \Gamma^{(1,1)}_{k,i}(\mathbf{p})$$
$$- \int_{\mathbf{q}} [\tilde{\partial}_t G_{k,i_1 i_2}(\mathbf{q})] \partial_{\phi_{i_2}} \Gamma^{(2,0)}_{k,i_3 i}(\mathbf{p}) G_{k,i_3 i_4}(\mathbf{p}+\mathbf{q}) \partial_{\phi_{i_1}} \Gamma^{(1,1)}_{k,i_4}(\mathbf{p}), \quad (4.50)$$

$$\partial_t \Gamma^{(0,2)}_k(\mathbf{p}) = \frac{1}{2} \int_{\mathbf{q}} [\tilde{\partial}_t G_{k,i_1 i_2}(\mathbf{q})] \partial_{\phi_{i_1} \phi_{i_2}} \Gamma^{(0,2)}_k(\mathbf{p})$$
$$- \int_{\mathbf{q}} [\tilde{\partial}_t G_{k,i_1 i_2}(\mathbf{q})] \partial_{\phi_{i_2}} \Gamma^{(1,1)}_{k,i_3}(\mathbf{p}) G_{k,i_3 i_4}(\mathbf{p}+\mathbf{q}) \partial_{\phi_{i_1}} \Gamma^{(1,1)}_{k,i_4}(\mathbf{p}). \quad (4.51)$$

Together with the flow equation of U_k (4.43) and that of $\Gamma^{(2,0)}_k$ (2.63), Eqs. (4.50) and (4.51) form a closed set of equations for the potential U_k and the vertices $\Gamma^{(2,0)}_k$, $\Gamma^{(1,1)}_k$ and $\Gamma^{(0,2)}_k$. From them, we deduce the flow equations for W_k, $Y_{k,A}$, $Y_{k,B}$ f_k and γ_k which are given in [72]. The flow equations for the additional functions f_k and γ_k involve the same threshold functions than those for W_k, $Y_{k,A}$ and $Y_{k,B}$. We define the field renormalization factor by

$$Z_k = \left. \frac{\partial \Gamma^{(2,0)}_{k,\mathrm{T}}(\mathbf{p}, \rho)}{\partial \mathbf{p}^2} \right|_{\mathbf{p}=0, \rho=\rho_{0,k}} = 1 + Y_{A,k}(\mathbf{p}=0, \rho_{0,k}), \quad (4.52)$$

where we recall that $Y_{A,k}$ is defined by Eq. (2.65). Z_k is defined at the minimum of the potential rather than at $\rho = 0$. Although the latter choice yields simpler equations for η_k the former is preferred as the point $\rho = 0$ is not easily accessible in the ordered phase.[4] Eq. (4.52) implies that

$$\Gamma^{(2,0)}_{k,\mathrm{T}}(\mathbf{p} \to 0, \rho_{0,k}) \simeq Z_k \mathbf{p}^2 + W_k(\rho_{0,k}) \quad (4.53)$$

[4] We remind that the potential $U_k(\rho)$ is convex in the ordered phase. The approach to the convexity of the potential is a source of numerical instabilities in the flow at small ρ. We further discuss how to deal with this instability in Section 4.1.4 and Appendix A.2.1.

so that in the ordered phase the stiffness is simply defined by $\rho_{s,k} = 2Z_k\rho_{0,k}$. If we use Eq. (4.53) to estimate the gap Δ in the disordered phase (where $\rho_{0,k=0} = 0$), we find

$$\Delta = \left(\frac{W_{k=0}(0)}{Z_{k=0}}\right)^{1/2}. \tag{4.54}$$

The numerical solution of the flow equations show that this expression is in very good agreement (with an error smaller than 1‰) with the exact determination of the gap obtained from the peak in the spectral function $\chi''_{\mathrm{L,T}}(\omega)$.

Large-N limit

In this Section, following [48], we show that the BMW equations become exact and can be solved analytically when $N \to \infty$. In this limit, $\Gamma_k[\boldsymbol{\phi}]$ is of order N and the field $\boldsymbol{\phi}$ is of order $\sqrt{N}$. This implies that γ_k is $O(N)$, W_k, $\Gamma_{k,\mathrm{A}}$ and f_k are $O(1)$ whereas $\Gamma_{k,B}$ is $O(1/N)$. It follows that

$$\partial_t Y_{A,k} = -\frac{N}{2} I^{\mathrm{TT}}_{k,2} Y'_{A,k}. \tag{4.55}$$

We drop here the $\mathbf{p}$ and ρ dependency of $Y_{A,k}$ and remind that the prime denotes the derivative with respect to ρ. We use the threshold functions defined by

$$J^{\mathrm{TT}}_{k,n}(\mathbf{p},\rho) = \int_{\mathbf{q}} [\partial_t R_k(\mathbf{q})] G^{n-1}_{k,\mathrm{T}}(\mathbf{q},\rho) G_{k,\mathrm{T}}(\mathbf{p}+\mathbf{q},\rho), \qquad I^{\mathrm{TT}}_{k,n}(\rho) = J^{\mathrm{TT}}_{k,n}(\mathbf{p}=0,\rho). \tag{4.56}$$

Since $Y_{A,\Lambda} = 0$, we deduce $Y_{A,k} = 0$: the momentum dependence of the transverse propagator is not renormalized in the large-N limit. The other equations then read

$$\partial_t W_k = \frac{N}{2} I^{\mathrm{TT}\prime}_{k,1}, \qquad \partial_t \Gamma_{k,B} = N J^{\mathrm{TT}}_{k,3} \Gamma^2_{k,B} - I^{\mathrm{TT}}_{k,2} \Gamma'_{k,B}, \tag{4.57}$$

$$\partial_t f_k = N J^{\mathrm{TT}}_{k,3} f_k \Gamma_{k,B} - \frac{N}{2} I^{\mathrm{TT}}_{k,2} f'_k, \qquad \partial_t \gamma_k = N J^{\mathrm{TT}}_{k,3} f^2_k - \frac{N}{2} I^{\mathrm{TT}}_{k,2} \gamma'_k. \tag{4.58}$$

To solve these equations, we set $W = W_k(\rho)$ and use the variables (k, W) instead of (k, ρ) [48, 72]. Introducing the function $g_k(W) = \rho$, one obtains

$$g_k(W) = \frac{3N}{u_0} - \frac{N}{2} \int_{\mathbf{q}} \left(\frac{1}{\mathbf{q}^2 + W + R_k(\mathbf{q})} - \frac{1}{\mathbf{q}^2 + W + R_\Lambda(\mathbf{q})} \right). \tag{4.59}$$

We used $g_\Lambda(W) = (3N/u_0)(W - r_0)$, which is true for $\Gamma_\Lambda[\boldsymbol{\phi}] = S[\boldsymbol{\phi}]$. This reproduces the known result in the large-N limit [50] (see also Section 3.3). For $R_\Lambda(\mathbf{q}) < \infty$, we obtain an apparent difference with the exact result, which is explained by the fact that $\Gamma_\Lambda[\boldsymbol{\phi}]$ is not given by $S[\boldsymbol{\phi}]$. This does not matter when one is interested in universal properties in the vicinity of the QCP: the microscopic physics can be directly parameterized by $\Gamma_\Lambda[\boldsymbol{\phi}]$, which we can choose to coincide with $S[\boldsymbol{\phi}]$.

Using $\Gamma_{\Lambda,B} = u_0/3N$, $f_\Lambda = -2$ and $\gamma_\Lambda = 0$ we obtain

$$\Gamma_{k,B}(\mathbf{p},\rho) = \frac{1}{\dfrac{3N}{u_0} + \dfrac{N}{2}[\Pi_k(\mathbf{p},\rho) - \Pi_\Lambda(\mathbf{p},\rho)]}, \tag{4.60}$$

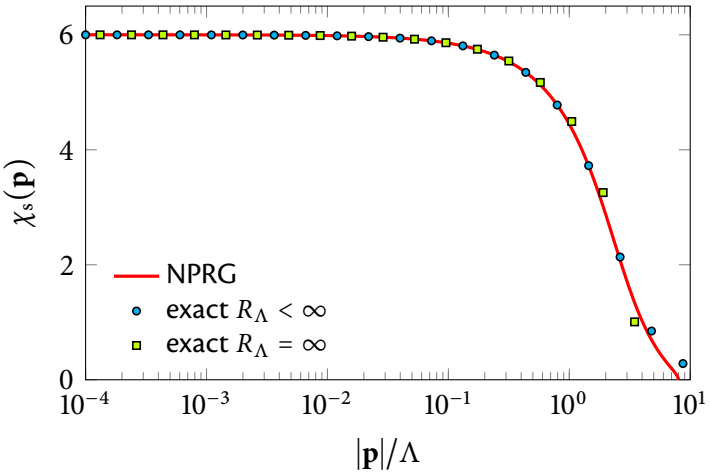

Figure 4.8: Spectral susceptibility $\chi_s(\mathbf{p})$ at the QCP for $N = 1000$ (solid line) compared to the exact large-N solution with $R_\Lambda < \infty$ (circles) and $R_\Lambda = \infty$ (squares). We use arbitrary units for χ_s.

$$f_k(\mathbf{p},\rho) = -\frac{6N}{u_0}\Gamma_{k,B}(\mathbf{p},\rho), \quad \gamma_k(\mathbf{p},\rho) = -\frac{12N}{u_0} + \left(\frac{6N}{u_0}\right)^2 \Gamma_{k,B}(\mathbf{p},\rho), \tag{4.61}$$

where

$$\Pi_k(\mathbf{p},\rho) = \int_{\mathbf{q}} \frac{1}{\mathbf{q}^2 + W_k(\rho) + R_k(\mathbf{q})} \frac{1}{(\mathbf{p}+\mathbf{q})^2 + W_k(\rho) + R_k(\mathbf{p}+\mathbf{q})}. \tag{4.62}$$

We recover the large-N results (4.12) and (4.17) when $R_\Lambda(\mathbf{q}) \to \infty$ and $\Pi_\Lambda \to 0$.

4.1.4 Universal spectral functions

We solve numerically the flow equations with $u_0 = 200$ and $\Lambda = 1$. We use a $(\tilde{p}, \tilde{\rho})$ grid of 80×200 points with $0 \le \tilde{p} \le \tilde{p}_{\max}$, $0 \le \tilde{\rho} \le \tilde{\rho}_{\max}$, $\tilde{p}_{\max} = 8$ and $\tilde{\rho}_{\max} = 6N$. The flow equations are integrated using an explicit Euler method with $\delta t = -10^{-4}$ ($t = \ln(k/\Lambda)$), see Appendix A for more information. In the ordered phase, to alleviate the difficulties caused by the approach to the convexity of the potential, we switch to a dimensionful grid in ρ, and drop the flow of the points for small ρ when the instabilities arise. This allows to continue the flow down to values of k of order $k_{\min} \sim 0.05\Delta$. A more subtle way to handle this issue is discussed in Appendix A.2.1.

A momentum dependent function $F(p) \equiv F_{k=0}(p)$ ($p = |\mathbf{p}|$), such as a two-point vertex or the scalar susceptibility, is obtained from the approximation $F(p) \simeq F_{k=p/\tilde{p}_{\max}}(p)$ where $k = p/\tilde{p}_{\max}$ is the smallest value of k for which the dimensionless momentum $\tilde{p} = p/k$ is still in the grid $[0, \tilde{p}_{\max}]$. We have verified, by increasing $\tilde{p}_{\max}$, that the flow of $F_k(p)$ for $k < p/\tilde{p}_{\max}$ is negligible (at least for the functions of interest to us). This is due to the fact that, in the cases we are considering here, p acts as an effective infrared cutoff, while only momenta of the order of k or smaller contribute to the flow, so that the flow of the function $F_k(p)$ effectively stops when $k \ll p$. $F(p)$ is analytically continued to $F^R(\omega)$ using Padé approximants. Selecting M points p_i, one constructs a rational function $F^{\text{Padé}}$ such that $F^{\text{Padé}}(p_i) = F(p_i)$ for $i = 1, \ldots, M$. We then approximate the analytic continuation of F by that of $F^{\text{Padé}}$, which can be done exactly; see Appendix A.2.2 for more details. Note that in the ordered phase, we cannot determine $F(p)$ for values of p below $k_{\min}\tilde{p}_{\max} = 8k_{\min} \simeq 0.4\Delta$, due to the method used to deal with the approach to convexity. This makes it hard to determine $F^R(\omega)$

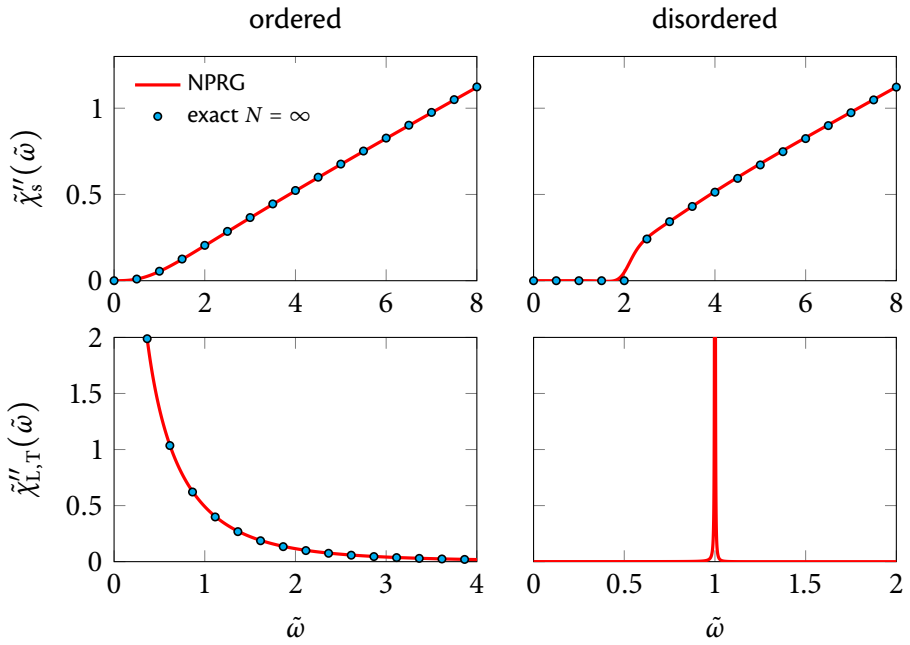

FIGURE 4.9: Spectral functions $\tilde{\chi}''_{L,T}(\tilde{\omega})$ and $\chi''_s(\tilde{\omega})$ in the ordered and disordered phase for $N = 1000$ (solid lines), compared to the exact large-N limit (symbols). In the disordered phase, the exact solution for $\tilde{\chi}''_{L,T}(\tilde{\omega}) \propto \delta(\omega - \Delta)$ is not shown.

for small ω. On the other hand, in the disordered phase, the spectral functions we are interested in vanish for $\omega < \Delta$ or $\omega < 2\Delta$ and there is no need to compute $F(p)$ and $F^R(\omega)$ for p or ω very close to 0.

As a check of our procedure we first discuss the numerical solution of the flow equations in the large-N limit where comparison with exact results is possible (see Section 4.1.3). Fig. 4.8 shows the scalar susceptibility $\chi_s(\mathbf{p})$ obtained for $N = 1000$ at the QCP. Except for momenta near the cutoff Λ, where a small residual difference due to the ultraviolet cutoff is present, we obtain a very good agreement with the exact solution (4.61) in the limit $N \to \infty$ taking into account the finite value of $R_\Lambda(\mathbf{p})$. For sufficiently small $|\mathbf{p}|$, when $\Pi_{k=0}(\mathbf{p})$ becomes very large, the scalar susceptibility becomes independent of the initial value R_Λ of the cutoff function. In any case, for universal properties, the value of R_Λ does not matter.

The spectral functions $\chi''_s(\omega)$ and $\chi''_{L,T}(\omega)$ are shown in Fig. 4.9 for $N = 1000$, in both the ordered and disordered phases, in the universal regime near the QCP. Again, the agreement with the exact results (including nonuniversal prefactors) in the limit $N \to \infty$ is very good. This validates our procedure to compute the momentum dependence of correlation functions as well as the Padé method to obtain the spectral functions.

In the following, we discuss the NPRG results obtained for finite N, in particular $N = 2$ and $N = 3$.

Quantum critical point

We first solve the equations to determine r_{0c} and the critical exponents ν and η, as detailed in Section 2.3.2. Fig. 4.10 shows $\chi_{L,T}(\mathbf{p})$ and $\chi_s(\mathbf{p})$ at criticality for $N = 2$ and $N = 3$. In the universal regime $|\mathbf{p}| \ll p_G$, where p_G is the inverse of the Ginzburg length $\xi_G \sim 24\pi/u_0$, we find $\chi_{L,T}(\mathbf{p}) \sim$

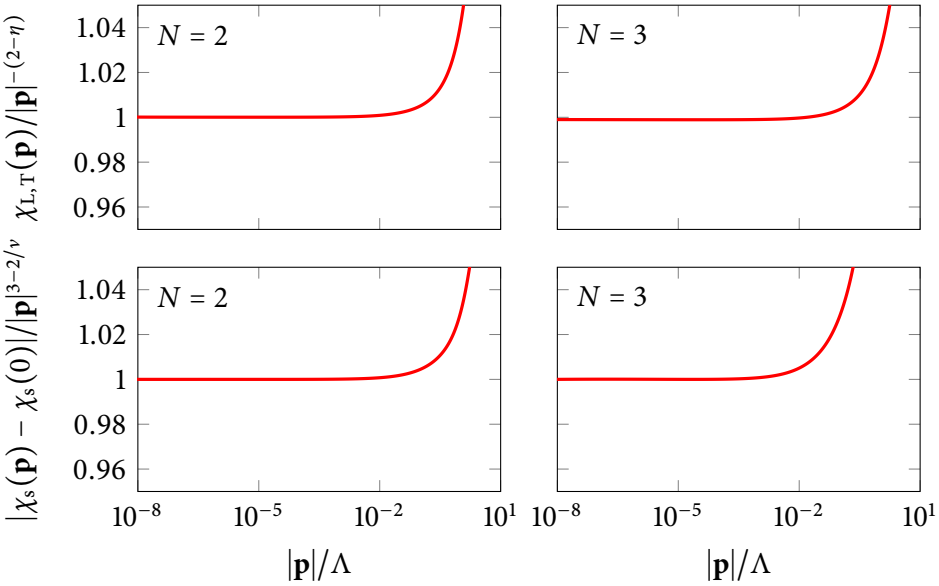

Figure 4.10: $\chi_{\mathrm{L,T}}(\mathbf{p})/|\mathbf{p}|^{-(2-\eta)}$ and $|\chi_s(\mathbf{p}) - \chi_s(0)|/|\mathbf{p}|^{3-2/\nu}$ at the QCP for $N = 2$ and $N = 3$. The normalization is chosen to have a ratio equal to one at $\mathbf{p} \to 0$.

N	from $\rho_{0,k}$	from χ_s	MC	CB
2	0.673	0.674	0.6717(1) [36]	0.67191(12) [33]
3	0.714	0.722	0.7112(5) [37]	0.7121(28) [33]
4	0.754	0.766	0.749(2) [38]	
5	0.787	0.804		
6	0.816	0.835		
8	0.860	0.879		
10	0.893	0.906		
100	0.990	0.992		
1000	0.999	0.999		

Table 4.1: Critical exponent ν obtained in the NPRG approach, from either $\rho_{0,k}$ (see Section 2.3.2) or χ_s [Eq. (4.38)], compared to Monte Carlo (MC) simulations and conformal bootstrap (CB) calculations.

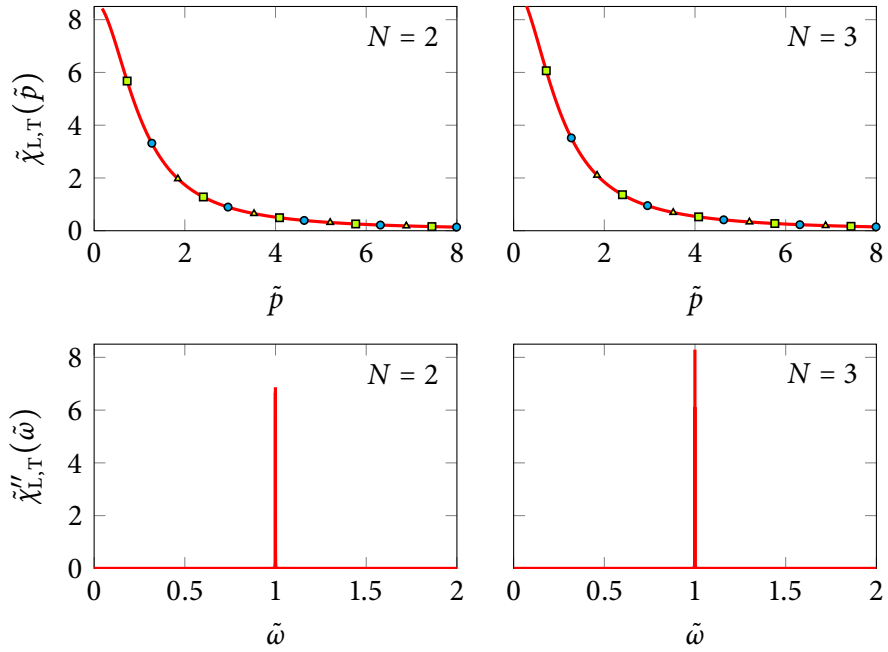

FIGURE 4.11: $\tilde{\chi}_{L,T}(\tilde{p})$ and $\tilde{\chi}''_{L,T}(\tilde{\omega})$ in the disordered phase for $N = 2$ and $N = 3$. The solid lines and symbols correspond to different values of $r_0 - r_{0c}$. We use arbitrary units.

$|\mathbf{p}|^{-2+\eta}$. As for the scalar susceptibility, we find $\chi_s(\mathbf{p}) \sim |\mathbf{p}|^{\theta}$ with $\theta \simeq 0.0345$ for $N = 2$ and $\theta \simeq 0.230$ for $N = 3$. If we use the expected relation $\theta = 3 - 2/\nu$ [see Eq. (4.38)], we obtain $\nu \simeq 0.674$ for $N = 2$ and $\nu \simeq 0.722$ for $N = 3$, in very good agreement with our previous estimates of ν based on the behavior of $\rho_{0,k}$ in the close vicinity of the fixed point, see Table 4.1.

Disordered phase

Figs. 4.11 and 4.12 show $\tilde{\chi}_{L,T}(\tilde{p})$ and $\tilde{\chi}_s(\tilde{p})$ and their spectral functions in the disordered phase for $N = 2$ and $N = 3$. The various curves, obtained for different values of $r_0 - r_{0c}$, show a data collapse in agreement with the scaling forms (4.29) and (4.38) expected in the critical regime. The excitation gap Δ, deduced from the peak in the spectral function $\chi''_{L,T}(\omega)$, is in very good agreement with the approximate expression $\sqrt{W_{k=0}(0)/Z_{k=0}}$.

The spectral function $\chi''_s(\omega)$ of the scalar susceptibility vanishes for $|\omega| < 2\Delta$. Contrary to previous conclusions based on QMC and NPRG [94, 95, 97], we find that $\chi''_s(\omega)$ rises smoothly above the threshold at $\omega = 2\Delta$ with no sign of a local maximum for $\omega \gtrsim 2\Delta$.[5] The authors of [96] argued that in spite of the maximum observed above the threshold in their MC simulations, there is inclusive evidence for a resonance at finite frequency in the disordered phase (the peak carries a small spectral weight and its position is not very robust). We also note that no resonance is obtained in the $4 - D$ expansion [98].

[5] An argument in favor of the presence of an amplitude mode in the disordered phase has been proposed by authors of [95]. The amplitude mode is excited by probing the system at intermediate energy scales, i.e. at finite distances. In that case the system may "seem" ordered, in which case a trace of the excitations of the ordered phase would be present in the disordered phase.

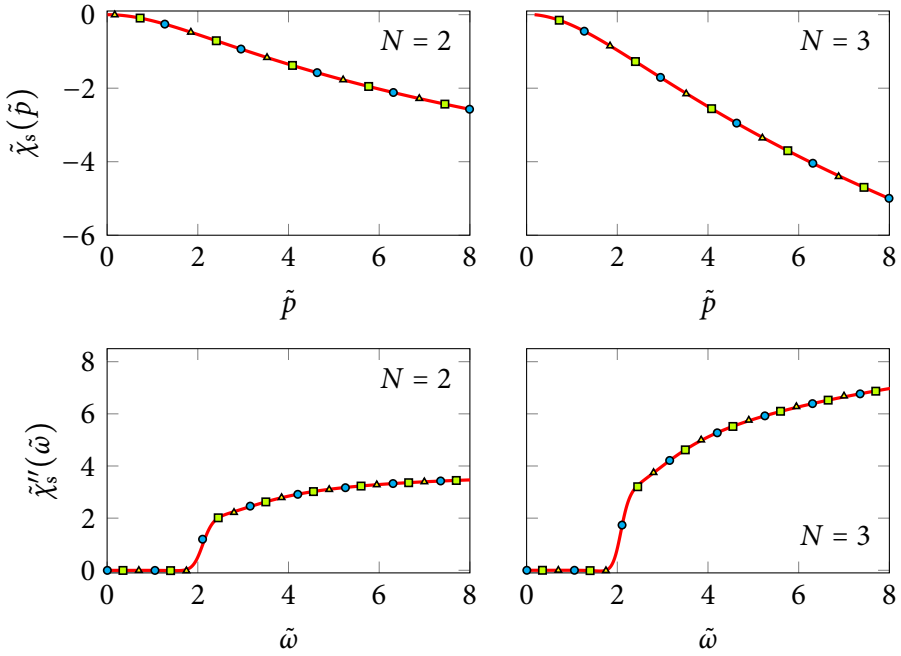

Figure 4.12: $\tilde{\chi}_s(\tilde{p})$ and $\tilde{\chi}_s''(\tilde{\omega})$ in the disordered phase for $N = 2$ and $N = 3$. The solid lines and symbols correspond to different values of $r_0 - r_{0c}$. We use arbitrary units.

N		3	2
NPRG BMW		2.7	2.2
NPRG	[97]		2.4
MC	[96]	2.2(3)	2.1(3)
QMC	[95]		3.3(8)
Perturbative RG	[98]	1.64	1.67
Lattice QMC	[99]	2.6(4)	
Exact diagonalization	[100, 101]	2.7(7)	2.1(2)

Table 4.2: Universal ratio m_H/Δ obtained from the NPRG in the BMW approximation. Also shown are previous less precise NPRG results [97] as well as results obtained from (Q)MC [95, 96, 99], perturbative RG [98] and exact diagonalization [100, 101].

Ordered phase

In Fig. 4.13 we show $\tilde{\chi}_s(\tilde{p})$ and $\tilde{\chi}_s''(\tilde{\omega})$ in the ordered phase for $N = 2$ and $N = 3$. Again, we observe data collapse in agreement with the scaling forms (4.38). For $N = 2$, we find a well-defined Higgs resonance whose position $\omega = m_H$ and full width at half-maximum vanishes as the QCP is approached. For $m_H \ll \omega \ll p_G$, we recover the critical scaling $\chi_s''(\omega) \sim \omega^{3-2/\nu}$. Up to a nonuniversal multiplicative factor the shape of the resonance, given by the universal scaling function χ_s'', is in very good agreement with the MC result of [62, 96]. The Higgs resonance is still visible, although less pronounced, for $N = 3$. This observation disagrees with previous less precise NPRG results [97] but agrees with the MC simulations of [62]. The universal ratio m_H/Δ, shown in Table 4.2, is compatible with the MC estimates of [62, 96]. Since in the ordered phase we must

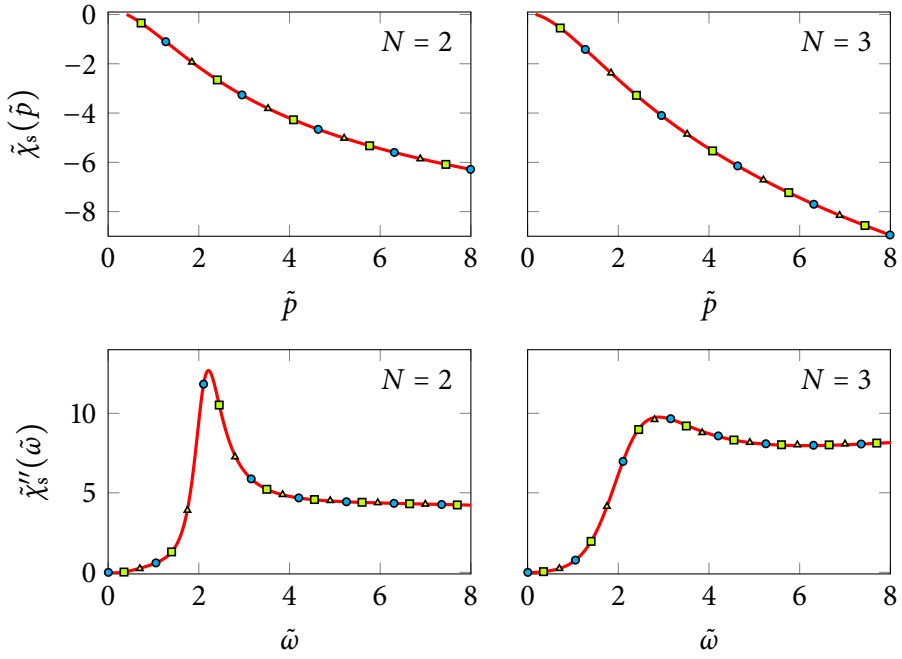

FIGURE 4.13: Spectral functions $\tilde{\chi}_s(\tilde{p})$ and $\tilde{\chi}_s''(\tilde{\omega})$ in the ordered phase for $N = 2$ and $N = 3$. The solid line and the symbols correspond to different values of $r_0 - r_{0c}$. We use arbitrary units for χ_s.

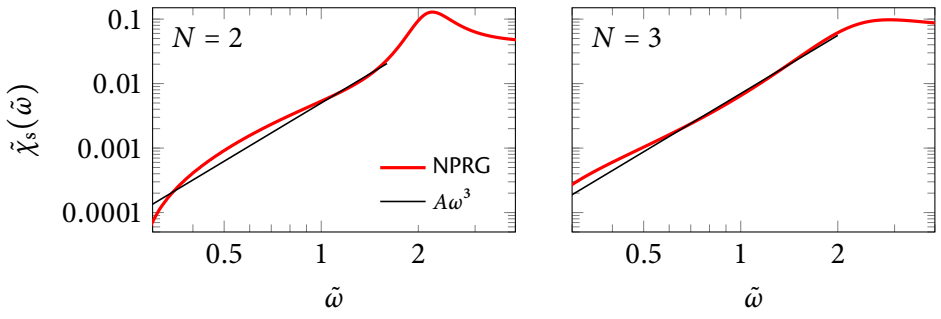

FIGURE 4.14: Log-log scale plot of $\tilde{\chi}_s''(\tilde{\omega})$ in the ordered phase for $N = 2$ and $N = 3$, showing the asymptotic behavior $\tilde{\chi}_s''(\tilde{\omega}) \sim \tilde{\omega}^3$ at low energies. We use arbitrary units.

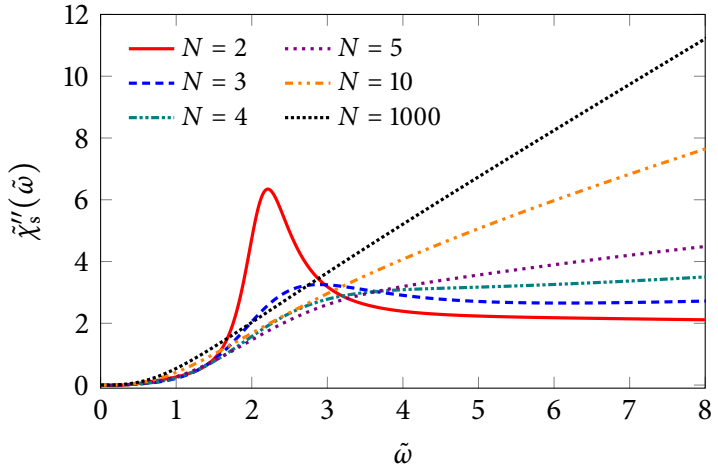

Figure 4.15: Spectral function $\tilde{\chi}''_s(\tilde{\omega})$ for various values of N in the ordered phase. We use arbitrary units for $\tilde{\chi}_s$ and the susceptibilities are rescaled by $1/N$.

stop the flow at a finite value $k_{\min}$, we cannot calculate reliably the spectral function $\chi''_s(\omega)$ for frequencies $\omega \lesssim k_{\min}$. Although for $k_{\min} \lesssim \omega \lesssim m_H$, our results are compatible with $\chi''_s(\omega) \sim \omega^3$ (see Fig. 4.14), the low-energy regime $\omega \ll \Delta$ where the spectral function is completely determined by the Goldstone modes is difficult to access. In Fig. 4.15 we show $\tilde{\chi}''_s(\tilde{\omega})$ for $N = 2, 3, 4, 5, 10, 1000$. Only for $N = 2$ and (to some extent) $N = 3$ does a Higgs resonance exist.

Finally we show the longitudinal susceptibility $\tilde{\chi}_L(\tilde{p})$ and its spectral function $\tilde{\chi}''_L(\tilde{\omega})$ in Fig. 4.16 for $N = 2$ and $N = 3$. For $\mathbf{p} \to 0$, the longitudinal susceptibility $\chi_L(\mathbf{p})$ diverges as $1/p$ as expected for a two-dimensional system[6] (see Fig. 4.17). This effect prevents the observation of a well-defined Higgs resonance in $\chi''_L(\omega)$. Nevertheless a broad peak, presumably due to the Higgs mode, can be seen for $\omega \sim m_H$ when $N = 2$ as evidenced in Fig. 4.16 (the position of the peak is observed at $\omega < m_H$ as expected). For $N = 3$, the peak has disappeared but a faint structure can still be seen.

4.1.5 Overview

We have studied the scalar and longitudinal susceptibilities in the quantum O(N) model using the NPRG. Comparison with QMC simulations [62, 94–96, 99], $\epsilon = 4 - D$ expansion [98] and exact diagonalization [100, 101] allows us to identify robust properties of the Higgs mode.

In the ordered phase, there is a well-defined Higgs resonance for $N = 2$ and to some extent for $N = 3$. The spectral function $\chi''_s(\omega)$ has been determined both from QMC and NPRG. Although, at the time of our study, there was some controversy regarding the value of the universal ratio m_H/Δ, our results and those of posterior studies (referenced in Table 4.2) seem to indicate that its value is close to 2.2 for $N = 2$ and 2.7 for $N = 3$, with a 10% uncertainty. In the disordered phase, there is no Higgs-like peak in $\chi''_s(\omega)$ above the absorption threshold.

There are two other important properties obtained from the NPRG that have not been studied with MC or other methods so far. First, the Higgs resonance is suppressed for $N \geq 4$. Second, for $N = 2$ the Higgs mode manifests itself in the longitudinal spectral function $\chi''_L(\omega)$ by a very broad peak.

[6] For $N = 2$, a numerical fit of $\tilde{\chi}''_L(\tilde{\omega})$ gives an exponent close to 0.8 instead of 1. A possible explanation is that the $\tilde{\chi}''_L(\omega) \sim 1/\tilde{\omega}$ behavior is only visible at lower frequencies where our procedure fails.

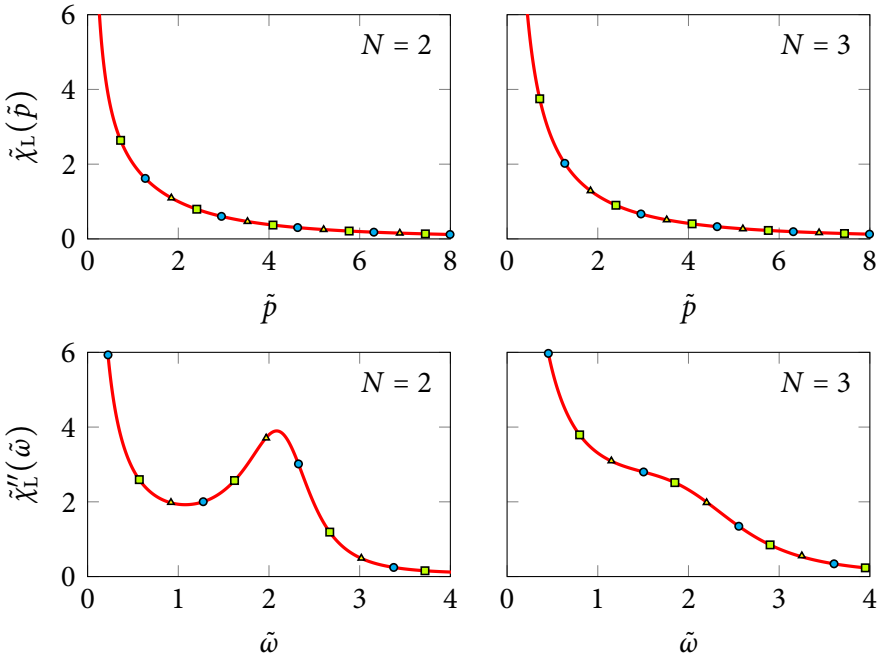

FIGURE 4.16: $\tilde{\chi}_{\mathrm{L}}(\tilde{p})$ and $\tilde{\chi}''_{\mathrm{L}}(\tilde{\omega})$ in the ordered phase for $N = 2$ and $N = 3$. The solid line and the symbols correspond to different values of $r_0 - r_{0\mathrm{c}}$.

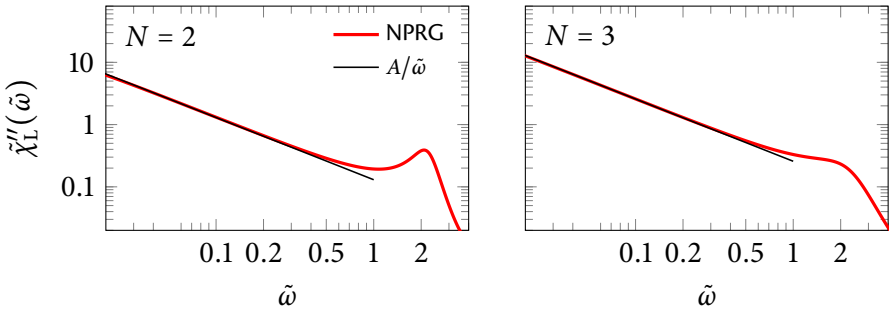

FIGURE 4.17: Log-log scale plot of $\tilde{\chi}''_{\mathrm{L}}(\tilde{\omega})$ in the ordered phase for $N = 2$ and $N = 3$, showing the asymptotic behavior $\tilde{\chi}''_{\mathrm{L}}(\omega) \sim 1/\omega$ at low energies.

As a final remark, let us mention some experimental results. The study of the Higgs mode in two dimensions remains a thoroughly investigated experimental topic. First, it has been indirectly observed in an ultracold atoms setting [10], where a resonance at finite energy is measured but the full response function remains inaccessible. It has been observed in superconducting films near a disorder-induced superconductor-insulator transition (SIT) [102], where its signature lies in the dynamical conductivity.[7] Alternatively, it has sparked recent attention in two-dimensional antiferromagnets [4, 5, 103]. In these experiments, the system can be tuned close to criticality

[7] A disordered superconductor may be described by a network of superconducting islands separated by weak links. The transition occurs at a critical value of disorder above which the system loses global phase coherence and becomes insulating, while the local superconducting order parameter remains finite. The relevant degree of freedom is the phase, and the transition belongs to the quantum O(2) universality class. We further discuss the SIT in Chapter 5.

and the spectral function χ_s'' is determined, although the agreement with our prediction remains qualitative. As only the ordered phase is studied no value of m_H/Δ is given. Lastly, we note that the Higgs mode has been observed in a Bose–Einstein condensate coupled to two optical cavities, which realize the O(2) model [104]. As all sites are coupled, the model is effectively infinite-dimensional; in that case the theory is described by mean-field. Nonetheless, the authors are able to observe the real-time dynamics of the model, and determine the Higgs spectral function in the whole phase diagram, recovering the mean-field value of $m_H/\Delta = \sqrt{2}$.

4.2 Bound states of the Ising model

Let us now turn our attention to the Ising model, the universality class of which is described by the φ^4 theory, the O(N) model for $N = 1$ (in which case the vector field $\boldsymbol{\varphi}$ reduces to a scalar). As the $O(1) \simeq Z_2$ symmetry is not a continuous symmetry, the physics of the ordered phase are radically different than that of the O($N > 1$) models. The Mermin–Wagner theorem is no longer valid. The lower critical dimension of the classical model is 1 and, in the two-dimensional quantum model, the ordered phase survives at low temperatures. There are no Goldstone modes in the ordered phase, which is fully gapped. We shall now study more accurately the excitation structure of the model, close to the criticality, and, in particular, we will focus on the bound states of the model. Their existence is made possible by the fact that the spectrum is gapped.

Bound states are excitations made of several quasi-particles with negative interaction energy and which therefore do not decay into elementary excitations. A common case of bound states in condensed matter physics is given by Cooper pairs in a superconductor. Low dimensional quantum systems, such as one-dimensional antiferromagetic spin chains [105] and ladders [106–109] are known to present bound states. Bound states are also important in the theory of nuclear forces [55, 110] and in quantum chemistry [111]. Focusing on strongly correlated systems, bound states arise in the theory of strong nuclear interactions, QCD [112, 113] and in strongly correlated electrons systems [89, 114, 115].

In the vicinity of its phase transition, the φ^4 field theory brings a simple example of a strongly correlated system. At low temperatures for the classical model, i.e. for large negative values of the φ^2 coupling, a hand-waving argument predicts the existence of a bound state. Consider a lattice ferromagnetic Ising model deep in the ordered phase. In the ground state all spins point in the same direction. A single-particle excitation is fabricated by flipping a single spin, with an energy (in units of the nearest-neighbor coupling) $\Delta = z$, the lattice connectivity. By flipping a second spin, one creates another excitation with a total energy $2\Delta = 2z$. If the second excitation is adjacent to the first one, there are two less frustrated links (one for each spin) and the energy of the excitation is lowered to $M = 2z - 2$: the two excitations form a stable bound state, whose energy threshold is below the multi-particle continuum. This argument explicitly depends on the microscopic structure of the model and is obviously not valid in the critical regime. In the following we study the fate of the bound state near the phase transition. We recall that, at the transition, the single-particle gap vanishes. Assuming the bound state remains an excitation of the system, its energy also vanishes. However, the ratio M/Δ of the bound state energy to that of the single-particle excitation is a universal number.

In the quantum $1+1$ case, or equivalently in the classical model with two spatial dimensions, the integrability of the Ising model allows one to completely determine the bound state spectrum [116, 117]. These results stem from the conformal invariance of the theory at criticality. In the language of the classical model, at criticality and in the presence of a small magnetic field, seven bound states

are known to exist, two of them lying below the multiple particle threshold.[8] The ratio between the energy of the first bound state and the single-particle gap is the universal number $(1+\sqrt{5})/2$, which has been experimentally observed in one-dimensional quantum magnets [2].

For the Ising model in three dimensions, the presence of a bound state in the symmetry-broken phase close to criticality has been first detected by MC simulations [118, 119] which predicted the ratio M/Δ of the energy of the bound state over the single-particle gap to be about 1.8. This prompted the use of resummed perturbative calculations by means of a Belthe–Salpeter equation, where the leading order yields 1.828, a result compatible with MC values [120, 121]. However, the series is ill-behaved and the next-to-leading order leads to an unphysical value $M/\Delta < 0$, suggesting a strongly nonperturbative behavior for the ratio. The bound state was also detected in the two-dimensional quantum Ising model at zero temperature within perturbation theory [122] and in an exact diagonalization study [123] which predicted $M/\Delta = 1.84$.

We shall now present a nonperturbative determination of the bound states in the symmetry broken phase of the φ^4 theory, for dimensions between $D = 2$ and 4. Excitations manifest themselves as poles on the imaginary axis in the two-point correlation function $\chi(\mathrm{i}\omega_n) = \chi(\mathbf{p} = 0, \mathrm{i}\omega_n) = \langle \varphi(0,\mathrm{i}\omega_n)\varphi(0,-\mathrm{i}\omega_n)\rangle_c$ (we adopt the quantum formalism). In the infrared, it behaves as

$$\chi(\mathrm{i}\omega_n) \underset{\omega_n\to 0}{\simeq} \frac{\mathcal{A}_1}{\omega_n^2+\Delta^2} + \frac{\mathcal{A}_2}{\omega_n^2+M^2} + \cdots, \tag{4.63}$$

and the bound states can be seen as peaks in the spectral function $\chi''(\omega)$. One thus needs to determine the correlation function at finite frequencies which is an important source of difficulty. It can be shown that at any finite order of perturbation theory around a free theory the ratio M/Δ can only be an integer [121], forbidding the observation of bound states. This problem remains in the approximation schemes within NPRG where a gradient expansion is performed, e.g. LPA and DE. This leads us to use the BMW formalism.

The remainder of this Section is organized as follows. In Section 4.2.1 we present the BMW formalism applied to the study of the bound states, the numerical solution of the flow equations, and the analytic continuation, before discussing the results in Section 4.2.2.

4.2.1 BMW formalism and numerical procedure

The BMW procedure is exactly that detailed in Section 2.3.4. In that Section, the procedure is given for the $\mathrm{O}(N>1)$ model, where the propagator has two components (transverse and longitudinal). In the φ^4 theory there are no transverse fluctuations and the propagator is a simple scalar, with no internal $\mathrm{O}(N)$ matrix structure. The two-point vertex is defined by

$$\Gamma^{(2)}(\mathbf{p},\rho) = p^2(1+Y(\mathbf{p},\rho)) + W(\rho) + 2\rho W'(\rho), \tag{4.64}$$

and the susceptibility is the propagator evaluated at the minimum of the potential,

$$\chi(\mathrm{i}\omega_n) = G(\mathrm{i}\omega_n,\rho_0) = [\Gamma^{(2)}(\mathrm{i}\omega_n,\rho_0)]^{-1}. \tag{4.65}$$

One constructs a k-dependent theory by adding to the microscopic action the regulator term $\int_{\mathbf{q}} \frac{1}{2}\varphi(\mathbf{q})R_k(\mathbf{q})\varphi(-\mathbf{q})$. By performing the BMW approximation on $\Gamma_k^{(3)}$ and $\Gamma_k^{(4)}$ one obtains flow equations for W_k and Y_k. Note that the flow equations can also be determined from the $\mathrm{O}(N)$

[8] At the critical point in the absence of magnetic field there is no bound state.

model in the limit $N \to 1$, in which case $\Gamma_k^{(2)}$ is given by $\Gamma_{A,k} + 2\rho\Gamma_{B,k}$ and Y_k by $Y_{A,k} + 2\rho Y_{B,k}$. The flow equations for W_k, $Y_{A,k}$ and $Y_{B,k}$ are given by Eqs. (2.63) and (4.43), see also [45, 72]. The adimensionning of the variables and functions and definition of η_k are the same as that explained in Section 2.3.2, again using the transverse part of the propagator Γ_A. That procedure had been previously used to determine the momentum-dependent correlation function of the Ising model at criticality and in the disordered phase [45].

If one neglects the nontrivial momentum dependence and set Y to only depend on ρ, in the ordered phase, $\chi^{-1}(\omega_n)$ only vanishes for $\omega_n = \pm i\Delta_0$,

$$\Delta_0 = \sqrt{2\rho_0 W_{k=0}(\rho_0)/Y_{k=0}(\rho_0)}. \tag{4.66}$$

In that case Δ_0 is the excitation gap and there are no bound states. Within the BMW approximation, this is no longer true and bound states may exist. The actual energy Δ of the elementary excitation is close to (but, unlike what happens for $N > 1$, not equal to) Δ_0. We keep Δ_0 as a useful energy scale as it needs not be extracted by analytic continuation.

The flow equations are integrated numerically using an explicit Euler method with a time step $\delta t = 10^{-4}$. For the momentum dependence of $\tilde{Y}_k(\tilde{p}, \tilde{\rho})$ we use a Chebyshev pseudo-spectral approximation (see [124]) while the ρ dependence is tackled with finite elements. We study the momentum dependence for $\tilde{p} \leq \tilde{p}_{\max} = 10$ and keep from 20 to 50 Chebyshev polynomials, and the $\tilde{\rho}$ dependence for $\tilde{\rho} \leq \tilde{\rho}_{\max} = 10$–$14$ with a step size $\delta\tilde{\rho} = 0.1$. We use the exponential regulator (2.23) and vary α to verify the stability of the results. Integrals are computed following the Gauss-Legendre method, see Appendix A.2. A good numerical accuracy is needed for $D < 3$.

As in the study of the Higgs mode, we estimate the function $\Gamma^{(2)}_{k=0}(\mathbf{p}, \rho_0)$ using the approximation

$$\Gamma^{(2)}_{k=0}(\mathbf{p}, \rho_0) \simeq \Gamma^{(2)}_{k=p/\tilde{p}_{\max}}(\mathbf{p}, \rho_0). \tag{4.67}$$

Since we study the ordered phase, we encounter at $k \ll \Delta_0$ an instability due to the approach to the convexity of the potential. We deal with this issue the same way we do in the study of the Higgs mode, by switching to a dimensionful grid for ρ and removing small values of ρ for which $W_k(\rho)$ is too negative, see Appendix A.2.1. This method allows us to integrate the flow down to $k \simeq 0.1\Delta_0$.

Once the flow is integrated, we perform the analytic continuation $i\omega_n \to \omega + i0^+$ by approximating $\chi(i\omega_n)$ by a Padé approximant, see Appendix A.2.2. We typically use 30 to 50 evenly spaced points between $\omega_{\min} \sim \Delta_0$ and $\omega_{\max} \sim 10\Delta_0$ to determine an even in ω_n approximant, which is then exactly analytically continued to the real axis.

For a given determination of the response function $\chi(i\omega_n)$, we show in Fig. 4.18 several Padé approximants in Euclidean space. Some special care is required when analyzing the results thus obtained; indeed, as we are investigating a rather subtle effect in the spectral function (a subleading lorentzian), the results tend to be more sensitive to the approximations made. To check the validity of this method, we vary the parameters N, $\omega_{\min}$ and $\omega_{\max}$ and compare about 20 different approximants. While they all (almost) coincide for imaginary frequencies, they vary a lot more when analytically continued, a signature of the fragility of the Padé procedure with respect to numerical errors. All approximants show a remarkable agreement for the pole at ω/Δ_0 close to $0.75\Delta_0$, corresponding to the single-particle excitation energy Δ where all curves are superimposed at this pole. Among the approximants, we eliminate those that exhibit unphysical spurious behavior, such as an additional pole at an energy $\omega \ll \Delta$, or a splitting of the gap pole into two peaks of energy around Δ. Furthermore, we eliminate approximants which present a gap more than 1% different

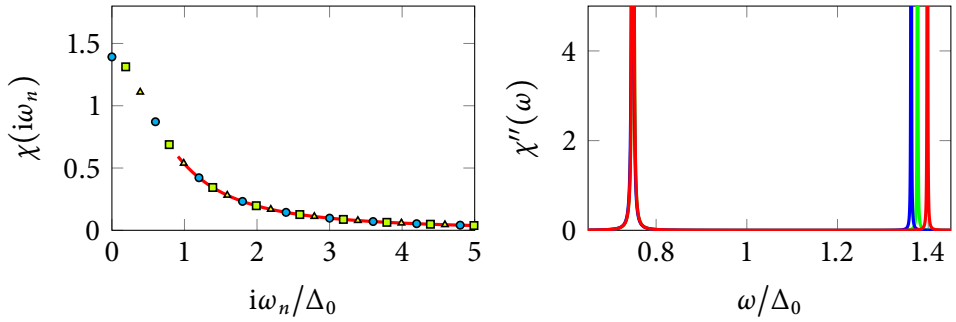

FIGURE 4.18: Comparison of three different Padé approximants of (left) $\chi(i\omega_n)$ and (right) $\chi''(\omega)$ in $D = 3$. Left: we show in arbitrary units $\chi(i\omega_n)$ (full red line) as well as its fit by three approximants (symbols). Right: the spectral function in arbitrary units obtained from the analytic continuation of these approximants. The three approximants show two poles, one at a frequency $\Delta \simeq 0.75\Delta_0$ whose position is very stable and one other at a frequency $M \simeq 1.3$–1.4Δ whose position depends slightly on the approximants.

from the others. Depending on the dimension, between one fourth $(D = 3)$ and one half $(D = 2)$ of the Padé approximants are rejected this way.

We observe that all the selected approximants present a single second pole at an energy $M > \Delta$, the value of M varying slightly from approximant to approximant (from 2% in $D = 3$ to less than 10% for $D \lesssim 2.6$). Depending on the dimension, we find two possibilities. In the first case, $M \gtrsim 2\Delta$, and the pole corresponds to two single-particle excitations coupled to the multi-particle continuum implying that there are no stable bound states. (In that case, as we use Padé approximants even in p, it is impossible to observe the lifetime of the excitations.) In the second case $\Delta < M < 2\Delta$ and a stable bound state exists with energy M.

As an additional check of the accuracy of the analytic continuation, we have verified that the position of the poles varies smoothly with the dimensionality of the system.

4.2.2 Results and overview

Let us start by discussing the results obtained in $D = 3$, where a bound state is clearly present in the broken symmetry phase, and absent in the symmetric phase. The corresponding values of M/Δ are displayed in Fig. 4.19 (left) as a function of $r_0 - r_{0c}$, where r_{0c} is the value of the parameter r_0 which makes the model critical. For a given value of the reduced temperature (which we identify with $r_0 - r_{0c}$), the value of the ratio M/Δ varies slightly between different approximants, which is the origin of the error bars shown in the figure. To test the accuracy of the method, we have also studied the variation of the results with the parameter α in front of the regulator function. In all cases this variation turns out to be much smaller than the error bars stemming from the Padé procedure.

Both in the universal regime $r_0 \simeq r_{0c}$, as well as for smaller values of the quadratic coupling r_0 within the non-universal regime, the ratio does not appear to vary significantly with r_0. Using a conservative error bar, we find $M/\Delta = 1.82(2)$, in agreement with previous results: 1.83(3) for Monte Carlo [119], 1.828(3) for the first order approximation of the Bethe-Salpeter equation [121], 1.84(3) for the results of perturbative continuous unitary transformations, and 1.84(1) for the most recent and accurate results from numerical diagonalization methods [123].

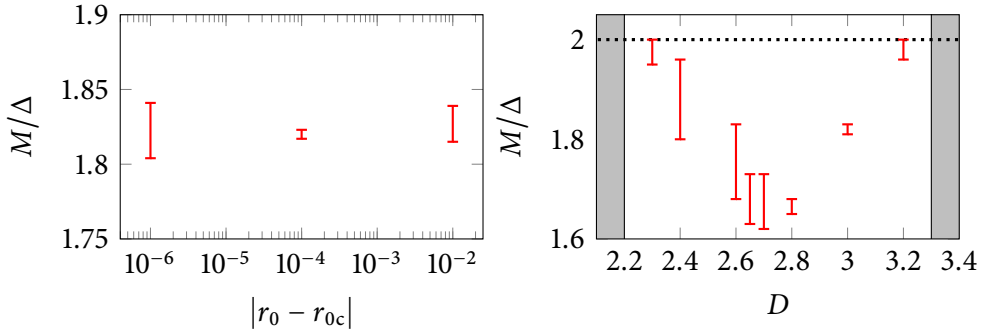

Figure 4.19: Left: values of the ratio M/Δ in $D = 3$ for several values of the reduced temperature, corresponding to different values of $r_0 - r_{0c}$ measuring the distance to criticality. For each temperature, the error bar indicates the extremal possible values obtained from the Padé approximants. Right: values of the ratio M/Δ in the critical regime for various dimensions. For each dimension, the error bar indicates the extremal possible values obtained from the Padé approximants. The shaded areas denotes the range of dimensions for which it is certain there are no bound states.

Next, we study the evolution of value of the M/Δ ratio at criticality as a function of the dimension, for $2 \leq D \leq 4$. The ratio is a smooth function of the dimension, as shown in Fig. 4.19 (right). It is found that there exists an upper and lower dimension, $D_{\mathrm{BS}}^{-} \sim 2.2$–$2.3$ and $D_{\mathrm{BS}}^{+} \sim 3.2$–$3.3$, such that for $D_{\mathrm{BS}}^{-} < D < D_{\mathrm{BS}}^{+}$ there is a bound state, whereas for dimensions outside this interval, there is none. This is consistent with the fact that there are no bound states in $D = 2$ in the absence of a magnetic field [117]. Furthermore, it shows that no bound state is to be expected in dimension $D = 4$.

We recall that for $N > 1$, due to the presence of gapless Goldstone modes, the existence of stable bound states is ruled out. This is confirmed by our determination of the longitudinal susceptibility in the ordered phase in $D = 3$ presented in Section 4.1.4.

To summarize, we studied the existence of a bound state in the φ^4 scalar theory in all dimensions between $D = 2$ and $D = 4$, and for a range of temperatures below the critical point. For $D = 3$, our results are within 1% of the previous Monte Carlo and numerical diagonalization values, using the BMW approximation of the Non-Perturbative Renormalization Group, which allows for the determination of the full-momentum dependence of the spectral function both in the universal and nonuniversal regimes. These results show once again the power of the BMW approximation for dealing with non-trivial physics at arbitrary momentum scales, even in cases where the quantities of interest require to perform analytic continuations of numerical data.

5

Transport

Hope clouds observation.

— F. Herbert, *Dune*.

In this Chapter, we study the transport properties of the O(N) model. Indeed, for $N \geq 2$, the O(N) symmetry is a continuous symmetry and there are associated conserved charges, and thus, currents. In the critical regime, near the zero-temperature QCP, the corresponding conductivity takes the form of a universal function, the determination of which has been a longstanding question [89]. Its behavior in the quantum critical regime remains mysterious to this day.

To go beyond perturbation theory, three approaches, each with its own strengths and weaknesses, have been used so far: Quantum Monte Carlo simulations [62, 125–130] (QMC), conformal field theory (CFT) methods [128, 130–133], and holographic models [128, 129, 133–136] based on the AdS/CFT correspondence. We provide here a NPRG approach to determine the conductivity at zero-temperature, a first step towards its study at finite temperature.

The outline of this Chapter is the following. In Section 5.1, we introduce the conductivity of the quantum O(N) model and give its definition, before discussing its general properties, based on symmetry and scaling considerations, in Section 5.2. Finally, in Section 5.3, we present a NPRG scheme to compute the conductivity in the critical regime, and present and compare our results with the literature.

Part of the work presented in this Chapter has been published [32, 137].

5.1 Introduction and definitions

We recall that the two-dimensional quantum O(N) model is defined at zero temperature by the (Euclidean) action

$$S = \int_{\mathbf{x}} \frac{1}{2}(\partial_\mu \boldsymbol{\varphi})^2 + \frac{r_0}{2}\boldsymbol{\varphi}^2 + \frac{u_0}{4!N}(\boldsymbol{\varphi}^2)^2, \tag{5.1}$$

where $\boldsymbol{\varphi}(\mathbf{x})$ is an N-component real field, $\mathbf{x} = (\mathbf{r}, \tau)$ with $\mathbf{r}$ a two-dimensional coordinate, τ an imaginary time and we set $\hbar = k_B = 1$. (In the following, we derive some expressions for generic dimensions d; for applications we set d to 2.) r_0 and u_0 are temperature-independent coupling constants and the (bare) velocity of the $\boldsymbol{\varphi}$ field is set to one. The model is regularized by an ultraviolet cutoff Λ. In order to maintain the Lorentz invariance of the action at zero temperature, it is natural to implement a cutoff on both momenta and frequencies.

In this Section, we define the conserved charge associated to the $\mathrm{O}(N)$ conductivity. For $N \geq 2$, the symmetry is continuous and there are indeed conserved charges and associated currents, as stated by the Noether theorem. The physical interpretation of these conserved quantities — an internal angular momentum — is not straightforward. For that reason, we chose to first present it with the Hamiltonian formulation in Section 5.1.1, before redefining it in the more convenient for us field-theoretical language in Section 5.1.2 and defining the conductivity from the linear response theory in Section 5.1.3.

5.1.1 Hamiltonian formulation

We recast the action (5.1) into a quantum Hamiltonian formulation. We start by going back to real time. The Lagrangian of the theory reads

$$L = \int \mathrm{d}^d\mathbf{r}\, \mathcal{L}, \qquad \mathcal{L} = \frac{1}{2}(\partial_t \boldsymbol{\varphi})^2 - \frac{1}{2}(\nabla\boldsymbol{\varphi})^2 - U(\boldsymbol{\varphi}^2/2) \tag{5.2}$$

with $\mathcal{L}$ the Lagrangian density and U the potential. The momentum $\boldsymbol{\pi}$ conjugate to the field $\boldsymbol{\varphi}$ is defined as

$$\boldsymbol{\pi}(\mathbf{r}) = \frac{\partial \mathcal{L}}{\partial[\partial_t \boldsymbol{\varphi}(\mathbf{r})]} \tag{5.3}$$

and the Hamiltonian is given by

$$H = \int \mathrm{d}^d\mathbf{r}\, [\boldsymbol{\pi}\cdot\partial_t\boldsymbol{\varphi}] - L = \int \mathrm{d}^d\mathbf{r}\, \frac{1}{2}\boldsymbol{\pi}^2 + \frac{1}{2}(\nabla\boldsymbol{\varphi})^2 + U(\boldsymbol{\varphi}^2/2). \tag{5.4}$$

With canonical quantization we promote this classical Hamiltonian to a quantum one,

$$\hat{H} = \int \mathrm{d}^d\mathbf{r}\, \frac{1}{2}\hat{\boldsymbol{\pi}}^2 + \frac{1}{2}(\nabla\hat{\boldsymbol{\varphi}})^2 + U(\hat{\boldsymbol{\varphi}}^2/2), \tag{5.5}$$

where $\hat{\boldsymbol{\varphi}}(\mathbf{r})$ is a N-component real operator field defined over a d-dimensional space and $\hat{\boldsymbol{\pi}}$ its conjugate field, $[\hat{\pi}_i(\mathbf{r}), \hat{\varphi}_j(\mathbf{r}')] = -\mathrm{i}\delta_{ij}\delta(\mathbf{r}-\mathbf{r}')$. The Hamiltonian is invariant under $\mathrm{O}(N)$ rotations in the internal space, $\hat{\boldsymbol{\phi}} \to \hat{\boldsymbol{\varphi}}' = O\hat{\boldsymbol{\varphi}}$, $\hat{\boldsymbol{\pi}} \to \hat{\boldsymbol{\pi}}' = O\hat{\boldsymbol{\pi}}$; the commutation relations are preserved. This incites to define an angular momentum, $\hat{L}(\mathbf{r}) = \hat{\boldsymbol{\pi}}(\mathbf{r}) \cdot T\hat{\boldsymbol{\varphi}}(\mathbf{r})$, where T is a skew symmetric matrix, by analogy with the angular momentum of a quantum particle $\hat{\mathbf{p}}\times\hat{\mathbf{r}}$. The conjugate variables $\hat{\boldsymbol{\varphi}}$ and $\hat{\boldsymbol{\pi}}$ play the role of position and momentum while T is analog to the cross product (we explain it further below in Section 5.1.2). As defined here, $\hat{L}$ is a scalar. However, as there are $N(N-1)/2$ possible independent choices for the skew-symmetric matrix T, there are as many conserved quantities.

Due to internal rotation symmetry, $\int \mathrm{d}\mathbf{r}\, \hat{L}$ commutes with the Hamiltonian and is thus a global conserved charge. Locally, its time evolution is given by the continuity equation

$$\frac{\partial \hat{L}}{\partial t} = \mathrm{i}[\hat{H}, \hat{L}] = -\nabla\cdot\hat{\mathbf{j}} \tag{5.6}$$

where we have defined the current $\hat{\mathbf{j}} = \nabla\hat{\boldsymbol{\varphi}}\cdot T\hat{\boldsymbol{\varphi}}$. Defining $\hat{j}_0 = \hat{L}$ and $\partial_0 = \partial_t$, the continuity equation is rewritten as

$$\partial_\mu \hat{j}_\mu = 0. \tag{5.7}$$

Let us now give interpretations of the current and conserved charge for $N = 2$ and 3. For $N = 2$, there is only one single independent skew-symmetric matrix, which can be chosen as minus the antisymmetric tensor ϵ_{ij}, and we find

$$\hat{j}_\mu = -\mathrm{i}[\hat{\psi}^* \partial_\mu \hat{\psi} - (\partial_\mu \hat{\psi}^*)\hat{\psi}], \tag{5.8}$$

where we define $\hat{\psi} = (\hat{\varphi}_1 + \mathrm{i}\hat{\varphi}_2)/\sqrt{2}$. We thus recover the standard expression of the current density of bosons described by a complex field $\hat{\psi}$. Remark that, however, the conserved charge, the density, is not given by the usual expression, $\hat{\psi}^*\hat{\psi}$, but rather by $-\mathrm{i}[\hat{\psi}^* \partial_\tau \hat{\psi} - (\partial_\tau \hat{\psi}^*)\hat{\psi}]$. This is due to the fact that the bosons display relativistic rather than Galilean invariance. For $N = 3$, the three possible choices for T are $T^{12} = -\mathrm{i}S^3$, $T^{13} = \mathrm{i}S^2$ and $T^{23} = -\mathrm{i}S^1$, where (S^1, S^2, S^3) are spin-one matrices: $\sum_i (S^i)^2 = 2$ and $[S^j, S^k] = \mathrm{i}\epsilon_{jkl} S^l$. The three angular momenta can be mapped to the coordinates of an angular momentum vector $\hat{\mathbf{L}}$ in the spin space and the current corresponds to a spin current, $j^i_\mu = -\mathrm{i}\epsilon_{ijk}(\partial_\mu \varphi_j)\varphi_k$. This expression agrees with the continuum limit of spin currents defined in lattice models [138]. This mapping does not hold for $N \geq 4$.

5.1.2 Gauge field

Having introduced the angular momentum and current in the Hamiltonian formulation, we now give it in the field theoretical formalism. The action of the D-dimensional $\mathrm{O}(N)$ model is invariant in the global rotation $\boldsymbol{\varphi}' = O\boldsymbol{\varphi}$ with $O \in \mathrm{SO}(N)$ a uniform rotation. We can make this global invariance a local one by introducing a gauge field A_μ in the action:

$$S = \int_{\mathbf{x}} \frac{1}{2}(\partial_\mu \boldsymbol{\varphi} - q A_\mu \boldsymbol{\varphi})^2 + \frac{r_0}{2}\boldsymbol{\varphi}^2 + \frac{u_0}{4!}(\boldsymbol{\varphi}^2)^2. \tag{5.9}$$

We set the charge q equal to unity in the following (it will be reintroduced in final expressions whenever necessary). A_μ is a $\mathbf{x}$-dependent skew-symmetric matrix of the Lie algebra $\mathrm{so}(N)$. It can be written as

$$A_\mu = A^a_\mu T^a, \tag{5.10}$$

where $\{T^a\}$ denotes a set of $\mathrm{so}(N)$ generators made of $N(N-1)/2$ linearly independent skew-symmetric matrices (see below). The action is invariant in the local gauge transformation

$$\boldsymbol{\varphi}' = O\boldsymbol{\varphi}, \qquad A'_\mu = O A_\mu O^T + (\partial_\mu O) O^T, \tag{5.11}$$

where O is a space-dependent $\mathrm{SO}(N)$ rotation. (Note that, *stricto sensu*, gauge invariance is satisfied only if it is not broken by the UV regularization. We shall assume here that this is the case and come back to this issue in Section 5.3.)

We do not consider A_μ as a dynamical gauge field but rather as a mere external source which allows us to define the current density

$$J^a_\mu(\mathbf{x}) = -\frac{\delta S}{\delta A^a_\mu(\mathbf{x})}. \tag{5.12}$$

To alleviate the notation we do not indicate the dependence of $J^a_\mu(\mathbf{x})$ on $\mathbf{A}$. From the action we obtain

$$J^a_\mu = j^a_\mu - A_\mu \boldsymbol{\varphi} \cdot T^a \boldsymbol{\varphi}, \qquad j^a_\mu = \partial_\mu \boldsymbol{\varphi} \cdot T^a \boldsymbol{\varphi}, \tag{5.13}$$

where j^a_μ and $-A_\mu \boldsymbol{\varphi} \cdot T^a \boldsymbol{\varphi}$ respectively denote the "paramagnetic" and "diamagnetic" parts of the current density. Eq. (5.13) can also be derived from Noether's theorem. In the two-dimensional quantum O(N) model, $\mathbf{j}^a = (j^a_x, j^a_y)$ corresponds to the current density (in the absence of external gauge field) defined in Section 5.1.1, whereas j^a_z, after a Wick rotation $z \equiv \tau \to \mathrm{i}t$, gives the conserved charge (angular momentum) density $L^a = -ij^a_z = -\partial_t \boldsymbol{\varphi} \cdot T^a \boldsymbol{\varphi}$ [89].

Lie algebra of rotation matrices

The skew-symmetric matrices $\{T^a\}$ can be chosen as any basis of the special orthogonal Lie algebra so(N). They satisfy the commutation relations

$$\left[T^a, T^b\right] = f_{abc} T^c, \tag{5.14}$$

which define the structure constants f_{abc}. The structure constants are real and antisymmetric under permutation of indices: $f_{abc} = -f_{bac} = -f_{cba}$, etc. A convenient basis of so(N), which we retain in the following, is

$$T^{IJ}_{ij} = -\delta_{I,i}\delta_{J,j} + \delta_{I,j}\delta_{J,i}, \tag{5.15}$$

where the integers I and J satisfy $1 \le I < J \le N$. T^{IJ} is the generator of rotations in the plane (I, J).

5.1.3 Linear response and conductivity

Now, we define the conductivity by the response function of the current to an external gauge field, in a similar manner as the conductivity in classical electrodynamics. To leading order in $\mathbf{A}$, the mean-value of the current density is given by

$$\left\langle J^a_\mu(\mathbf{x}) \right\rangle = \int_{\mathbf{x}'} K^{ab}_{\mu\nu}(\mathbf{x} - \mathbf{x}') A^b_\nu(\mathbf{x}') + O(A^2), \tag{5.16}$$

where

$$K^{ab}_{\mu\nu}(\mathbf{x} - \mathbf{x}') = \left. \frac{\delta^2 \ln \mathcal{Z}[\mathbf{A}]}{\delta A^a_\mu(\mathbf{x}) \delta A^b_\nu(\mathbf{x}')} \right|_{\mathbf{A}=0}, \tag{5.17}$$

with $\mathcal{Z}[\mathbf{A}]$ the partition function in the presence of the external gauge field. Differentiating twice the free energy gives

$$K^{ab}_{\mu\nu}(\mathbf{x} - \mathbf{x}') = \Pi^{ab}_{\mu\nu}(\mathbf{x} - \mathbf{x}') - \delta_{\mu\nu}\delta(\mathbf{x} - \mathbf{x}') \left\langle T^a \boldsymbol{\varphi} \cdot T^b \boldsymbol{\varphi} \right\rangle, \tag{5.18}$$

where

$$\Pi^{ab}_{\mu\nu}(\mathbf{x} - \mathbf{x}') = \left\langle j^a_\mu(\mathbf{x}) j^b_\nu(\mathbf{x}') \right\rangle \tag{5.19}$$

is the paramagnetic current-current correlation function.

In the quantum model, the response to a uniform time-dependent gauge field is given by $K^{ab}_{\mu\nu}(\mathrm{i}\omega_n) \equiv K^{ab}_{\mu\nu}(\mathbf{p} = 0, \mathrm{i}\omega_n)$ and the frequency-dependent conductivity is equal to

$$\sigma^{ab}_{\mu\nu}(\mathrm{i}\omega_n) = -\frac{1}{\omega_n} K^{ab}_{\mu\nu}(\mathrm{i}\omega_n). \tag{5.20}$$

The real-frequency conductivity is thus defined by

$$\sigma^{ab}_{\mu\nu}(\omega) = \frac{1}{\mathrm{i}(\omega + \mathrm{i}0^+)} K^{ab\,\mathrm{R}}_{\mu\nu}(\omega), \tag{5.21}$$

where $K^{ab\,\mathrm{R}}_{\mu\nu}(\omega) = K^{ab}_{\mu\nu}(\mathrm{i}\omega_n \to \omega + \mathrm{i}0^+)$ denotes the retarded part of $K^{ab}_{\mu\nu}(\mathrm{i}\omega_n)$.

For $N = 2$, the conductivity tensor reduces to a single component defined by the current-current correlation function obtained from the usual definition (5.8).

For $N = 3$, the conductivity can be interpreted as the response of the current to a time-dependent, spatially-uniform magnetic field gradient $\nabla H^a(\mathbf{r}, \tau)$:[1]

$$\left\langle J^a_\mu \right\rangle = \sigma^{ab}_{\mu\nu}(\omega)\partial_\nu H^b \tag{5.22}$$

To show that the definitions (5.20) and (5.22) are equivalent one uses gauge invariance to transform the space- and time-dependent magnetic field H^a into a spatially constant time-dependent gauge field A_μ [1]. The same formulation exists for $N \neq 3$ but in that case H^a can no longer be interpreted as a magnetic field.

5.2 Properties of the conductivity

Having defined the conductivity, we now discuss its properties. First, in Section 5.2.1, we use general considerations to express the components of the conductivity in both phases and define the universal scaling functions which characterize it. Then, in Section 5.2.2, we define the effective action formalism and derive Ward identities for the conductivity.

5.2.1 Generalities

We begin with some elementary remarks on the properties of conductivity. Due to space-time symmetry, the tensor is diagonal in space, $\sigma^{ab}_{\mu\nu}(\omega) = \delta_{\mu\nu}\sigma^{ab}(\omega)$. Furthermore, as a consequence of the $\mathrm{O}(N)$ invariance, the conductivity tensor is invariant under rotations in the skew-symmetric matrix space, as such a rotation can be compensated by a corresponding rotation in spin space. Because of this, there are at most two independent components to the conductivity tensor, just as there are at most two independent components to the propagator. We establish properly this statement in Section 5.2.2.

In the ordered phase, for $N \geq 3$ the conductivity tensor has two components, $\sigma_A(\omega)$ and $\sigma_B(\omega)$, corresponding respectively to generators of rotations acting on the order parameter $\bar{\boldsymbol{\phi}}$ (the rotation is said to belong to class A) and generators of rotations around the order parameter (class B generators), i.e.

$$T^a\bar{\boldsymbol{\phi}} \neq 0 \text{ for } a \in \text{class A}, \qquad T^a\bar{\boldsymbol{\phi}} = 0 \text{ for } a \in \text{class B}. \tag{5.23}$$

Assuming the order parameter lies along the first direction, $\bar{\phi}_i = \sqrt{2\rho_0}\delta_{1i}$ and using the basis (5.15), class A generators are the $N-1$ matrices T^{IJ} with $1 = I < J$ (generators of rotations in planes in which lays the order parameter) and class B generators are the $(N-1)(N-2)/2$ matrices T^{IJ} with $1 < I < J$ (generators of rotation in planes orthogonal to the order parameter). Remark that for a generic basis T^a the conductivity tensor is not necessarily diagonal. For $N = 2$ there is only one $\mathrm{so}(N)$ generator, which belongs to class A.

Since A_μ enters the action in the gauge invariant combination $D_\mu = \partial_\mu - A_\mu$, its scaling dimension at the QCP must be $[A_\mu] = [\partial_\mu] = 1$. From Eq. (5.17) it follows that $[K(\mathrm{i}\omega_n)] = d - 1$ and

[1] In the path integral formalism the magnetic field couples to the field through $\partial_\tau\varphi_i \to \partial_\tau\varphi_i - \mathrm{i}H^a T^a_{ij}\varphi_j$. H^a causes a precession of the $\boldsymbol{\varphi}$ field.

$[\sigma(\mathrm{i}\omega_n)] = d - 2$. For $d = 2$, in the vicinity of the QCP the conductivity satisfies the scaling form [139, 140]

$$\sigma(\omega) = \sigma_{\mathrm{Q}}\Sigma_{+}\left(\frac{\omega}{\Delta}\right), \qquad \sigma_{A,B}(\omega) = \sigma_{\mathrm{Q}}\Sigma_{-}^{A,B}\left(\frac{\omega}{\Delta}\right), \tag{5.24}$$

where $\Sigma_{\pm}$ is a universal scaling function, Δ a characteristic energy scale and the index $+/-$ refers to the disordered/ordered phase. Here, $\sigma_{\mathrm{Q}} = q^2/h$ is the quantum of conductance and q the charge; setting q to unity, $\sigma_{\mathrm{Q}} = 1/2\pi$ in natural units. As in Chapter 4, in the disordered phase Δ is the excitation gap, and in the ordered phase, we choose Δ to be given by the excitation gap at the point of the disordered phase located symmetrically with respect to the QCP (i.e., corresponding to the same value of $|r_0 - r_{0\mathrm{c}}|$). At the QCP, the universal scaling functions reach a nonzero limit $\Sigma_{\pm}(\infty)$; denoting $\sigma^* = \sigma(\omega \to 0, \Delta = 0) = \sigma_{\mathrm{Q}}\Sigma_{\pm}(\infty)$ the ratio $\sigma^*/\sigma_{\mathrm{Q}}$ is universal [139].

Let us now discuss qualitatively the low frequency ($\omega \ll \Delta$) behavior of the conductivity in both phases. In the disordered phase and at the QCP, the conductivity tensor has only one component (and is diagonal), as the system is rotationally invariant. The system is insulating and at low frequencies is expected to behave like a capacitor,

$$\sigma(\omega) = -\mathrm{i}\omega C_{\mathrm{dis}}. \tag{5.25}$$

Since in the ordered phase the system is superfluid-like, we may expect that one of the components of the current-current correlation function (i.e. K) has a finite limit at zero-frequency, equal to the superfluid stiffness [141]. Because of that, for class A generators at low frequencies,

$$\sigma_A(\omega) = \mathrm{i}\frac{\rho_{\mathrm{s}}}{(\omega + \mathrm{i}0^+)} = \rho_{\mathrm{s}}\left(\frac{\mathrm{i}}{\omega} + \pi\delta(\omega)\right), \tag{5.26}$$

with ρ_{s} the superfluid stiffness.[2] The system thus behaves as a perfect inductor,

$$\sigma_A(\omega) = \mathrm{i}\frac{1}{L_{\mathrm{ord}}(\omega + \mathrm{i}0^+)}, \tag{5.27}$$

with (by analogy with a superfluid) inductance

$$L_{\mathrm{ord}} = \frac{1}{\rho_{\mathrm{s}}} = \frac{\hbar}{2\pi\sigma_{\mathrm{Q}}\rho_{\mathrm{s}}}, \tag{5.28}$$

where we restore natural units in the second equality. Comparing the definitions of the capacitance (5.25) and inductance (5.27) with the scaling forms (5.24) one remarks that the ratios $C_{\mathrm{dis}}\Delta/\sigma_{\mathrm{Q}}$ and $1/L_{\mathrm{ord}}\Delta\sigma_{\mathrm{Q}}$ are universal in the critical regime; hence, at two symmetric points with respect to the transition the ratio $C_{\mathrm{dis}}/L_{\mathrm{ord}}\sigma_{\mathrm{Q}}^2$ is universal.

For $\sigma_B(\omega)$, the case is more complex; we shall see later that it reaches a finite limit σ_B^* in the low frequency regime, which is a universal number in units of σ_{Q} (as is σ^* at the QCP).

[2] This is true for $N = 2$ where the system is superfluid. For $N \geq 2$, class A generators play a similar role than the sole generator for $N = 2$, which is why we expect σ_A to take the form $\sigma_A(\omega) = \mathrm{i}\rho_{\mathrm{s}}/(\omega + \mathrm{i}0^+)$.

Vortex-charge duality

Inspired by the discussion in [11], we rephrase the above statements about the low-frequency limit of the conductivity in the terms of the superconductor-insulator transition in zero-temperature two-dimensional film systems (belonging to the universality class of the quantum O(2) model), to provide a physical picture. Near the transition, the low-energy physics is described by an effective bosonic Hamiltonian, the relevant degrees of freedom being the phase of the local superconducting order parameter. The effective model is that of a Josephson-junction array, with superconducting islands, separated by weak links where phase slips can occur. The transport properties are dominated by the behavior of the links.

Consider such a weak link, between two superconducting islands whose phases differ by θ. The source of resistance in the link is the presence of vortices, whose flow induces a voltage difference. The voltage across the weak link is given by the Josephson relation

$$V = \frac{\hbar}{q}\frac{\mathrm{d}\theta}{\mathrm{d}t} = \frac{h}{q}\Phi_{\mathrm{v}}, \tag{5.29}$$

where we use the fact that the rate of phase slip is proportional to the flux Φ_{v} of vortices across the link perpendicular to the current, each vortex carrying a phase slip of $\pm 2\pi$ (depending on its direction). The charge $q = 2e$ is that of a Cooper pair. The current is similarly given by the flow Φ_{C} of Cooper pairs between the electrodes,

$$I = q\Phi_{\mathrm{C}}, \tag{5.30}$$

so that the conductivity is

$$\sigma = \frac{I}{V} = \sigma_{\mathrm{Q}}\frac{\Phi_{\mathrm{C}}}{\Phi_{\mathrm{v}}}. \tag{5.31}$$

In the insulating phase there is no charge flow and the conductivity vanishes, while in the superconducting phase vortices bind together and there is no vortex flux: the conductivity is infinite. It is natural to assume that at the transition both charges and vortices are mobile and the conductivity σ^* is some number times σ_{Q}.

Furthermore, it turns out that there exist a duality transformation of the path integral description of the system which exchanges the role played by charges and vortices [139, 142]. That transformation maps the superconducting (ordered) phase of the particle model onto an insulating (disordered) phase for the vortices and, conversely, the insulating phase of the particle model is mapped onto a phase where vortices condense into a vacuum state. If the system were self-dual at the transition, i.e. invariant under this duality transformation, one would have $\Phi_{\mathrm{C}} = \Phi_{\mathrm{v}}$ and thus $\sigma^* = \sigma_{\mathrm{Q}}$. One does not expect the model to be self-dual at the transition: for instance, vortices interact with a logarithmic interaction whereas Cooper pairs interact via the Coulomb force. For a detailed discussion see [142]. The value of σ^* at the transition thus measures the closeness to self-duality. We shall see in Sections 5.2.5 and 5.3.3 that the value of $\sigma^*/\sigma_{\mathrm{Q}}$ is close to 0.35.

Finite temperature behavior

Let us briefly examine the finite temperature behavior of the conductivity, basing our remarks on [134, 140]. We confine the discussion to this Section and remain here purely qualitative, as we have not (up to now) devised a RG-based computation to study the conductivity at finite temperature.

At finite temperature a new energy scale, T, is introduced and the conductivity is defined by three scaling functions (one in the disordered phase and two, for class A and B generators, in the ordered phase) of two variables: $\sigma(\omega, T, r_0) = \sigma_Q \Sigma(\hbar\omega/\Delta, \hbar\omega/k_B T)$. It is especially important here to remark that the limits $\omega \to 0$, $\Delta \to 0$ and $T \to 0$ do not commute. Most theoretical approaches are done at zero temperature, and the function $\Sigma(x, \infty)$ is computed. For computations done at finite temperature in imaginary time (e.g. Monte Carlo), an analytic continuation $i\omega_n \to \omega + i0^+$ has to be done, and it is notoriously hard to determine the function for values $\omega \lesssim \omega_1 = 2\pi T$. However, in experiments, the temperature is always finite while the frequency can be arbitrarily small. An important theoretical issue is thus to determine the conductivity in the limit $\omega \ll T$ (the hydrodynamic, incoherent regime), i.e. the long-time response at finite temperature, which is *a priori* different from the large-frequency ($\Delta, T \ll \omega \ll \Lambda$) conductivity (the collisionless coherent regime).

In the case where a system whose excitations are weakly-interacting quasiparticles, the Boltzmann equation can be used to study transport. In the critical regime ($\Delta \ll T$) the system cannot be described in terms of quasiparticles and such an approach fails. To evidence this, let us concentrate on the case of the superfluid-insulator transition ($N = 2$), and let us try to extrapolate results from the quantum disordered and renormalized classical regimes to the quantum critical region.

In the insulating phase the system is gapped and has particle and hole excitations. The simplest picture is that the conductivity at finite temperature comes from the directed Brownian motion of the thermally excited particles and holes under an electric field. The motion is described by a Drude equation with a collision time τ_c, and at low frequencies the conductivity is given by

$$\sigma(\omega) = \frac{\sigma_0}{1 - i\omega\tau_c}. \tag{5.32}$$

Assuming (without justification) that this form holds in the critical regime (with a collision time determined by the only energy scale of the system, $\tau_c \sim T^{-1}$) one finds that the real part of the conductivity is a decreasing Lorentzian at small frequencies and at high frequencies reaches its zero-temperature quantum critical limit. However, the same approach can be done in the superfluid phase, using the duality mapping hinted at in the last Section to describe the system using the vortices as elementary degrees of freedom. In that description the system is an insulator whose primary (gapped) excitations are vortices. Following the same steps as in the disordered phase, one determines the conductivity of the vortices; at low frequencies it is given by Eq. (5.32). However, the physical conductivity of the underlying particle model is equal to the resistivity of the vortex-like particles [139, 142]. From this we expect the low-frequency conductivity at the quantum critical point to be roughly the inverse of Eq. (5.32), with $\sigma(\omega = 0)$ a local minimum.

Thus, depending on which regime we extrapolate the results from, there are two qualitatively incompatible predictions for the low-frequency behavior of $\sigma(\Delta \ll T, \omega \ll T)$. Although large-$N$ and dimensional expansion predict that the insulator scenario (particle-like transport) is valid, there has not been to this point a nonperturbative answer to decisively discriminate both scenarios. A Monte-Carlo study also hints towards the insulator scenario [126]. The work we present in this Chapter should be considered a stepping stone towards the determination of conductivity at finite temperature.

5.2.2 Effective action formalism

We proceed in a similar manner to what is done in Section 4.1.3 to define an effective action formalism suited to the determination of the Higgs mode. Let us consider the partition function

$$\mathcal{Z}[\mathbf{J},\mathbf{A}] = \int \mathcal{D}[\boldsymbol{\varphi}]\, \exp\left(-S[\boldsymbol{\varphi},\mathbf{A}] + \int_{\mathbf{x}} \mathbf{J}\cdot\boldsymbol{\varphi}\right) \tag{5.33}$$

in the presence of both the gauge field $\mathbf{A}$ and an external source $\mathbf{J}$ which couples linearly to the $\boldsymbol{\varphi}$ field. The action $S[\boldsymbol{\varphi},\mathbf{A}]$ is defined by Eq. (5.9). The order parameter is obtained from

$$\boldsymbol{\phi}[\mathbf{x};\mathbf{J},\mathbf{A}] = \frac{\delta \ln \mathcal{Z}[\mathbf{J},\mathbf{A}]}{\delta \mathbf{J}(\mathbf{x})}. \tag{5.34}$$

The effective action

$$\Gamma[\boldsymbol{\phi},\mathbf{A}] = -\ln \mathcal{Z}[\mathbf{J},\mathbf{A}] + \int_{\mathbf{x}} \mathbf{J}\cdot\boldsymbol{\phi} \tag{5.35}$$

is defined as the Legendre transform of $-\ln \mathcal{Z}[\mathbf{J},\mathbf{A}]$ with respect to the linear source $\mathbf{J}$, at fixed $\mathbf{A}$. Again, note the similarity with the effective action (4.24). Γ satisfies the equation of state

$$\frac{\delta\Gamma[\boldsymbol{\phi},\mathbf{A}]}{\delta\boldsymbol{\phi}(\mathbf{x})} = \mathbf{J}[\mathbf{x};\boldsymbol{\phi},\mathbf{A}]. \tag{5.36}$$

The effective potential $U(\rho) = (1/V)\Gamma[\boldsymbol{\phi},\mathbf{A}]|_{\boldsymbol{\phi}=\text{const.},\mathbf{A}=0}$ determines the thermodynamics, with $\rho = \boldsymbol{\phi}^2/2$ the $\mathrm{O}(N)$ invariant and ρ_0 the minimum of the potential. Correlation functions can be reconstructed from the one-particle irreducible (1PI) vertices defined by

$$\Gamma^{(n,m)\{a_j\}}_{\{i_j\},\{\mu_j\}}[\{\mathbf{x}_j\},\{\mathbf{y}_j\};\boldsymbol{\phi},\mathbf{A}] = \frac{\delta^{n+m}\Gamma[\boldsymbol{\phi},\mathbf{A}]}{\delta\phi_{i_1}(\mathbf{x}_1)\cdots\delta\phi_{i_n}(\mathbf{x}_n)\delta A^{a_1}_{\mu_1}(\mathbf{y}_1)\cdots\delta A^{a_m}_{\mu_m}(\mathbf{y}_m)}. \tag{5.37}$$

The correlation functions evaluated for $\mathbf{A}=0$ and in a uniform field configuration are determined by the vertices

$$\Gamma^{(n,m)\{a_j\}}_{\{i_j\},\{\mu_j\}}(\{\mathbf{x}_j\},\{\mathbf{y}_j\};\boldsymbol{\phi}) = \Gamma^{(n,m)\{a_j\}}_{\{i_j\},\{\mu_j\}}[\{\mathbf{x}_j\},\{\mathbf{y}_j\};\boldsymbol{\phi},\mathbf{A}]\Big|_{\boldsymbol{\phi}=\text{const.},\ \mathbf{A}=0}. \tag{5.38}$$

In particular, the (connected) propagator $G_{ij}(\mathbf{p},\boldsymbol{\phi}) = \langle\varphi_i(\mathbf{p})\varphi_j(-\mathbf{p})\rangle - \langle\varphi_i(\mathbf{p})\rangle\langle\varphi_j(-\mathbf{p})\rangle$ in a uniform field and for $\mathbf{A}=0$ is obtained from the matrix equation $G(\mathbf{p},\boldsymbol{\phi}) = \Gamma^{(2,0)-1}(\mathbf{p},\boldsymbol{\phi})$ where $\Gamma^{(2,0)}(\mathbf{p},\boldsymbol{\phi}) \equiv \Gamma^{(2,0)}(\mathbf{p},-\mathbf{p},\boldsymbol{\phi})$. The two independent components Γ_A and Γ_B of $\Gamma^{(2,0)}$, as well as the longitudinal (L) and transverse (T) parts of the propagator, are defined following Eqs. (2.17) and (2.18).

Conductivity from the vertices

The conductivity can be expressed in terms of the 1PI vertices. From Eqs. (5.17) and (5.35) we deduce

$$K^{ab}_{\mu\nu}(\mathbf{y}-\mathbf{y}') = \frac{\delta^2 \ln \mathcal{Z}[\mathbf{J},\mathbf{A}]}{\delta A^a_\mu(\mathbf{y})\delta A^b_\nu(\mathbf{y}')}\bigg|_{\mathbf{J}=\mathbf{A}=0} = -\frac{\bar\delta^2\Gamma[\boldsymbol{\phi}[\mathbf{A}],\mathbf{A}]}{\bar\delta A^a_\mu(\mathbf{y})\bar\delta A^b_\nu(\mathbf{y}')}\bigg|_{\mathbf{A}=0} \tag{5.39}$$

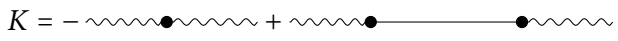

FIGURE 5.1: Diagrammatic representation of the conductivity kernel. Dots with n straight lines and m wavy lines stand for the vertex $\Gamma^{(n,m)}$ and full lines represent the propagator $G = \Gamma^{(2,0)-1}$.

where the order parameter $\boldsymbol{\phi}[\mathbf{A}]$ is defined by

$$\left.\frac{\delta\Gamma[\boldsymbol{\phi},\mathbf{A}]}{\delta\boldsymbol{\phi}(\mathbf{x})}\right|_{\boldsymbol{\phi}=\boldsymbol{\phi}[\mathbf{A}]} = 0. \tag{5.40}$$

Here $\bar{\delta}/\bar{\delta}A^a_\mu(\mathbf{y})$ is a total derivative which acts both on $\boldsymbol{\phi}[\mathbf{A}]$ and the explicit $\mathbf{A}$-dependence of the functional $\Gamma[\boldsymbol{\phi},\mathbf{A}]$. Following the same steps than in Section 4.1.3 [Eqs. (4.30) to (4.35)] one shows that

$$K^{ab}_{\mu\nu}(\mathbf{p}) = -\Gamma^{(0,2)ab}_{\mu\nu}(\mathbf{p},\bar{\boldsymbol{\phi}}) + \Gamma^{(1,1)a}_{i\mu}(-\mathbf{p},\bar{\boldsymbol{\phi}})\Gamma^{(2,0)-1}_{ij}(\mathbf{p},\bar{\boldsymbol{\phi}})\Gamma^{(1,1)b}_{j\nu}(\mathbf{p},\bar{\boldsymbol{\phi}}), \tag{5.41}$$

where $\bar{\boldsymbol{\phi}} = \boldsymbol{\phi}[\mathbf{A}=0]$ is the (uniform) order parameter in the absence of the gauge field and we use the notation $\Gamma^{(n,m)}(\mathbf{p}) \equiv \Gamma^{(n,m)}(\mathbf{p},-\mathbf{p})$ for both vertices $\Gamma^{(1,1)}$ and $\Gamma^{(0,2)}$. The second term in the right hand side of Eq. (5.41) corresponds to the part of $K^{ab}_{\mu\nu}$ which is not 1PI; we shall see that it does not contribute to the conductivity $\sigma^{ab}_{\mu\nu}(\omega)$ of the quantum model. Eq. (5.41) is shown diagrammatically in Fig. 5.1.

As in the case of $\Gamma^{(2,0)}$, one can take advantage of the symmetries of the model to write the vertices in the form

$$\Gamma^{(1,1)a}_{j\mu}(\mathbf{p},\boldsymbol{\phi}) = \mathrm{i}p_\mu(T^a\boldsymbol{\phi})_j\Psi_A, \tag{5.42}$$

$$\Gamma^{(0,2)ab}_{\mu\nu}(\mathbf{p},\boldsymbol{\phi}) = p_\mu p_\nu[\delta_{ab}\Psi_B + (T^a\boldsymbol{\phi})\cdot(T^b\boldsymbol{\phi})\Psi_C] + \delta_{\mu\nu}[\delta_{ab}\bar{\Psi}_B + (T^a\boldsymbol{\phi})\cdot(T^b\boldsymbol{\phi})\bar{\Psi}_C], \tag{5.43}$$

where $\Psi_A, \Psi_B, \Psi_C, \bar{\Psi}_B, \bar{\Psi}_C$ are functions of ρ and $\mathbf{p}^2$. This leads to

$$\begin{aligned} K^{ab}_{\parallel}(\mathbf{p}) = &-\delta_{ab}[\bar{\Psi}_B(\mathbf{p},\rho_0) + \mathbf{p}^2\Psi_B(\mathbf{p},\rho_0)] \\ &-(T^a\boldsymbol{\phi})\cdot(T^b\boldsymbol{\phi})[\bar{\Psi}_C(\mathbf{p},\rho_0) + \mathbf{p}^2\Psi_C(\mathbf{p},\rho_0) - \mathbf{p}^2 G_{\mathrm{T}}(\mathbf{p},\rho_0)\Psi_A(\mathbf{p},\rho_0)^2] \end{aligned} \tag{5.44}$$

and

$$K^{ab}_{\perp}(\mathbf{p}) = -\delta_{ab}\bar{\Psi}_B(\mathbf{p},\rho_0) - (T^a\bar{\boldsymbol{\phi}})\cdot(T^b\bar{\boldsymbol{\phi}})\bar{\Psi}_C(\mathbf{p},\rho_0), \tag{5.45}$$

where $K^{ab}_{\parallel}$ and $K^{ab}_{\perp}$ are the longitudinal and transverse components of $K^{ab}_{\mu\nu}$,

$$K^{ab}_{\mu\nu}(\mathbf{p}) = \hat{p}_\mu\hat{p}_\nu K^{ab}_{\parallel}(\mathbf{p}) + (\delta_{\mu\nu} - \hat{p}_\mu\hat{p}_\nu)K^{ab}_{\perp}(\mathbf{p}), \tag{5.46}$$

with $\hat{\mathbf{p}} = \mathbf{p}/|\mathbf{p}|$ a unit vector parallel to $\mathbf{p}$.

5.2.3 Ward identities

To further simplify the expression of $K^{ab}_{\mu\nu}$, we derive Ward identities for the conductivity. Indeed, the functions $\Psi_A, \Psi_B, \Psi_C, \bar{\Psi}_B, \bar{\Psi}_C$ are not independent but related. The effective action $\Gamma[\phi,\mathbf{A}]$ inherits from the symmetries of the microscopic action (5.9) and must therefore be invariant under the gauge transformation (5.11), $\Gamma[\boldsymbol{\phi}',\mathbf{A}'] = \Gamma[\boldsymbol{\phi},\mathbf{A}]$. For an infinitesimal transformation, i.e., $O = 1 + \theta^a T^a$ with $\theta^a \to 0$,

$$\boldsymbol{\phi}' = \boldsymbol{\phi} + \theta^a T^a\boldsymbol{\phi}, \qquad A^{a\,\prime}_\mu = A^a_\mu + \partial_\mu\theta^a + f_{abc}\theta^b A^c_\mu, \tag{5.47}$$

where we denote by f_{abc} the structure constants of the so(N) Lie algebra, see Eq. (5.14). Gauge invariance then implies, for all x and a and for any configuration of the fields,

$$\Gamma_i^{(1,0)}[\mathbf{x};\boldsymbol{\phi},\mathbf{A}](T^a\boldsymbol{\phi})_i - \partial_\mu \Gamma_\mu^{(0,1)a}[\mathbf{x};\boldsymbol{\phi},\mathbf{A}] - f_{abc}\Gamma_\mu^{(0,1)b}[\mathbf{x};\boldsymbol{\phi},\mathbf{A}]A_\mu^c = 0. \tag{5.48}$$

As a consequence of the gauge invariance, we obtain a local identity. Taking functional derivatives with respect to the fields and then setting $\mathbf{A}$ to zero and $\boldsymbol{\phi}$ uniform nets the Ward identities

$$\mathbf{p}^2\Psi_A(\mathbf{p},\rho) = \Gamma_A(\mathbf{p},\rho) - U'(\rho), \tag{5.49}$$
$$\mathbf{p}^2\Psi_B(\mathbf{p},\rho) + \bar{\Psi}_B(\mathbf{p},\rho) = 0, \tag{5.50}$$
$$\mathbf{p}^2\Psi_C(\mathbf{p},\rho) + \bar{\Psi}_C(\mathbf{p},\rho) = \Psi_A(\mathbf{p},\rho). \tag{5.51}$$

The first equation implies $\lim_{\mathbf{p}\to 0}\Psi_A(\mathbf{p},\rho) = Z(\rho)$ where the field renormalization $Z(\rho)$ is defined from the low-momentum behavior of $\Gamma^{(2,0)}$ by

$$Z(\rho) = \lim_{\mathbf{p}\to 0}\frac{\Gamma_A(\mathbf{p},\rho) - U'(\rho)}{\mathbf{p}^2} \tag{5.52}$$

Relations (5.49) to (5.51) imply that $K_{\mu\nu}^{ab}$ is transverse,

$$K_\parallel^{ab}(\mathbf{p}) = -(T^a\bar{\boldsymbol{\phi}})\cdot(T^b\bar{\boldsymbol{\phi}})\Psi_A(\mathbf{p},\rho_0)U'(\rho_0)G_{\mathrm{T}}(\mathbf{p},\rho_0) = 0, \tag{5.53}$$

where we have used $G_{\mathrm{T}}(\mathbf{p},\rho) = \Gamma_A(\mathbf{p},\rho)^{-1}$ and the fact that, depending on the phase, either $U'(\rho_0) = 0$ or $\bar{\boldsymbol{\phi}} = 0$. This identity is the "$f$-sum rule"

$$K_\parallel^{ab}(\mathbf{p}) = \Pi_\parallel^{ab}(\mathbf{p}) - \left\langle (T^a\boldsymbol{\varphi})\cdot(T^b\boldsymbol{\varphi})\right\rangle = 0 \tag{5.54}$$

relating the diamagnetic term $\langle(T^a\boldsymbol{\varphi})\cdot(T^b\boldsymbol{\varphi})\rangle$ to the paramagnetic current-current correlation function $\Pi_\parallel^{ab}$. $K_{\mu\nu}^{ab}$ can thus be written as

$$K_{\mu\nu}^{ab}(\mathbf{p}) = (\delta_{\mu\nu} - \hat{p}_\mu\hat{p}_\nu)K_\perp^{ab}(\mathbf{p}). \tag{5.55}$$

5.2.4 Conductivity in the quantum model

To obtain the frequency-dependent conductivity in the quantum model, one sets $\mathbf{p} = (0,0,\omega_n)$ and $\mu,\nu = x,y$ so that $p_\mu = p_\nu = 0$ and the one-particle-reducible contribution in Eq. (5.41) vanishes. This way $K_{\mu\nu}^{ab}(\mathrm{i}\omega_n) = -\Gamma_{\mu\nu}^{(0,2)ab}(\mathrm{i}\omega_n,\bar{\boldsymbol{\phi}})$, i.e., using the Ward identities (5.49) to (5.51),

$$K_{\mu\nu}^{ab}(\mathrm{i}\omega_n) = \delta_{\mu\nu}\left\{\omega_n^2\delta_{ab}\Psi_B(\mathrm{i}\omega_n,\rho_0) + (T^a\bar{\boldsymbol{\phi}})\cdot(T^b\bar{\boldsymbol{\phi}})[\omega_n^2\Psi_C(\mathrm{i}\omega_n,\rho_0) - \Psi_A(\mathrm{i}\omega_n,\rho_0)]\right\}. \tag{5.56}$$

We retrieve the form of the conductivity presented in Section 5.2.1: in the disordered phase and at the QCP the conductivity tensor is diagonal equal to

$$\sigma(\omega) = \mathrm{i}\omega\Psi_B(\omega,\rho=0), \tag{5.57}$$

and restoring physical units we deduce the expression of the capacitance introduced in Eq. (5.25),

$$C_{\mathrm{dis}} = -2\pi\hbar\sigma_{\mathrm{Q}}\Psi_B(\mathrm{i}\omega_n = 0,\rho = 0). \tag{5.58}$$

In the ordered phase, assuming for simplicity that the order parameter is along the first direction, i.e., $\bar{\phi}_i = \delta_{i,1}\sqrt{2\rho_0}$, and choosing the basis $\{T^{IJ}\}$ introduced in Eq. (5.15), one finds

$$K^{ab}_{\mu\nu}(\mathrm{i}\omega_n) = \delta_{\mu\nu}\delta_{ab}\{\omega_n^2\Psi_B(\mathrm{i}\omega_n,\rho_0) + 2\rho_0\delta_{a\in A}[\omega_n^2\Psi_C(\mathrm{i}\omega_n,\rho_0) - \Psi_A(\mathrm{i}\omega_n,\rho_0)]\}, \tag{5.59}$$

where $\delta_{a\in A}$ is equal to unity if T^a is in class A and vanishes otherwise.

For class A generators, at low frequencies

$$\sigma_A(\omega) = \mathrm{i}\frac{2\rho_0\Psi_A(\mathrm{i}\omega_n = 0,\rho_0)}{\omega + \mathrm{i}0^+} + O(\omega) \tag{5.60}$$

is as expected [see Eq. (5.27)] characteristic of a perfect inductor (based on perturbation theory arguments the constant term $O(\omega^0)$ vanishes [92]). Note that the coefficient $2\rho_0\Psi_A(\mathrm{i}\omega_n = 0,\rho_0) = 2\rho_0 Z(\rho_0)$ is indeed the superfluid stiffness ρ_s [defined by the small-momentum behavior of the transverse propagator, see Eq. (3.3)] as a consequence of the Ward identity (5.49).

For class B generators,

$$\sigma_B(\omega) = \mathrm{i}(\omega + \mathrm{i}0^+)\Psi_B^R(\omega,\rho_0), \tag{5.61}$$

where $\Psi_B^R(\omega,\rho)$ denotes the retarded part of $\Psi_B(\mathrm{i}\omega_n,\rho)$. We will argue in Section 5.3 (see also Section 5.2.5 for the calculation of Ψ_B in the large-N limit) that in the ordered phase $\Psi_B(\mathrm{i}\omega_n,\rho)$ diverges as $1/|\omega_n|$ for $\omega_n \to 0$ so that $\sigma_B(\omega)$ takes a finite value in the limit $\omega \to 0$. As a result $\sigma_B(\omega\to 0)/\sigma_Q$ is a universal number in the whole ordered phase.

5.2.5 Large-N limit

The general expression of $\sigma(\omega)$ is verified in the large-N limit. We briefly present here known results, obtainable e.g. by resumming RPA diagrams as in Section 4.1.1, whose derivation is detailled in [1, 73]. Note that it is important in the computation to cut off the momenta in the ultraviolet to handle divergences (we do not implement a cutoff on frequencies).

In the disordered phase $K^{aa}(\mathrm{i}\omega_m) \equiv K(\mathrm{i}\omega_m)$ does not depend on a. Recalling the expression of the large-N propagator ($c = 1$)

$$G(\mathbf{q},\mathrm{i}\omega_n) = (\mathbf{q}^2 + \omega^2 + \Delta^2)^{-1} \tag{5.62}$$

Omitting terms of order $O(|\omega_m|/\Lambda)$,

$$\begin{aligned} K(\mathrm{i}\omega_m) &= 2\int_{\mathbf{q},\omega_n} \mathbf{q}^2 G(\mathbf{q},\mathrm{i}\omega_n)[G(\mathbf{q},\mathrm{i}\omega_n + \mathrm{i}\omega_m) - G(\mathbf{q},\mathrm{i}\omega_n)] \\ &= -\frac{\omega_m^2}{2}\int_{\mathbf{q}} \frac{\mathbf{q}^2}{(\mathbf{q}^2+\Delta^2)^{3/2}(\omega_m^2 + 4\mathbf{q}^2 + 4\Delta^2)} = -\frac{\omega_m^2}{24\pi\Delta} + O\left(\frac{\omega_m^4}{\Delta^3}\right) \end{aligned} \tag{5.63}$$

for $T = 0$ and $d = 2$, i.e., $\Psi_B(\mathrm{i}\omega_m = 0, \rho = 0) = -1/24\pi\Delta$. We thus obtain

$$C_{\mathrm{dis}} = \frac{\hbar\sigma_Q}{12\Delta}, \tag{5.64}$$

restoring physical units.

At the QCP, $\Delta \to 0$. Evaluating the integral in Eq. (5.63) for $\Delta = 0$ yields the universal value $K(\mathrm{i}\omega_m) = -|\omega_m|/16$, i.e. [11]

$$\sigma(\mathrm{i}\omega_m) = \frac{\pi}{8}\sigma_Q. \tag{5.65}$$

Note that at the QCP, in the critical regime, $\Psi_B(i\omega_m, \rho = 0)$ behaves as $1/|\omega_m|$.

In the ordered phase, for a class B generator, the calculation of the conductivity is similar to the case of the disordered phase with $\Delta = 0$; K_B is given by the integral in Eq. (5.63), which gives $K_B(i\omega_m) = -|\omega_m|/16$ and

$$\sigma_B(i\omega_m) = \frac{\pi}{8}\sigma_Q, \tag{5.66}$$

in agreement with [130]. $\Psi_B(i\omega_m, \rho_0)$ behaves as $1/|\omega_m|$.

For a class A generator, to leading order in the large-N limit, $\Psi_A(i\omega_m, \rho_0) = 1$ and $\Psi_C(i\omega_m, \rho_0) = 0$. For $\omega_m \to 0$, $K_A(i\omega_m) = \rho_s/\omega_m$ with $\rho_s = 2\rho_0$, which yields

$$\frac{C_{dis}}{N\sigma_Q^2 L_{ord}} = \frac{\pi}{6}\frac{\rho_s}{N\Delta} = \frac{1}{24}, \tag{5.67}$$

where the last result is deduced using Eq. (3.26), $\rho_s/N\Delta = 1/4\pi$.

5.3 Non-perturbative renormalization group scheme

In this Section we show how the NPRG allows us to compute the effective action $\Gamma[\boldsymbol{\phi}, \mathbf{A}]$.

5.3.1 Scale-dependent effective action

As done in Section 2.2 we build a family of models indexed by a momentum scale k such that fluctuations are smoothly taken into account as k is lowered from the microscopic scale Λ down to 0. This is achieved by adding to the action (5.9) an infrared regulator term. Note that the standard expression (2.20) for the regulator breaks down gauge invariance due to the gradient term. We thus explicitly propose a gauge-invariant regulator,

$$\Delta S_k[\boldsymbol{\varphi}, \mathbf{A}] = \frac{1}{2}\int_{\mathbf{x}} \boldsymbol{\varphi}(\mathbf{x}) \cdot R_k\big(-\mathbf{D}(\mathbf{x})^2\big)\boldsymbol{\varphi}(\mathbf{x}) = \frac{1}{2}\int_{\mathbf{x},\mathbf{x}'} \boldsymbol{\varphi}(\mathbf{x}) \cdot \mathcal{R}_k[\mathbf{x}, \mathbf{x}', \mathbf{A}]\boldsymbol{\varphi}(\mathbf{x}'), \tag{5.68}$$

where

$$\mathcal{R}_k[\mathbf{x}, \mathbf{x}', \mathbf{A}] = \frac{1}{2}\Big[R_k\big(-\mathbf{D}(\mathbf{x})^2\big) + R_k\big(-\mathbf{D}(\mathbf{x}')^2\big)^T\Big]\delta(\mathbf{x} - \mathbf{x}') \tag{5.69}$$

and $\mathbf{D}^2 = D_\mu D_\mu$ with $D_\mu(\mathbf{x}) = \partial_{x_\mu} - A_\mu(\mathbf{x})$. The cutoff function R_k is chosen as in Section 2.2; in practice we use an exponential regulator (2.23). In the absence of the external gauge field, we recover the usual regulator term. By replacing ∂_μ by the covariant derivative D_μ in the regulator term, we ensure that the action $S + \Delta S_k$ remains gauge invariant. Gauge-invariant regulators have been considered before in the context of gauge theories [143–147]. As in our case $\mathbf{A}$ is not dynamical and is set to zero before integrating the flow equations, a gauge-invariant regulator is much easier to handle than for gauge theories.

We define in the usual way the k-dependent partition function

$$\mathcal{Z}_k[\mathbf{J}, \mathbf{A}] = \int \mathcal{D}[\boldsymbol{\varphi}] \exp\left(-S[\boldsymbol{\varphi}, \mathbf{A}] - \Delta S_k[\boldsymbol{\varphi}, \mathbf{A}] + \int_{\mathbf{x}} \mathbf{J} \cdot \boldsymbol{\varphi}\right). \tag{5.70}$$

The scale-dependent effective action

$$\Gamma_k[\boldsymbol{\phi}, \mathbf{A}] = -\ln \mathcal{Z}_k[\mathbf{J}, \mathbf{A}] + \int_{\mathbf{x}} \mathbf{J} \cdot \boldsymbol{\phi} - \Delta S_k[\boldsymbol{\phi}, \mathbf{A}] \tag{5.71}$$

is defined as a modified Legendre transform of $-\ln \mathcal{Z}_k[\mathbf{J},\mathbf{A}]$ which includes the subtraction of $\Delta S_k[\boldsymbol{\phi},\mathbf{A}]$. Here $\boldsymbol{\phi}(\mathbf{x}) = \langle \boldsymbol{\varphi}(\mathbf{x})\rangle$ is the order parameter in the presence of the external source $\mathbf{J}$ and the gauge field $\mathbf{A}$. As in Section 2.2 the boundary conditions for $k = \Lambda$ and $k = 0$ are

$$\Gamma_\Lambda[\boldsymbol{\phi},\mathbf{A}] = S[\boldsymbol{\phi},\mathbf{A}], \qquad \Gamma_{k=0}[\boldsymbol{\phi},\mathbf{A}] = \Gamma[\boldsymbol{\phi},\mathbf{A}]. \tag{5.72}$$

The variation of the effective action with k is given by the Wetterich equation (2.27)

$$\partial_t \Gamma_k[\boldsymbol{\phi},\mathbf{A}] = \frac{1}{2}\operatorname{Tr}[\partial_t \mathcal{R}_k[\mathbf{A}](\Gamma_k^{(2,0)}[\boldsymbol{\phi},\mathbf{A}] + \mathcal{R}_k[\mathbf{A}])^{-1}], \tag{5.73}$$

where we recall that $t = \ln(k/\Lambda)$ is a (negative) RG "time". The regulator $\mathcal{R}_k$ ensures that high momenta do not contribute to the flow and the momentum integrals can be safely extended up to infinity. Thus the regulator term ΔS_k provides us with a gauge-invariant UV regularization. The k-dependent effective action inherits all properties of the effective action discussed in Section 5.2.2. Thus, the computation of the conductivity requires to determine the vertices $\Gamma^{(1,1)}_{k=0}$ and $\Gamma^{(0,2)}_{k=0}$ in addition to the effective potential $U_{k=0}$ and the inverse propagator $\Gamma^{(2,0)}_{k=0}$.

From this we deduce the flow of U_k (2.30) and $\Gamma^{(2,0)}_k$ (2.31). For the vertices $\Gamma^{(1,1)}_k$ and $\Gamma^{(0,2)}_k$, one has to take into account the fact that $\mathcal{R}_k$ depends on the gauge field, and yields a contribution when taking functional derivatives with respect to $\mathbf{A}$. Dropping the $\boldsymbol{\phi}$ dependency of the vertices and propagators, their flows read

$$\begin{aligned}\partial_t \Gamma^{(1,1)a}_{k,i\mu}(\mathbf{p}) = \frac{1}{2}\tilde{\partial}_t \int_{\mathbf{q}} \operatorname{tr}\Big\{ & G_k(\mathbf{q})\Gamma^{(3,1)a}_{k,i\mu}(\mathbf{q},-\mathbf{q},\mathbf{p},-\mathbf{p}) - G_k(\mathbf{q})\Gamma^{(3,0)}_{k,i}(\mathbf{p},\mathbf{q},-\mathbf{p}-\mathbf{q})G_k(\mathbf{p}+\mathbf{q}) \\ & \times\big[\Gamma^{(2,1)a}_{k,\mu}(\mathbf{p}+\mathbf{q},-\mathbf{q},-\mathbf{p}) + \mathcal{R}^{(1)a}_{k,\mu}(\mathbf{p}+\mathbf{q},-\mathbf{q},-\mathbf{p})\big]\Big\},\end{aligned} \tag{5.74}$$

$$\begin{aligned}\partial_t \Gamma^{(0,2)ab}_{k,\mu\nu}(\mathbf{p}) = \frac{1}{2}\tilde{\partial}_t \int_{\mathbf{q}} \operatorname{tr}\Big\{ & G_k(\mathbf{q})\big[\Gamma^{(2,2)ab}_{k,\mu\nu}(\mathbf{q},-\mathbf{q},\mathbf{p},-\mathbf{p}) + \mathcal{R}^{(2)ab}_{k,\mu\nu}(\mathbf{q},-\mathbf{q},\mathbf{p},-\mathbf{p})\big] \\ & - G_k(\mathbf{q})\big[\Gamma^{(2,1)a}_{k,\mu}(\mathbf{q},-\mathbf{p}-\mathbf{q},\mathbf{p}) + \mathcal{R}^{(1)a}_{k,\mu}(\mathbf{q},-\mathbf{p}-\mathbf{q},\mathbf{p})\big]G_k(\mathbf{p}+\mathbf{q}) \\ & \times\big[\Gamma^{(2,1)b}_{k,\nu}(\mathbf{p}+\mathbf{q},-\mathbf{q},-\mathbf{p}) + \mathcal{R}^{(1)b}_{k,\nu}(\mathbf{p}+\mathbf{q},-\mathbf{q},-\mathbf{p})\big]\Big\}.\end{aligned} \tag{5.75}$$

Here tr denotes the trace with respect to the $\mathrm{O}(N)$ indices. Eqs. (5.74) and (5.75) are shown diagrammatically in Fig. 5.2. They differ from usual flow equations by the appearance of derivatives of the cutoff function with respect to the gauge field,

$$\mathcal{R}^{(1)a}_{k,\mu}(\mathbf{x},\mathbf{x}',\mathbf{y}) = \left.\frac{\delta\mathcal{R}[\mathbf{x},\mathbf{x}',\mathbf{A}]}{\delta A^a_\mu(\mathbf{y})}\right|_{\mathbf{A}=0}, \qquad \mathcal{R}^{(2)ab}_{k,\mu\nu}(\mathbf{x},\mathbf{x}',\mathbf{y},\mathbf{y}') = \left.\frac{\delta^2\mathcal{R}[\mathbf{x},\mathbf{x}',\mathbf{A}]}{\delta A^a_\mu(\mathbf{y})\delta A^b_\nu(\mathbf{y}')}\right|_{\mathbf{A}=0}. \tag{5.76}$$

The explicit expressions of $\mathcal{R}^{(1)a}_{k,\mu}(\mathbf{p}_1,\mathbf{p}_2,\mathbf{p}_3)$ and $\mathcal{R}^{(2)ab}_{k,\mu\nu}(\mathbf{p}_1,\mathbf{p}_2,\mathbf{p}_3,\mathbf{p}_4)$ are derived in [32] and read (we drop the k index)

$$\mathcal{R}^{(1)a}_{\mu}(\mathbf{p}_1,\mathbf{p}_2,\mathbf{p}_3) = \delta_{\sum \mathbf{p}_i,0}\, T^a(\mathrm{i}p_{1\mu} - \mathrm{i}p_{2\mu})\frac{R(\mathbf{p}_1^2) - R(\mathbf{p}_2^2)}{\mathbf{p}_1^2 - \mathbf{p}_2^2}, \tag{5.77}$$

$$\begin{aligned}\mathcal{R}^{(2)ab}_{\mu\nu}(\mathbf{p}_1,\mathbf{p}_2,\mathbf{p}_3,\mathbf{p}_4) = \delta_{\sum \mathbf{p}_i,0}\Big\{ & -\delta_{\mu\nu}\{T^a,T^b\}\frac{R(\mathbf{p}_1^2) - R(\mathbf{p}_2^2)}{\mathbf{p}_1^2 - \mathbf{p}_2^2} - \Big[T^aT^b(2p_{1\mu} + p_{3\mu})(2p_{2\nu} + p_{4\nu}) \\ & \times \frac{R(\mathbf{p}_1^2)[(\mathbf{p}_1+\mathbf{p}_3)^2 - \mathbf{p}_2^2] + R\left((\mathbf{p}_1+\mathbf{p}_3)^2\right)(\mathbf{p}_2^2 - \mathbf{p}_1^2) + R(\mathbf{p}_2^2)\left[\mathbf{p}_1^2 - (\mathbf{p}_1+\mathbf{p}_3)^2\right]}{[(\mathbf{p}_1+\mathbf{p}_3)^2 - \mathbf{p}_2^2](\mathbf{p}_2^2 - \mathbf{p}_1^2)[\mathbf{p}_1^2 - (\mathbf{p}_1+\mathbf{p}_3)^2]} \\ & + (a\leftrightarrow b, \mu\leftrightarrow\nu, \mathbf{p}_3\leftrightarrow\mathbf{p}_4)\Big]\Big\}.\end{aligned} \tag{5.78}$$

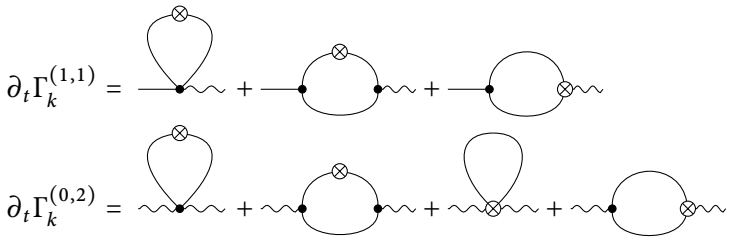

Figure 5.2: Diagrammatic representation of the RG equations (5.74) and (5.75). Signs and symmetry factors are not shown. Dots with n straight lines and m wavy lines stand for the vertex $\Gamma_k^{(n,m)}$, solid lines represent the full propagator $G_k = (\Gamma_k^{(2,0)} + R_k)^{-1}$, the cross stands for $\partial_t R_k$ and the cross with n wavy lines stands for $\partial_t \mathcal{R}_k^{(n)}$.

5.3.2 Approximation schemes

Let us now discuss the approximation schemes we use to solve the above flow equations and determine the functions $\Psi_{A,B,C}$ and $\bar{\Psi}_{A,B,C}$. We wish to compute the conductivity at finite frequencies and, for that reason, one needs an appropriate approximation scheme. A natural idea is thus to implement, as in Chapter 4, a BMW-like scheme on the vertices $\Gamma_k^{(2,1)}$, $\Gamma_k^{(3,1)}$ and $\Gamma_k^{(2,2)}$ to close the equations. However, it is difficult to conciliate this approach with the gauge invariance of the theory. The reason is that these vertices bear a nontrivial momentum dependence. Consider for instance the vertex $\Gamma_k^{(2,1)}$. The BMW approximation reads

$$\Gamma_{k,ij\mu}^{(2,1)a}(\mathbf{p}+\mathbf{q},-\mathbf{q},-\mathbf{p}) \to \Gamma_{k,ij\mu}^{(2,1)a}(\mathbf{p},0,-\mathbf{p}) = \mathrm{i}p_\mu \left\{ T_{ij}^a \Psi_A(\mathbf{p},\rho) + \phi_j (T^a \boldsymbol{\phi})_i \Psi_A'(\mathbf{p},\rho) \right\}. \tag{5.79}$$

Compare this with the mean-field result $\mathrm{i}(p_\mu + 2q_\mu) T_{ij}^a$: one remarks the momenta structure is different (as expected since $\mathbf{q}$ is set to zero in the BMW approximation). This breaks gauge invariance. The difference with the BMW approximation for the standard n-point functions and for the Higgs model presented in Sections 2.3.4 and 4.1.3 is that the vertices do not depend only on the modulus of the momenta but also on their direction, preventing this issue from arising. In shorter terms, in the action the gauge-invariant term is $q_\mu - A_\mu$: setting carelessly $\mathbf{q}$ to zero while retaining $\mathbf{A}$ breaks down gauge invariance.

A tentative workaround is to modify the BMW scheme to take this into account, e.g. by writing using the symmetries

$$\Gamma_{k,ij\mu}^{(2,1)a}(\mathbf{p}+\mathbf{q},-\mathbf{q},-\mathbf{p}) = p_\mu f_{k,ij}^a(\mathbf{p},\mathbf{q}) + q_\mu g_{k,ij}^a(\mathbf{p},\mathbf{q}) \tag{5.80}$$

and approximating $f_{k,ij}^a(\mathbf{p},\mathbf{q}), g_{k,ij}^a(\mathbf{p},\mathbf{q}) \to f_{k,ij}^a(\mathbf{p},0), g_{k,ij}^a(\mathbf{p},0)$. The issue is that it has not been possible to find a closed expression for $g_{k,ij}^a(\mathbf{p},0)$ within the BMW approximation. For this reason, we drop the BMW approximation and rather use *Ansatz*-based schemes, for which gauge invariance is easily enforced.

Derivative expansion

We first propose a derivative expansion (DE) scheme [32], see Section 2.3.1. We recall that such an expansion is made possible by the regulator term ΔS_k which ensures that all vertices $\Gamma_k^{(n,m)}$ are smooth functions of momenta $\mathbf{p}_i$ and can be expanded in powers of $\mathbf{p}_i^2/k^2$ when $|\mathbf{p}_i| \ll k$, even

at criticality. DE does not allow us to obtain the full frequency dependence of the conductivity but is sufficient to determine the low-frequency limit of $\sigma(\omega)$ and $\sigma_A(\omega)$ defined by C_{dis} and L_{ord}. The case of $\sigma_B(\omega)$ and $\sigma(\omega)$ at the QCP is more subtle. At low frequencies, the vertices that define $\sigma_B(\omega \to 0)$ and σ^* diverge like $1/\omega$ (this is the case in the large-N limit derived in Section 5.2.5; we verify it for all N through RG). Because of this, DE cannot be used to determine these quantities.

The derivative expansion is fully determined by the symmetries of the system. We remind the reader that, for $\mathbf{A} = 0$, the most general $\mathrm{O}(N)$ invariant effective action to second order in derivatives,

$$\Gamma_k[\boldsymbol{\phi}] = \int_{\mathbf{x}} \frac{1}{2} Z_k(\rho)(\partial_\mu \boldsymbol{\phi})^2 + \frac{1}{4} Y_k(\rho)(\partial_\mu \rho)^2 + U_k(\rho) \tag{5.81}$$

is defined by three functions. When $\mathbf{A} \neq 0$, the effective action must be invariant under gauge transformations. This can be done by replacing ∂_μ by the covariant derivative D_μ. It may also include terms depending on the field strength

$$F_{\mu\nu} = -[D_\mu, D_\nu] = \partial_\mu A_\nu - \partial_\nu A_\mu - [A_\mu, A_\nu]. \tag{5.82}$$

Although $F_{\mu\nu}$ is not gauge invariant (it transforms under (5.11) as $F'_{\mu\nu} = O F_{\mu\nu} O^T$), it allows us to construct two invariant terms, namely $\mathrm{tr}(F_{\mu\nu}^2)$ and $(F_{\mu\nu}\boldsymbol{\phi})^2$.[3] This leads to the effective action

$$\begin{aligned} \Gamma_k[\boldsymbol{\phi}, \mathbf{A}] = & \int_{\mathbf{x}} \frac{1}{2} Z_k(\rho) D_\mu \boldsymbol{\phi} \cdot D_\mu \boldsymbol{\phi} + \frac{1}{4} Y_k(\rho)(\partial_\mu \rho)^2 + U_k(\rho) \\ & + \frac{1}{4} X_{1,k}(\rho) F^a_{\mu\nu} F^a_{\mu\nu} + \frac{1}{4} X_{2,k}(\rho) \sum_{\mu\nu} (F^a_{\mu\nu} T^a \boldsymbol{\phi})^2, \end{aligned} \tag{5.83}$$

where we use $F_{\mu\nu} = F^a_{\mu\nu} T^a$ and $\mathrm{tr}(F^2_{\mu\nu}) = -2 F^a_{\mu\nu} F^a_{\mu\nu}$ with

$$F^a_{\mu\nu} = \partial_\mu A^a_\nu - \partial_\nu A^a_\mu - f_{abc} A^b_\mu A^c_\nu \tag{5.84}$$

where the structure constants f_{abc} of the $\mathrm{so}(N)$ Lie algebra are defined by Eq. (5.14). Note that we restrict ourselves to terms of second order in $\mathbf{A}$, as higher-order terms do not contribute to the conductivity.[4] The effective action $\Gamma_k[\boldsymbol{\phi}, \mathbf{A}]$ is determined by $X_{1,k}(\rho)$ and $X_{2,k}(\rho)$ in addition to $U_k(\rho)$, $Z_k(\rho)$ and $Y_k(\rho)$. From the action (5.83) we obtain

$$\Psi_{A,k}(\mathbf{p}, \rho) = Z_k(\rho), \quad \Psi_{B,k}(\mathbf{p}, \rho) = -X_{1,k}(\rho), \quad \Psi_{C,k}(\mathbf{p}, \rho) = -X_{2,k}(\rho), \tag{5.85}$$

$$\tilde{\Psi}_{B,k}(\mathbf{p}, \rho) = \mathbf{p}^2 X_{1,k}(\rho), \quad \tilde{\Psi}_{C,k}(\mathbf{p}, \rho) = Z_k(\rho) + \mathbf{p}^2 X_{2,k}(\rho), \tag{5.86}$$

to lowest order of the derivative expansion. Hence, the flow of $\Gamma_k^{(0,2)}$ is sufficient to determine $X_{1,k}(\rho)$ and $X_{2,k}(\rho)$. Eqs. (5.85) and (5.86) satisfy the Ward identities (5.49) to (5.51). From this one determines the capacitance $C_{\text{dis}} = X_{1,k=0}(\rho_{0,k=0})$ [Eq. (5.25) in the disordered phase] and the inductance [Eq. (5.27)] through the stiffness $\rho_s = 2\rho_{0,k=0} Z(\rho_{0,k=0})$ in the ordered phase. In the large-N limit the exact solution for C_{dis} is retrieved. The values obtained for the ratio $C_{\text{dis}}/\sigma_Q^2 L_{\text{ord}}$ is given in Table 5.1 in Section 5.3.3. For the conductivity σ at the QCP and σ_B in the ordered phase, however, one finds that in the $k, \omega \to 0$ limit

$$\sigma(\omega) = \frac{\omega}{k} \tilde{X}_1^{*\text{crit}}, \qquad \sigma_B(\omega) = \frac{\omega}{k} \tilde{X}_1^{*\text{ord}} \tag{5.87}$$

[3] Topological terms such as $\epsilon_{\mu\nu\rho\sigma} F_{\mu\nu} F_{\rho\sigma}$ can in principle be included but do not contribute to the conductivity.

[4] As a consequence the last term in the right-hand side of Eq. (5.84) does not matter.

where $\tilde{X}_1^{*\mathrm{crit}}$ and $\tilde{X}_1^{*\mathrm{ord}}$ are the fixed point values of the (dimensionless) function $\tilde{X}_{1,k} = k^{4-D} X_{1,k}(\tilde{\rho})$ ($D = 3$) evaluated at the minimum of the potential $\tilde{\rho}_{0,k}$ respectively at the QCP and in the ordered phase. The zero-frequency limit is thus ill-defined, as the DE breaks down due to the singular behavior of the $\Psi_{B,k=0}(\mathbf{p}, \rho_0)$ for $\mathbf{p} \to 0$. One can still try to determine the low-frequency with a qualitative argument. Consider some arbitrarily small frequency ω. It defines an energy scale, which cuts the flow as, for instance, a mass does in the disordered phase. Stopping the flow at $k \sim \omega$ in Eq. (5.87), we see that $\sigma(\omega)$ and $\sigma_B(\omega)$ reach finite limits σ^* and σ_B^* in the low-frequency limit, but they cannot be determined within this approach.

LPA″

To determine the conductivity at finite frequencies, inspired by the DE, we opt for an LPA″ scheme. As done in Section 2.3.3, we start with the LPA′ *Ansatz*, which is given by approximating the four functions $Z_k(\rho)$, $Y_k(\rho)$, $X_{1,k}(\rho)$ and $X_{2,k}(\rho)$ of the DE *Ansatz* (5.81) by ρ-independent numbers Z_k, Y_k, $X_{1,k}$ and $X_{2,k}$. We then promote these numbers to functions of $-\mathbf{D}^2 \equiv -D_\mu^2$. The LPA″ *Ansatz* thus reads

$$\begin{aligned}\Gamma_k[\boldsymbol{\phi}, \mathbf{A}] = \int_{\mathbf{x}} & \frac{1}{2} D_\mu \boldsymbol{\phi} \cdot Z_k(-\mathbf{D}^2) D_\mu \boldsymbol{\phi} + \frac{1}{4} (\partial_\mu \rho) Y_k(-\boldsymbol{\partial}^2)(\partial_\mu \rho) + U_k(\rho) \\ & + \frac{1}{4} F^a_{\mu\nu} X_{1,k}(-\mathbf{D}^2) F^a_{\mu\nu} + \frac{1}{4} F^a_{\mu\nu} T^a \boldsymbol{\phi} \cdot X_{2,k}(-\mathbf{D}^2) F^b_{\mu\nu} T^b \boldsymbol{\phi}. \end{aligned} \tag{5.88}$$

Note that as the covariant derivative of a scalar is equal to its regular derivative Y_k is a function of $-\boldsymbol{\partial}^2 \equiv -\partial_\mu^2$. We emphasize that $U_k(\rho)$ only depends on the field while $Z_k(\mathbf{p})$, $Y_k(\mathbf{p})$, $X_{1,k}(\mathbf{p})$ and $X_{2,k}(\mathbf{p})$ are all functions of a momentum (actually of its modulus square $\mathbf{p}^2$). Let us remark that because we do not include any dependence on ρ in the vertices, this scheme does not reproduce the large-N exact solution in the disordered phase. Indeed, we see by integrating the DE equations in the large-N limit that the dependence on ρ is necessary to recover the exact solution [32]. At the QCP and in the ordered phase, however, the $N \to \infty$ limit is correctly retrieved, because for all k one has $W_k(\rho_0, k) = 0$ and the dependence on ρ of the vertices is not necessary [137]. Within this *Ansatz*, the vertices read

$$\Psi_{A,k}(\mathbf{p}, \rho) = Z_k(\mathbf{p}), \quad \Psi_{B,k}(\mathbf{p}, \rho) = -X_{1,k}(\mathbf{p}), \quad \Psi_{C,k}(\mathbf{p}, \rho) = -X_{2,k}(\mathbf{p}), \tag{5.89}$$

$$\bar{\Psi}_{B,k}(\mathbf{p}, \rho) = \mathbf{p}^2 X_{1,k}(\mathbf{p}), \quad \bar{\Psi}_{C,k}(\mathbf{p}, \rho) = Z_k(\mathbf{p}) + \mathbf{p}^2 X_{2,k}(\mathbf{p}). \tag{5.90}$$

As in Section 2.3.3 we obtain the flows of $X_{1,k}(\mathbf{p})$ and $X_{2,k}(\mathbf{p})$ by evaluating the flow of $\Gamma_k^{(0,2)}$ at the running minimum of the potential $\rho_{0,k}$.

The k-dependent conductivities read

$$\sigma_k(\mathrm{i}\omega_n) = 2\pi\sigma_{\mathrm{Q}} \omega_n X_{1,k}(\mathrm{i}\omega_n) \tag{5.91}$$

in the disordered phase and at the QCP and

$$\sigma_{k,A}(\mathrm{i}\omega_n) = 2\pi\sigma_{\mathrm{Q}} \left\{ \frac{2\rho_{0,k} Z_k(\mathrm{i}\omega_n)}{\omega_n} + \omega_n \left[X_{1,k}(\mathrm{i}\omega_n) + 2\rho_{0,k} X_{2,k}(\mathrm{i}\omega_n) \right] \right\}, \tag{5.92}$$

$$\sigma_{k,B}(\mathrm{i}\omega_n) = 2\pi\sigma_{\mathrm{Q}} \omega_n X_{1,k}(\mathrm{i}\omega_n) \tag{5.93}$$

in the ordered phase.

	$\hbar\sigma_Q/2\pi C_{dis}\Delta$				$C_{dis}/NL_{ord}\sigma_Q^2$	
N	DE	LPA″	MC	ED	DE	LPA″
2	1.98	2.00	2.1(1) [127]	2.0(4) [63]	0.105	0.0975
3	1.98	1.98			0.0742	0.0706
4	1.98	1.96			0.0598	0.0587
5	1.97	1.94			0.0520	0.0526
6	1.97	1.92			0.0475	0.0493
8	1.96	1.90			0.0431	0.0461
10	1.96	1.88			0.0415	0.0448
100	1.92	1.80			0.0413	0.0443
1000	1.91	1.79			0.0416	0.0446

TABLE 5.1: Ratios $\hbar\sigma_Q/2\pi C_{dis}\Delta$ and $C_{dis}/NL_{ord}\sigma_Q^2$ obtained from the NPRG approach, compared to Monte Carlo (MC) simulations and exact diagonalization (ED). The exact results for $N \to \infty$ are $6/\pi \simeq 1.90986$ and $1/24 \simeq 0.041667$, respectively.

5.3.3 Results

Let us start with the conductivities $\sigma(\omega)$ in the disordered phase and $\sigma_A(\omega)$ in the ordered phase, in the limit $\omega \to 0$. Both DE and LPA″ yield predictions for the universal ratios $\hbar\sigma_Q/2\pi C_{dis}\Delta$ and $C_{dis}/NL_{ord}\sigma_Q^2$, which we display in Table 5.1. In the limit $N \to \infty$, the DE results agree with the exact results $6/\pi$ and $1/24$, but the LPA″ is wrong by about 5–10%. The error for LPA″ arises from the fact that $X_1(\mathbf{p})$, and thus C_{dis} is incorrectly determined in the disordered phase (see above Section); conversely, L_{ord}, which is defined by the inverse of the spin stiffness in the ordered phase, is correcly computed, see Table 3.2 for the values of $\rho_s/N\Delta$ within LPA″. For $N = 2$, the difference between DE and LPA″ is smaller and we find $\hbar\sigma_Q/2\pi C_{dis}\Delta \simeq 1.98$ for DE and 2.00 for LPA″, in reasonable agreement with the Monte Carlo and exact diagonalization results.

Let us now turn our attention to the finite-frequency behavior of the conductivity. In the following, we thus only discuss LPA″ results.

Quantum critical point

We start with the universal conductivity σ^*/σ_Q at the QPC. Following what is done in Section 2.3.2, we switch to dimensionless variables in which the flow equations admit fixed point solutions at the QPC. We rewrite the k-dependent conductivity $\sigma_k(i\omega_n)$ given in Eq. (5.91) as

$$\sigma_k(i\omega_n) = 2\pi\sigma_Q\omega_n X_{1,k}(i\omega_n) = 2\pi\sigma_Q\tilde{\omega}_n\tilde{X}_{1,k}(i\tilde{\omega}_n) \tag{5.94}$$

Here $\tilde{\omega}_n = \omega_n/k$ is a dimensionless frequency and $\tilde{X}_{1,k}(i\tilde{\omega}_n) = kX_{1,k}(i\tilde{\omega}_n)$ a dimensionless function of ω_n^2. At the QCP, the function $\tilde{X}_{1,k}$ reaches a k-independent fixed-point value $\tilde{X}_1^{*crit}$ and the conductivity takes the form $\sigma_k(i\omega_n) = 2\pi\sigma_Q\tilde{\omega}_n\tilde{X}_1^{*crit}(i\tilde{\omega}_n)$. The low-frequency universal conductivity is obtained by taking first the limit $k \to 0$ and then $\omega_n \to 0$, i.e. $\tilde{\omega}_n \to \infty$: $\sigma^*/2\pi\sigma_Q = \lim_{\tilde{\omega}_n\to\infty}\tilde{\omega}_n\tilde{X}_1^{*crit}(i\tilde{\omega}_n)$ is thus determined by the $1/\tilde{\omega}_n$ behavior of $\tilde{X}_1^{*crit}(i\tilde{\omega}_n)$ at high frequencies, see Fig. 5.3 (left). This $1/\tilde{\omega}_n$ high-frequency tail corresponds to the $1/\omega_n$ divergence of $X_{1,k=0}(\omega_n)$ for $\omega_n \to 0$ responsible of the breakdown of DE. The value of σ^* depends weakly on the regulator,

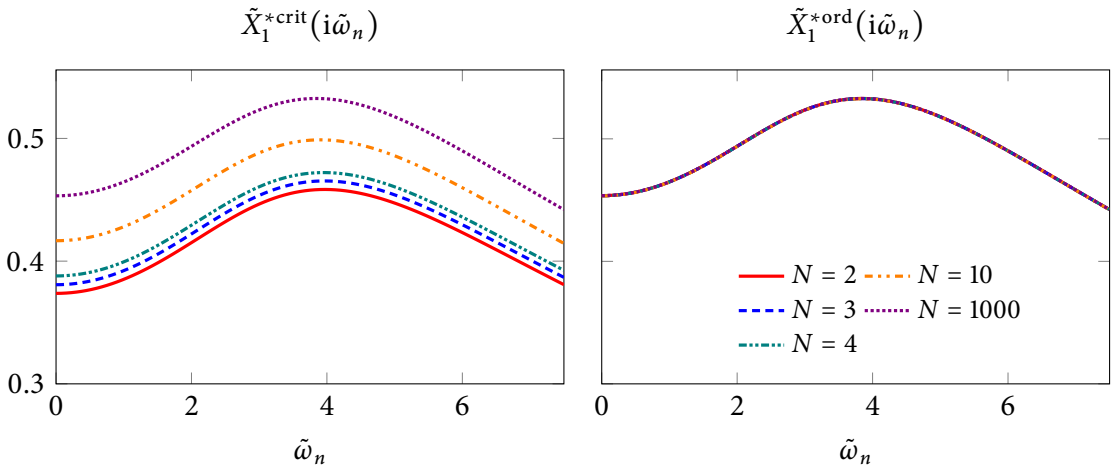

Figure 5.3: Fixed-point functions $\tilde{X}_1^{*\mathrm{crit}}(\mathrm{i}\tilde{\omega}_n)$ (left) and $\tilde{X}_1^{*\mathrm{ord}}(\mathrm{i}\tilde{\omega}_n)$ (right) within LPA″ at the QCP for various values of N. The universal conductivities σ^* and σ_B^* are determined by the $1/\tilde{\omega}_n$ high-frequency tail of the functions. The collapse of the curves for $\tilde{X}_1^{*\mathrm{ord}}(\mathrm{i}\tilde{\omega}_n)$ indicates that σ_B^* is N-independent.

N	LPA″	$O(1/N)$	ϵ expansion	QMC	CB
2	0.3218	0.2512	0.315 [148]	0.355–0.361 [62, 126, 128, 129]	0.3554(6) [132]
3	0.3285	0.2984			
4	0.3350	0.3220			
10	0.3599	0.3644			
1000	0.3927	0.3924			

Table 5.2: Universal conductivity σ^*/σ_Q at the QCP, obtained within LPA″ with a regulator parameter value of $\alpha = 2.25$, compared to results obtained from dimensional expansion, large-N to $O(1/N)$ expansion (the result is $\sigma^* = \pi/8(1 - 64/9\pi^2 N)$ [11]), quantum Monte Carlo simulations (QMC) and conformal bootstrap (CB). The exact value for $N \to \infty$ is $\pi/8 \simeq 0.3927$.

through the arbitrary parameter α in the definition of the exponential regulator (2.23). There is no value of α which fulfills the "principle of minimal sensitivity" for the conductivity; however, σ^* varies at most only by a few percents when α varies in the range $[1, 100]$. We retain $\alpha = 2.25$, which yields decent estimates for the critical exponents η and ν. This dependence on α decreases as N increases, and at $N = \infty$ the results do not depend on α and the exact value $\sigma^*/\sigma_Q = \pi/8$ is recovered. The universal conductivity σ^* is shown in Table 5.2 for various values of N. For $N = 2$ we find a value close to ϵ expansion and in reasonable agreement with (although 10% smaller than) results from QMC and conformal bootstrap.

Disordered phase

In the disordered phase, away from the QCP, Eq. (5.94) still holds since the order parameter vanishes. In Fig. 5.4 we show the real-frequency conductivity $\sigma(\omega)$ obtained from $\sigma_{k=0}(\mathrm{i}\omega_n)$ by analytical continuation using Padé approximants (see Appendix A.2.2). As expected, the system is insulating. The real part of the conductivity vanishes below the two-particle excitation gap 2Δ and the system

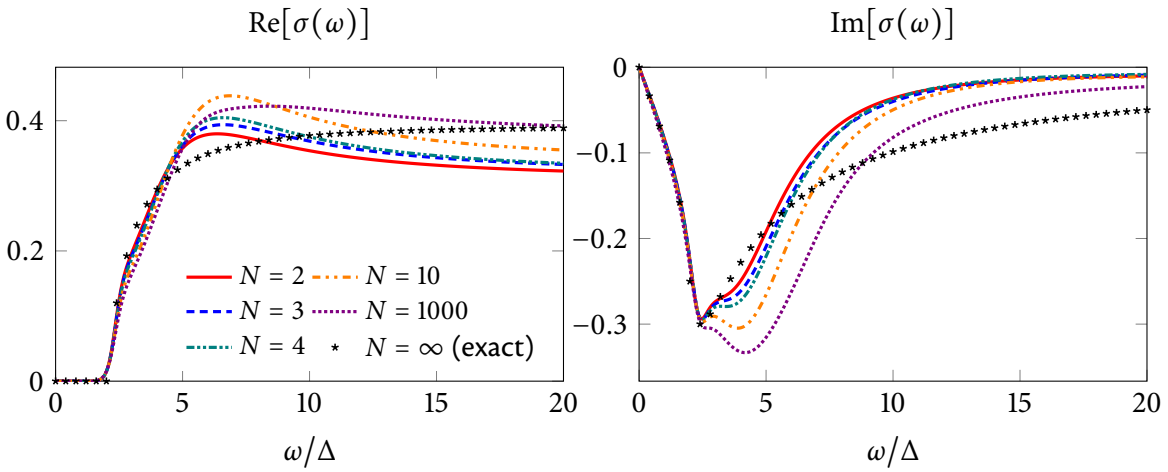

FIGURE 5.4: Real and imaginary parts of the universal conductivity $\sigma(\omega)$ in the disordered phase for various values of N. Black stars show the exact large-N solution.

behaves as a perfect capacitor for $|\omega| \ll \Delta$, i.e. with a conductivity $\sigma(\omega) \sim -\mathrm{i}C_{\mathrm{dis}}\omega$. We however recall that for large-N, there is a discrepancy in the disordered phase between the exact solution and our computation. Furthermore, the analytic continuation is made difficult by the singularity at $\omega = 2\Delta$ so that the frequency dependence of $\sigma(\omega)$ above 2Δ should be taken with caution. In particular, the features of $\sigma(\omega)$ above 2Δ, e.g. the presence of a local extrema in the real or imaginary part, are not stable with the Padé approximant. By contrast, the analytic continuation of data in the ordered phase (see next Section) is very stable.

Ordered phase and superuniversality

Let us finally discuss the two elements σ_A and σ_B of the conductivity tensor in the ordered phase where the $\mathrm{O}(N)$ symmetry is spontaneously broken. Following Eq. (5.94) we write Eqs. (5.92) and (5.93) in a dimensionless form (for the definition of $\tilde{\rho}$ and $\tilde{Z}_k$ see Eqs. (2.40) and (2.41))

$$\sigma_{k,A}(\mathrm{i}\omega_n) = 2\pi\sigma_{\mathrm{Q}}\left\{\frac{2\tilde{\rho}_{0,k}\tilde{Z}_k(\mathrm{i}\tilde{\omega}_n)}{\tilde{\omega}_n} + \tilde{\omega}_n\left[\tilde{X}_{1,k}(\mathrm{i}\omega_n) + 2\tilde{\rho}_{0,k}\tilde{X}_{2,k}(\mathrm{i}\tilde{\omega}_n)\right]\right\}, \tag{5.95}$$

$$\sigma_{k,B}(\mathrm{i}\omega_n) = 2\pi\sigma_{\mathrm{Q}}\tilde{\omega}_n\tilde{X}_{1,k}(\mathrm{i}\tilde{\omega}_n) \tag{5.96}$$

At low frequencies, the leading contribution to $\sigma_{A,k}$, $2\rho_{0,k}Z_k(0)/\omega_n$, is indeed characteristic of a superfluid system with stiffness $\rho_{\mathrm{s},k} = 2\rho_{0,k}Z_k(0)$. $\sigma_A(\omega)$, with the superfluid contribution subtracted, is shown in Fig. 5.5 (top). Our results seem to indicate the absence of a constant $O(\omega_n^0)$ term in agreement with the predictions of perturbation theory [92]. Furthermore we see a marked difference in the low-frequency behavior of the real part of the conductivity between the cases $N = 2$ and $N > 2$, but our numerical results are not precise enough to resolve the low-frequency power laws (predicted [92] to be ω and ω^5 for $N > 2$ and $N = 2$, respectively). On the other hand we find that $\sigma_B(\omega)$ reaches a nonzero universal value σ_B^* in the limit $\omega \to 0$ (Fig. 5.5, bottom). As for the conductivity $\sigma_B^*/\sigma_{\mathrm{Q}}$ at the QCP, this universal value is determined by the $1/\tilde{\omega}_n$ high-frequency tail of the fixed-point value $\tilde{X}_1^{*\mathrm{ord}}(\mathrm{i}\tilde{\omega}_n)$ of the dimensionless function $\tilde{X}_{1,k}(\mathrm{i}\tilde{\omega}_n)$.

Quite surprisingly, contrary to $\tilde{X}_1^{*\mathrm{crit}}$ (Fig. 5.3, left), $\tilde{X}_1^{*\mathrm{ord}}$ turns out to be N independent: the relative change in $\tilde{X}_1^{*\mathrm{ord}}$ is less than 10^{-6} when N varies (Fig. 5.3, right). Noting that the obtained

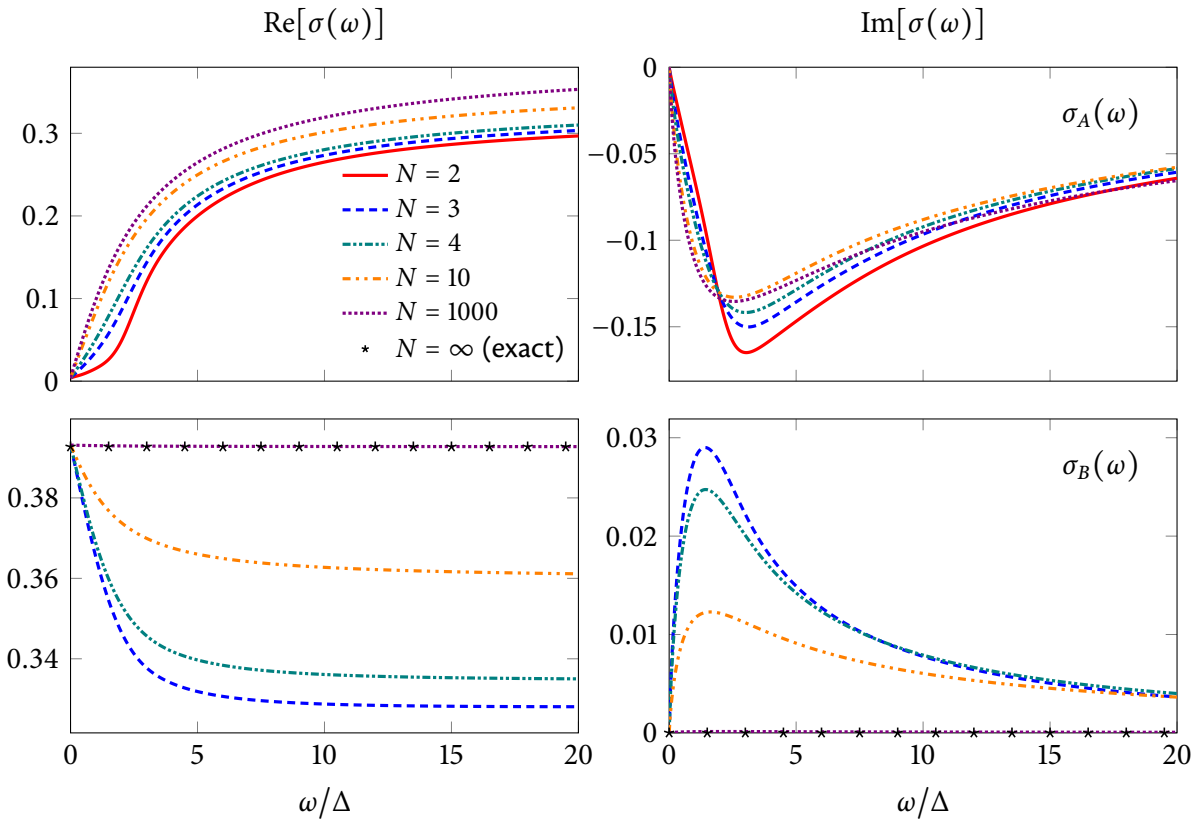

FIGURE 5.5: Real and imaginary parts of the universal conductivities $\sigma_A(\omega)$ and $\sigma_B(\omega)$ in the ordered phase for various values of N. Top: $\sigma_A(\omega)$ with the superfluid contribution $\mathrm{i}\rho_s/(\omega + \mathrm{i}0^+) = \rho_s(\pi\delta(\omega) + \mathrm{i}/\omega)$ subtracted. Bottom: $\sigma_B(\omega)$. Black stars show the exact large-N solution $\sigma_B(\omega) = \pi/8$ (no simple analytic form of $\sigma_A(\omega)$ has been obtained).

value $\sigma_B^*/\sigma_Q \simeq 0.3927$ is equal to the large-N result $\pi/8$ within numerical precision, we conjecture that $\sigma_B^*/\sigma_Q = \pi/8$ for all values of N.

This result can be simply understood by noting that Goldstone bosons become effectively noninteracting in the infrared limit. The most general gauge-invariant effective action for the transverse modes takes of the form

$$\Gamma[\boldsymbol{\pi}, \mathbf{A}] = Z \int_{\mathbf{q},\omega_n} [(\partial_\mu - A_\mu)\boldsymbol{\pi}]^2 + \cdots \tag{5.97}$$

with $Z = \rho_s/2\rho_0$ the field renormalization factor. The dots stand for higher-order terms in $\boldsymbol{\pi}$ (which are irrelevant) and in the gauge field. The theory being noninteracting the correlator $\langle j_\mu^a j_\nu^b \rangle$, which yields the conductivity for a class B generator, can be computed using Wick's theorem and is defined by the bubble diagram. Schematically,

$$\left\langle j_\mu^a j_\mu^a \right\rangle|_{\mathbf{p},\mathrm{i}\omega_m} \sim \int_{\mathbf{q},\mathrm{i}\omega_n} \Gamma_{a\mu}^{(2,1)}(\dots) G_T(\mathbf{q}, \mathrm{i}\omega_n) \Gamma_{a\mu}^{(2,1)}(\dots) G_T(\mathbf{p}+\mathbf{q}, \mathrm{i}\omega_n + \mathrm{i}\omega_m) \tag{5.98}$$

with $G_T(\mathbf{p}, \mathrm{i}\omega_n) = [Z(\mathbf{p}^2 + \omega_n^2)]^{-1}$ the propagator and $\Gamma_{a\mu}^{(2,1)} = Z$. The value of the bubble is given by the integral in Eq. (5.63) (setting Δ to 0). Additionally, each propagator G_T and vertex $\Gamma_{a\mu}^{(2,1)}$ brings

a factor Z^{-1} and Z which cancel. The fact that the same Z intervenes in both the propagator and $\Gamma^{(2,1)}$ is a consequence of the Ward identity (5.48) and follows from the gauge invariance of (5.97). We finally obtain $\sigma_B^*/\sigma_Q = \pi/8$ in agreement with the NPRG result.[5]

Overview

We have determined the frequency-dependent zero-temperature conductivity near a relativistic $(2+1)$-dimensional QCP with $O(N)$-symmetric order parameter. We solve the RG equations using DE and LPA″ schemes, which respect the local gauge invariance of the theory. LPA″ allows to determine the full frequency dependence of the conductivity. Besides the frequency dependence of the conductivity both in the ordered and disordered phases, our main result is the conjecture that $\sigma_B(\omega \to 0)/\sigma_Q$ takes the superuniversal (N-independent) value $\sigma_B^*/\sigma_Q = \pi/8$. Note that universal quantities, in general, depend on N. To our knowledge there are very few exceptions. The critical energy density of $O(N)$ models on d-dimensional lattice with long-range interactions are known to be all equal to the one of the Ising model [149]. The same is true for all $O(N)$ models on a one-dimensional lattice with nearest-neighbor interactions. It has been conjectured [150] that this superuniversality should hold for all d-dimensional $O(N)$ models but a firm numerical confirmation has not been provided so far [151].

The universal character of $\sigma_B(\omega \to 0)$ could in principle be verified in experiments in two-dimensional antiferromagnets, where quantum criticality has been observed [4, 103]. In that case the conserved quantity is the local spin density and the observation would necessitate the measurement of spin transport.

[5] A similar Ward identify exists in Fermi-liquid theory, ensuring that the quasi-particle weight does not appear in physical response functions.

6

Conclusion and perspectives

> I'm drinking a glass of water in the empty hotel bar at the Principe di Savoia and staring at the mural behind the bar and in the mural there is a giant mountain, a vast field spread out below it where villagers are celebrating in a field of long grass that blankets the mountain dotted with tall white flowers, and in the sky above the mountain it's morning and the sun is spreading itself across the mural's frame, burning over the small cliffs and the low-hanging clouds that encircle the mountain's peak, and a bridge strung across a path through the mountain will take you to any point beyond that you need to arrive at, because behind that mountain is a highway and along that highway are billboards with answers on them — who, what, where, when, why — and I'm falling forward but also moving up toward the mountain, my shadow looming against its jagged peaks, and I'm surging forward, ascending, sailing through dark clouds, rising up, a fiery wind propelling me, and soon it's night and stars hang in the sky above the mountain revolving as they burn.
>
> The stars are real.
>
> The future is that mountain.
>
> — Bret Easton Ellis, *Glamorama*.

In this thesis, we determined universal thermodynamical and dynamical properties of the two-dimensional relativistic quantum O(N) model, which describes several quantum phase transitions in strongly correlated cold atoms and condensed matter systems.

The tool we used is the nonperturbative renormalization group (NPRG), an implementation of Wilson's renormalization group idea based on the effective action formalism. The NPRG is a method well suited to quantitatively study criticality in statistical physics which we presented in Chapter 2. The NPRG is a complementary approach to other existing theoretical and numerical tools: perturbative methods, such as the perturbative renormalization group or large-N expansion, exact diagonalization, quantum Monte Carlo or holographic methods based on AdS/CFT correspondence. Each method has its strong points and drawbacks: perturbation theory is mathematically well-controlled by an expansion parameter ($\epsilon = 4 - D, 1/N$) but may break down for the physical case ($\epsilon = 1$, $N = 2$ or 3); exact diagonalization is restricted to very small systems, and involved finite-size scaling analysis is needed to extrapolate the results to the thermodynamic limit; Monte Carlo methods are powerful to study thermodynamics or determine imaginary-time correlation functions, but suffer from the difficulty of analytically continuing data to real time; holographic models provide real-time results but their relationship to relativistic field theories of interest in condensed matter is not always clear.

NPRG is not exempt of drawbacks, either. Its main strength, the possibility to devise qualitatively nonperturbative approximation schemes, also means that there is no control parameter. Still, NPRG has proven to be a very powerful method for determining the thermodynamical and zero-

temperature dynamical properties of a broad class of systems in statistical physics, quantum many-body problems and high-energy physics.

During this thesis, we appropriated this technique, and improved on it with respect to the literature. From a purely technical point of view, our main achievements within NPRG are the computation of four-point correlation functions using an external source, the inclusion of a static gauge field in a condensed-matter setting, and the extension of LPA″ to the determination of response functions at all momenta.

Let us now briefly recall the main results we have obtained. In a first part, in Chapter 3, we studied the thermodynamics of the model, and determined the scaling functions which govern the energy gap, the free energy, and the internal energy density at finite temperature in the critical regime, illustrating quantitatively the phase diagram of the model. Furthermore, thanks to the celebrated quantum-classical mapping, we were able to compare our results for the two-dimensional quantum model to Monte Carlo simulations done for classical spin models in three dimensions in the context of critical Casimir forces, showing a very good agreement.

We then investigated the zero-temperature dynamical properties of the model. In Chapter 4, we examined the excitation spectrum of the model, determining the spectral function in the very different cases of $N = 1$ and $N \geq 2$. For $N = 2$ and, to some extent, 3, we established the existence of a well-defined "Higgs" amplitude mode in the ordered phase of the model in two space dimensions. We determined the energy of the mode, in good agreement with other numerical studies (exact diagonalization, quantum Monte Carlo) done both before and after ours. For $N = 1$, the ordered phase is gapped, and we showed the existence of a bound state below the multi-particle excitation continuum, whose energy we determined in agreement with exact diagonalization and field theoretical calculations. We studied the dependence of the energy of the bound state with dimension and showed its disappearance in dimensions one and three (in the quantum model).

In Chapter 5, we focused our attention on the transport properties of the model, namely the dynamical conductivity, whose frequency dependence we determined at zero temperature. We determined the universal ratio $C_{\text{dis}}/L_{\text{ord}}$, constructed from the low-frequency behavior of the conductivity in both phases. We also computed the universal conductivity at the QCP. Our results compare well with QMC and conformal bootstrap results. Even more, we were able to make the strong conjecture that one of the components of the conductivity tensor in the ordered phase is, at low frequencies, "superuniversal", depending neither on the distance to the critical point nor on N.

Let us now stress again that the extent of the work on the dynamics of the model we present in this thesis is restricted to zero-temperature. This limitation, common to all numerical approaches in imaginary time, comes from the difficulty of performing the analytic continuation for frequencies smaller with than the temperature. A natural continuation of our effort would be to devise a scheme to circumvent this issue and determine spectral functions at finite temperature. Several efforts have been made in this direction in the literature [152–158].

A first possibility would be to perform the analytic continuation beforehand, directly on the flow equations, and solve them in real time [152]. This necessitates both an involved numerical effort and the development of sensible approximation schemes, as the flow equations in real time are ill-behaved. Another idea, inspired by Strodthoff and coworkers' steps [153–155], could be to modify LPA″ so that sums over frequencies in the flow could be determined analytically. This

would allow to integrate the flow equations in real time while avoiding many numerical difficulties. Such a scheme would require using a regulator only on momenta and appropriately simplifying the right-hand side of the flow equations, e.g. by using DE propagators and approximating vertices.

Such a scheme would allow us to determine the conductivity at finite temperature in the hydrodynamic incoherent regime, an unanswered question discussed in Chapter 5. Among the new physics that could be explored at finite temperature, let us mention the hydrodynamics of the $\mathrm{O}(N)$ model, and the determination of the dynamical viscosity tensor. Viscosity is the set of transport coefficients describing the relaxation of a deviation of the momentum density from its equilibrium value. For instance, string theory arguments predict the generic inequality

$$\frac{\eta}{s} \geq \frac{\hbar}{4\pi k_{\mathrm{B}}}, \tag{6.1}$$

valid for relativistic quantum field theories [159], where η is the shear viscosity and s the entropy density. Authors of [159] claim strong interactions are needed to approach that bound, saturated by theories with gravity duals. It would be fascinating to verify this conjecture for the $\mathrm{O}(N)$ model using NPRG.

A

Numerical procedures

> Never build a dungeon you wouldn't be happy to spend the night in yourself. The world would be a happier place if more people remembered that.
>
> — Terry Pratchett, *Guards! Guards!*

Except in some very specific cases, the flow equations one obtains within the NPRG framework cannot be solved analytically. Hence, they need to be numerically integrated.

In this Appendix, we detail various procedures used to numerically integrate RG flows. First, in Appendix A.1 we explain very briefly the explicit Euler method we use to integrate the partial differential flow equations encountered throughout this manuscript, so that a motivated reader could reproduce our results. We remain very concise and for more involved discussion we refer to applied mathematics textbooks [160]. In Appendix A.2 we discuss other numerical subtleties related to the integration of RG flows, including the analytic continuation of results using Padé approximants.

A.1 Finite elements

The most general form of a PDE is

$$\partial_t f(t,x) = \Phi(t,x,f). \tag{A.1}$$

Here, the unknown is a function (or a set of functions) f that depends on a "time" $t \geq 0$ and a "space" variable x. The initial condition $f(t=0,x)$ as well as the functional Φ describing the time evolution are given and we want to determine $f(t,x)$ at all times.

In the NPRG framework, f can represent a set of coupling constants (within e.g. LPA′), the functions that determine the vertices (within full-potential DE or LPA″) or the vertices themselves (within BMW). t is (up to a sign change) the RG time, while x can belong to a 0, 1 or 2-dimensional space depending on whether we retain the momentum or the field dependence of vertices.[1]

As computers can only handle discrete numbers, it is necessary to discretize the continuous space and time variables. To that effect, two main methods exist: finite elements, where the continuous dimensions are replaced with a grid or lattice, and spectral methods, where the functions

[1] Assuming we retain only a set of coupling constants the partial differential equation reduces to a regular differential equation.

are projected onto a finite set of linearly independent functions and one keeps track of the finite number of coefficients.[2] In this manuscript, we (almost exclusively) use the simplest method: finite elements with an explicit Euler prescription, which is sufficient for us. There exist however some cases where more involved spectral methods are necessary to integrate NPRG flows, see [124].

To implement the finite element method, we discretize space and time variables, with finite steps δx and δt. Then, we approximate the function $f(t,x)$ by a discretized version $f_{n,i} = f(n\delta t, i\delta x)$, i and n taking integer values. In practice the index i belongs to a finite grid, e.g. $0 \leq i \leq i_{\max}$, and $n \geq 0$. The next step is to construct a discrete version of Eq. (A.1) which can be solved numerically. We seek for a discrete version of derivatives, integrals, and so on, which leaves a certain freedom. For instance, in explicit Euler method we approximate the time derivative by

$$\partial_t f(t = n\delta t, x = i\delta x) \to \frac{f_{n+1,i} - f_{n,i}}{\delta t}. \tag{A.2}$$

and the PDE (A.1) becomes

$$\frac{f_{n+1,i} - f_{n,i}}{\delta t} = [\Phi f]_{i,n} \tag{A.3}$$

with $[\Phi f]$ a discretized version of $\Phi(t,x,f)$. Obviously, the explicit dependence of $\Phi(t,x,f)$ on space and time variables as well as on the functions are discretized as $t, x, f(x,t) \to n\delta t, i\delta x, f_{n,i}$. The situation is more complex for differential operators and integrals, $\partial_x f$, $\int_x f$. In the following paragraph we explain how to discretize them. For clarity, as we work at fixed $t = n\delta t$, we drop the n index in the remainder of this section.

Discretization of derivatives and integrals

In the case of a one-dimensional space variable, we discretize differentials using finite differences: we approximate $(\partial^k f)_i$ by a linear combination of m different f_{i_j},

$$(\partial^k f)_i \simeq \sum_{j=1}^{m} a_j f_{i_j}. \tag{A.4}$$

To obtain the coefficients, we impose that the series expansion around $i\delta x$ of the linear combination to be equal to $(\partial^k f)_i + O((\delta x)^{m+1-k})$. We have used 5-points derivatives centered around i and for them the expressions read

$$(\partial_x f)_i \simeq \frac{1}{12\delta x}\left(f_{i-2} - 8f_{i-1} + 8f_{i+1} - f_{i+2}\right), \tag{A.5}$$

$$(\partial^2_{xx} f)_i \simeq \frac{1}{12(\delta x)^2}\left(-f_{i-2} + 16f_{i-1} - 30f_i + 16f_{i+1} - f_{i+2}\right). \tag{A.6}$$

As the i grid is compact, we also need non-centered finite differences expressions for the edges. If we note $i = 0$ the position of the left edge, we have

$$(\partial_x f)_0 \simeq \frac{1}{12\delta x}\left(-25f_0 + 48f_1 - 3f_2 + 16f_3 - 3f_4\right), \tag{A.7}$$

$$(\partial_x f)_1 \simeq \frac{1}{12\delta x}\left(-3f_0 - 10f_1 + 18f_2 - 6f_3 + f_4\right), \tag{A.8}$$

[2] The finite element method is a special case of the spectral method, where the basis set is made of piecewise linear functions vanishing on every point of the grid but one.

$$(\partial^2_{xx} f)_0 \simeq \frac{1}{12(\delta x)^2}\left(35 f_0 - 104 f_1 + 114 f_2 - 56 f_3 + 11 f_4\right), \tag{A.9}$$

$$(\partial^2_{xx} f)_1 \simeq \frac{1}{12(\delta x)^2}\left(11 f_0 - 20 f_1 + 6 f_2 + 4 f_3 - f_4\right). \tag{A.10}$$

The corresponding expressions for the right edge can be deduced by symmetry; first and second derivatives are respectively odd and even under space inversion.

One dimensional integrals are computed using a composite Simpson's rule of order $O((\delta x)^3)$ which is valid for odd and even intervals [161]

$$\int_0^{\delta x} \mathrm{d}x\, g(x) \simeq \frac{\delta x}{24}(12 g_0 + 12 g_1), \tag{A.11}$$

$$\int_0^{2\delta x} \mathrm{d}x\, g(x) \simeq \frac{\delta x}{24}(8 g_0 + 32 g_1 + 8 g_2), \tag{A.12}$$

$$\int_0^{3\delta x} \mathrm{d}x\, g(x) \simeq \frac{\delta x}{24}(9 g_0 + 27 g_1 + 27 g_2 + 9 g_3), \tag{A.13}$$

$$\int_0^{4\delta x} \mathrm{d}x\, g(x) \simeq \frac{\delta x}{24}(9 g_0 + 28 g_1 + 22 g_2 + 28 g_3 + 9 g_4), \tag{A.14}$$

$$\int_0^{5\delta x} \mathrm{d}x\, g(x) \simeq \frac{\delta x}{24}(9 g_0 + 28 g_1 + 23 g_2 + 23 g_3 + 28 g_4 + 9 g_5), \tag{A.15}$$

$$\int_0^{x_{\max}} \mathrm{d}x\, g(x) \simeq \frac{\delta x}{24}\left(9 g_0 + 28 g_1 + 23 g_2 + 24 \sum_{i=3}^{i=i_{\max}-3} g_i + 23 g_{i_{\max}-2} + 28 g_{i_{\max}-1} + 9 g_{i_{\max}}\right). \tag{A.16}$$

Step size and stability

The choice of step sizes stems not only from a compromise between accuracy and computation time but also takes into account the issue of stability. Contrary to what a naive intuition could suggest, it is not enough to send step sizes to zero to obtain a correct approximation of the flow. Indeed, with our explicit Euler method, if the step size in the step variables is too small compared to the time step, the flow can be unstable, that is, small errors in the calculation get amplified to the point the approximated solution diverges. The idea behind this phenomena is that if space derivatives are computed with a too high precision compared to time derivatives, the numerical integration "overshoots" the solution. A more comprehensive discussion can be found in applied mathematics textbooks [160]. It is instructive to solve exactly the discretized version of the one-dimensional heat equation and perform a stability analysis to check it. Considering the complexity of our equations, we were unable to do so. In practice, the orders of magnitude are $\delta t \sim 10^{-4}$, $\delta\rho \sim 10^{-1}$, $\delta q \sim 10^{-1}$ (after rescaling $\rho \to \rho/N$ in the case of a N component field).

A.2 Specificities of NPRG flows

The above procedure can be used to integrate generic partial differential equations. In the case of RG flows which interest us, however, some specificities arise. We deal with them in this Section.

Anomalous dimension

The running anomalous dimension $\eta_k = -\partial_t \log Z_k$ (defined by (2.44)) is given by a renormalization condition $\partial_t \tilde{f} = 0$ where $\tilde{f}$ is a quantity related to the vertex $\Gamma^{(2)}$ (e.g. within DE $\tilde{f}$ is $Z(\rho)$ and

within BMW $\tilde{f}$ is $Y_A(p,\rho)$ for arbitrary renormalization points ρ and p). At a given time step, η_k and the other quantities have to be determined in a consistent way, so that $\partial_t \tilde{f}$ is indeed zero.

In the flow equation of $\tilde{f}$, η_k appears explicitly in two places: the dimensional terms and the time derivatives of the regulator, since $R_k(\mathbf{q}) = Z_k \mathbf{q}^2 r(\mathbf{q}^2/k^2)$ (with $r(y)$ some function) involves a Z_k factor in its definition. Both these dependencies are linear in η_k. Thanks to this, the implicit equation defining η_t can be easily inverted, and a closed expression for η_t obtained.

Minimum of the potential

We need to know the minimum of the potential $\rho_{0,t}$ as well as in the values taken by the functions at $\rho_{0,t}$. To determine $\rho_{0,t}$ we use two approaches. When using a fixed dimensionless grid $[0, \tilde{\rho}_{\max}]$, we first find the point in the grid where W changes sign, then use polynomial interpolation [162] around this point to approximate W. We estimate $\rho_{0,t}$ as the zero of the polynomial. Conversely, we use interpolation to determine the value of the different functions at $\rho_{0,t}$.

Multidimensional integrals

The flows involve multidimensional integrals which we reduce to one or two dimensional integrals, depending on the symmetry of the integrand.

For rotationally invariant integrals one has trivially

$$\int \frac{\mathrm{d}^D\mathbf{q}}{(2\pi)^D} g(\mathbf{q}^2) = \int_{\mathbf{q}} g(\mathbf{q}^2) = \frac{S_D}{(2\pi)^D} \int_0^{+\infty} \mathrm{d}q\, q^{D-1} g(q^2), \tag{A.17}$$

where S_d is the volume of the unit sphere in D dimensions. For integrals of the type

$$I(\mathbf{p}^2) = \int_{\mathbf{q}} g(\mathbf{q}^2, (\mathbf{p}+\mathbf{q})^2) \tag{A.18}$$

where $\mathbf{p}$ is some external momenta, it is possible to use the invariance of the integral under rotations around $\mathbf{p}$ to obtain after a change of variables [44]

$$I(\mathbf{p}^2) = \frac{S_{D-1}}{(2\pi)^D} \int_0^{+\infty} \mathrm{d}q\, \frac{q^{D-2}}{p} \int_{|p-q|}^{p+q} \mathrm{d}\xi\, \xi \mathcal{J}_D(\xi,p,q) g(q^2,\xi^2). \tag{A.19}$$

Here $p = |\mathbf{p}|$ and

$$\mathcal{J}_D(\xi,p,q) = \left[1 - \left(\frac{\xi^2 - p^2 - q^2}{2pq}\right)^2\right]^{(D-3)/2} \tag{A.20}$$

is the Jacobian of the change of variables. This expression presents several advantages: first, the needed integration points for ξ fall in the grid so that no interpolation is needed to get access to them. Second, for $D = 3$ the Jacobian reduces to unity, which further simplifies the computation.

However, for $D \neq 3$, the Jacobian tends to be ill-behaved at the boundaries of the integral on ξ. For $D = 2$ and 4, it respectively diverges like the inverse square root or goes to zero like the square root. To circumvenient this issue, one exploits the fact that the Jacobian is known *analytically* while the rest of the integral is known *numerically* on the grid, and uses the Gauss-Legendre method rather than the chained Simpson integral. Considering an integral of the form

$$\int_0^{2\delta x} \mathrm{d}x\, J(x) g(x) \tag{A.21}$$

with J known analytically and g numerically, we approximate it by a linear combination $\sum_{i=0}^{2} a_i g_i$ $(x = i\delta x)$ where the coefficients – which depend implicitly on J – are chosen so that the expression is exact for second order polynomials. This cures the problems induced by the Jacobian's divergences as the error committed in doing so is of the order of $O(g^{(3)})$ rather than $O((Jg)^{(3)})$ for the equivalent 3-point Simpson method.

A.2.1 Exploring the ordered phase

In this Section we swiftly present the method to pursue the NPRG flows in the ordered phase by following the dimensionless minimum of the potential.

In the ordered phase one encounters three separate issues while integrating the flow. First, as the minimum of the potential $\rho_{0,k}$ runs to the actual minimum ρ_0, its dimensionless counterpart $\tilde{\rho}_{0,k} \sim k^{d-2+\eta}\rho_{0,k}$ diverges. Second, for small values of ρ, because of the approach to convexity, the dimensionless potential becomes too negative and a pole in the propagator appears. The last issue, which we do not discuss here, is that for some models the dimensionless potential itself becomes singular at criticality.

A very simple method is to simply drop the points ρ for which the potential is negative. This method allows to prolongate the flow, but not indefinitely. Another much more effective solution is to follow the minimum of the potential while keeping dimensionless variables. To that effect, let us introduce the k-dependent change of variables $\tilde{\rho} \to \rho_{0,k} + \delta\tilde{\rho}$. When the minimum of the potential starts to grow and leaves the dimensionless grid $[0, \tilde{\rho}_{\max}]$, we perform the change of variables and switch to a grid $[\delta\tilde{\rho}_{\min}, \delta\tilde{\rho}_{\max}]$, with $\delta\tilde{\rho}_{\min} \leq 0 \leq \delta\tilde{\rho}_{\max}$ such that the minimum of the potential $\delta\tilde{\rho} = 0$ is within the grid. In the original dimensionless variables, it corresponds to a $\tilde{\rho}$ window of fixed length that follows $\tilde{\rho}_{0,k}$ as it flows to infinity. In the dimensionful variables, the grid shrinks around the minimum of the potential.

The equations for the functions are only changed minimally. Let us consider a certain function $\tilde{f}(\tilde{\rho})$ (which can be $\tilde{W}$, $\tilde{Z}$, and so on), and $\bar{f}(\delta\tilde{\rho})$ the same function after the change of variables. As $\bar{f}(\delta\tilde{\rho}) = \tilde{f}(\delta\tilde{\rho} + \rho_{0,k})$,

$$\partial_t \bar{f}(\delta\tilde{\rho}) = \partial_t \bar{f}(\delta\tilde{\rho})|_{\tilde{\rho}} - \frac{\partial_t \bar{W}(0)|_{\tilde{\rho}}}{\bar{W}'(0)} \bar{f}'(\delta\tilde{\rho}) \tag{A.22}$$

where $\partial_t \cdot |_{\tilde{\rho}}$ denotes the derivative at fixed $\tilde{\rho}$ and the second term comes from the fact that the change of variable is k-dependent. We use the exact expression of $\partial_t \rho_{0,k}$ obtained from differentiating $W(\rho_{0,k}) = 0$.

Note that $\rho_{0,k}$ now appears explicitly in the equations. However, it cannot be deduced from W any more because of the change of variables. Rather, we compute it by integrating its flow equation

$$\partial_t \rho_{0,k} = -\frac{\partial_t \bar{W}(0)|_{\tilde{\rho}}}{\bar{W}'(0)}. \tag{A.23}$$

At finite temperature in the classical renormalized regime, it is possible that in the flow the system first appears ordered then becomes disordered. Because of that, the minimum of the potential can become very large, only to go to zero as $k \to 0$. As the minimum grows, we perform the change of variable $\rho \to \rho_{0,k} + \delta\rho$. Then, as $\tilde{\rho}_{0,k}$ goes to zero, eventually the smallest point in the grid $\tilde{\rho}_{\min,k} = \tilde{\rho}_{0,k} + \delta\tilde{\rho}_{\min}$ becomes close to zero. As this happens, we switch back to the original fixed grid $[0, \tilde{\rho}_{\max}]$.

A.2.2 Padé approximants

To obtain the retarded dynamical function $F^R(\omega)$, we compute $F(p)$ for M momentum values p_l $(l = 1, \dots, M)$ with typically M in the range 50–100. One then constructs a M-point Padé approximant $F_P(p)$ which coincides with $F(p)$ for all p_l's. An algorithm [163] allows to do so. Then, $F^R(\omega)$ is approximated by $F_P(-i\omega + \epsilon)$.

The analytic continuation of numerical data is a subject of importance in condensed matter physics. The crude scheme explained above is often found to be insufficient. For instance, Padé approximants are highly sensitive to numerical noise, and a slight error in the data can cause huge noise in the continuation. Several other approaches have been proposed [164, 165]. For instance, the maximum entropy method finds an approximant by minimizing some fictitious free energy over a function space, which disfavors aberrant approximants (e.g. by enclosing a priori knowledge about the data). Such methods are not necessary for us, and Padé approximants are sufficient because NPRG provide precise results, i.e. the data we wish to continue is made of smooth functions and is free of numerical error.

Bibliography

[1] S. Sachdev, *Quantum phase transitions*, 2nd ed. (Cambridge University Press, Cambridge, UK, 2011).

[2] R. Coldea, D. A. Tennant, E. M. Wheeler, E. Wawrzynska, D. Prabhakaran, M. Telling, K. Habicht, P. Smeibidl, and K. Kiefer, "Quantum Criticality in an Ising Chain: Experimental Evidence for Emergent E_8 Symmetry," Science **327**, 177 (2010), arXiv:1103.3694 [cond-mat.str-el].

[3] C. Rüegg, B. Normand, M. Matsumoto, A. Furrer, D. F. McMorrow, K. W. Krämer, H. U. Güdel, S. N. Gvasaliya, H. Mutka, and M. Boehm, "Quantum Magnets under Pressure: Controlling Elementary Excitations in $TlCuCl_3$," Phys. Rev. Lett. **100**, 205701 (2008), arXiv:0803.3720 [cond-mat.str-el].

[4] A. Jain, M. Krautloher, J. Porras, G. H. Ryu, D. P. Chen, D. L. Abernathy, J. T. Park, A. Ivanov, J. Chaloupka, G. Khaliullin, B. Keimer, and B. J. Kim, "Higgs mode and its decay in a two-dimensional antiferromagnet," Nat. Phys. (2017), 10.1038/nphys4077, arXiv:1705.00222 [cond-mat.str-el].

[5] T. Hong, M. Matsumoto, Y. Qiu, W. Chen, T. R. Gentile, S. Watson, F. F. Awwadi, M. M. Turnbull, S. E. Dissanayake, H. Agrawal, R. Toft-Petersen, B. Klemke, K. Coester, K. P. Schmidt, and D. A. Tennant, "Higgs amplitude mode in a two-dimensional quantum antiferromagnet near the quantum critical point," Nat. Phys. **13**, 638 (2017), letter, arXiv:1705.06172 [cond-mat.str-el].

[6] D. Jaksch, C. Bruder, J. I. Cirac, C. W. Gardiner, and P. Zoller, "Cold Bosonic Atoms in Optical Lattices," Phys. Rev. Lett. **81**, 3108 (1998), cond-mat/9805329.

[7] M. Greiner, O. Mandel, T. Esslinger, T. W. Hansch, and I. Bloch, "Quantum phase transition from a superfluid to a Mott insulator in a gas of ultracold atoms," Nature **415**, 39 (2002).

[8] T. Stöferle, H. Moritz, C. Schori, M. Köhl, and T. Esslinger, "Transition from a Strongly Interacting 1D Superfluid to a Mott Insulator," Phys. Rev. Lett. **92**, 130403 (2004), cond-mat/0312440.

[9] I. B. Spielman, W. D. Phillips, and J. V. Porto, "Mott-Insulator Transition in a Two-Dimensional Atomic Bose Gas," Phys. Rev. Lett. **98**, 080404 (2007), cond-mat/0606216.

[10] M. Endres, T. Fukuhara, D. Pekker, M. Cheneau, P. Schauß, C. Gross, E. Demler, S. Kuhr, and I. Bloch, "The 'Higgs' amplitude mode at the two-dimensional superfluid/Mott insulator transition," Nature **487**, 454 (2012), arXiv:1204.5183 [cond-mat.quant-gas].

[11] M.-C. Cha, M. P. A. Fisher, S. M. Girvin, M. Wallin, and A. P. Young, "Universal conductivity of two-dimensional films at the superconductor-insulator transition," Phys. Rev. B **44**, 6883 (1991).

[12] S. Doniach, "The Kondo lattice and weak antiferromagnetism," Physica B & C **91**, 231 (1977).

[13] H. V. Löhneysen, A. Rosch, M. Vojta, and P. Wölfle, "Fermi-liquid instabilities at magnetic quantum phase transitions," Rev. Mod. Phys. **79**, 1015 (2007), cond-mat/0606317.

[14] S. Sachdev and J. Ye, "Universal Quantum-Critical Dynamics of Two-Dimensional Antiferromagnets," Phys. Rev. Lett. **69**, 2411 (1992).

[15] B. Keimer, S. A. Kivelson, M. R. Norman, S. Uchida, and J. Zaanen, "From quantum matter to high-temperature superconductivity in copper oxides," Nature **518**, 179 (2015), arXiv:1409.4673 [cond-mat.supr-con].

[16] A. Schröder, G. Aeppli, E. Bucher, R. Ramazashvili, and P. Coleman, "Scaling of Magnetic Fluctuations near a Quantum Phase Transition," Phys. Rev. Lett. **80**, 5623 (1998), cond-mat/9803004.

[17] A. Altland and B. D. Simons, *Condensed Matter Field Theory*, 2nd ed. (Cambridge University Press, Cambridge, UK, 2010).

[18] J. Berges, N. Tetradis, and C. Wetterich, "Non-perturbative renormalization flow in quantum field theory and statistical physics," Phys. Rep. **363**, 223 (2002), arXiv:hep-ph/0005122.

[19] P. Kopietz, L. Bartosch, and F. Schütz, *Introduction to the Functional Renormalization Group*, 2nd ed. (Springer, Berlin, Germany, 2010).

[20] B. Delamotte, "Renormalization Group and Effective Field Theory Approaches to Many-Body Systems," (Springer, Berlin, Heidelberg, 2012) Chap. An Introduction to the Nonperturbative Renormalization Group, pp. 49–132, arXiv:cond-mat/0702365.

[21] M. Le Bellac, *Quantum and Statistical Field Theory* (Oxford University Press, Oxford, UK, 1991).

[22] K. G. Wilson, "Renormalization Group and Critical Phenomena. I. Renormalization Group and the Kadanoff Scaling Picture," Phys. Rev. B **4**, 3174 (1971).

[23] K. G. Wilson, "Renormalization Group and Critical Phenomena. II. Phase-Space Cell Analysis of Critical Behavior," Phys. Rev. B **4**, 3184 (1971).

[24] K. Wilson, "The renormalization group: Critical phenomena and the Kondo problem," Rev. Mod. Phys. **47**, 773 (1975).

[25] J. Polchinski, "Renormalization and effective lagrangians," Nucl. Phys. B **231**, 269 (1984).

[26] J. F. Nicoll, T. S. Chang, and H. E. Stanley, "Approximate Renormalization Group Based on the Wegner-Houghton Differential Generator," Phys. Rev. Lett. **33**, 540 (1974).

[27] A. Hasenfratz and P. Hasenfratz, "Renormalization group study of scalar field theories," Nucl. Phys. B **270**, 687 (1986).

[28] C. Wetterich, "Exact evolution equation for the effective potential," Phys. Lett. B **301**, 90 (1993), arXiv:1710.05815 [hep-th].

[29] T. R. Morris, "The Exact Renormalization Group and Approximate Solutions," Int. J. Mod. Phys. A **9**, 2411 (1994), hep-ph/9308265.

[30] U. Ellwanger, "Collective fields and flow equations," Z. Phys. C **58**, 619 (1993).

[31] M. Bonini, M. D'Attanasio, and G. Marchesini, "Perturbative renormalization and infrared finiteness in the Wilson renormalization group: the massless scalar case," Nucl. Phys. B **409**, 441 (1993), hep-th/9301114.

[32] F. Rose and N. Dupuis, "Nonperturbative functional renormalization-group approach to transport in the vicinity of a $(2+1)$-dimensional $\mathrm{O}(N)$-symmetric quantum critical point," Phys. Rev. B **95**, 014513 (2016), arXiv:1610.06476 [cond-mat.str-el].

[33] F. Kos, D. Poland, D. Simmons-Duffin, and A. Vichi, "Precision islands in the Ising and $O(N)$ models," J. High Energy Phys. **8**, 36 (2016), arXiv:1603.04436 [hep-th].

[34] M. Hasenbusch, "Finite size scaling study of lattice models in the three-dimensional Ising universality class," Phys. Rev. B **82**, 174433 (2010), arXiv:1004.4486 [cond-mat.stat-mech].

[35] A. A. Pogorelov and I. M. Suslov, "Estimate of the critical exponents from the field-theoretical renormalization group: mathematical meaning of the "Standard Values"," J. Exp. Theor. Phys. **106**, 1118 (2008), arXiv:1010.3389 [cond-mat.stat-mech].

[36] M. Campostrini, M. Hasenbusch, A. Pelissetto, and E. Vicari, "Theoretical estimates of the critical exponents of the superfluid transition in ^{4}He by lattice methods," Phys. Rev. B **74**, 144506 (2006), arXiv:cond-mat/0605083.

[37] M. Campostrini, M. Hasenbusch, A. Pelissetto, P. Rossi, and E. Vicari, "Critical exponents and equation of state of the three-dimensional Heisenberg universality class," Phys. Rev. B **65**, 144520 (2002), arXiv:cond-mat/0110336.

[38] M. Hasenbusch, "Eliminating leading corrections to scaling in the three-dimensional $\mathrm{O}(N)$-symmetric ϕ^4 model: $N = 3$ and 4," J. Phys. A **34**, 8221 (2001), arXiv:cond-mat/0010463.

[39] R. Guida and J. Zinn-Justin, "Critical exponents of the N-vector model," J. Phys. A **31**, 8103 (1998), cond-mat/9803240.

[40] S. A. Antonenko and A. I. Sokolov, "Critical exponents for a three-dimensional $\mathrm{O}(n)$-symmetric model with $n \geq 3$," Phys. Rev. E **51**, 1894 (1995).

[41] M. Moshe and J. Zinn-Justin, "Quantum field theory in the large N limit: a review," Phys. Rep. **385**, 69 (2003), hep-th/0306133.

[42] G. v. Gersdorff and C. Wetterich, "Nonperturbative renormalization flow and essential scaling for the Kosterlitz-Thouless transition," Phys. Rev. B **64**, 054513 (2001), arXiv:hep-th/0008114.

[43] N. Hasselmann, "Effective-average-action-based approach to correlation functions at finite momenta," Phys. Rev. E **86**, 041118 (2012), arXiv:1206.6121 [cond-mat.stat-mech].

[44] F. Benitez, J. P. Blaizot, H. Chaté, B. Delamotte, R. Méndez-Galain, and N. Wschebor, "Solutions of renormalization group flow equations with full momentum dependence," Phys. Rev. E **80**, 030103 (2009), arXiv:0901.0128 [cond-mat.stat-mech].

[45] F. Benitez, J. P. Blaizot, H. Chaté, B. Delamotte, R. Méndez-Galain, and N. Wschebor, "Nonperturbative renormalization group preserving full-momentum dependence: Implementation and quantitative evaluation," Phys. Rev. E **85**, 026707 (2012), arXiv:1110.2665 [cond-mat.stat-mech].

[46] S. Ledowski, N. Hasselmann, and P. Kopietz, "Self-energy and critical temperature of weakly interacting bosons," Phys. Rev. A **69**, 061601 (2004), cond-mat/0311043.

[47] N. Hasselmann, S. Ledowski, and P. Kopietz, "Critical behavior of weakly interacting bosons: A functional renormalization-group approach," Phys. Rev. A **70**, 063621 (2004), cond-mat/0409167.

[48] J.-P. Blaizot, R. Méndez-Galain, and N. Wschebor, "A new method to solve the nonperturbative renormalization group equations," Phys. Lett. B **632**, 571 (2006), arXiv:hep-th/0503103.

[49] G. R. Golner, "Exact renormalization group flow equations for free energies and N-point functions in uniform external fields," ArXiv e-prints (1998), hep-th/9801124.

[50] A. Rançon, O. Kodio, N. Dupuis, and P. Lecheminant, "Thermodynamics in the vicinity of a relativistic quantum critical point in 2 + 1 dimensions," Phys. Rev. E **88**, 012113 (2013), arXiv:1303.6559 [cond-mat.quant-gas].

[51] A. Rançon, L.-P. Henry, F. Rose, D. Lopes Cardozo, N. Dupuis, P. C. W. Holdsworth, and T. Roscilde, "Critical Casimir forces from the equation of state of quantum critical systems," Phys. Rev. B **94**, 140506(R) (2016), arXiv:1606.03205 [cond-mat.stat-mech].

[52] P. Chaikin and T. Lubensky, *Principles of Condensed Matter Physics* (Cambridge University Press, Cambridge, UK, 2000).

[53] J. M. Kosterlitz and D. J. Thouless, "Ordering, metastability and phase transitions in two-dimensional systems," J. Phys. C **6**, 1181 (1973).

[54] S. K. Ma, *Modern theory of critical phenomena*, Frontiers in Physics (Benjamin-Cummings, Reading, MA, USA, 1976).

[55] J. Zinn-Justin, *Phase Transitions and Renormalisation Group* (Oxford University Press, Oxford, UK, 2007).

[56] D. R. Nelson and J. M. Kosterlitz, "Universal Jump in the Superfluid Density of Two-Dimensional Superfluids," Phys. Rev. Lett. **39**, 1201 (1977).

[57] H. B. G. Casimir, "On the attraction between two perfectly conducting plates," Proc. K. Ned. Akad. Wet. **51**, 793 (1948).

[58] M. E. Fisher and P.-G. de Gennes, "Wall phenomena in a critical binary mixture," C. R. Acad. Sci. Ser B **287**, 207 (1978).

[59] M. Fukuto, Y. F. Yano, and P. S. Pershan, "Critical Casimir Effect in Three-Dimensional Ising Systems: Measurements on Binary Wetting Films," Phys. Rev. Lett. **94**, 135702 (2005).

[60] R. Garcia and M. H. W. Chan, "Critical Casimir Effect near the ^{3}He-^{4}He Tricritical Point," Phys. Rev. Lett. **88**, 086101 (2002).

[61] A. Ganshin, S. Scheidemantel, R. Garcia, and M. H. W. Chan, "Critical Casimir Force in ^{4}He Films: Confirmation of Finite-Size Scaling," Phys. Rev. Lett. **97**, 075301 (2006), cond-mat/0605663.

[62] S. Gazit, D. Podolsky, A. Auerbach, and D. P. Arovas, "Dynamics and conductivity near quantum criticality," Phys. Rev. B **88**, 235108 (2013), arXiv:1309.1765 [cond-mat.str-el].

[63] Y. Nishiyama, "Duality-mediated critical amplitude ratios for the $(2+1)$-dimensional $S = 1$ XY model," Eur. Phys. J. B **90**, 173 (2017), arXiv:1710.02927 [cond-mat.stat-mech].

[64] D. Dantchev and M. Krech, "Critical Casimir force and its fluctuations in lattice spin models: Exact and Monte Carlo results," Phys. Rev. E **69**, 046119 (2004), cond-mat/0402238.

[65] O. Vasilyev, A. Gambassi, A. Maciołek, and S. Dietrich, "Universal scaling functions of critical Casimir forces obtained by Monte Carlo simulations," Phys. Rev. E **79**, 041142 (2009), arXiv:0812.0750 [cond-mat.stat-mech].

[66] A. Hucht, D. Grüneberg, and F. M. Schmidt, "Aspect-ratio dependence of thermodynamic Casimir forces," Phys. Rev. E **83**, 051101 (2011), arXiv:1012.4399 [cond-mat.stat-mech].

[67] D. Lopes Cardozo, *Finite size scaling and the critical Casimir force : Ising magnets and binary fluids*, Ph.D. thesis, École normale supérieure de Lyon (2015).

[68] P. Jakubczyk, N. Dupuis, and B. Delamotte, "Reexamination of the nonperturbative renormalization-group approach to the Kosterlitz-Thouless transition," Phys. Rev. E **90**, 062105 (2014), arXiv:1409.1374 [cond-mat.stat-mech].

[69] A. Rançon, *Quantum criticality and universality of a Bose gas in the vicinity of the Mott transition*, Ph.D. thesis, Université Pierre et Marie Curie - Paris VI (2012).

[70] C.-L. Hung, X. Zhang, N. Gemelke, and C. Chin, "Observation of scale invariance and universality in two-dimensional Bose gases," Nature **470**, 236 (2011), arXiv:1009.0016 [cond-mat.quant-gas].

[71] T. Yefsah, R. Desbuquois, L. Chomaz, K. J. Günter, and J. Dalibard, "Exploring the Thermodynamics of a Two-Dimensional Bose Gas," Phys. Rev. Lett. **107**, 130401 (2011), arXiv:1106.0188 [cond-mat.quant-gas].

[72] F. Rose, F. Léonard, and N. Dupuis, "Higgs amplitude mode in the vicinity of a $(2+1)$-dimensional quantum critical point: A nonperturbative renormalization-group approach," Phys. Rev. B **91**, 224501 (2015), arXiv:1503.08688 [cond-mat.quant-gas].

[73] F. Rose, F. Benitez, F. Léonard, and B. Delamotte, "Bound states of the ϕ^4 model via the nonperturbative renormalization group," Phys. Rev. D **93**, 125018 (2016), arXiv:1604.05285 [cond-mat.stat-mech].

[74] P. W. Higgs, "Broken Symmetries and the Masses of Gauge Bosons," Phys. Rev. Lett. **13**, 508 (1964).

[75] F. Englert and R. Brout, "Broken Symmetry and the Mass of Gauge Vector Mesons," Phys. Rev. Lett. **13**, 321 (1964).

[76] G. S. Guralnik, C. R. Hagen, and T. W. B. Kibble, "Global Conservation Laws and Massless Particles," Phys. Rev. Lett. **13**, 585 (1964).

[77] G. Aad, T. Abajyan, B. Abbott, J. Abdallah, S. Abdel Khalek, A. A. Abdelalim, O. Abdinov, R. Aben, B. Abi, M. Abolins, *et al.*, "Observation of a new particle in the search for the Standard Model Higgs boson with the ATLAS detector at the LHC," Phys. Lett. B **716**, 1 (2012), arXiv:1207.7214 [hep-ex].

[78] P. W. Anderson, "Plasmons, Gauge Invariance, and Mass," Phys. Rev. **130**, 439 (1963).

[79] R. Sooryakumar and M. V. Klein, "Raman Scattering by Superconducting-Gap Excitations and Their Coupling to Charge-Density Waves," Phys. Rev. Lett. **45**, 660 (1980).

[80] P. B. Littlewood and C. M. Varma, "Amplitude collective modes in superconductors and their coupling to charge-density waves," Phys. Rev. B **26**, 4883 (1982).

[81] M.-A. Méasson, Y. Gallais, M. Cazayous, B. Clair, P. Rodière, L. Cario, and A. Sacuto, "Amplitude Higgs mode in the 2H-NbSe2 superconductor," Phys. Rev. B **89**, 060503 (2014), arXiv:1401.1025 [cond-mat.supr-con].

[82] C. M. Varma, "Higgs Boson in Superconductors," J. Low Temp. Phys. **126**, 901 (2002), arXiv:cond-mat/0109409.

[83] C. Rüegg, A. Furrer, D. Sheptyakov, T. Strässle, K. W. Krämer, H.-U. Güdel, and L. Mélési, "Pressure-Induced Quantum Phase Transition in the Spin-Liquid $TlCuCl_3$," Phys. Rev. Lett. **93**, 257201 (2004).

[84] P. Merchant, B. Normand, K. W. Krämer, M. Boehm, D. F. McMorrow, and C. Rüegg, "Quantum and classical criticality in a dimerized quantum antiferromagnet," Nat. Phys. **10**, 373 (2014), arXiv:1405.2391 [cond-mat.str-el].

[85] U. Bissbort, S. Götze, Y. Li, J. Heinze, J. S. Krauser, M. Weinberg, C. Becker, K. Sengstock, and W. Hofstetter, "Detecting the Amplitude Mode of Strongly Interacting Lattice Bosons by Bragg Scattering," Phys. Rev. Lett. **106**, 205303 (2011), arXiv:1010.2205 [cond-mat.quant-gas].

[86] H. D. Scammell and O. P. Sushkov, "Asymptotic freedom in quantum magnets," Phys. Rev. B **92**, 220401 (2015), arXiv:1506.08934 [cond-mat.str-el].

[87] M. Fidrysiak and J. Spałek, "Stable high-temperature paramagnons in a three-dimensional antiferromagnet near quantum criticality: Application to $TlCuCl_3$," Phys. Rev. B **95**, 174437 (2017), arXiv:1701.07406 [cond-mat.str-el].

[88] A. Patashinskiĭ and V. Pokrovskiĭ, "Longitudinal susceptibility and correlations in degenerate systems," Zh. Eksp. Teor. Fiz. **64**, 1445 (1973).

[89] S. Sachdev, "Universal relaxational dynamics near two-dimensional quantum critical points," Phys. Rev. B **59**, 14054 (1999), arXiv:cond-mat/9810399.

[90] W. Zwerger, "Anomalous Fluctuations in Phases with a Broken Continuous Symmetry," Phys. Rev. Lett. **92**, 027203 (2004), arXiv:cond-mat/0304153.

[91] N. Dupuis, "Infrared behavior in systems with a broken continuous symmetry: Classical O(N) model versus interacting bosons," Phys. Rev. E **83**, 031120 (2011), arXiv:1011.3324 [cond-mat.quant-gas].

[92] D. Podolsky, A. Auerbach, and D. P. Arovas, "Visibility of the amplitude (Higgs) mode in condensed matter," Phys. Rev. B **84**, 174522 (2011), arXiv:1108.5207 [cond-mat.supr-con].

[93] D. Podolsky and S. Sachdev, "Spectral functions of the Higgs mode near two-dimensional quantum critical points," Phys. Rev. B **86**, 054508 (2012), arXiv:1205.2700 [cond-mat.quant-gas].

[94] L. Pollet and N. Prokof'ev, "Higgs Mode in a Two-Dimensional Superfluid," Phys. Rev. Lett. **109**, 010401 (2012), arXiv:1204.5190 [cond-mat.quant-gas].

[95] K. Chen, L. Liu, Y. Deng, L. Pollet, and N. Prokof'ev, "Universal Properties of the Higgs Resonance in (2 + 1)-Dimensional U(1) Critical Systems," Phys. Rev. Lett. **110**, 170403 (2013), arXiv:1301.3139 [cond-mat.stat-mech].

[96] S. Gazit, D. Podolsky, and A. Auerbach, "Fate of the Higgs Mode Near Quantum Criticality," Phys. Rev. Lett. **110**, 140401 (2013), arXiv:1212.3759 [cond-mat.quant-gas].

[97] A. Rançon and N. Dupuis, "Higgs amplitude mode in the vicinity of a (2 + 1)-dimensional quantum critical point," Phys. Rev. B **89**, 180501(R) (2014), arXiv:1402.3098 [cond-mat.quant-gas].

[98] Y. T. Katan and D. Podolsky, "Spectral function of the Higgs mode in $4 - \epsilon$ dimensions," Phys. Rev. B **91**, 075132 (2015), arXiv:1412.4546 [cond-mat.str-el].

[99] M. Lohöfer, T. Coletta, D. G. Joshi, F. F. Assaad, M. Vojta, S. Wessel, and F. Mila, "Dynamical structure factors and excitation modes of the bilayer Heisenberg model," Phys. Rev. B **92**, 245137 (2015), arXiv:1508.07816 [cond-mat.str-el].

[100] Y. Nishiyama, "Critical behavior of the Higgs- and Goldstone-mass gaps for the two-dimensional $S = 1$ XY model," Nucl. Phys. B **897**, 555 (2015), arXiv:1506.04199 [cond-mat.stat-mech].

[101] Y. Nishiyama, "Universal scaled Higgs-mass gap for the bilayer Heisenberg model in the ordered phase," Eur. Phys. J. B **89**, 31 (2016), arXiv:1601.04772 [cond-mat.stat-mech].

[102] D. Sherman, U. S. Pracht, B. Gorshunov, S. Poran, J. Jesudasan, M. Chand, P. Raychaudhuri, M. Swanson, N. Trivedi, A. Auerbach, M. Scheffler, A. Frydman, and M. Dressel, "The Higgs mode in disordered superconductors close to a quantum phase transition," Nat. Phys. **11**, 188 (2015), arXiv:1412.0068 [cond-mat.supr-con].

[103] S.-M. Souliou, J. Chaloupka, G. Khaliullin, G. Ryu, M. Le Tacon, and B. Keimer, "Raman scattering from Higgs mode oscillations in the two-dimensional antiferromagnet Ca_2RuO_4," ArXiv e-prints (2017), arXiv:1704.04991 [cond-mat.str-el].

[104] J. Léonard, A. Morales, P. Zupancic, T. Donner, and T. Esslinger, "Monitoring and manipulating Higgs and Goldstone modes in a supersolid quantum gas," ArXiv e-prints (2017), arXiv:1704.05803 [cond-mat.quant-gas].

[105] G. S. Uhrig and H. J. Schulz, "Magnetic excitation spectrum of dimerized antiferromagnetic chains," Phys. Rev. B **54**, R9624 (1996), cond-mat/9606001.

[106] S. Trebst, H. Monien, C. J. Hamer, Z. Weihong, and R. R. P. Singh, "Strong-Coupling Expansions for Multiparticle Excitations: Continuum and Bound States," Phys. Rev. Lett. **85**, 4373 (2000), cond-mat/0007192.

[107] C. Knetter, K. P. Schmidt, M. Grüninger, and G. S. Uhrig, "Fractional and Integer Excitations in Quantum Antiferromagnetic Spin 1/2 Ladders," Phys. Rev. Lett. **87**, 167204 (2001), cond-mat/0106077.

[108] W. Zheng, C. J. Hamer, R. R. Singh, S. Trebst, and H. Monien, "Linked cluster series expansions for two-particle bound states," Phys. Rev. B **63**, 144410 (2001), cond-mat/0010354.

[109] M. Windt, M. Grüninger, T. Nunner, C. Knetter, K. P. Schmidt, G. S. Uhrig, T. Kopp, A. Freimuth, U. Ammerahl, B. Büchner, and A. Revcolevschi, "Observation of Two-Magnon Bound States in the Two-Leg Ladders of $(Ca,La)_{14}Cu_{24}O_{41}$," Phys. Rev. Lett. **87**, 127002 (2001), cond-mat/0103438.

[110] C. Cohen-Tannoudji and D. Guery-Odelin, *Advances in Atomic Physics* (World Scientific Publishing Company, Singapore, 2011).

[111] I. N. Levine, *Quantum Chemistry*, 7th ed. (Prentice Hall, Upper Saddle River, NJ, USA, 2013).

[112] R. J. Jaffe, "Multiquark hadrons. I. Phenomenology of $Q^2\overline{Q}^2$ mesons," Phys. Rev. D **15**, 267 (1977).

[113] M. Shifman, A. Vainshtein, and V. Zakharov, "QCD and resonance physics. Theoretical foundations," Nucl. Phys. B **147**, 385 (1979).

[114] J. Vidal, B. Douçot, R. Mosseri, and P. Butaud, "Interaction Induced Delocalization for Two Particles in a Periodic Potential," Phy. Rev. Lett. **85**, 3906 (2000), cond-mat/0005215.

[115] B. Douçot and J. Vidal, "Pairing of Cooper Pairs in a Fully Frustrated Josephson-Junction Chain," Phys. Rev. Lett. **88**, 227005 (2002), cond-mat/0202115.

[116] A. B. Zamolodchikov, "Integrals of Motion and S-Matrix of the (scaled) $T = T_c$ Ising Model with Magnetic Field," Int. J. Mod. Phys. A **4**, 4235 (1989).

[117] P. Fonseca and A. Zamolodchikov, "Ising field theory in a magnetic field: analytic properties of the free energy," ArXiv e-prints (2001), hep-th/0112167.

[118] V. Agostini, G. Carlino, M. Caselle, and M. Hasenbusch, "The spectrum of the 2 + 1-dimensional gauge Ising model," Nucl. Phys. B **484**, 331 (1997), hep-lat/9607029.

[119] M. Caselle, M. Hasenbusch, and P. Provero, "Non-perturbative states in the $3D$ φ^4 theory," Nucl. Phys. B **556**, 575 (1999), hep-lat/9903011.

[120] M. Caselle, M. Hasenbusch, P. Provero, and K. Zarembo, "Bound states in the three-dimensional φ^4 model," Phys. Rev. D **62**, 017901 (2000), hep-th/0001181.

[121] M. Caselle, M. Hasenbusch, P. Provero, and K. Zarembo, "Bound states and glueballs in three-dimensional Ising systems," Nucl. Phys. B **623**, 474 (2002), hep-th/0103130.

[122] S. Dusuel, M. Kamfor, K. P. Schmidt, R. Thomale, and J. Vidal, "Bound states in two-dimensional spin systems near the Ising limit: A quantum finite-lattice study," Phys. Rev. B **81**, 064412 (2010), arXiv:0912.1463 [cond-mat.str-el].

[123] Y. Nishiyama, "Universal critical behavior of the two-magnon-bound-state mass gap for the $(2+1)$-dimensional Ising model," Physica A **413**, 577 (2014), arXiv:1407.8243 [cond-mat.stat-mech].

[124] F. Léonard, *Criticalité et phase brisée de modèles avec symétrie discrète*, Ph.D. thesis, Université Pierre et Marie Curie - Paris VI (2016).

[125] J. Šmakov and E. Sørensen, "Universal Scaling of the Conductivity at the Superfluid-Insulator Phase Transition," Phys. Rev. Lett. **95**, 180603 (2005), cond-mat/0509671.

[126] K. Chen, L. Liu, Y. Deng, L. Pollet, and N. Prokof'ev, "Universal Conductivity in a Two-Dimensional Superfluid-to-Insulator Quantum Critical System," Phys. Rev. Lett. **112**, 030402 (2014), arXiv:1309.5635 [cond-mat.str-el].

[127] S. Gazit, D. Podolsky, and A. Auerbach, "Critical Capacitance and Charge-Vortex Duality Near the Superfluid-to-Insulator Transition," Phys. Rev. Lett. **113**, 240601 (2014), arXiv:1407.1055 [cond-mat.str-el].

[128] E. Katz, S. Sachdev, E. S. Sørensen, and W. Witczak-Krempa, "Conformal field theories at nonzero temperature: Operator product expansions, Monte Carlo, and holography," Phys. Rev. B **90**, 245109 (2014), arXiv:1409.3841 [cond-mat.str-el].

[129] W. Witczak-Krempa, E. S. Sørensen, and S. Sachdev, "The dynamics of quantum criticality revealed by quantum Monte Carlo and holography," Nat. Phys. **10**, 361 (2014), arXiv:1309.2941 [cond-mat.str-el].

[130] A. Lucas, S. Gazit, D. Podolsky, and W. Witczak-Krempa, "Dynamical response near quantum critical points," Phys. Rev. Lett. **118**, 056601 (2017), arXiv:1608.02586 [cond-mat.str-el].

[131] W. Witczak-Krempa, "Constraining Quantum Critical Dynamics: $(2+1)D$ Ising Model and Beyond," Phys. Rev. Lett. **114**, 177201 (2015), arXiv:1501.03495 [cond-mat.str-el].

[132] F. Kos, D. Poland, D. Simmons-Duffin, and A. Vichi, "Bootstrapping the O(N) archipelago," J. High Energy Phys. **11**, 106 (2015), arXiv:1504.07997 [hep-th].

[133] R. C. Myers, T. Sierens, and W. Witczak-Krempa, "A holographic model for quantum critical responses," J. High Energy Phys. **2016**, 1 (2016), arXiv:1602.05599 [hep-th].

[134] S. Sachdev, "What Can Gauge-Gravity Duality Teach Us About Condensed Matter Physics?" Annu. Rev. Condens. Matter Phys. **3**, 9 (2012), arXiv:1108.1197 [cond-mat.str-el].

[135] W. Witczak-Krempa and S. Sachdev, "Quasinormal modes of quantum criticality," Phys. Rev. B **86**, 235115 (2012), arXiv:1210.4166 [cond-mat.str-el].

[136] W. Witczak-Krempa and S. Sachdev, "Dispersing quasinormal modes in $(2+1)$-dimensional conformal field theories," Phys. Rev. B **87**, 155149 (2013), arXiv:1302.0847 [cond-mat.str-el].

[137] F. Rose and N. Dupuis, "Superuniversal transport near a $(2+1)$-dimensional quantum critical point," Phys. Rev. B **96**, 100501 (2017), arXiv:1705.03905 [cond-mat.str-el].

[138] A. Rückriegel and P. Kopietz, "Spin currents, spin torques, and the concept of spin superfluidity," Phys. Rev. B **95**, 104436 (2017), arXiv:1701.05505 [cond-mat.mes-hall].

[139] M. P. A. Fisher, G. Grinstein, and S. M. Girvin, "Presence of quantum diffusion in two dimensions: Universal resistance at the superconductor-insulator transition," Phys. Rev. Lett. **64**, 587 (1990).

[140] K. Damle and S. Sachdev, "Nonzero-temperature transport near quantum critical points," Phys. Rev. B **56**, 8714 (1997), arXiv:cond-mat/9705206.

[141] P. Nozieres and D. Pines, *Theory Of Quantum Liquids* (Avalon Publishing, New York, NY, USA, 1999).

[142] X. G. Wen and A. Zee, "Universal conductance at the superconductor-insulator transition," Int. J. Mod. Phys. B **04**, 437 (1990).

[143] T. R. Morris, "A gauge invariant exact renormalisation group. (I)," Nucl. Phys. B **573**, 97 (2000), hep-th/9910058.

[144] T. R. Morris, "A gauge invariant exact renormalization group II," J. High Energy Phys. **12**, 012 (2000), hep-th/0006064.

[145] S. Arnone, A. Gatti, and T. R. Morris, "Towards a manifestly gauge invariant and universal calculus for Yang-Mills theory," Acta Phys. Slovaca **52**, 621 (2002), arXiv:hep-th/0209130.

[146] L. Bartosch, "Corrections to scaling in the critical theory of deconfined criticality," Phys. Rev. B **88**, 195140 (2013), arXiv:1307.3276 [cond-mat.str-el].

[147] A. Codello, R. Percacci, L. Rachwał, and A. Tonero, "Computing the effective action with the functional renormalization group," Eur. Phys. J. C **76**, 226 (2016), arXiv:1505.03119 [hep-th].

[148] R. Fazio and D. Zappalà, "ϵ expansion of the conductivity at the superconductor–Mott-insulator transition," Phys. Rev. B **53**, R8883 (1996).

[149] A. Campa, A. Giansanti, and D. Moroni, "Canonical solution of classical magnetic models with long-range couplings," J. Phys. A: Math. Gen. **36**, 6897 (2003), cond-mat/0206173.

[150] L. Casetti, C. Nardini, and R. Nerattini, "Microcanonical Relation between Continuous and Discrete Spin Models," Phys. Rev. Lett. **106**, 057208 (2011), arXiv:1011.4164 [cond-mat.stat-mech].

[151] R. Nerattini, A. Trombettoni, and L. Casetti, "Critical energy density of $O(n)$ models in $d = 3$," J. Stat. Mech. Theor. Exp. **12**, 12001 (2014), arXiv:1407.7966 [cond-mat.stat-mech].

[152] S. Floerchinger, "Analytic continuation of functional renormalization group equations," J. High Energy Phys. **5**, 21 (2012), arXiv:1112.4374 [hep-th].

[153] R. A. Tripolt, N. Strodthoff, L. von Smekal, and J. Wambach, "Finite-Temperature Spectral Functions from the Functional Renormalization Group," in *Proceedings of the 31st International Symposium on Lattice Field Theory*, LATTICE 2013 (PoS, Mainz, Germany, 2013) p. 457, arXiv:1311.4304 [hep-lat].

[154] K. Kamikado, N. Strodthoff, L. von Smekal, and J. Wambach, "Real-time correlation functions in the model from the functional renormalization group," Eur. Phys. J. C **74**, 2806 (2014), arXiv:1302.6199 [hep-ph].

[155] J. Wambach, R.-A. Tripolt, N. Strodthoff, and L. von Smekal, "Spectral functions from the functional renormalization group," Nucl. Phys. A **928**, 156 (2014), arXiv:1404.7312 [hep-ph].

[156] J. M. Pawlowski and N. Strodthoff, "Real time correlation functions and the functional renormalisation group," Phys. Rev. D **92**, 094009 (2015), arXiv:1508.01160 [hep-ph].

[157] J. Pawlowski and A. Rothkopf, "Thermal dynamics on the lattice with exponentially improved accuracy," ArXiv e-prints (2016), arXiv:1610.09531 [hep-lat].

[158] N. Strodthoff, "Self-consistent spectral functions in the $O(N)$ model from the functional renormalization group," Phys. Rev. D **95**, 076002 (2017), 1611.05036 [hep-th].

[159] P. K. Kovtun, D. T. Son, and A. O. Starinets, "Viscosity in Strongly Interacting Quantum Field Theories from Black Hole Physics," Phys. Rev. Lett. **94**, 111601 (2005), hep-th/0405231.

[160] G. Evans, J. Blackledge, and P. Yardley, *Numerical Methods for Partial Differential Equations*, Springer Undergraduate Mathematics Series (Springer-Verlag, London, UK, 2000).

[161] J. W. Hollingsworth and H. F. Hunter, "Simpson's Rule for an Odd Number of Intervals," in *Preprints of Papers Presented at the 14th National Meeting of the Association for Computing Machinery*, ACM '59 (ACM, New York, NY, USA, 1959) p. 1.

[162] W. H. Press, B. P. Flannery, S. A. Teukolsky, and W. T. Vetterling, *Numerical Recipes in C: The Art of Scientific Computing, Second Edition* (Cambridge University Press, Cambridge, UK, 1992).

[163] H. J. Vidberg and J. W. Serene, "Solving the Eliashberg equations by means of N-point Padé approximants," J. Low Temp. Phys. **29**, 179 (1977).

[164] J. Schött, E. G. C. P. van Loon, I. L. M. Locht, M. I. Katsnelson, and I. Di Marco, "Comparison between methods of analytical continuation for bosonic functions," Phys. Rev. B **94**, 245140 (2016), arXiv:1607.04212 [cond-mat.str-el].

[165] O. Goulko, A. S. Mishchenko, L. Pollet, N. Prokof'ev, and B. Svistunov, "Numerical analytic continuation: Answers to well-posed questions," Phys. Rev. B **95**, 014102 (2017), arXiv:1609.01260 [cond-mat.other].

Félix Rose **19 septembre 2017**

Sujet : Dynamique et transport au voisinage d'une transition de phase quantique en dimension deux

Résumé Nous étudions le modèle O(N) relativiste, une généralisation quantique de la théorie φ^4 utilisée en physique statistique pour étudier des transitions de phase. Ce modèle décrit certaines transitions de phase quantiques telles que la transition isolant de Mott-superfluide dans un gaz de bosons piégés dans un réseau optique ou la transition paramagnétique-antiferromagnétique dans un aimant. En deux dimensions d'espace, ces systèmes sont fortement corrélés près de la transition. Nous les étudions à l'aide du groupe de renormalisation non perturbatif, une formulation du groupe de renormalisation de Wilson. Nous nous intéressons aux propriétés universelles au voisinage de la transition de phase quantique à température nulle.

Ainsi, nous déterminons les fonctions d'échelle universelles qui définissent la thermodynamique et démontrons que ces fonctions sont reliées à celles décrivant la force de Casimir critique dans un système classique tridimensionel. Ensuite, nous étudions le spectre d'excitation dans la phase ordonnée à température nulle. Pour $N = 2$ et 3, nous établissons l'existence d'un mode d'amplitude aussi appelé « mode de Higgs » par analogie avec le mécanisme de Higgs en physique des hautes énergies. Pour $N = 1$, nous montrons l'existence d'un état lié pour des dimensions proches de trois. Enfin, nous calculons la dépendance en fréquence de la conductivité à température nulle et confirmons son universalité, en particulier à la transition. Nous établissons que l'une des composantes du tenseur de conductivité dans la phase ordonnée est une quantité « superuniverselle », ne dépendant ni de la distance au point critique ni de N.

Mots-clés Transition de phase quantique ; groupe de renormalisation non perturbatif ; équation d'état ; Higgs ; conductivité.

Subject: Dynamics and transport in the vicinity of a two-dimensional quantum phase transition

Abstract We study the relativistic O(N) model, a quantum generalization of the φ^4 theory used in statistical physics to study some phase transitions. This model describes quantum phase transitions such as the Mott insulator-superfluid transition in boson gases trapped in optical lattices or the paramagnetic-antiferromagnetic transition in magnets. In two space dimensions, these systems exhibit strong correlations near the transition. We study them using the nonperturbative renormalization group, an implementation of Wilson's renormalization group. We focus on the universal properties in the vicinity of the zero-temperature quantum phase transition.

We determine the universal scaling functions which define the thermodynamics and we show that these functions are related to those describing the critical Casimir forces in a three-dimensional system. Then, we study the excitation spectrum in the zero-temperature ordered phase. For $N = 2$ and 3, we establish the existence of an amplitude mode, also called "Higgs mode" by analogy with the Higgs mechanism in high-energy physics. For $N = 1$, we show the existence of a bound state at dimensions close to three. Finally, we compute the frequency-dependent conductivity at zero temperature and confirm its universal character, in particular at the transition. We prove that one of the components of the conductivity tensor in the ordered phase is a "superuniversal" quantity, depending neither on the distance to the critical point nor on N.

Keywords Quantum phase transition; nonperturbative renormalization group; equation of state; Higgs; conductivity.